WL-TR-1997-7006

AERODYNAMIC TESTING IN A FREE-FLIGHT SPARK RANGE

G.L.Winchenbach

WL/MNAV
Flight Vehicles Branch
Weapon Flight Mechanics Division
Eglin AFB FL 32542-6810

April 1997

FINAL REPORT FOR PERIOD JUNE 1990 - MARCH 1997

<div style="border:1px solid black">

APPROVED FOR PUBLIC RELEASE: DISTRIBUTION UNLIMITED

</div>

19970822 021

DTIC QUALITY INSPECTED 3

WRIGHT LABORATORY, ARMAMENT DIRECTORATE

Air Force Materiel Command ■ United States Air Force ■ Eglin Air Force Base

NOTICE

When Government drawings, specifications, or other data are used for any purposes other than in connection with a definitely Government-related procurement, the United States Government incurs no responsibility or any obligation whatsoever. The fact that the Government may have formulated or in any way supplied the said drawings, specifications, or other data, is not to be regarded by implication, or otherwise as in any manner construed, as licensing the holder, or any other person or corporation; or as conveying any rights or permission to manufacture, use, or sell any patented invention that may be related thereto.

This technical report has been reviewed and is approved for publication.

FOR THE COMMANDER

L. Bruce Simpson
Technical Director
Weapon Flight Mechanics Division

Even though this report may contain special release rights held by the controlling office, please do not request copies from the Wright Laboratory, Armament Directorate. If you qualify as a recipient, release approval will be obtained from the originating activity by DTIC. Address your request for additional copies to:

ATTN: DTIC-OCP
Defense Technical Information Center
8725 John J. Kingman Road
Fort Belvoir, VA 22060-6218

If your address has changed, if you wish to be removed from our mailing list, or if your organization no longer employs the addressee, please notify WL/MNAV, 101 W. Eglin Blvd., Suite 219, Eglin AFB FL 32542-6810, to help us maintain a current mailing list.

Do not return copies of this report unless contractual obligations or notice on a specific document requires that they be returned.

REPORT DOCUMENTATION PAGE

Form Approved
OMB No, 0704-0188

1. AGENCY USE ONLY *(Leave blank)*	2. REPORT DATE April 1997	3. REPORT TYPE AND DATES COVERED Final Report June 1990 - March 1997

4. TITLE AND SUBTITLE	5. FUNDING NUMBERS
Aerodynamic Testing in a Free-Flight Spark Range	PE: 62602F
	PR: 2502
6. AUTHOR(S) Winchenbach, G. L.	TA: 67
	WU: 03

7. PERFORMING ORGANIZATION NAME(S) AND ADDRESS(ES) Wright Laboratory Armament Directorate Weapon Flight Mechanics Division Flight Vehicles Branch(WL / MNAV), Eglin AFB FL 32542-6810	8. PERFORMING ORGANIZATION REPORT NUMBER

9. SPONSORING/MONITORING AGENCY NAME(S) AND ADDRESS(ES) Wright Laboratory Armament Directorate Weapon Flight Mechanics Division Flight Vehicles Branch (WL / MNAV), Eglin AFB FL 32542-6810 Point of Contact : G.L. Winchenbach, WL/ MNAV, 904-882-4085	10. SPONSORING/MONITORING AGENCY REPORT NUMBER WL-TR-1997 - 7006

11. SUPPLEMENTARY NOTES

12a. DISTRIBUTION/AVAILABILITY STATEMENT Approved for Public Release: Distribution Unlimited	12b. DISTRIBUTION CODE A

13. ABSTRACT *(Maximum 200 words)*

The U.S. Air Force Wright Laboratory operates the Aeroballistic Research Facility. This facility is located at Eglin AFB FL and is an enclosed free-flight range used to perform aerodynamic tests and research. This report documents the theoretical and experimental considerations required by the test engineers, facility operators, and data analysts to effectively conduct their duties. These duties include, pretest planning, conducting the tests, trajectory analysis, data correlation, and the continued development of advanced and /or improved techniques.

14. SUBJECT TERM Spark Range Testing, Trajectory Measurements, Trajectory Analysis, Aerodynamics	15. NUMBER OF PAGES 166
	16. PRICE CODE

17. SECURITY CLASSIFICATION OF REPORT UNCLASSIFIED	18. SECURITY CLASSIFICATION OF THIS PAGE UNCLASSIFIED	19. SECURITY CLASSIFICATION OF ABSTRACT UNCLASSIFIED	20. LIMITATION OF ABSTRACT SAR

NSN 7540-01-280-5500

Standard Form 298 (Rev. 2-89)
Prescribed by ANSI Std. 239-18

PREFACE

The information documented in the publication is meant to provide the free-flight ballistics test engineer with the basic insights and understandings he requires to accomplish his research duties. However, it certainly does not attempt to provide all the information the ballistic range practitioner needs to fulfill these duties. There are numerous outstanding references available to the researcher. Some of these are listed herein and those references will refer to even more outstanding publications associated with ballistic technologies. It is hoped that the information contained herein will be of assistance to the ballistic range test personnel, especially those involved in free-flight spark ranges.

This publication was drafted intermittently from December 1990 through March 1997. Information was extracted from numerous papers, reports, and text books. Hopefully, credit has been given where due but after practicing over 30 years in a technology area it is difficult to remember where all the information one possesses originally came from. Nevertheless applicable references have been provided throughout this publication and a bibliography of related publications is also provided for the interested reader. Because much of the information was extracted from other sources and collected over a period of time the units used throughout are a hodge podge of English and Metric and in many cases mixed. The author apologizes for this inconvenience but has attempted to at least clearly identify the units used.

Even after the above statement, it is still necessary to acknowledge certain individuals, i.e., Bob Whyte and Wayne Hathaway of Arrow Tech, Inc., Burlington VT, Dr. C. H. Murphy, Army Research Laboratory, Aberdeen MD, Dr. John D. Nicolaides, California Polytechnical Inst. (retired), and Dr. Gary Chapman, University of California, Berkeley. Although all of these individuals have been referenced they are the persons primarily responsible for much of the information provided herein. Very little, if any, of the information presented in this publication was original work by the author. Some of the derivations included herein may appear to differ from those in previous publications; however, this is only due to the author's style.

There is always the desire and inclination to add one more section or present another derivation. Also, since modern computational techniques and electronics are rapidly evolving some sections have required significant rewrites during the drafting process. In fact this could be a continuous process. But, eventually an end must be reached and the work product delivered in the hope that it adds something to the available literature. In that hope this document is submitted.

(This page is blank)

CONTENTS

CONTENTS

CONTENTS

CONTENTS

LIST OF FIGURES

CONTENTS

Partial List of Symbols

A	= reference area, $\pi d^2/4$
a	= speed of sound
a_c	= Coriolis acceleration
A.F.	= amplification factor, see Eq. 6.32
A.J.	= aerodynamic jump, see Eq. 7.32
C_F	= generalized force coefficient, $F/(1/2\ \rho\ V^2 A)$
C_X	= force coefficient in the x direction
C_D	= drag coefficient
C_L	= lift force coefficient
$C_{L\alpha}$	= lift force coefficient derivative
C_N	= normal force coefficient
$C_{N\alpha}$	= normal force coefficient derivative
C_m	= pitching moment coefficient, $m\ /\ (1/2\ \rho\ V^2 Ad)$
$C_{m\alpha}$	= pitching moment coefficient derivative
C_n	= yawing moment coefficient, $n\ /\ (1/2\ \rho\ V^2 Ad)$
$C_{n\alpha}$	= yawing moment coefficient derivative
$C_{mq}+C_{m\dot\alpha}$	= damping-in-pitch derivatives
$C_{np\alpha}$	= Magnus moment derivative
d	= model diameter, reference length
d_b	= barrel diameter
g	= acceleration due to gravity
I_x, I_y, I_z	= moments of inertia about the x, y, and z axes
I_{xy}	= cross product of inertia
K_N, K_P, K_T	= nutational, precessional, and trim vector magnitudes
K_p, K_δ	= coefficients of the roll equation, see Eq. 6.10
k_a, k_t	= axial and transverse radiuses of gyration
L	= model length
L_{cg}	= distance from model nose to center-of-gravity
L_{cp}	= distance from model nose to center-of-pressure
L_{WB}	= length of projectile wheel base, see Eq. 7.34
l, m, n	= moments about the x, y, and z axes
M	= Mach number
m_a	= model mass
m_e, n_e, p_e	= direction cosines, see Eq. 5.14
P_i	= partial derivative, see Eq. 6.61
p, q, r	= angular rates about the x, y, and z axes
R	= gas constant, for air $R = 53.34$ (ft-lb$_f$ / lb$_m$ °R)
Re	= Reynolds number
Re_L	= Reynolds number based on model length
RSQ	= sum of the residuals squared, see Eq. 6.68

S_d = dynamic stability parameter, see Eq. 7.22
S_g = gyroscopic stability factor, see Eq. 7.11
t = time
T = absolute temperatue, degrees Rankine, $T_F + 460$
T_F = temperature, deg. F
u, v, w = velocities in the x, y, and directions
V = model velocity
V_{REF} = reference velocity, see Eq. 6.60
$\bar{\alpha}$ = total angle-of-attack
α, β = components of the total angle of attack, see Section 2.3.1
β = ballistic coefficient, see Section 6.1.1
γ = aerodynamic roll angle, see Eq. 2.10
γ = ratio of specific heats, for air $\gamma = 1.4$
δ_R = Earth's azimuth of test facility
λ_R = Earth's latitude of test facility
ε = sine $\bar{\alpha}$, see Eq. 2.14
ρ = air density
ω = frequency of oscillation, see Eq. 3.2
ω_e = earth's rotational rate, 7.272×10^{-5} rad/sec
ϕ = roll orientation
ϕ_N', ϕ_P' = nutational and precessional frequencies
μ = viscosity of flow medium, see Eq. 1.3
μ_N, μ_P = nutational and precessional damping rates
θ_m, ψ_m = missile angles, see Section 2.2.2
θ_{FP}, ψ_{FP} = fixed plane angles, see Section 2.2.2

Superscripts

$\cdot, \cdot\cdot$ = first and second derivatives with respect to time
$', ''$ = first and second derivatives with respect to distance

List of Abbreviations

ARF = Aeroballistic Research Facility
ARFDAS = Aeroballistic Research Facility Data Analysis System
BEF = Ballistic Experimentation Facility
BRL = Ballistic Research Laboratory
BTU = British Thermal Unit
CADRA = Comprehensive Automated Aerodynamic Data Reduction System
cal = caliber
CCD = charge couple device
CEP = circular error probable
CFD = computational fluid dynamics
cg = center-of-gravity

cm	= centimeters
deg	= degrees
Eq.	= equation
F	= Fahrenheit
ft	= feet
Fig.	= Figure
gms	= grams
Hg	= Mercury
i.e.	= for example
in.	= inch
kg	= kilogram
km	= kilometers
^{o}K	= degrees Kelvin
lb	= pound
lb_f	= pound force
lb_m	= pound mass
m	= meters
mb	= millibars
Mhz	= megahertz
MLM	= Maximum Likelihood Method
mm	= millimeters
msec	= milliseconds
NI	= numerical integration
OI	= operating instruction
PRODAS	= Projectile Design and Analysis System
psi	= pounds / in^2
rad	= radian
^{o}R	= degrees Rankine
Ref.	= reference
Rev.	= revolution
sec	= second
typ	= typical
WLS	= weighted least squares
1kx1k	= 1000 by 1000
2kx2k	= 2000 by 2000
2DOF	= two degrees of freedom
6DOF	= six degrees of freedom
μsec	= microsecond

I. INTRODUCTION

1.1 HISTORICAL BACKGROUND

Ballistics could very well be the oldest technology known to man. It certainly predates fire making and may even predate the use of primitive tools. Undoubtedly one of man's two legged ancestors, in a fit of anger, picked up a stone and threw it at a perceived enemy or rival. After this rival figured out that he could do likewise, an enterprising individual must have recognized that whoever could throw the stone the farthest had a distinct advantage. Especially if the stone could be thrown with any accuracy.

This recognition would have led to the development of crude slings which can still be found in use by primitive tribes even today. Although we'll never know for certain whether or not this scenario is correct we do know that strife and war have been the engine driving the development of ballistics as a science during the following ages. These crude slings evolved to become bows and arrows which were used as personal weapons and even later as catapults which were the medieval equivalent of artillery.

However, the engine really didn't get into high gear until the Chinese invention of gun powder was brought to Europe by Marco Polo in the 13th century. This invention not only made it possible to project force even farther using guns or rockets but also the projectile could carry an explosive charge and hence deliver more energy to the target than just the kinetic energy of the projectile itself. This single event totally altered western civilization as well as warfare because castles suddenly became very vulnerable to attack. Since the sole purpose of these damp musty piles of stone was to provide protection to the nobility and ruling classes and this protection was no longer available the residents of these castles moved into the more comfortable towns and villages. This intermingling of the ruling classes with the masses of the people was the beginning of the breakdown of the existing social structure. From this breakdown followed the establishment of a new social order which has progressed to the modern concepts of personal and religious freedoms that we enjoy today.

Nevertheless the original concept that whoever could throw the stone the farthest had an advantage over his enemies was still valid. Napoleon used this concept by first using sabots in firing subscale projectiles from large bore guns. These subscale projectiles could be fired much farther since the total in gun weight of the projectile plus sabot was significantly less than the weight of the full scale projectile. This permitted Napoleon's gunners to engage the enemy troops long before they could return fire. Although the use of sabots added a complexity to the accuracy of which the projectiles could be fired, Napoleon's artillery tactics became legendary and accounted for much of his military successes.

Very early in the development of ballistics as a science, ballisticians realized that if a projectile could be fired at a high enough velocity then the curvature of the trajectory due to gravity would equal the curvature of the Earth. Since the projectile would then essentially fall around the Earth, orbit would be achieved. This is the basic concept from which orbital mechanics was derived. Obviously, once we had developed the capability to fire a projectile at this orbital velocity we had reached the ultimate ability to throw our stone to the farthest possible distance.

The purpose of this historical diatribe is not to provide a history lesson of the world but to give the reader a basic understanding of the importance that ballistics has played in the development of civilization and science as we know it today.

1.2 EXTERIOR BALLISTICS

Since we have now reached the ultimate of throwing our stone the farthest possible distance, future advances in ballistics will be primarily directed in three general areas. First to improve the efficiency of the launch systems in order to optimize the velocity and mass of the payload that we want to deliver. Secondly, to improve our ability to hit the target of interest. And lastly, to deliver more energy and maximize damage to the target. These three areas are the distinct technologies commonly called interior, exterior, and terminal ballistics.

Interior ballistics is the study of the processes which occur while the projectile is in the barrel of the gun. Exterior ballistics is concerned with the understanding of the forces and moments acting on the projectile during its flight. Terminal ballistics is the science of what happens when the projectile hits the target. Although all three of these areas will be mentioned in varying degrees herein, the primary discussion will be associated with the exterior ballistics of the projectile or missile.

The historical event from which exterior ballistics became a true science occurred in the mid 18th century. At that time Benjamin Robbins used a ballistic pendulum to measure the muzzle velocity of a projectile. Until then muzzle velocities were estimated by measuring the distance the projectile flew and calculating the velocity using the point mass kinematic relations derived by Newton and others a hundred years earlier. Since these relations ignored the air density they grossly underestimated the associated muzzle velocities. This apparent discrepancy between the measured muzzle velocity as determined by Robbins and the best theoretical estimates of the time led to the understanding that the air itself provided a resistance force to the passage of the projectile. The concept of aerodynamic drag was henceforth developed and a realization that this force was a function of the shape of the projectile formed the basis for the science of aerodynamics.

Since Robbins made his muzzle velocity measurements many individuals have contributed to the science of exterior ballistics. Much of the more recent work accomplished by some of these individuals will be described and referenced herein.

1.3 FREE - FLIGHT SPARK RANGES

A free-flight spark range is an enclosed facility containing a number of orthogonal spark photography stations and assorted other instrumentation systems. Various aerodynamic configurations of interest are flown through the facility and shadowgrams are obtained at each of the spark stations. These shadowgrams are then processed and analyzed to provide an experimentally measured position-attitude-time history of the free-flight configuration. The theoretical equations of motion are then fit to the experimentally measured trajectory and the unknown aerodynamic coefficients and derivatives extracted. These aerodynamic parameters are the basic data required to understand, predict, or improve the exterior ballistics performance of the configuration of interest. This complete process will be described and discussed in some detail in the following sections.

Many varieties of test ranges must have been used by researchers over the centuries. But, the first spark photograph of a free-flight object was obtained by Ernst Mach late in the 19th century. This development was put to good use by A.C. Charters when he constructed and operated the first modern free-flight spark range [1.1,1.2] at Aberdeen Proving Ground, Maryland, during World War II. That facility proved very useful in solving many ballistic problems and provided the impetus in developing theoretical free-flight dynamic analysis techniques. That facility is still a very valuable research tool and the technologies developed there have been used throughout the world.

Since World War II ballistic ranges have been adapted to study many different physical phenomena, i.e., impact mechanics, basic material properties, reentry physics, ablative properties of various materials, wake studies, radar cross-section measurements, planetary entry probes, and many others. As a result ballistic range technology has become a diverse and multifaceted mature science[1.3]. This is not to suggest that we know everything there is know about this technology area, but only that the beginner has a lot to know about before he can become expert in the field.

The primary discussion herein will be related to free-flight spark ranges as applied to aerodynamic testing which was Charters primary purpose in constructing that first facility. The facilities that have been constructed since have varied considerably in size, number of spark photography stations, geometry, and capabilities. Hence, the facility used herein to describe the various processes and considerations associated with free-flight aerodynamic testing is the Aeroballistic Research Facility (ARF)[1.4] located at Eglin AFB, Florida and operated by the Wright Laboratory Armament Directorate.

This atmospheric test/research facility, see Fig. 1.1, became operational in 1976. It contains 55 orthogonal shadowgraph stations, see Fig. 1.2, along with other instrumentation systems, i.e., interferometry, Schlieren, front lighted LASER

3

photography, atmospheric measuring instruments, and a master chronograph system. This enclosed facility is about 800 ft long with 660 ft (~ 200 meters) of instrumented length and has been used to evaluate the free-flight characteristics of various objects from subsonic to hypersonic velocities. A list and locations of the instrumentation systems presently contained in the ARF are presented in Appendix 1.
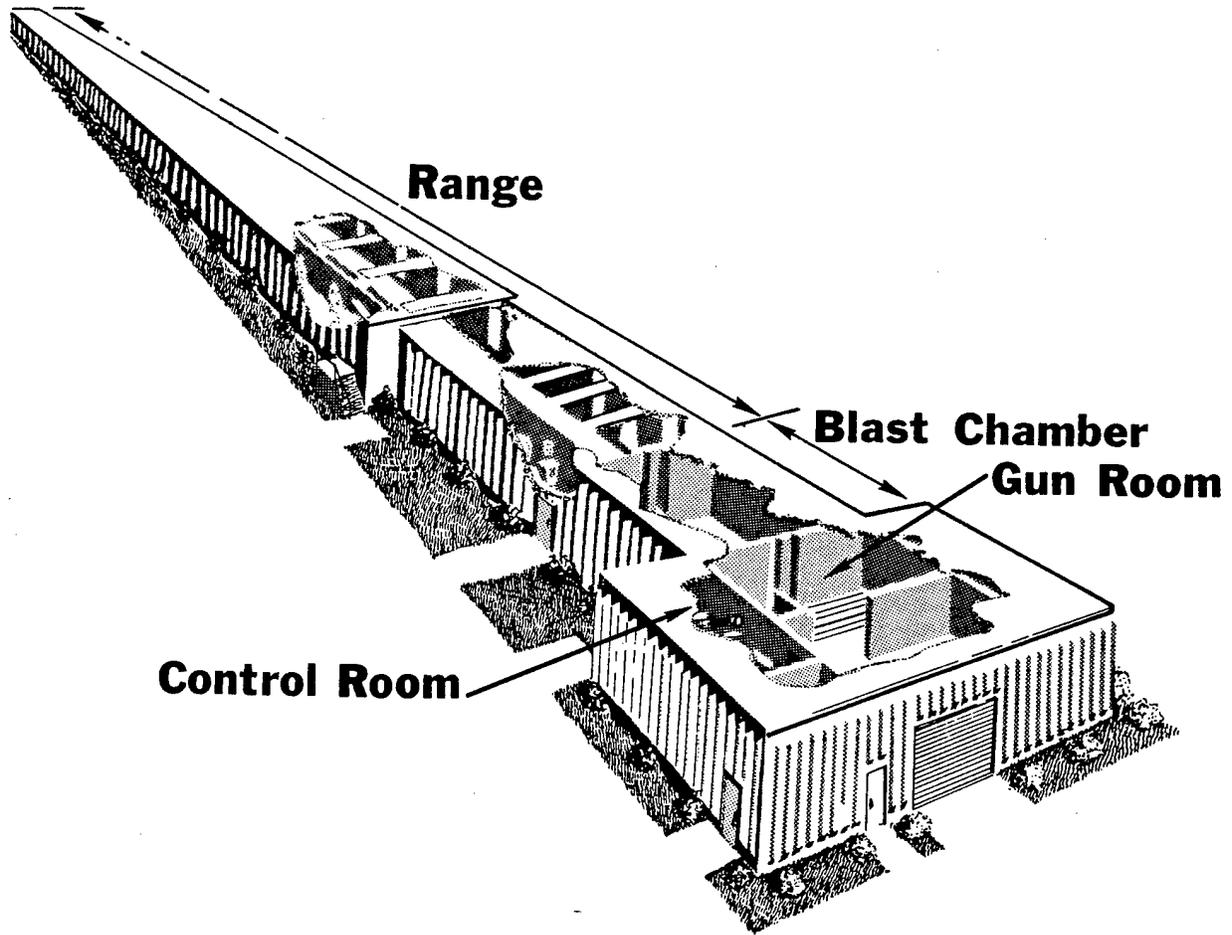
Figure 1.1 Sketch of the Aeroballistic Research Facility
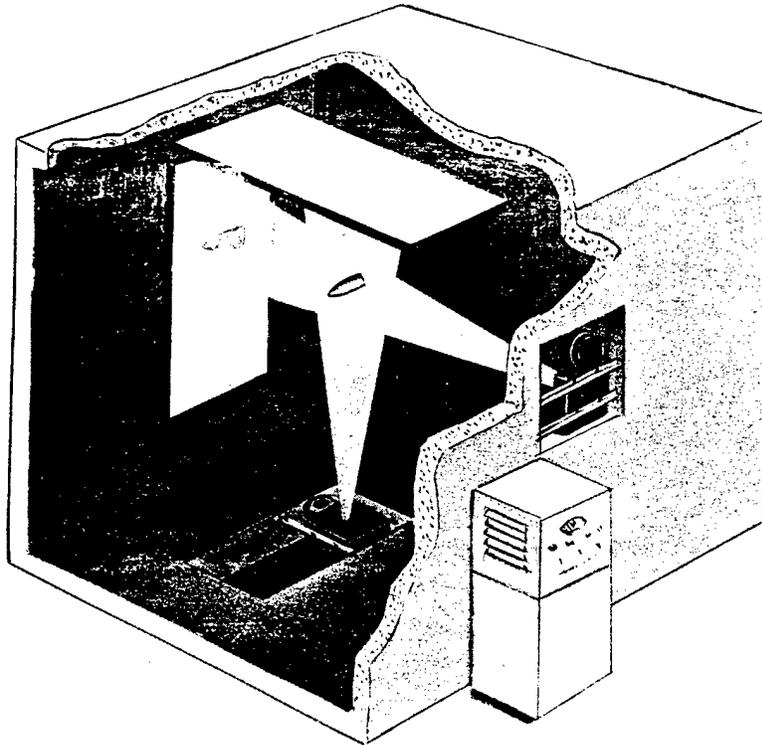
Figure 1.2 Schematic of a Shadowgraph Station

1.4 AERODYNAMIC TESTING

Webster's definition of aerodynamics is " the dynamics of gases, especially of atmospheric interactions with moving objects ". Therefore, aerodynamic testing is the measurement / determination of these atmospheric interactions. The basic tenet in wind tunnel testing is that instead of moving the object (model) the object is held and the atmosphere (air / gas) is moved over the model. The idea being that the interactions occurring between the atmosphere and model is independant of whether or not the model or the gas is moving. Although this is generally true there are many issues concerning the quality of flow in wind tunnels which can affect the resulting aerodynamic data. Some of these issues are the tunnel wall effects, variation of the velocity across the tunnel test section, flow turbulence, interactions caused by the mounting system, i.e., model base flow interference effects, condensation of the flow and others. Many of these aspects associated with wind tunnel testing are discussed in various publications, see Pope's book entitled "Low-speed Wind Tunnel Testing" [1.5].

In contrast to wind tunnel testing, ballistic range testing is the study of the interaction of ' moving ' objects in a quiet or still atmosphere. Hence the concerns associated with the quailty of flow are eliminated. Nevertheless, in whichever type of facility is used there are flow properties which must be matched in order to duplicate the full scale flight conditions or to compare data from facility to facility. Two of the most important of these are Mach number ,(M), and Reynolds number ,(Re_L). These are defined as:

5

$$M = V / a \qquad\qquad 1.1$$

and

$$Re_L = \rho V L / \mu \qquad\qquad 1.2$$

where :

    V = velocity of the model , or velocity of the flow in the test section
    a = speed of sound (local), $(\gamma R g T)^{1/2}$
    ρ = density of flow medium
    L = model length
    μ = viscosity of flow medium

Since air viscosity is insensitive to pressure a linear relationship for μ exists for the 60-90 degree Fahrenheit temperature range. This relationship for μ of air is ,

$$\mu = 3.7463 \times 10^{-7} + (0.005515 \times 10^{-7})(T_F - 60) \qquad\qquad 1.3$$

where μ has the units of lb.sec. / ft.^{3} and T_F is in degrees F. Flow Reynolds numbers are frequently presented as per unit length, or, $Re = \rho V / \mu$, where the model length is not included. There are many other numbers which are used to identify and qualify various flow regimes, i.e., Knudsen number $\sim M / Re$, but it is not our purpose here to discuss all of these various flow quantification parameters.

The test engineer should also recognize that when testing subscale objects, parameters other than flow conditions should also be matched with the full scale object if possible. The center-of-gravity , L_{cg} / L , and the inertia ratio , I_x / I_y , are two such model characteristics that should be matched when feasible. Although the aerodynamic moment data can be shifted to any L_{cg} / L position this shift, as will be shown in Section VII, requires a determination of the normal force coefficient and if this determination is in error the shifted moment data will also possess errors. Therefore it is wise to design the subscale models with L_{cg} / L positions as close to the full scale vehicle as practical and minimize the required shift in the moment data. Also since the inertia ratio can affect the free-flight angular motion pattern, this ratio should be representative of the full scale vehicle.

Here a precautionary note concerning subscale testing in any facility must be mentioned. Boundary layers do not scale! Therefore, the boundary layer thickness will be overly large compared to the full scale configuration. This overly large boundary layer can affect the effectiveness of the control surfaces (i.e. fins) immersed in the boundary layer and result in misleading results and conclusions. Also the boundary layer transition point (laminar to turbulent flow) will not scale. Frequently an experimentalist will force the boundary layer to transition, using trips, at the equivalent location of the full scale object in order to better simulate the actual flow conditions. Tripping boundary layers can be an art in itself and beads, grooves, grit, and other mechanisms are used.

When comparing dynamic data (free-flight, air bearing, forced oscillation, etc.) two additional parameters can be important. These are the reduced frequency parameter, $\omega d / 2V$, and the nondimensionalized spin parameter, $pd / 2V$. Omega, ω, is the frequency of oscillation and in the free-flight facility is normally assumed to be equal to the nutational frequency, ϕ_N', and p is spin rate. The characteristic length (d) is usually the model diameter but when testing aircraft type configurations is frequently defined as the aerodynamic chord of a wing or fin. These parameters should be recorded, and the determined aerodynamic results plotted versus $\omega d / 2V$ and $pd / 2V$ to determine if they are affecting the results. Examples of cases where they have affected the results are discussed in Refs. 1.6 and 1.7.

The ultimate purpose of aerodynamic testing is to measure those interactions between the test model and the atmosphere in such a way as to quantify those interactions . This quantification is accomplished by measuring the forces and moments acting on the test object as a result of these interactions. Once these forces and moments have been measured they can be used to predict the performance of the object at conditions other than those tested. Hence the vehicle's flight performance is known and a flight control system can be designed. Obviously for those configurations which do not have a flight control system, i.e., dumb bombs, purely ballistic missiles, bullets, artillery shells, etc., the accurate determination of these forces and moments are an absolute necessity in order to predict the trajectory from the platform to the target.

REFERENCES

1.1 Schmidt, E. M., " The Aerodynamic Range : A National Historic Mechanical Engineering Landmark ", Special Publication ARBRL-SP-00028, May 1983.

1.2 Braun, W.F., " The Free-Flight Aerodynamics Range", BRL Report No. 1048, 1958, AD202249.

1.3 Canning, T.N., Seiff, A., and Jones, C.S., " Ballistic Range Technology ", AGARD-AG-138-70, August 1970.

1.4 Kittyle, R.L., Packard, J.D., and Winchenbach, G.L., " Description and Capabilities of the Aerballistic Research Facility ", AFATL-TR-87-08, May 1987.

1.5 Pope, Alan, and Harper, John, " Low-Speed Wind Tunnel Testing " , Wiley and Sons, 1966.

1.6 Welsh, C.J., and Winchenbach, G.L., " Free-Flight Investigation of Ablation Effects on the Stability of Conical Reentry Configurations ", Paper presented at the Ninth Navy Symposium on Aeroballistics, May 9-11,1972, John Hopkins University, Maryland.

1.7 Dupris, A.D., " Aeroballistic Range Tests of the Flechette Anti-Tank Penetrator ", Defense Research Establishment, Valcartier Report 4443 / 88, April 1988.

II. DEFINITIONS

2.1 COEFFICIENT AND DERIVATIVE NOMENCLATURE

The purpose of the aerodynamic nondimensionalized nomenclature is to represent the aerodynamic forces and moments acting on a body in a manner such that these forces and moments can be easily used in conjunction with the equations of motion to predict the flight performance of the body in question. This nomenclature permits measuring the aerodynamic parameters using a subscale body, i.e., from either a wind tunnel or free-flight spark range, and using these measurements directly in the predictions. It also permits direct comparison of the aerodynamic forces and moments as measured from various scale models in different facilities.

In general forces are represented by capital letters, i.e. F, and moments are represented by lower case letters, i.e. m. The nondimensionalized force coefficient is defined as,

$$C_F \equiv F / (1/2) \rho V^2 A \qquad\qquad 2.1$$

and the moment coefficient as,

$$C_m \equiv m / (1/2) \rho V^2 A d \qquad\qquad 2.2$$

Where A and d are the model's reference area and reference length respectively. The reference area and length should always be clearly specified when presenting or documenting results. The aerodynamic coefficients are useless in comparing results or predicting the flight performance if these reference values are not specified. It is also imperative to specify the moment reference location as well. This is normally the center-of-gravity location for the free-flight models; however, not always.

The forces in the x,y,z directions are therefore defined as:

$$
\left.
\begin{aligned}
F_x &\equiv C_x \,(1/2)\, \rho\, V^2 A \\
F_y &\equiv C_y \,(1/2)\, \rho\, V^2 A \\
F_z &\equiv C_z \,(1/2)\, \rho\, V^2 A
\end{aligned}
\right\} \qquad 2.3
$$

And the moments about the x,y,z axis respectively are defined as:

$$
\left.
\begin{aligned}
l &\equiv C_l \,(1/2)\, \rho\, V^2 A\, d \\
m &\equiv C_m \,(1/2) \rho\, V^2 A\, d \\
n &\equiv C_n \,(1/2) \rho\, V^2 A\, d
\end{aligned}
\right\} \qquad 2.4
$$

Since the x axis is associated with the direction of flight (see Section 2.2.2) l is the rolling moment, m is the pitching moment, and n is the yawing moment. The derivative nomenclature of the force and moment coefficients is illustrated by the examples below:

$$\partial C_x / \partial M \equiv C_{xM} \qquad\qquad 2.5$$

and

$$\partial C_m / \partial \alpha \equiv C_{m\alpha} \qquad\qquad 2.6$$

where M is Mach number and α is the angle of attack. Hence, C_{xM} in Eq. 2.5 represents the slope of the force coefficient in the x direction with respect to Mach number. Likewise , $C_{m\alpha}$, in Eq. 2.6 represents the slope of the pitching moment with respect to the angle of attack. This moment coefficient derivative , $C_{m\alpha}$, is frequently referred to as the static stability derivative and will be discussed in detail in the later sections.

The aerodynamic nomenclature as defined above is used throughout the following sections and is the basic nomenclature system used by most designers and researchers around the world. However, in the past some organizations / countries did not include the 1/2 in the force and moment definitions of Eqs. 2.1 and 2.2. Therefore, when comparing data or using the results from other organizations one should be alert to how the force and moment coefficients are defined.

2.2 AXES SYSTEMS

2.2.1 Facility Axis System

When conducting aerodynamic tests in a free-flight spark range, the time-position-attitude history of the test item is precisely measured at various locations along its trajectory. These precise position and attitude measurements are obtained by reading and numerically coding the positions of the test item's shadow with respect to the range reference system as derived from photographs. The determination of these positions and attitudes from the shadow measurements will be explained in detail in Section V.

The range reference system in the ARF consists of four Kevlar® fiber bundles (henceforth called wires) with reference beads positioned at ±45.72 cm about 1.52 meter centers over the entire length of the instrumented range. Two of these wires are strung in front of the wall-mounted reflective screens and two are strung below the ceiling-mounted reflective screens. With the positioning described above, eight beads on each of four wires are located in front of each of the 131 potential station locations (windows). At each of the 50 windows which house fully operational dual plane shadowgraph stations, two beads on each of two wires are in the field of view of each camera.

Once the wires and reference beads have been positioned and calibrated, see Section 3.5.3, they are maintained in this position by the alignment system[2.1]. The zero-zero-zero coordinate of the ARF axis system corresponds to the first bead on the lower wall wire at

window 1(there is no shadowgraph station at window 1). Emanating from this bead and pointing downrange is the X axis, pointing to the left, looking downrange, is the Y axis, and Z is vertically up. A sketch of the range axis system is shown in Fig. 2.1.

2.2.2 Aerodynamic Axis Systems

2.2.2.1 Fixed Plane Equations of Motions

The fixed plane axis system is defined as shown in the sketch below.
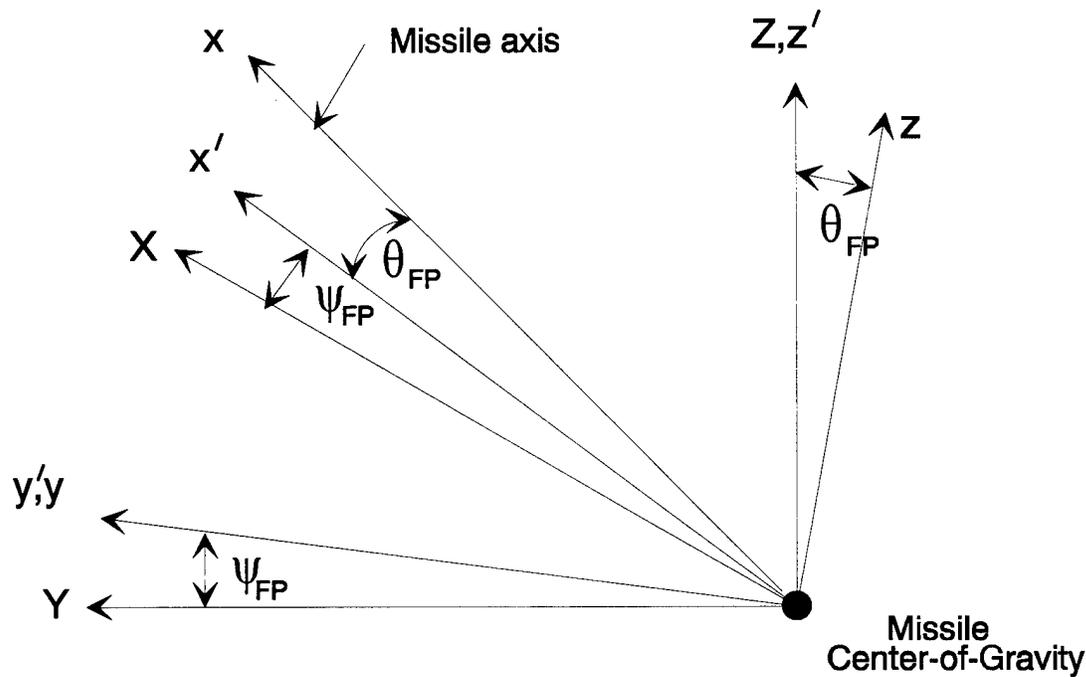
X,Y,Z Earth fixed coordinates, parallel to the ARF axis system, Fig.2.1
x',y',z' First rotation about the Z (ψ_{FP}) yields intermediate coordinate system
x,y,z   Second rotation about y' (θ_{FP}) yields fixed plane coordinate system

Where u,v,w are the velocities along the missile axes x,y,z ; p,q,r, are the angular rates about the x,y,z axes ; and, l,m,n are the moments about the x,y,z axes. The total velocity of the missile ,V, is therefore,

$$V = (u^2 + v^2 + w^2)^{1/2} \qquad\qquad 2.7$$

The fixed plane coordinate system is positive in the same direction as the Earth fixed system X,Y,Z of the ARF as shown in Fig. 2.1. Or, x is positive downrange, y is positive to the left looking downrange , and z is positive up. The missile angles, θ_m and ψ_m , are defined as shown in the sketches below.
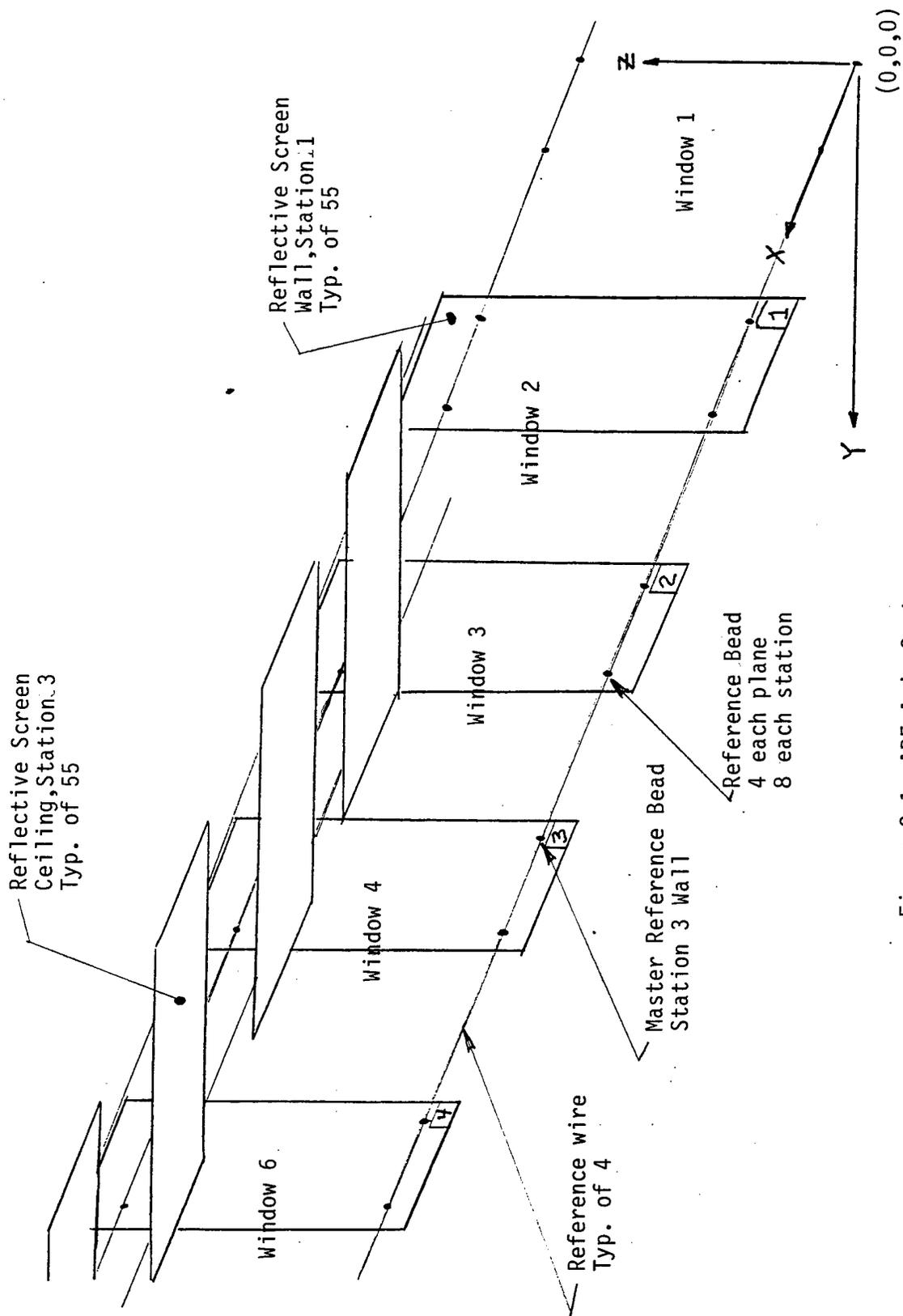
Figure 2.1 ARF Axis System
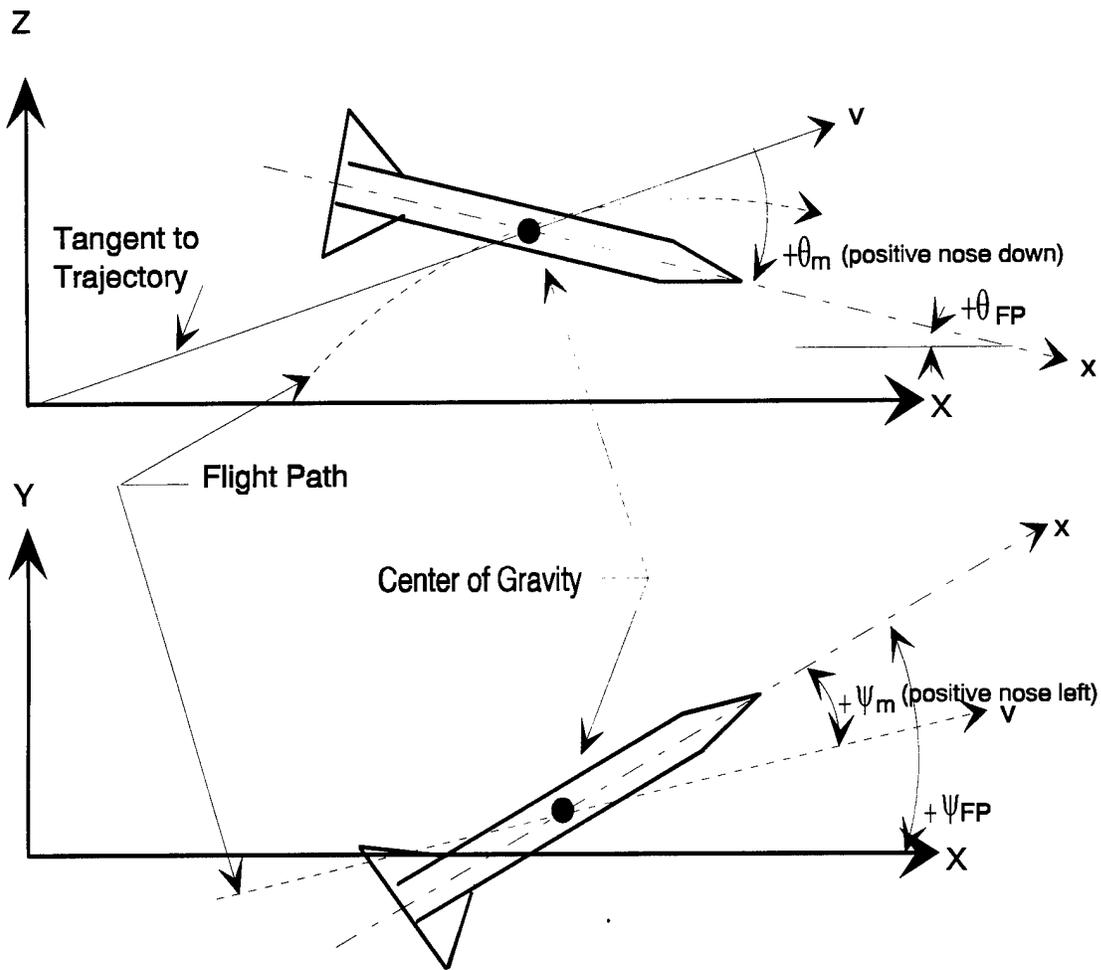
Note that if the trajectory (x) is parallel to the X axis (flight parallel to the range alignment system) θ_m is equal to θ_{FP}. Also, since the direction cosines (m_e, n_e, p_e) are what are actually measured from the shadowgraph images, then

and

$$\theta_{FP} = -\sin^{-1}(n_e)$$

$$\psi_{FP} = \sin^{-1}[\ m_e / (\ m_e^2 + p_e^2\ )^{1/2}\ ] \qquad \Bigg\} \quad 2.8$$

The missile angles θ_m and ψ_m are then obtained by subtracting the instantaneous trajectory angles from θ_{FP} and ψ_{FP}. It should be recognized that during the fitting process the instantaneous trajectory will vary slightly and hence the missile angles θ_m and ψ_m will also vary with each iteration.

The roll orientation , ϕ , is defined in the sketch below,

Z

Note: When viewing from the rear ϕ is
positive clockwise looking downrange

Ψ_{FP}, Ψ_m, Y

ϕ_1

Reference fin or
Ref. spin pin

θ_{FP}
θ_m
W

α

ϕ

Vertical, parallel to Z

v
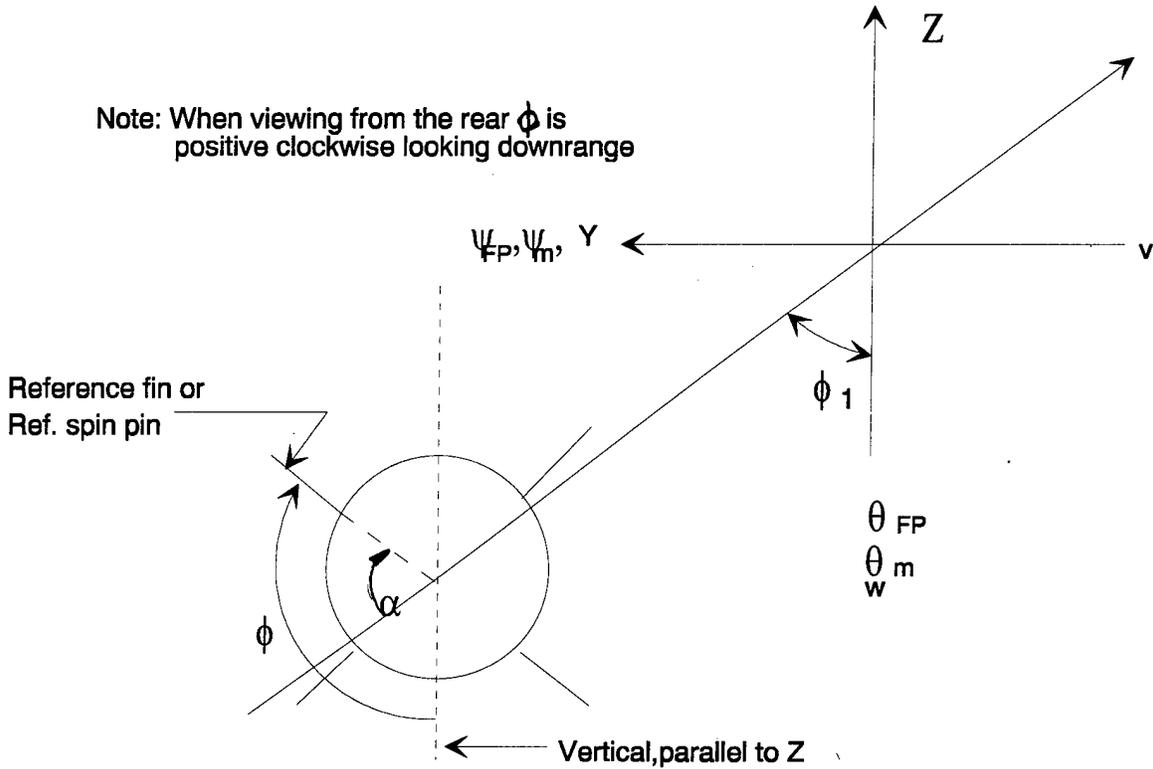
The aerodynamic roll angle , γ , is therefore defined as,

$$\gamma = \phi - \phi_1 \qquad\qquad 2.9$$

where $\phi_1 = \tan^{-1}(-v / w)$

Normally the aerodynamic roll angle is calculated in the analysis routine using the following relation,

$$\gamma = \tan^{-1}(v_b / w_b) \qquad\qquad 2.10$$

where

$$v_b = v \cos \phi + w \sin \phi$$
$$w_b = w \cos \phi - v \sin \phi$$

Note that when the reference fin (or the spin pin) is vertically down ϕ is equal to zero ; and, the missile's measured roll orientations will be between 0 and 360 degrees. During the process of fitting the theoretical equations of motion to the experimental measurements a continuous roll orientation profile is required. Hence, we are required to determine when the roll passes through each 360 degree revolution. This 'unwinding' of the raw roll angles can be one of the more difficult tasks to accomplish when analyzing free-flight spark range trajectories. Although tools have been developed and incorporated into the analysis routines to assist the analyst in accomplishing this task, it can still be

difficult when the roll rate is rapidly changing or when full spin is not imparted by the barrel's rifling.

The 6DOF fixed plane equations of motion have been derived in Refs. 2.2 and 2.3 and are listed below. These equations include the Coriolis accelerations and recognize that θ is θ_m and ψ is ψ_m in these relations.

$$\dot{x} = u \cos \theta \cos \psi - v \sin \psi + w \sin \theta \cos \psi$$

$$\dot{y} = u \cos \theta \sin \psi + v \cos \psi + w \sin \theta \sin \psi$$

$$\dot{z} = -u \sin \theta + w \cos \theta$$

$$\dot{\theta} = q$$

$$\dot{\psi} = r \cos \theta$$

$$\dot{\phi} = p + r \tan \theta$$

$$\dot{u} = g \sin \theta - q w + r v - a_{cu} + F_x / m_a$$

$$\dot{v} = -r u - r w \tan \theta - a_{cv} + F_y / m_a$$

$$\dot{w} = -g \cos \theta + r v \tan \theta + q u - a_{cw} + F_z / m_a$$

$$\dot{p} = 1 / I_x$$

$$\dot{q} = -r^2 \tan \theta - r p \, I_x / I_y + m / I_y$$

$$\dot{r} = q r \tan \theta + q p \, I_x / I_y + n / I_y$$

2.11

where : m_a = projectile mass
g = acceleration due to gravity

The Coriolis effects included above are defined as,

$$a_{cu} = a_{cx} \cos \theta \cos \psi + a_{cy} \cos \theta \sin \psi - a_{cz} \sin \theta$$
$$a_{cv} = -a_{cx} \sin \psi + a_{cy} \cos \psi$$
$$a_{cw} = a_{cx} \sin \theta \cos \psi + a_{cy} \sin \theta \sin \psi + a_{cz} \cos \theta$$

and

$$a_{cx} = -2 \omega_e (\dot{y} \sin \lambda_R + \dot{z} \cos \lambda_R \sin \delta_R)$$

$$a_{cy} = 2 \omega_e (\dot{x} \sin \lambda_R - \dot{z} \cos \lambda_R \cos \delta_R)$$

$$a_{cz} = 2 \omega_e (\dot{x} \cos \lambda_R \sin \delta_R + \dot{y} \cos \lambda_R \cos \delta_R)$$

where :

ω_e is the Earth's rotation rate , 7.272×10^{-5} rad / sec
λ_R is Earth latitude of test facility , 30.5 deg for ARF
δ_R is Earth azimuth of test facility , 126.0 deg for ARF

The above equations of motion are applicable for symmetrical spin stabilized or fin stabilized free-flight missile configurations. Because of the symmetry assumptions the missiles must have at least three fins.

2.2.2.2 Body Fixed Equations of Motion

The body fixed axis system is simply the fixed plane system defined in the previous section but is allowed to roll with the missile. Or,
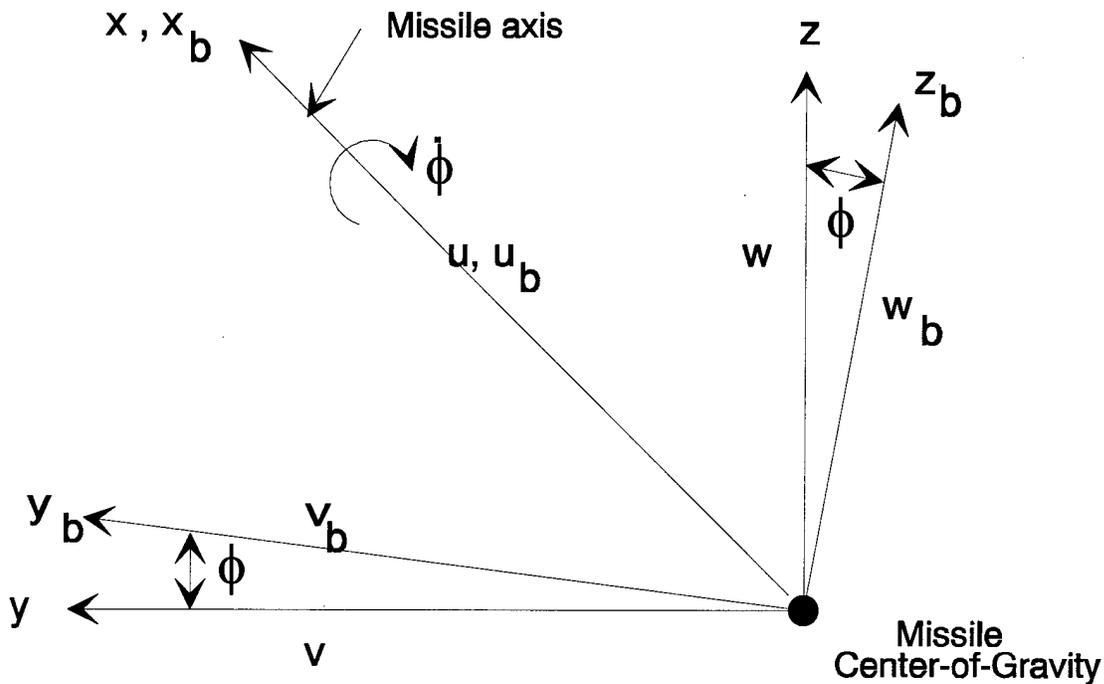
This coordinate system (x_b , y_b , z_b) is defined with x_b aligned with the longitudinal axis of the missile and points out the nose. The y_b axis points out the left wing (or equivalent) and the z_b axis points up with respect to the body. The body fixed coordinate system is rigidly attached to the missile and rotates with the missile about the x_b axis as shown above.

The equations of motion in this system can then be defined as shown below, see Refs. 2.4 and 2.5. Again $\theta = \theta_m$ and $\psi = \psi_m$ in these relations.

$$\dot{x} = u_b \cos\theta \cos\psi + v_b (\sin\theta \sin\phi \cos\psi - \cos\phi \sin\psi)$$
$$+ w_b (\sin\theta \cos\phi \cos\psi + \sin\phi \sin\psi)$$

$$\dot{y} = u_b \cos\theta \sin\psi + v_b (\sin\theta \sin\phi \sin\psi + \cos\phi \cos\psi)$$
$$+ w_b (\sin\theta \cos\phi \sin\psi - \sin\phi \cos\psi)$$

$$\dot{z} = -u_b \sin\theta + v_b \cos\theta \sin\phi + w_b \cos\theta \cos\phi$$

$$\dot{\theta} = q_b \cos\phi - r_b \sin\phi$$
$$\dot{\psi} = (q_b \sin\phi + r_b \cos\phi) / \cos\theta$$
$$\dot{\phi} = p_b + \tan\theta (q_b \sin\phi + r_b \cos\phi)$$

$$\dot{u}_b = r_b v_b - q_b w_b - a_{cub} + (F_{Xb} / m_a) + g \sin\theta$$
$$\dot{v}_b = p_b w_b - r_b u_b - a_{cub} + (F_{Yb} / m_a) - g \sin\phi \cos\theta \qquad \left.\right\} \ 2.12$$
$$\dot{w}_b = q_b u_b - p_b v_b - a_{cub} + (F_{Zb} / m_a) - g \cos\phi \cos\theta$$

$$\dot{p}_b = [I_y l_b + I_{xy} m_b - (I_x + I_y - I_z) I_{xy} p_b r_b] / (I_x I_y - I_{xy}^2)$$
$$+ [(I_{xy}^2 + I_y (I_y - I_z)) q_b r_b] / (I_x I_y - I_{xy}^2)$$

$$\dot{q}_b = [I_x m_b + I_{xy} l_b + (I_x + I_y - I_z) I_{xy} q_b r_b] / (I_x I_y - I_{xy}^2)$$
$$+ [(I_x (I_z - I_Y) - I_{xy}^2) p_b r_b] / (I_x I_y - I_{xy}^2)$$

$$\dot{r}_b = [n_b + I_{xy} (p_b^2 - q_b^2) + (I_x - I_y) p_b q_b] / I_z$$

Note that the Coriolis accelerations are also included in the body fixed equations of motion. The moments of inertia about the x,y,z axes are I_x, I_y, and I_z respectively. There is only one product of inertia, I_{xy}, because it is assumed that there is one plane of symmetry, i.e., $I_{xy} = I_{yz}$. If the model's principal axis is aligned with the body axis then I_{xy} is also equal to zero. This could be a symmetric body with wings or a body with an oval shaped cross section with or without wings.

2.3 AERODYNAMIC MODELS

2.3.1 Body Fixed

As previously stated the interaction between the atmosphere and the missile results in forces and moments acting on the missile. These forces and moments are illustrated in the sketch below for an asymmetric configuration.
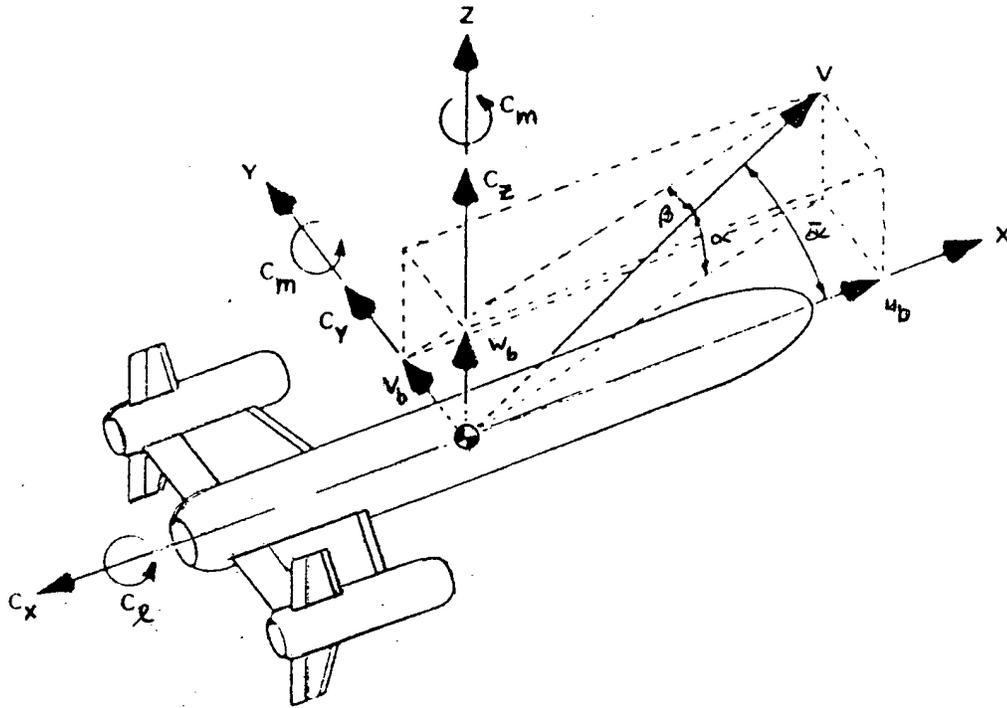
Using the aerodynamic nomenclature as defined in Section 2.1 the forces can be written as,

$$F_X = -(1/2)\rho \, V^2 A \, C_X + m_a \, g \sin \theta_{FP}$$

$$F_Y = (1/2) \, \rho \, V^2 A \, C_Y - m_a \, g \cos \theta_{FP} \sin \phi$$

$$F_Z = (1/2) \, \rho \, V^2 A \, C_Z - m_a \, g \cos \theta_{FP} \cos \phi$$

$$\left. \right\} \quad 2.13$$

The aerodynamic coefficients C_X, C_Y, and C_Z are expanded as functions of the total angle of attack, $\bar{\alpha}$, or the components of the total angle of attack, α and β, as shown in the sketch above. These expanded coefficients can also be assumed to be functions of Mach number and the aerodynamic roll angle. The nonlinearities with respect to $\bar{\alpha}$ or α and β have been assumed to be functions of their respective sines, i.e.,

$$\sin \bar{\alpha} = (w_b^2 + v_b^2)^{1/2} / V \equiv \varepsilon$$
$$\sin \alpha = w_b / V$$
$$\sin \beta = v_b / V$$

$$\left. \right\} \quad 2.14$$

The resulting expansions for C_X, C_Y, and C_Z are then,

$$C_X = C_{X0} + C_{X\alpha} (w_b / V) + C_{X\alpha2} (w_b / V)^2 + C_{X\beta2} (v_b / V)^2 + C_{XM} (M_i - M_{REF}) \quad 2.15$$

$$C_Y = C_{Y0} + C_{Y\beta} (v_b / V) + C_{Y\beta3} (v_b / V)^3 + C_{Yp\alpha} (pd / 2V) (w_b / V) \\ + C_{Y\gamma\overline{\alpha}} \, \varepsilon^2 (w_b / V) \cos (N \gamma) \quad\quad 2.16$$

$$C_Z = C_{Z0} + C_{Z\alpha} (w_b / V) + C_{Z\alpha2} (w_b / V)^2 + C_{Z\alpha3} (w_b / V)^3 \\ + C_{Zp\beta} (pd / 2V) (v_b / V) - C_{Z\gamma\overline{\alpha}} \, \varepsilon^2 (v_b / V) \cos (N \gamma) \quad\quad 2.17$$

and N = number of planes of symmetry. Substituting these expansions for C_X, C_Y, and C_Z into Eq. 2.13 yields the associated force definitions.

Again using the moment definitions of Section 2.1,

$$l = (1/2) \, \rho \, V^2 \, A \, d \, C_l$$

$$m = (1/2) \, \rho \, V^2 \, A \, d \, C_m$$

$$n = (1/2) \, \rho \, V^2 \, A \, d \, C_n$$

and similarly expanding C_l, C_m, and C_n as we did for the associated forces, we define

$$C_l = C_{l0} + C_{lp} (pd / 2V) + C_{l\beta} (v_b / V) + C_{l\gamma\overline{\alpha}2} \, \varepsilon^2 \sin (N\gamma) \quad\quad 2.18$$

$$C_m = C_{m0} + C_{m\alpha} (w_b / V) + C_{m\alpha2} (w_b / V)^2 + C_{m\alpha3} (w_b / V)^3 \\ + C_{m\gamma\overline{\alpha}3} \, \varepsilon^2 (w_b / V) \sin (N\gamma) + C_{mq} (q_b d / 2V) \\ + C_{mq\alpha2} (w_b / V)^2 (q_b d / 2V) + C_{m\gamma\overline{\alpha}3} \, \varepsilon^2 (v_b / V) \sin (N\gamma) \quad 2.19$$

$$C_n = C_{n0} + C_{n\beta} (v_b / V) + C_{n\beta3} (v_b / V)^3 + C_{nr} (r_b d / 2V) \\ - C_{n\gamma\overline{\alpha}3} \, \varepsilon^2 (v_b / V) \sin (N\gamma) + C_{n\gamma\beta2} (v_b / V)^2 (r_b d / 2V) \\ + C_{n\gamma\overline{\alpha}3} \, \varepsilon^2 (w_b / V) \sin (N\gamma) \quad\quad 2.20$$

Again substituting Eqs. 2.18 through 2.20 into the moment definitions above one arrives at the general moment expansions.

It should be noted that the general force and moment expansions (Eqs. 2.15 to 2.20) are modified and extended as required. When analyzing experimentally measured trajectory data the analyst should strive to fit the measurements to the experimental accuracy of the data. This may necessitate modifying the force and moment expansions above. Knowing what expansions and terms to extend or modify can be difficult at best and usually requires considerable experience and insight.

2.3.2 Fixed Plane

Unlike the body fixed axis system which rotates with the body, this system does not rotate but rides along with the missile and is defined as previously discussed in Section 2.2.2. However, since the missile is symmetric with at least 3 planes of symmetry, certain of the aerodynamic force and moment coefficients are equal.
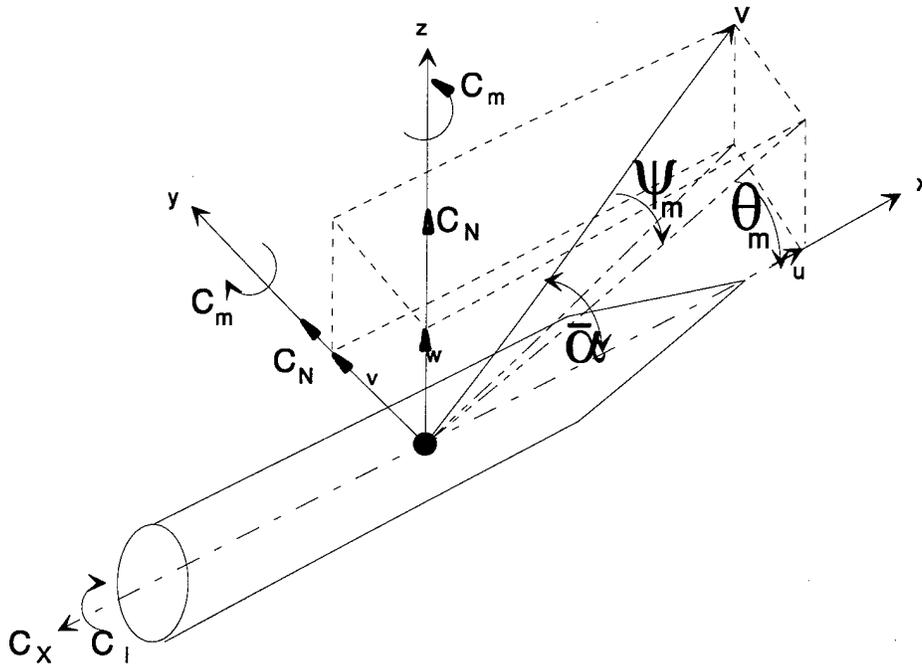
The above sketch illustrates that,

$$
\left.
\begin{aligned}
C_{m\alpha} &= C_{n\beta} \\
C_{mq} &= C_{nr} \\
C_{Z\alpha} &= C_{Y\beta} \equiv C_{N\alpha} \\
C_{yp\alpha} &= C_{zp\beta} \\
C_{my\alpha} &= C_{ny\beta} \quad , \text{ etc.}
\end{aligned}
\right\} \qquad 2.21
$$

The forces and moments are expanded similarly as the body fixed forces and moments in the previous section. However, the nonlinearities for this case are assumed to be only a function of the sine of the total angle-of-attack , $\overline{\alpha}$, and not the components of the total angle-of-attack as was for the body fixed case. Again,

$$
\sin \overline{\alpha} = (v^2 + w^2)^{1/2} / V \equiv \varepsilon
$$

where :

$$
\left.
\begin{aligned}
\sin \theta_m &= w / (u^2 + w^2)^{1/2} \\
\sin \psi_m &= - v / V
\end{aligned}
\right\} \qquad 2.22
$$

Note that

$$
\sin^2 \overline{\alpha} \neq \sin^2 \theta_m + \sin^2 \psi_m
$$

The force equations are therfore written as :

$$F_X = -(1/2)\, \rho\, V^2\, A\, [\, C_{X0} + C_{X\bar{\alpha}2}\, \varepsilon^2 + C_{x\bar{\alpha}4}\, \varepsilon^4 + C_{XM}\, (\, M_i - M_{REF}\,) \\ + C_{XY\bar{\alpha}2}\, \varepsilon^2\, \cos(N\gamma) \qquad\qquad\qquad\qquad\qquad 2.23$$

$$F_Y = (1/2)\, \rho\, V^2\, A\, [\, -C_{N\bar{\alpha}}\,(\,v\,/\,V\,) - C_{N\bar{\alpha}3}\, \varepsilon^2\,(\,v\,/\,V\,) - C_{N\bar{\alpha}5}\, \varepsilon^4\,(\,v\,/\,V\,) \\ - C_{N\gamma\bar{\alpha}3}\, \varepsilon^2\,(\,v\,/\,V\,)\, \cos\,(N\gamma) + C_{Yp\bar{\alpha}}\,(\,pd\,/\,2V\,)\,(\,w\,/\,V\,) \\ + C_{Yp\bar{\alpha}3}\, \varepsilon^2\,(\,pd\,/\,2V\,)\,(\,w\,/\,V\,) + C_{Y\gamma\bar{\alpha}3}\, \varepsilon^2\,(\,w\,/\,V\,)\, \sin\,(N\gamma) \\ + C_{N\delta}\, \delta_A\, \sin\phi \; - \; C_{N\delta}\, \delta_B\, \cos\phi\,] \qquad\qquad\qquad\qquad 2.24$$

$$F_Z = (1/2)\, \rho\, V^2\, A\, [\, -C_{N\bar{\alpha}}\,(\,w\,/\,V\,) - C_{N\bar{\alpha}3}\, \varepsilon^2\,(\,w\,/\,V\,) - C_{N\bar{\alpha}5}\, \varepsilon^4\,(\,w\,/\,V\,) \\ - C_{N\gamma\bar{\alpha}3}\, \varepsilon^2\,(\,w\,/\,V\,)\, \cos\,(\,N\gamma\,) + C_{Yp\bar{\alpha}}\,(\,pd\,/\,2V\,)\,(\,v\,/\,V\,) \\ + C_{Yp\bar{\alpha}3}\, \varepsilon^2\,(\,pd\,/\,2V\,)\,(\,v\,/\,V\,) - C_{Y\gamma\bar{\alpha}3}\, \varepsilon^2\,(\,v\,/\,V\,)\, \sin\,(N\gamma) \\ - C_{N\delta}\, \delta_A\, \cos\phi \; - \; C_{N\delta}\, \delta_B\, \sin\phi\,] \qquad\qquad\qquad\qquad 2.25$$

and the moment equations are :

$$l = (1/2)\, \rho\, V^2\, A\, d\, [\, C_{l0} + (\,pd\,/\,2V\,)\, C_{lp} + (\,pd\,/\,2V\,)\, C_{lp\bar{\alpha}2}\, \varepsilon^2 \\ + (\,pd\,/\,2V\,)\, C_{lpM}\, (\, M_i - M_{REF}\,) + C_{l\gamma\bar{\alpha}2}\, \varepsilon^2\, \sin\,(N\gamma)\,] \qquad 2.26$$

$$m = (1/2)\, \rho\, V^2\, A\, d\, [\, C_{m\bar{\alpha}}\,(\,w\,/\,V\,) + C_{m\bar{\alpha}3}\, \varepsilon^2\,(\,w\,/\,V\,) + C_{m\bar{\alpha}5}\, \varepsilon^4\,(\,w\,/\,V\,) \\ + C_{m\bar{\alpha}M}\,(\, M_i - M_{REF}\,)\,(\,w\,/\,V\,) + C_{m\gamma\bar{\alpha}3}\, \varepsilon^2\,(\,w\,/\,V\,)\, \cos\,(N\gamma) \\ + C_{mq}\,(\,qd\,/\,2V\,) + C_{mq\bar{\alpha}2}\, \varepsilon^2\,(\,qd\,/\,2V\,) + C_{mq\bar{\alpha}4}\, \varepsilon^4\,(\,qd\,/\,2V\,) \\ + C_{n\bar{\alpha}}\,(\,v\,/\,V\,) + C_{np\bar{\alpha}}\,(\,pd\,/\,2V\,)\,(\,v\,/\,V\,) + C_{np\bar{\alpha}3}\, \varepsilon^2\,(\,pd\,/\,2V\,)\,(\,v\,/\,V\,) \\ + C_{np\bar{\alpha}5}\, \varepsilon^4\,(\,pd\,/\,2V\,)\,(\,v\,/\,V\,) + C_{n\gamma\bar{\alpha}3}\, \varepsilon^2\,(\,v\,/\,V\,)\, \sin\,(N\gamma) \\ + C_{m\delta}\, \delta_A\, \cos\phi \; - \; C_{m\delta}\, \delta_B\, \sin\phi\,] \qquad\qquad\qquad 2.27$$

$$n = (1/2)\, \rho\, V^2\, A\, d\, [\, -C_{m\bar{\alpha}}\,(\,v\,/\,V\,) - C_{m\bar{\alpha}3}\, \varepsilon^2\,(\,v\,/\,V\,) - C_{m\bar{\alpha}5}\, \varepsilon^4\,(\,v\,/\,V\,) \\ - C_{m\bar{\alpha}M}\,(\, M_i - M_{REF}\,)\,(\,v\,/\,V\,) - C_{m\gamma\bar{\alpha}3}\, \varepsilon^2\,(\,v\,/\,V\,)\, \cos\,(N\gamma) \\ + C_{mq}\,(\,rd\,/\,2V\,) + C_{mq\bar{\alpha}2}\, \varepsilon^2\,(\,rd\,/\,2V\,) + C_{mq\bar{\alpha}4}\, \varepsilon^4\,(\,rd\,/\,2V\,) \\ + C_{n\bar{\alpha}}\,(\,w\,/\,V\,) + C_{np\bar{\alpha}}\,(\,pd\,/\,2V\,)\,(\,w\,/\,V\,) + C_{np\bar{\alpha}3}\, \varepsilon^2\,(\,pd\,/\,2V\,)\,(\,w\,/\,V\,) \\ + C_{np\bar{\alpha}5}\, \varepsilon^4\,(\,pd\,/\,2V\,)\,(\,w\,/\,V\,) + C_{n\gamma\bar{\alpha}3}\, \varepsilon^2\,(\,w\,/\,V\,)\, \sin(N\gamma) \\ + C_{m\delta}\, \delta_A\, \sin\phi \; + \; C_{m\delta}\, \delta_B\, \cos\phi\,] \qquad\qquad\qquad 2.28$$

Again N = number of planes of symmetry (i.e. number of fins) and

$$\gamma = \tan^{-1}\,(v_b\,/\,w_b)$$

where

$$\left.\begin{array}{l} v_b = v\, \cos\phi \; + \; w\, \sin\phi \\ w_b = -\,v\, \sin\phi \; + \; w\, \cos\phi \end{array}\right\} \qquad 2.29$$

2.4 IDENTITIES

2.4.1. Angular Relationships

Missile Angles

$$\sin \overline{\alpha}_m = (\sin^2 \psi_m + \cos^2 \psi_m \ \sin^2 \theta_m)^{1/2}$$
$$\sin \theta_m = \sin \chi_m / \cos \psi_m$$
$$\sin \theta_m = \sin \alpha_m$$
$$\sin \psi_m = - \sin \beta_m \ \cos \chi_m$$
$$\tan \beta_m = - \tan \psi_m \ / \ \cos \theta_m$$

Missile Angles to Earth Angles

$$\theta = \theta_m - \sin^{-1} (\sin \gamma_e / \cos \psi_m)$$
$$\psi = \sin^{-1} (\sin \psi_m / \cos \gamma_e) + \delta_e$$

Direction Cosines (m_e , n_e , p_e) to Fixed Plane

$$\theta = - \sin^{-1} n_e$$
$$\psi = \sin^{-1} [m_e / (m_e^2 + p_e^2)^{1/2}]$$

2.4.2 Velocity Relationships

Missile Velocities to Missile Angles

$$v = -V \sin \psi_m$$
$$w = V \cos \psi_m \sin \theta_m$$
$$u = V \cos \psi_m \cos \theta_m$$

Body Fixed to Fixed Plane

$$u = u_b$$
$$v = v_b \cos \phi - w_b \ \sin \phi$$
$$w = v_b \sin \phi + w_b \cos \phi$$
$$p = p_b$$
$$q = q_b \cos \phi - r_b \sin \phi$$
$$r = q_b \sin \phi + r_b \cos \phi$$

Fixed Plane to Body Fixed

$$u_b = u$$
$$v_b = v \cos \phi + w \sin \phi$$
$$w_b = -v \sin \phi + w \cos \phi$$
$$p_b = p$$
$$q_b = q \cos \phi + r \sin \phi$$
$$r_b = -q \sin \phi + r \cos \phi$$

2.4.3 Missile Angle Definitions

ANGLE	SINE	COSINE	TANGENT
χ_m	$\dfrac{w}{\sqrt{u^2 + v^2 + w^2}}$	$\dfrac{\sqrt{u^2 + v^2}}{\sqrt{u^2 + v^2 + w^2}}$	$\dfrac{w}{\sqrt{u^2 + v^2}}$
ψ_m	$\dfrac{-v}{\sqrt{u^2 + v^2 + w^2}}$	$\dfrac{\sqrt{u^2 + w^2}}{\sqrt{u^2 + v^2 + w^2}}$	$\dfrac{-v}{\sqrt{u^2 + w^2}}$
θ_m	$\dfrac{w}{\sqrt{u^2 + w^2}}$	$\dfrac{u}{\sqrt{u^2 + w^2}}$	$\dfrac{w}{u}$
α_m	$\dfrac{w}{\sqrt{u^2 + w^2}}$	$\dfrac{u}{\sqrt{u^2 + w^2}}$	$\dfrac{w}{u}$
β_m	$\dfrac{v}{\sqrt{u^2 + v^2}}$	$\dfrac{u}{\sqrt{u^2 + v^2}}$	$\dfrac{v}{u}$
$\bar{\alpha}_m$	$\dfrac{\sqrt{v^2 + w^2}}{\sqrt{u^2 + v^2 + w^2}}$	$\dfrac{u}{\sqrt{u^2 + v^2 + w^2}}$	$\dfrac{\sqrt{v^2 + w^2}}{u}$

2.4.4 Trajectory Angle Definitions

ANGLE	SINE	COSINE	TANGENT
γ_e	$\dfrac{\dot{z}}{V}$	$\dfrac{(\dot{x}^2 + \dot{y}^2)^{\frac{1}{2}}}{V}$	$\dfrac{\dot{z}}{(\dot{x}^2 + \dot{y}^2)^{\frac{1}{2}}}$
δ_e	$\dfrac{\dot{y}}{(\dot{x}^2 + \dot{y}^2)^{\frac{1}{2}}}$	$\dfrac{\dot{x}}{(\dot{x}^2 + \dot{y}^2)^{\frac{1}{2}}}$	$\dfrac{\dot{y}}{\dot{x}}$

2.4.5 Coordinate System Transformations

Fixed Plane - Missile to Earth

$$\dot{x} = u \cos\theta \cos\psi - v \sin\psi + w \sin\theta \cos\psi$$
$$\dot{y} = u \cos\theta \sin\psi + v \cos\psi + w \sin\theta \sin\psi$$
$$\dot{z} = -u \sin\theta + w \cos\theta$$

Fixed Plane - Earth to Missile

$$u = \dot{x} \cos\theta \cos\psi + \dot{y} \cos\theta \sin\psi - \dot{z} \sin\theta$$
$$v = -\dot{x} \sin\psi + \dot{y} \cos\psi$$
$$w = \dot{x} \sin\theta \cos\psi + \dot{y} \sin\theta \sin\psi + \dot{z} \cos\theta$$

Body Fixed - Missile to Earth

$$\dot{x} = u_b \cos\theta\cos\psi + v_b(\sin\theta\sin\phi\cos\psi - \cos\phi\sin\psi) + w_b(\sin\theta\cos\phi\cos\psi + \sin\phi\sin\psi)$$
$$\dot{y} = u_b \cos\theta \sin\psi + v_b(\sin\theta\sin\phi\sin\psi + \cos\phi\cos\psi) + w_b(\sin\theta\cos\phi\sin\psi - \sin\phi\cos\psi)$$
$$\dot{z} = -u_b \sin\theta + v_b \cos\theta \sin\phi + w_b \cos\theta \cos\phi$$

Body Fixed - Earth to Missile

$$u_b = \dot{x} \cos\theta \cos\psi + \dot{y} \cos\theta \sin\psi - \dot{z} \sin\theta$$
$$v_b = \dot{x}(\sin\theta \sin\phi \cos\psi - \cos\phi \sin\psi) + \dot{y}(\sin\theta \sin\phi \sin\psi + \cos\phi \cos\psi) + \dot{z}(\cos\theta \sin\phi)$$
$$w_b = \dot{x}(\sin\theta \cos\phi \cos\psi + \sin\phi \sin\psi) + \dot{y}(\sin\theta \cos\phi \sin\psi - \sin\phi \cos\psi) + \dot{z}(\cos\theta \cos\phi)$$

REFERENCES

2.1 Sullivan, J. A., and Cipolla, J. R., " A Unique Alignment System", paper presented at the 26 th meeting of the Aeroballistic Range Association, San Leandro, CA, 30 September 1975.

2.2 Whyte, R. H., and Hathaway, W. H., " Aeroballistic Range Data Reduction Technique Utilizing Numerical Integration", AFATL -TR - 74 - 41, February 1974.

2.3 Fischer, M. ,and Hathaway ,W. H., " Aeroballistic Research Facility Data Analysis System (ARFDAS)", AFATL - TR - 88 - 48 , September 1988.

2.4 Hathaway ,W. H. , and Whyte R. H., " Aeroballistic Range Data Analysis for Non Symmetric Configurations", AFATL - TR - 76 - 109 , September 1976.

2.5 Whyte, R.H., Winchenbach, G. L., Hathaway, W. H., " Subsonic Free-Flight Data for a Complex Asymmetric Missile", AIAA paper , Journal of Guidance and Control, Vol 4 , Number 1, January - February 1981, pg 59.

III. TEST PREPARATION

3.1 TEST OBJECTIVES

The first step in solving any problem is gaining an understanding of what the problem is. This encompasses the two questions of : why are the tests to be accomplished, and what needs to be determined ? The test engineer cannot plan and design a test / research program without knowing the answers to these basic questions. For example, if the primary purpose of the program is to determine the allowable range of the center-of-gravity for a particular configuration then the center-of-pressure location must be determined. As will be shown in Section 7.3.1 this requires that both the pitching moment and normal force derivatives be accurately measured. Although the pitching moment derivative is normally one of the easiest and most accurately determined measurements obtained from free-flight trajectories the normal force derivative can be difficult to precisely determine. The test engineer may therefore need to design the model and / or test procedure in such a manner as to maximize his ability to determine this derivative. Since the normal force derivative is primarily obtained from the swerving motion in the y - z directions, this could mean minimizing the model's mass in order to ensure that the maximum amount of swerving motion is obtained. If the test engineer has no control over the model's mass, i.e., frequently he is handed the models and told to "shoot these", then his only other option to maximize the swerving motion is to attempt to augment the angular motion by some means. The increased angles of attack increase the normal force acting on the test item and hence increase the resulting swerving motion. Methods of augmenting the initial disturbances will be discussed later in this section.

Another example of why the test engineer needs to understand the purpose of the test program could be that the drag data are required for a fire control system and / or the round dispersion is also required for probability of hit calculations. For this purpose it may not be desirable to augment the angular motions because this could contaminate the primary data required from the tests. The increased angles of attack would require a correction to be made to the measured drag coefficients in order to obtain the zero yaw drag coefficient needed for the fire control algorithm. These corrections can certainly be made, see Section 6.2.1. However, they can potentially add an error source into the C_{D0} results. Also, the round dispersion is a function of the initial angles of attack, see Section 7.4.1, and artificially increasing the angular motions will likewise increase the resulting dispersion.

The purpose of this discussion is to underscore the need for the test engineer to understand the purpose of the tests and what data / measurements are required to obtain the needed information. This understanding between the test engineer and the user / sponsor should be one of the primary goals of the initial test plan meeting or test request correspondence.

3.2 PRETEST PLANNING

Once the test engineer understands what data are required by the user it then becomes necessary to consider, early in the planning process, how this may affect the facility configuration, the launcher to be used, and the instrumentation requirements. Facility considerations may include whether or not the complete range is to be used or if the flight is to be terminated early. Many flights are terminated prior to the end of the instrumented section of the facility. Usually these flights are terminated because the drop in the trajectory due to gravity means that the model will fall below the instrumentation window (i.e. below the camera's field of view or the IR detection system). These flights are therefore terminated before the model impacts any of the instrumentation, i.e. cameras mounted in the pits on the floor of the facility. Other flights may be terminated early to avoid hitting the facility walls caused by high dispersion or high lift configurations.

A portable projectile trap is used to terminate these flights and installation requires scheduling a fork lift and ensuring that the armor plating is sufficient to stop the test item. There may also be considerations associated with any potential blast chamber modifications. These may encompass the size and location of the stripper hole leading from the blast chamber into the instrumented range, or any required witness panels in the blast chamber, or range proper. These preparations may require considerable lead times in order to procure or manufacture the needed components. Hence, the planning for such preparations should be accomplished as early as possible.

The launcher to be used for the proposed tests should also be identified early in the planning process. The general capabilities of the available launchers are shown in Fig. 3.1. Once the test conditions are determined the appropriate launcher can be selected using this figure. Where the figure indicates that more than one launcher is capable of achieving the desired test conditions, considerations such as simplicity of design, ease of operation, or minimizing launch loads should be involved in the decision as to which system is to be used. For example the two-stage light gas gun generally has a lower in bore peak acceleration than the single stage powder guns. However, it is a much more complex and costly system to operate and requires several additional expendables other than the normal model, sabot and propellant needed for the single stage guns. These additional expendables include pistons, diaphragms, and Helium. Nevertheless the trade off between lower acceleration and complexity are the kinds of decisions that must be considered when selecting the system to be used.

For some test conditions Fig. 3.1 indicates that there is only one available system capable of achieving the desired launch conditions and this certainly simplifies the decision process. Also, the figure illustrates that there are many launch conditions that cannot, at present, be achieved using any of the available systems, (large mass at high velocities). We should always be interested in investigating new and advanced systems which have the potential of expanding our capabilities into these areas, i.e., electromagnetic launchers, wave guns, or ram accelerators.
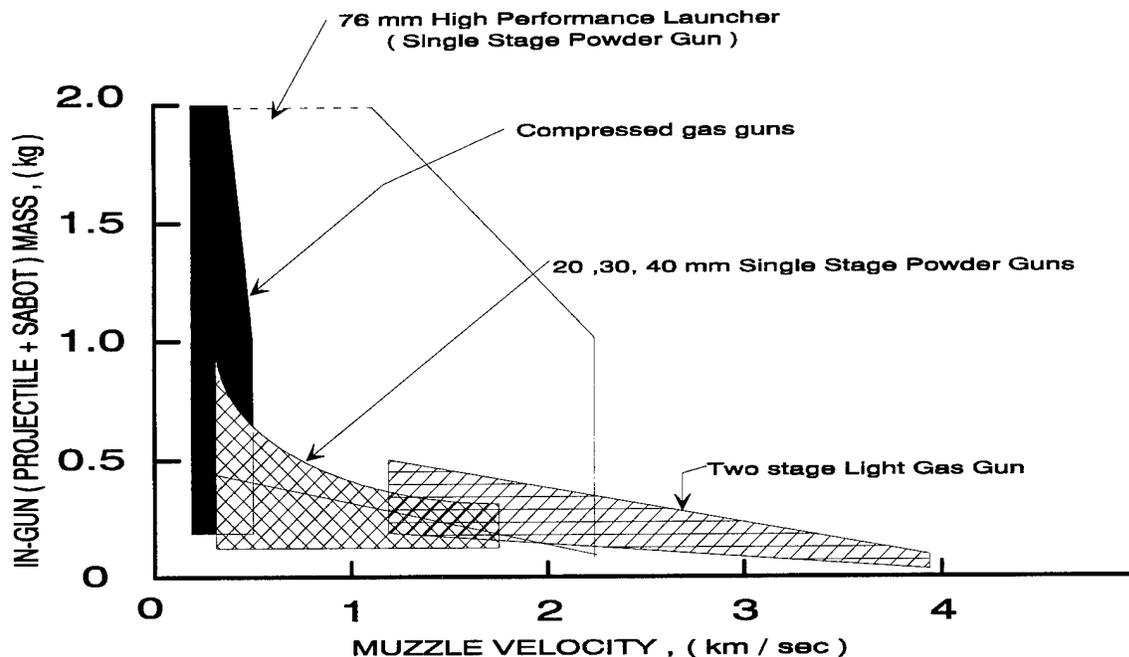
Figure 3.1   Launch Capability of Available Gun Systems

The requirements for any special instrumentation systems should also be considered very early in the planning process. This could include Doppler radar, interferometry, schlieren, or any other specified systems which require advanced preparation and planning. Prior thought into these various aspects of the proposed tests will improve significantly the chances of success and save time and resources.

3.3 MODEL / SABOT DESIGN

Some outstanding tools have been developed and provided to the test engineer in order to assist in designing models and sabots. One of these tools is the Projectile Design and Analysis System , PRODAS [3.1]. It is not our purpose herein to discuss all of the capabilities of this system or to instruct the reader in its use. However, it will be used to illustrate the general applications and some of the considerations of which the designer must be alert to. Figure 3.2 shows a simple spin stabilized configuration designed using this system. The total model mass properties along with the elemental mass properties of this design are also shown in this figure. The projectile shown was designed using only one material, aluminum, with no fins or internal cavities but these do not represent restrictions within PRODAS. This routine can be used to design very complex configurations with many elements, using different materials, with or without cavities. The primary restriction on PRODAS is that only symmetrical projectiles with circular cross sections can be designed. PRODAS has many other capabilities helpful to the designer / test engineer and some of these will be mentioned in the following sections.
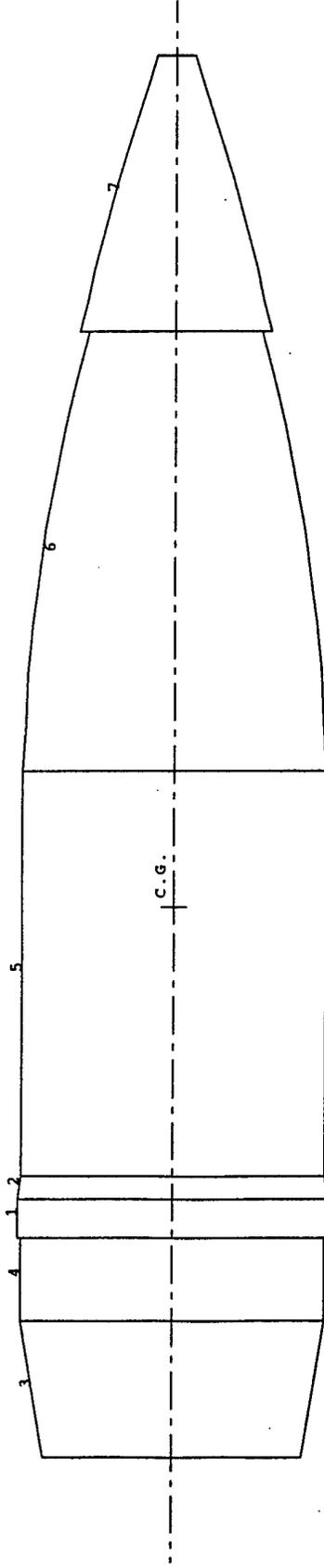
27

PRODAS VERSION 5.5

FILENAME: SC105MIMO 10-DEC-93   :subscale 105 ml modified fuse

PROJECTILE	OGIVE	C.G. FROM	AXIAL	TRANSVERSE	TOTAL	PROJECTILE	SABOT	PENETRATOR	FILLER
DIAMETER	LENGTH	LENGTH	NOSE	MOMENT	MOMENT	WEIGHT	WEIGHT	WEIGHT	WEIGHT	WEIGHT
(IN)	(IN)	(IN)	(IN)	(LBM-IN**2)	(LBM-IN**2)					
1.178	5.535	2.802	3.347	0.69170E-01	0.78533	0.449	0.449	0.000	0.000	0.000 LBM
						3145.259	3145.259	0.000	0.000	0.000 GRAINS
						203.728	203.728	0.000	0.000	0.000 GRAMS

I	CODE	LEFT DIAMETER (IN)	RIGHT DIAMETER (IN)	LENGTH (IN)	REFERENCE LOCATION (IN)	DENSITY (LBM/IN**3)	WEIGHT (LBM)	AXIAL MOMENT (LBM-IN**2)	TRANSVERSE MOMENT (LBM-IN**2)	CENTER OF GRAVITY (IN)	RADIUS (IN)
1	3	1.206	1.206	0.157	0.871	0.100	0.0180	0.32681E-02	0.16712E-02	0.079	
2	3	1.206	1.178	0.093	1.028	0.100	0.0104	0.18421E-02	0.92853E-03	0.046	
3	5	1.006	1.178	0.543	0.000	0.100	0.0510	0.76679E-02	0.50789E-02	0.286	
4	0	1.178	1.178	0.327	0.543	0.100	0.0357	0.61811E-02	0.34088E-02	0.164	
5	0	1.178	1.178	1.612	1.121	0.100	0.1756	0.30433E-01	0.53231E-01	0.806	
6	4	1.178	0.677	1.723	2.733	0.100	0.1377	0.18860E-01	0.39627E-01	0.725	7.285
7	4	0.743	0.146	1.079	4.456	0.100	0.0209	0.91234E-03	0.17898E-02	0.341	10.000

ELEMENT CODES

-2 – BOOM	-1 – SABOT	0 – PROJECTILE BODY
1 – PENETRATOR	2 – HE	3 – BAND
4 – OGIVE	5 – BOATTAIL	6 – FINS
7 – TRACER	8 – NOT USED	9 – SPIKE
10 – CONICAL FIN		

Figure 3.2   Example of Model Design Using PRODAS

The location of the model's center-of-gravity (cg) is one of the major design considerations. Obviously the model must be either spin stabilized or aerodynamically stable in flight, see Section 7.2, because unlike wind tunnel tests the model must possess static stability to successfully fly through the instrumented facility. Also, it can be advantageous to match the cg location of the full scale vehicle. Although as mentioned previously, the pitching moment can be shifted to any moment reference location using the relations derived in Section 7.3.2 this shift can induce errors. Especially, when large shifts are required or when the normal force data are ill defined. Some of the other derivatives, i.e. Magnus and damping-in-pitch, cannot be easily shifted and in fact usually are not. Therefore the data obtained about the model's cg location is assumed to be representative of the full scale vehicle. Hence, if the model's cg is designed to be consistent with the full scale vehicle these potential error sources are eliminated.

Normally for most test configurations it is good design policy to minimize the projectile mass. This not only improves the precision of the normal force as previously mentioned but many of the other coefficients as well. For example, the accuracy of the drag measurements are improved by increasing the model's deceleration experienced during the flight through the instrumented range. It should be noted that like the pitching moment derivative the drag measurements are normally very precise, less than 1% error. But if the model experiences very little deceleration, i.e. in a reduced density environment, minimizing the model mass may be advantageous in accurately measuring the drag.

The reduced mass also minimizes the angular momentum of the model thereby maximizing the aerodynamic damping effects on the model's motions. This in turn is reflected in better determined damping derivatives, pitch-yaw and roll. Minimizing the model's mass usually produces several other beneficial effects. Firstly, the lesser mass reduces the acceleration loads experienced by the model during launch. This increases the probability that the model will survive launch without any structural failures. It also simplifies the sabot design which should result in a lighter and stronger sabot since the forces acting on the sabot are likewise reduced. The lighter masses, both model and sabot, makes it easier to terminate their respective flights without causing undue damage to the blast chamber walls or the projectile trap at the end of the range. Lastly, the reduced model / sabot package mass requires less of a propellant charge and hence less of an over pressure in the blast chamber of the facility.

Nevertheless it may not always be wise to minimize model mass. When testing high lift configurations a heavy model may be desirable in order to reduce the lift effect on the model's trajectory. These configurations can exhibit large deviations in their flight paths and culminate in the model impacting the facility walls or even worse the facility instrumentation systems. One technique frequently used to control the trajectories of high lift configurations is to purposely induce a roll rate during launch and / or flight. This ensures that the lift force is not always pointed in the same direction and tends to cause the model to fly in a spiral trajectory. Obviously the goal is to make the diameter of the spiral less than the diameter of the instrumentation window of the facility. Other

common shapes which actually require heavy models are blunt entry configurations, i.e. planetary probes. These configurations have such large drag coefficients and hence high decelerations that the test engineer usually attempts to minimize the deceleration the model experiences in the range.

Spin pins are frequently inserted into the model's base in order to measure the roll orientation, and therefore the roll rate (spin) as the model traverses the instrumented range. See Section 5.2.3 for a discussion of these measurements and the design criteria that should be considered. When testing subscale models of missiles or projectiles that operate at high roll rates it is desirable to match as best as possible the nondimensionalized spin parameter, $pd / 2V$, as mentioned in the Section 1.4. This simulates the rotational flow about the full scale missile in flight. Some of the more common methods used to accomplish this match include using rifled launch tubes, grooved sabots, and canted fins.

One more consideration the model designer should take into account is the possibility that aerodynamic heating may cause the model to ablate during flight. This ablation process can cause shape changes to occur. These shape changes can be especially severe on the model's nose or fin leading edges and effectively alters the configuration being tested. This can be a serious problem at hypersonic Mach numbers (above 6) and may require certain heat resistant materials to be used for these conditions. This ablation can be predicted and materials selected to minimize this problem using the curve presented in Fig. 3.3 in combination with the data shown in Table 3.1. Figure 3.3 and Table 3.1 were extracted from Ref. 3.2 and illustrate that ablation is a function of the material properties, atmospheric pressure, and flight distance. Note that ablation occurs for all conditions below the curve in Fig. 3.3. Obviously when making predictions using this curve the flight length should be assumed to be the length of the range. By judiciously selecting materials the designer should attempt to minimize these ablation effects during the test and therefore eliminate them from the resulting aerodynamic coefficients and derivatives.

At the present time the designer does not have a user friendly software package to assist in designing sabots, computing stress levels, and predicting potential sabot failure modes. Although there is an on going effort along these lines and such a tool may be available in the near future. PRODAS can be used to model the sabot and compute the mass properties and there are several outstanding references, i.e. Ref. 1.3 and Refs. 3.3 and 3.4 , which can also be used to assist the designer. Unfortunately some aspects of sabot design are still more of an art than a science but this is rapidly changing with the use of modern finite element programs. There is a considerable body of literature which discusses various point designs also available[3.5,3.6].

The graph axes and labels:

y-axis: $\dfrac{\rho C k \; r_N \; (T_M-300)^2}{p_\infty \; S}$

y-axis values: 10^3, 10^2, 10^1, 10^0, 10^{-1}, 10^{-2}, 10^{-3}

Box label: " ABLATION "

$\rho C k$ - Material Properties Listed in Table I

r_N - Model Nose Radius, ft

S - Distance Travelled, ft

T_M - Material Melting Temperature^{O}K - Table I

p_∞ - Pressure, mm Hg

x-axis: Velocity, kft/sec

x-axis values: 5, 10, 15, 20, 25, 30
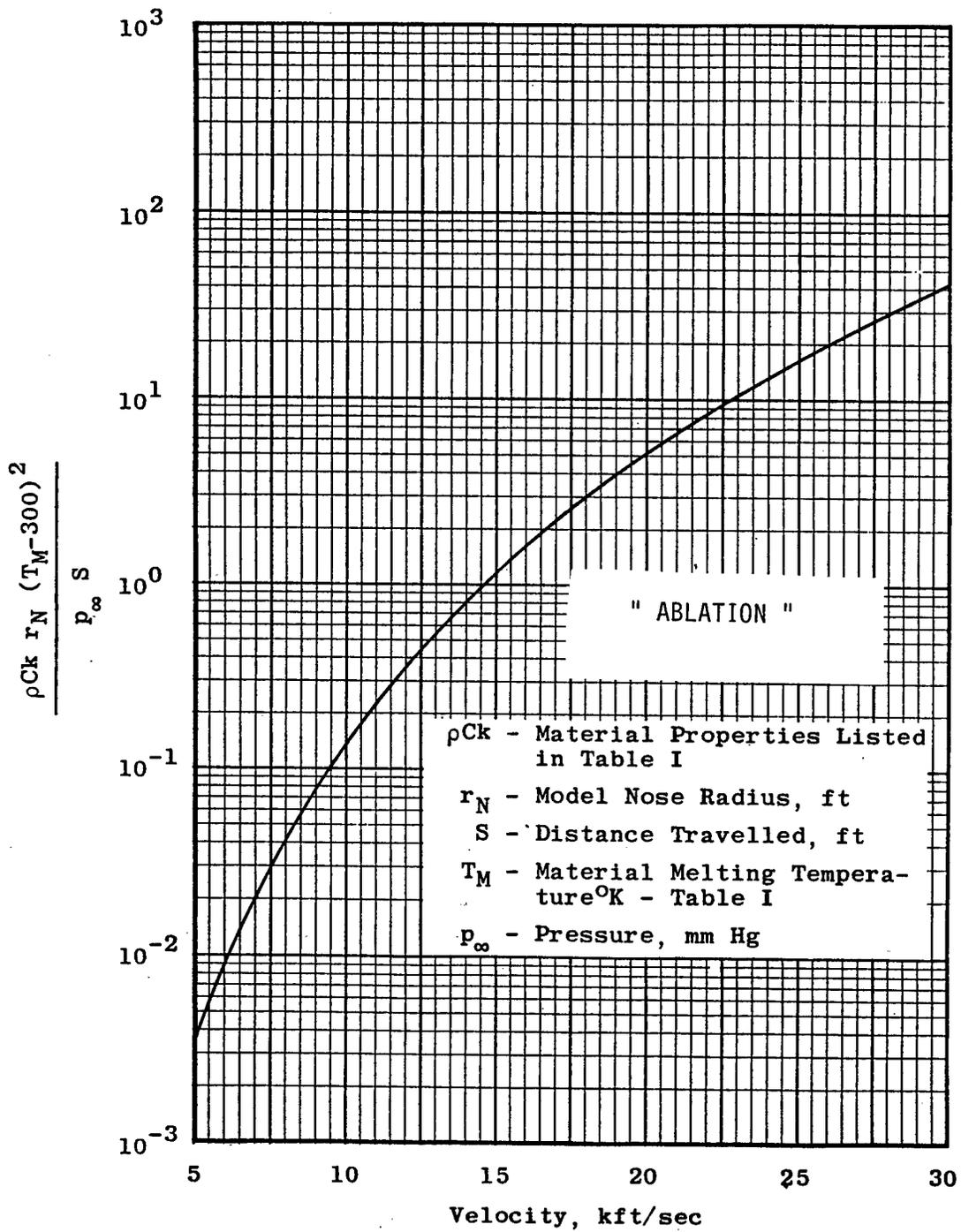
Figure 3.3   Flight Conditions Which Will Give Material
Melting Temperatures at the Stagnation Point
(Fig. 26 , Ref. 3.3)

31

Table 3.1

Material Properties

Material	Density, lb/ft³		Thermal Conductivity, K, Btu/sec/ft2/°K/ft		Specific Heat, C, Btu/lb/°K		ρCk,2 Btu2/ft⁴°K²sec		Melting Temperature, T_m, °K	
	High	Low	High	Low	High	Low	High	Low	High	Low
Aluminum (a)	184.7	160.4	0.068	0.026	0.415	0.396	5.21	1.65	930	761
Beryllium	115.2	---	0.0428	---	0.81	---	3.99	---	1555	---
Copper	558.5	554.7	0.113	0.098	0.18	0.162	11.36 -	8.81 -	1355	1337
Epoxies	149.8	69.9	0.0004	0.00005	---	---	---	---	533 (c)	394 (c)
Epoxies, pre-foamed	20.0	5.0	0.00001	---	---	---	---	---	344 (d)	---
Glass	268.3	156.0	0.001	0.00025	0.36	0.288	0.096	0.011	1955	855
Gold	1204.3	---	0.086	---	0.056	---	5.80	---	1336	---
Magnesium (a)	109.8	104.8	0.040	0.012	0.441	---	1.94	0.556	923	717
Nylons 6,11,66, 610 (e)	71.1	68.0	0.00007	0.00007	1.08	0.54	0.005	0.0018	339 (c)	310 (c)
Polycarbonate (e) LEX*N	94.2	74.9	0.00005	0.000025	0.54	---	0.003	0.001	558 (b)	---
Polyethylene (e)	59.9	56.8	0.00009	0.00005	0.99	0.828	0.006	0.002	355 (c)	313 (c)
Polystyrene	66.8	64.9	0.0004	0.00003	0.63	0.594	0.002	0.0011	355 (c)	336 (c)
Polystyrene, pre-foamed	10.0	2.0	0.00001	---	0.486	---	0.00005	0.00001	352 (d)	341 (d)
Silver	655.2	---	0.119	---	0.101	---	7.87	---	1235	---
Steel (a)	500.5	463.6	0.019	0.004	0.252	0.162	2.4	0.3	1813	1645
Titanium	295.2	276.4	0.005	0.002	0.234	0.216	0.34	0.12	1945	1775
Tungsten	1210.6	---	0.048	---	0.0613	---	3.56	---	3690	---
Urethane foam	25.0	0.5	0.000015	0.000005	0.8	0.76	0.0003	0.0000019	477 (d)	394 (d)

(a) includes alloys, (b) melting point (crystalline), (c) deflection temperature for 264-psi stress, (d) maximum recommended service temperature, (e) typical sabot material

Note: A "Materials Selector Issue" of "Materials in Design Engineering," published by Reinhold Publishing Corporation should be consulted for more detailed information.

(Table I , Ref. 3.2)

3.4 PRETEST PREDICTIONS

It is extremely advisable to make a concerted effort at predicting the various aspects and potential results associated with the test program. These predictions should be accomplished prior to testing and include such things as the required launcher conditions, test item aerodynamics, expected trajectories, and any other aspect pertinent to the program. Predictions are generally thought of as computations of some sort and as such will be discussed in the following sections. However, predictions can also include personal experiences or experiences documented by other individuals conducting related programs. For example if good records are available and maintained from previous test programs these can be an excellent source of predictions for future tests. This is one of the primary reasons why all test organizations maintain test logs which include such data as are listed below.

a. Launcher conditions (i.e.)
    bore diameter
    rifling rate(twist)
    propellant type(s) and charge(s)
    piston mass
    diaphragm rupture pressure
    pump tube gas and pressure

b. Sabot description (i.e.)
    pusher, puller
    number of petals
    mass
    materials
    sketches

c. Model description (i.e.)
    mass
    moments-of inertia
    center-of-gravity
    lengths, diameters
    materials
    drawings

d. Facility test conditions
    temperature
    relative humidity
    pressure

e. Results
    velocity / Mach number
    Reynolds number
    flight (length, time)
    instrumentation obtained or missed
    model / sabot integrity
    general comments

Published data reports and technical papers of previous tests are also an excellent source of predictions. Hence a literature search should be conducted for archival information of similar previous test programs. In fact any new data resulting from the proposed tests should be compared with any previous data of a similar configuration and test conditions. Such comparisons provide insights as to the viability of the test results and hence provides a measure of reliability to the test methods and processes used. In fact once the tests are in progress any and all predictions should be compared with the actual results as soon as possible and the differences analyzed by the test engineer. Such comparisons can yield valuable information which can alert the test engineer to potential problems or anomalies present during testing. These comparisons can also lead to potential advances of the existing predictive capabilities which will assist the designer in future programs.

3.4.1 Launcher

Once the test engineer has identified the launcher to be used either from Fig. 3.1 or other means there exists numerous techniques to predict launcher performance and the resulting muzzle conditions. Certainly the operations crew need to know the required load / charge conditions to achieve the desired muzzle velocity. Likewise the model / sabot designer needs to know what in-bore accelelerations are going to be applied to the test package. Depending on the type of launcher selected different prediction methods are used. For example if a single stage powder gun is used, PRODAS[3.1] is frequently used to predict these interior ballistic characteristics. A simple PRODAS prediction is shown in Fig. 3.4. The model configuration shown in this figure is the same one shown in Fig. 3.2 when the model design features of PRODAS were discussed. The interior ballistic calculations shown in Fig. 3.4 represent an abbreviated output and much more information is available to the user if required. Again it is not our purpose herein to instruct the reader on how to use this computer program but only to indicate that it can be a source of interior ballistics predictions.

If the two stage light gas gun is used as the launcher of preference other predictive tools are available. Some of these two stage light gas gun programs are complex and requires considerable expertise in successfully obtaining accurate estimates. However, some relatively simple routines are also available, for example, the "Light Gas Gun Program, LGG"[3.7] was written specifically for the small launcher operated by the Vehicles Branch, Wright Laboratory, Eglin AFB, FL. This code is applicable for 20, 30, and 40 mm launch tubes and only requires 5 additional inputs as listed below:
1. amount of propellant,
2. piston mass,
3. helium pressure in the pump tube,
4. diaphragm rupture pressure,
5. model / sabot package weight.
All of the other geometric aspects associated with the launcher are fixed. Obviously the estimates provided by this routine are not as precise as the more complex programs but this is more than made up for in ease and simplicity of operation. A summary plot of

PRODAS VERSION 5.5

FILENAME: SC105MIMO 10-DEC-93   :subscale 105 ml modified fuse

INTERIOR BALLISTICS SIMULATION

IGNITER CHARACTERISTICS

WEIGHT	(LBM)	0.0276
IMPETUS	(IN-LBF/LBM)	2000000.
GAMMA		1.20
FLAME TEMPERATURE	(DEG K)	3400.

PROPELLANT CHARACTERISTICS

		PROPELLANT NUMBER 1
TIME DELAY	(SEC)	0.000000
WEIGHT	(LBM)	2.8440
IMPETUS	(IN-LBF/LBM)	3660000.
GAMMA		1.26
COVOLUME	(IN**3/LBM)	30.5700
FLAME TEMPERATURE	(DEG K)	2417.
DENSITY	(LBM/IN**3)	0.0567
BURN RATE EXPONENT		0.670000
GRAIN DIAMETER	(IN)	0.0370
GRAIN LENGTH	(IN)	0.3500
PERFORATION DIAMETER	(IN)	0.0100
NUMBER OF PERFORATIONS		1
WEB	(IN)	0.0135
INITIAL BURN RATE	(IN/SEC/PSI)	0.00165
FINAL BURN RATE	(IN/SEC/PSI)	0.00165
SLOPE	(IN/SEC/PSI/IN)	0.00000
PMC (%)		0.00000

PROJECTILE CHARACTERISTICS

| WEIGHT | (LBM) | 0.4491 |

GUN CHARACTERISTICS

BARREL LENGTH	(IN)	110.0000
CHAMBER VOLUME	(IN**3)	153.0000
BORE DIAMETER	(IN)	1.1800
BORE AREA	(IN**2)	13.7850
PIDDUCK-KENT CONSTANT		3.0240
BASE PRESSURE "F" CONSTANT		0.0000
SHOT START PRESSURE	(PSI)	2000.0000
MAXIMUM GUN PRESSURE	(PSI)	150000.00

subscale 105 ml modified fuse
BODY LENGTH =	5.535 (IN)
OGIVE LENGTH =	2.802 (IN)
BOATTAIL LENGTH =	0.543 (IN)
BAND LENGTH =	0.350 (IN)

c.g.

S U M M A R Y

INTERIOR BALLISTICS SIMULATION
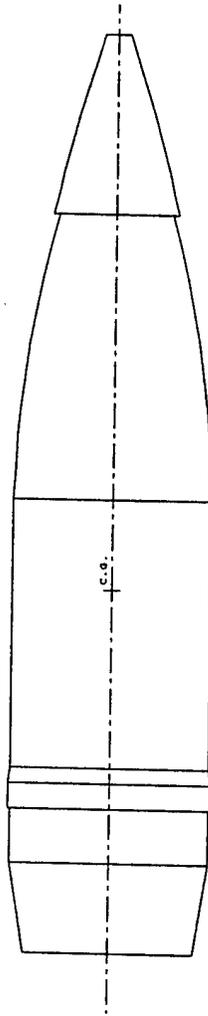
| MUZZLE VELOCITY (FT/SEC) | MUZZLE PRESSURE (PSI) | BORE LENGTH (IN) | MASS FRACTION AT EXIT |
| 1769. | 1628. | 86. | 0.434 PROPELLANT NUMBER 1 |

| MAXIMUM BREECH PRESSURE (PSI) | TIME AT MAXIMUM BREECH PRESSURE (MSEC) | TRAVEL AT MAXIMUM BREECH PRESSURE (IN) |
| 11431. | 0.65 | 1.3209 |

| MAXIMUM BASE PRESSURE (PSI) | TIME AT MAXIMUM BASE PRESSURE (MSEC) | TRAVEL AT MAXIMUM BASE PRESSURE (IN) | MAXIMUM ACCELERATION (GEES) |
| 9795. | 0.65 | 1.32 | 22969. |

| IMPULSE LBF-SEC AT EXIT 29.435 | IMPULSE LBF-SEC AT 20 MSEC 34.347 |

Figure 3.4 Example of Interior Ballistics Using PRODAS

propellant weight vs. muzzle velocity is shown in Fig. 3.5 for convenience. If peak accelerations are required or more specific information needed the user is encouraged to execute this simple routine or any other routine he may have access to.
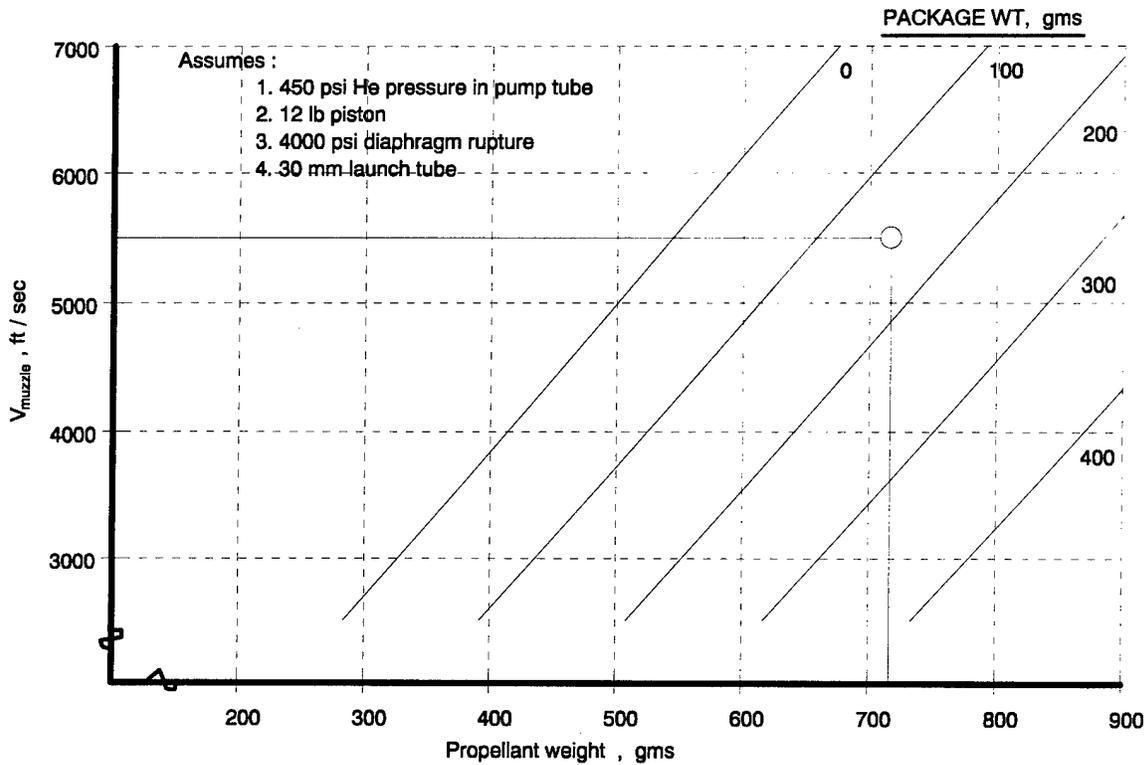
Figure 3.5 Propellant vs Velocity Relationship for the Eglin Light Gas Gun

If the test models are large and the launch velocities relatively low then a compressed gas gun may be the launcher of choice (see Fig. 3.1). Subsonically the launcher performance can be predicted using the relationship below:

$$V_p = E_f \ [\ 2P_c \ V_c \ (\ 1 - K^{1-\gamma}) / (\gamma - 1) \ m_a \ ]^{1/2} \qquad 3.1$$

where $K \equiv (A_b \ L_b + V_c) / Vc$

and V_p = muzzle velocity of the projectile
           P_c = chamber pressure
           V_c = chamber volume
           γ = ratio of specific heats (air = 1.4)
           m_a = projectile mass
           A_b = launch tube cross sectional area
           L_b = launch tube length
           E_f = efficiency factor (assumed to be 0.87)

36

Equation 3.1 was obtained from Ref. 3.8 and is applicable for subsonic launches. A unique variation of this relationship was derived for a double barreled compressed air launcher as is shown in Ref. 3.9. The efficiency factor, E_f, was experimentally measured as 0.87 and included in Eq. 3.1 during the tests discussed in Ref. 3.9.

If a supersonic launch is required ($M \rightarrow 1.5$) using the compressed gas gun then Eq. 3.1 should not be used and the compressibility of the gas must be included. These relationships have been developed[3.10,3.11] and a predictive routine , GUNPAI, exists which utilizes these relationships. Example performance curves using GUNPAI are shown in Fig. 3.6 and illustrate the difference in performance when helium is used in place of air as the propelling gas. Also shown in this figure are experimental data for comparison purposes.

Obviously any prediction should be evaluated using existing data from previous tests. Especially when the user has data of similar in-gun weights and fired at nearly the same velocities. This provides an excellent mechanism for predicting launcher performance in future tests.

3.4.2 Aerodynamics / Trajectory

The test item's expected aerodynamics should also be predicted and used to compare with the experimentally determined coefficients and derivatives. These predicted aerodynamics can be extremely useful in illustrating the expected trends, (i.e., vs Mach number , angle of attack, etc.) and can be used as an indicator of the experimental viability. The test engineer should carefully analyze any large deviations between experiment and prediction to ensure that the experiment was properly conducted and that the results are reasonable. Previous data on similar configurations at similar conditions should also be used for this purpose. Obviously the test engineer should be concerned if similar configurations at similar conditions yield significantly different trends and immediate evaluation of these differences is in order.

The PRODAS program discussed previously is capable of fulfilling this requirement for symmetrical spin stabilized or statically stable, i.e. finned, configurations. Table 3.2 illustrates the PRODAS aerodynamic predictions for the example model shown in Fig. 3.2. This routine is based on previous data and theoretical relationships are used to extrapolate between configurational and test condition variations. Hence if the test item configuration falls within the bounds of the existing data reasonable predictions are normally obtained.

Once the aerodynamics have been predicted this routine can also generate trajectories using these aerodynamics in conjunction with the model's physical characteristics and the atmospheric conditions. Either 6DOF or 2DOF trajectories can be generated for most launch conditions. A typical 2DOF trajectory representing a flight through the ARF is

FNF = Coefficient of friction between sabot and gun

f = Fluid friction coefficient
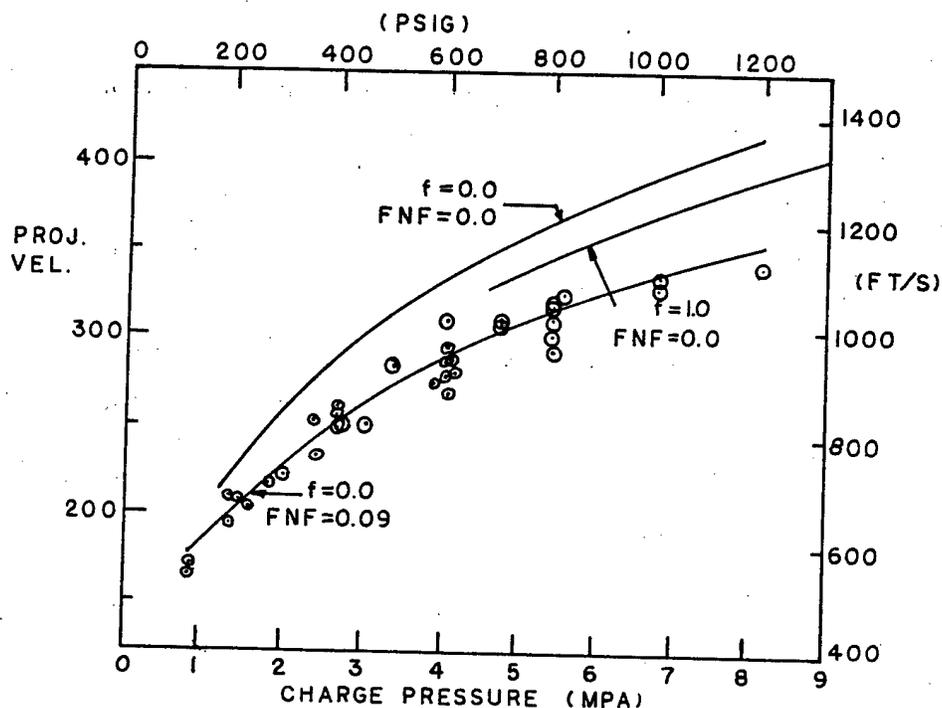
a. Air Propellent (Fig. 5 , Ref. 3.10)
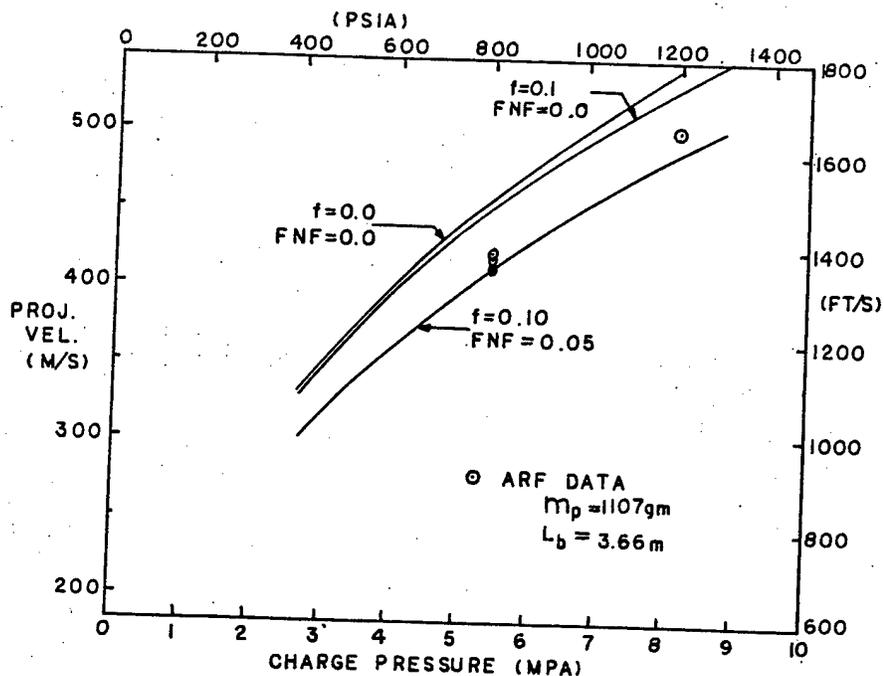
b. Helium Propellent (Fig. 7 , Ref. 3.10)

Figure 3.6 Comparison of GUNPAI Predictions with
Experimental Results , 151mm I.D.,
3.66 m Long Launch Tube , 1 Kg Package

Table 3.2
Aerodynamic Predictions Using PRODAS

FILENAME: SC105M1MO 10-DEC-93   :subscale 105 m1 modified fuse

STABILITY RESULTS

	PROJECTILE LENGTH	OGIVE LENGTH	BOATTAIL LENGTH	BOOM LENGTH	C.G. FROM NOSE	BAND DIAMETER	MEPLAT DIAMETER	OGIVE RADIUS	RIFLING TWIST
IN INCHES	5.535	2.802	0.543	0.000	3.347	1.206	0.146	7.285	21.240/REV
IN CALIBERS	4.699	2.379	0.461	0.000	2.841	1.024	0.124	6.184	18.000/REV

DIAMETER (IN)	WEIGHT (LBM)	GUN BORE (IN)	TEMPERATURE (DEG F)	AIR DENSITY (SLUGS/FT**3)	AXIAL MOM. (LBM-IN**2)	TRANS. MOM. (LBM-IN**2)
1.178	0.449	1.180	59.000	0.002376	0.06917	0.78533

AERODYNAMIC COEFFICIENTS

SPINNER PREDICTION

MACH	CX	CX2	CNA	CMA	CPN	CYPA	MAGNUS AT ANGLE OF ATTACK (DEG)				NON-LINEAR MAGNUS		CMQ	CLP
							CNPA-0	CNPA-2	CNPA-5	CNPA-10	CNPA3	CNPA5		
0.010	0.147	2.618	1.617	3.684	0.563	-0.794	-0.405	0.121	0.422	0.72	132.57	-3133.	-11.4	-0.028
0.600	0.147	2.618	1.617	3.684	0.563	-0.794	-0.405	0.121	0.422	0.72	132.57	-3133.	-11.4	-0.028
0.800	0.134	3.149	1.683	3.796	0.585	-0.794	-0.255	0.196	0.497	0.80	120.22	-2808.	-10.3	-0.028
0.900	0.168	3.696	1.813	3.982	0.644	-0.888	0.014	0.310	0.564	1.03	85.23	-1701.	-11.8	-0.028
0.950	0.223	4.111	1.928	4.108	0.710	-1.123	0.258	0.474	0.690	1.34	63.92	-932.	-14.5	-0.026
1.000	0.348	4.603	2.042	4.003	0.880	-1.029	0.361	0.558	0.657	0.90	45.93	-922.	-16.9	-0.024
1.050	0.388	5.137	2.156	3.888	1.037	-0.935	0.444	0.587	0.623	0.71	28.36	-641.	-19.3	-0.023
1.100	0.402	5.696	2.219	3.807	1.126	-0.888	0.479	0.581	0.606	0.69	19.92	-425.	-20.2	-0.022
1.200	0.403	6.241	2.295	3.694	1.231	-0.794	0.482	0.557	0.572	0.65	14.00	-281.	-21.0	-0.022
1.350	0.381	5.614	2.411	3.552	1.367	-0.794	0.497	0.557	0.572	0.65	11.53	-216.	-19.3	-0.022
1.500	0.359	5.057	2.513	3.471	1.460	-0.794	0.504	0.557	0.572	0.65	10.29	-184.	-17.6	-0.022
1.750	0.332	4.480	2.649	3.372	1.568	-0.794	0.512	0.565	0.572	0.65	9.06	-151.	-17.2	-0.022
2.000	0.307	3.917	2.775	3.290	1.656	-0.794	0.520	0.565	0.572	0.65	7.82	-119.	-17.3	-0.021
2.500	0.264	3.161	2.890	3.050	1.785	-0.794	0.527	0.565	0.572	0.65	6.59	-86.	-18.8	-0.019
3.000	0.220	2.614	2.815	2.685	1.887	-0.794	0.535	0.565	0.572	0.65	5.35	-54.	-21.9	-0.015
4.000	0.180	2.144	2.715	2.586	1.889	-0.794	0.535	0.565	0.572	0.65	5.35	-54.	-22.0	-0.015
5.000	0.159	1.675	2.615	2.487	1.890	-0.794	0.535	0.565	0.572	0.65	5.35	-54.	-21.3	-0.015
6.000	0.143	1.488	2.565	2.438	1.891	-0.794	0.535	0.565	0.572	0.65	5.35	-54.	-21.1	-0.015
8.000	0.133	1.399	2.535	2.408	1.891	-0.794	0.535	0.565	0.572	0.65	5.35	-54.	-20.9	-0.015
10.000	0.126	1.305	2.515	2.388	1.892	-0.794	0.535	0.565	0.572	0.65	5.35	-54.	-20.7	-0.015

presented in Fig. 3.7. This trajectory illustrates the expected drop due to gravity and the velocity decay of the previously used example model (see Fig 3.2).

3.4.3 Initial Motion Augmentation

Frequently it is necessary to augment the model's initial angular disturbance as it exits the launch tube. This is required because the naturally occurring disturbance is not adequate to impart an angular motion large enough for accurate determination of the aerodynamic coefficients and derivatives. Over the years numerous techniques have been used to increase the initial disturbances including modifications to the muzzle of the launcher, plates near the muzzle to cause asymmetric flow upon exit, offsetting the model in the sabot, etc. All of these techniques and many others have had some success; however, quite often what worked for one test configuration did not work for the next. Also the amount of disturbance could not be predicted prior to testing. Many of these techniques tended to impart an undesirable transverse velocity as well as the desired angular disturbance. This transverse velocity can result in the model impacting the walls of the facility, or worse the instrumentation systems in the facility.

The problem outlined above still applies for statically stable configurations because no systematic procedure has ever been developed which is predictable and reliable for these configurations. On the other hand a reliable and predictable method has been developed for spin stabilized projectiles. This method uses the model's gyroscopic stability as a means of imparting the initial angular disturbance without a corresponding transverse velocity. The gyroscopic stability factor , S_g , is discussed in some detail in Section VII but for our purposes here it is sufficient to note that if S_g is less than 1.0 the model is gyroscopically unstable and the angular motion will increase. The relationship developed in Section VII for S_g is ,

$$S_g = (2\, I_x\, P^2)\, /\, (I_y\, \rho\, \pi\, d^3\, C_{m\alpha}) \qquad (\text{see Eq. 7.11 })$$

where :

I_x = axial moment of inertia
I_y = transverse moment of inertia
P = spin rate
d = model diameter
$C_{m\alpha}$ = pitching moment derivative
ρ = atmospheric density

From this equation it can be seen that if the atmospheric density is increased sufficiently S_g can be forced to a value less than unity.

This represents the crux of the technique and operationally is accomplished by flying the model through a relatively short tube (~ 3 m) containing a high density gas. The tube has both ends sealed with a diaphragm, the air is pumped out, and a sufficient amount of high density gas is bled into the evacuated tube. An environmentally safe

40

Subscale 105mm with M1 Modified Fuse
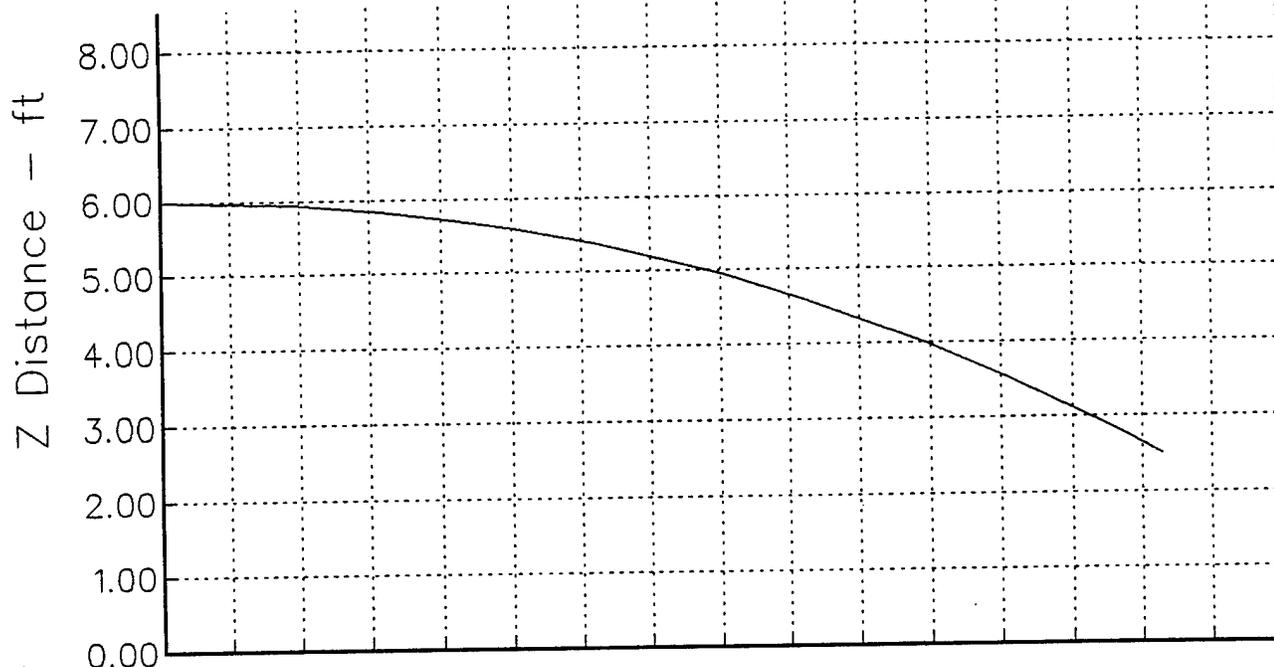
a. Altitude vs Distance Traveled (Gravity drop)
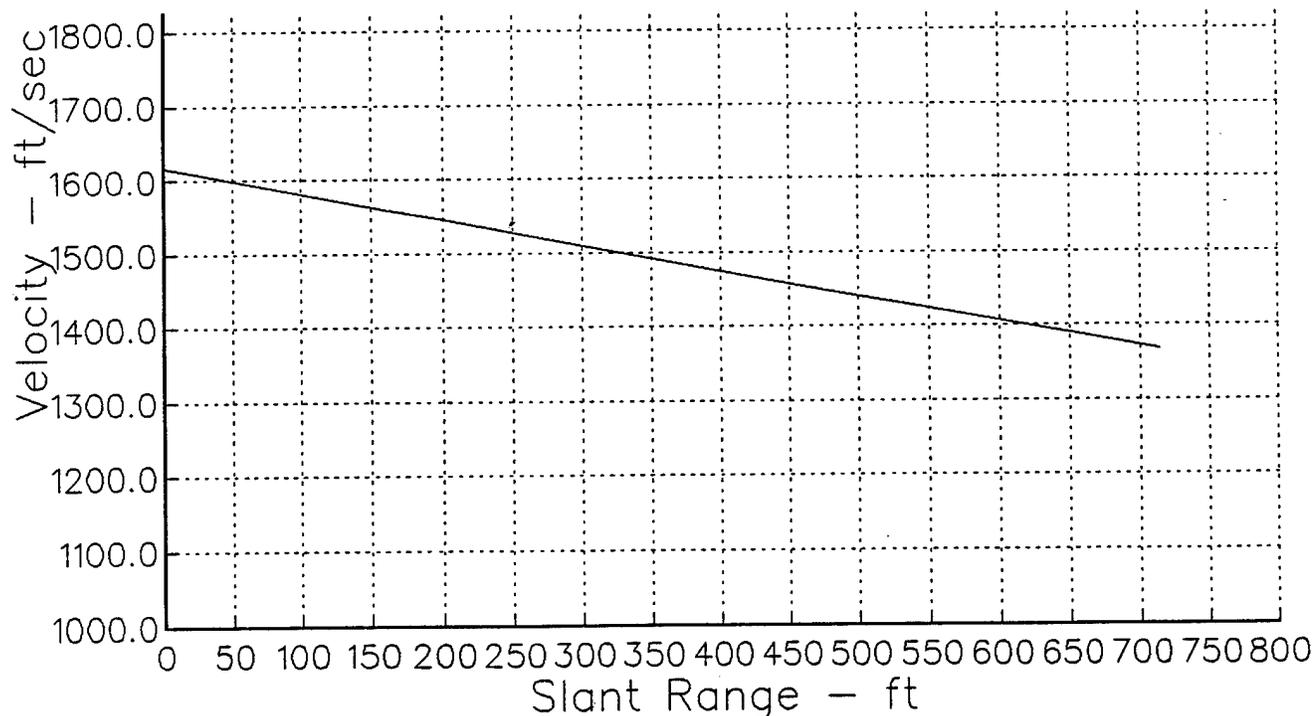
b. Velocity vs Distance Traveled

Figure 3.7 Facility Trajectory Predictions Using PRODAS

Freon compound is used for this purpose. When computing the required amount of gas, using the equation above, an estimate of $C_{m\alpha}$ must be available. This can be obtained either from similar data or PRODAS as mentioned previously. It should be recognized that $C_{m\alpha}$ varies with Mach number and the Mach number in the tube will be significantly different than the Mach number in air (for Freon about twice as high) . Once the model punctures the diaphragm and enters the tube the angular motion will increase because it is gyroscopically unstable. Upon exit from the tube the augmented angular motion can be measured and analyzed as discussed in the later sections herein.

3.5 PRETEST MEASUREMENTS

It should be obvious that whatever can be measured (i.e., model's physical characteristics, range and test conditions, instrumentation calibration, etc.) should be measured and recorded prior to any testing being accomplished. Nevertheless the lack of obtaining such measurements causes more difficulties during the post test analysis than any other single cause. For some complex full scale flight tests these measurements can be difficult to obtain. For example the atmospheric conditions, i.e. temperature, pressure, wind, etc. , are all functions of altitude and the model's geometry can be variable as well, i.e. cg movements, fin deflections, etc. Difficult or not these measurements are absolutely necessary in order to completely analyze the test results. This is just as true for the simpler case of testing subscale models within an indoor facility. Model measurements and facility conditions are absolute requirements and not only obtained but should also be examined for reasonableness and consistency prior to testing. During this pretest measurement process it is also a good time to obtain photographs of the models and sabots for later documentation purposes.

3.5.1 Model Physical Properties

The physical characteristics of the models include the linear dimensions, mass, center-of-gravity, and moments of inertia. There are numerous methods and instruments by which the dimensional measurements can be obtained. Not only should the obvious measurements of length and diameter be obtained but also any other potentially pertinent measurements such as nose bluntness or fin cant. Small variations in nose bluntness can significantly affect the aerodynamic drag measurements and changes in fin cant can seriously alter the rolling motion and hence the overall flight dynamics of the test model. The test engineer should be alert to any potential model variation which could affect the results and insure that the required measurements are obtained.

The distance between the model's nose and the center-of-gravity (L_{cg}) is usually measured using a simple beam balance type system as illustrated in the sketch on the following page. Writing the moment equation about the pivot point, A , leads to the relation:

$$X_1 = W X_2 / m_a$$

from which the models L_{cg} distance can be determined. Note that m_a is the model mass
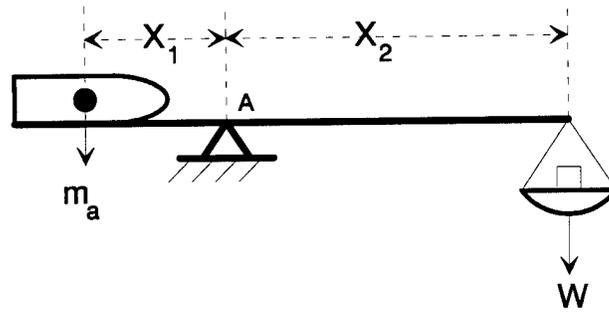
and W is the counter balancing weight. In application such systems can become fairly complex[3.12]; although, this is the basic principle which is normally applied.

The model's moments of inertia, transverse and axial, are usually obtained using a torsional pendulum system. Sketches illustrating this principle are shown below.
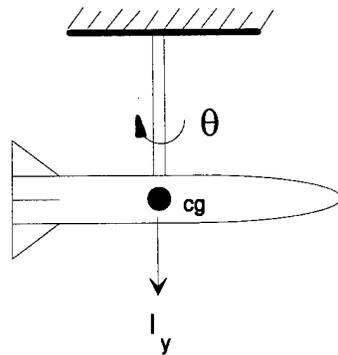
Transverse Inertia
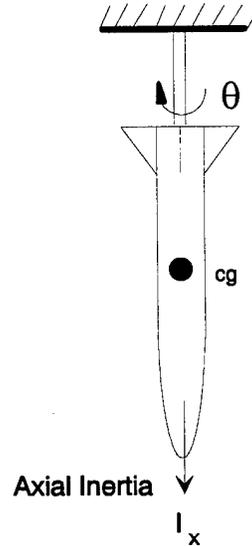
Axial Inertia

Assuming small angles of oscillation (θ) the differential equation governing the rotational motion of the pendulum is,

$$I (d^2\theta / dt^2) + K \theta = 0$$

The frequency of oscillation (ω) is given by the relation,

$$\omega = (1 / 2\pi) (K / I)^{1/2} \qquad 3.2$$

where,

$$K \equiv \text{stiffness constant of the wire}$$

Once the constant K is determined by measuring the frequency of an object with a known inertia (i.e. a solid homogenous cylinder) an unknown inertia, for example a test item, can be determined using Eq. 3.2 and measuring its rotational frequency about the axis of

the torsion bar. There are several commercially built instruments presently available for this purpose[3.12] and most use the principle as outlined above.

3.5.2 Atmosphere

When accomplishing free-flight tests in an indoor facility these measurements are relatively easy and consists of temperature, pressure, and relative humidity. For large (long) facilities it is recommended that multiple measurements along the flight path be recorded at about the same time the tests are conducted. As previously mentioned when testing on an outdoor facility or full scale flight profiles are duplicated these atmospheric measurements along with the existing winds should be obtained throughout the altitude range of interest. Since these are also frequently time dependent it is desirable to obtain the measurements as near the test time as possible. A whole host of commercial instruments are readily available for these purposes. However, those which do not require human recordings and / or interpretation are preferred. Regardless of which instruments are chosen, these measurements are highly recommended because failure to obtain or record these parameters can make the post test analysis extremely difficult if not impossible.

3.5.3 Range / Instrumentation Calibration

As pointed out in the previous sections it is critical to measure and record the physical characteristics of the models, range conditions (atmosphere) during the tests and any other parameter that could be expected to affect the final results. Obviously the instruments used to obtain these measurements should be periodically calibrated to ensure that the measurements are reliable. Most research / test organizations have processes in place which accomplish this periodic evaluation and these should be faithfully adhered to because unreliable measurements can render the final results suspect and hence useless. Some instruments cannot easily be sent to a calibration lab for evaluation and procedures must be established to calibrate / evaluate these instruments / systems in place. This can be accomplished by periodically evaluating a standard and maintaining a running log of the measurement which will highlight any unexpected variation. These periodic evaluations can be for simple instruments imbedded in a more complex system or the complex system itself. For example, the calibration of the facility and the determination of the its overall accuracy in positions, attitudes and time.

Free-flight spark range calibration is generally defined as the precise determination of the spatial locations of the facility's reference system, spark sources, cameras, and other critical components. In the early days of free-flight spark ranges these determinations were accomplished by physically measuring all of these critical components using calibrated tapes, optical scopes, and a myriad of special fixtures and tools, i.e. see the discussion in Ref. 1.2. More recently these determinations have been done by mathematical means, Refs. 3.13 to 3.16. The mathematical technique developed in Ref. 3.13 and utilized in Ref. 3.16 essentially uses known points in space to compute the spatial coordinates of the reference beads and spark locations, see the abbreviated

discussion in Appendix 2. The technique discussed in Ref. 3.15 determines the biases at each station by maintaining a record of the various fits to the experimental data and subtracting these biases from the raw measurements during analysis. In practice both methods should be utilized. The more precise technique of Ref. 3.13 should be periodically utilized, once every year or so, unless the reference system is damaged by a projectile impact, then it should be accomplished as soon as the repair is completed. The method of Ref. 3.15 should be used on a continuing basis for evaluating the facility accuracy and updating the station bias files. This technique is very powerful and caution must be used to ensure that the residuals between the experimental data and the fitted trajectories are caused by random measurement noise and not modeling inadequacies.

If the range calibration becomes suspect it can readily be examined by launching several standard spin stabilized projectiles whose aerodynamics and flight dynamics are known. If these residuals demonstrate a noticeable trend (i.e. a sine wave function) this usually indicates an aerodynamic modeling problem. However, if the residuals at an individual station have a tendency to always be positive (or negative) then this indicates a potential calibration problem. The decision as to when a facility recalibration is required and which method to use hinges on several factors. These include but are not limited to: 1) the purpose of the tests and whether or not the required results would be noticeably impacted by the suspected errors, 2) the magnitude and quantity of the suspected errors, 3) how much time is available for the calibration.

REFERENCES

3.1 Burnet, J. R., Hathaway, W. H., and Whyte, R H., " Projectile Design and Analysis System (PRODAS-81)" , AFATL-TR-81-43, April 1981.

3.2 Bailey, A.B., and Koch, K.E., "Data for Use with Hypervelocity Ballistic Ranges", AEDC-TM-65-16, June 1965.

3.3 DeWitt, J., " Procedure for Design of Models and Sabots for Range G Launchers" , AEDC-TMR-92-P6, May 1992.

3.4 Lockheed Propulsion Co., " Sabot Technology Engineering Handbook", Final Report Jan. 1968 through Feb. 1969, Report 913-F, August 1969.

3.5 Strange, D., Swift, H., " Sabot Designs for Launching a Selection of Massive Rods from the 82.6 mm Solid Propellant Gun at the U.S. Army Waterways Experiment Station", Physics Applications, Inc., 7635 Wilmington Pike, Dayton, Ohio, August 1994.

3.6 Abate, G.L., "Launch Technique for High Length / Diameter (L / D) Configurations", paper presented at the 39th Meeting of the Aeroballistic Range Association, Albuquerque, NM, October 1988.

3.7 Courter, R., and Patin, R. M., " Light Gas Gun Performance Analysis and
Test Design by Microprocessor", paper presented at the 36th Meeting of the
Aeroballistic Range Association, San Antonio, TX, October 1985.

3.8 Strange, D.E., and Swift, H.F., " Approximate Methods for Evaluating Light-Gas Gun
Performance", paper presented at the 43th Meeting of the Aeroballistic Range
Association, Columbus, Ohio, October 1992.

3.9 Winchenbach, G.L., Aldegren, R., and McClenahan, C., "Launching a Surf Zone
Mine Countermeasure Explosive Array from a Double Barreled Single Stage
Compressed Gas Gun", paper presented at the 44th Meeting of the Aeroballistic
Range Association, Munich, Germany, September 1993.

3.10 Boehman, L.I., Swift, H.F., "Analysis of Captured -Piston Compressed Gas Guns",
AFATL-TR-81-98, November 1981.

3.11 Boehman, L.I., and Swift, H.F., and Winchenbach, G.L , "Analysis of Captured-
Piston Compressed -Gas Launchers", paper presented at the 33rd Meeting of the
Aeroballistic Range Association, Santa Barbara, CA, August 1982.

3.12 Parish, G.E., " Projectile Measurement and Instrumentation Laboratory Mass
Property Measurements", AFATL-TR-74-156, September 1974.

3.13 Winchenbach, G.L., and Davis, T.D., "A Mathematical Technique of Free-Flight
Spark Range Calibration", paper presented at the 30th Meeting of the Aeroballistic
Range Association, Burlington, VT, September 1979.

3.14 Pitsch, K.H., and Winchenbach, G.L., "An Improved Range Calibration Technique",
paper presented at the 41st Meeting of the Aeroballistic Range Association,
San Diego, CA, October 1990.

3.15 Whyte, R.H., and Hathaway, W.H., "Dynamic Calibration of Spark Aeroballistic
Ranges", paper presented at the 44th Meeting of the Aeroballistic Range Association
Munich, Germany, September 1993.

3.16 Dupris, A. " Calibration Methodology and Procedure for the DREV Aeroballistic
Range", paper presented at the 41st Meeting of the Aeroballistic Range Association
San Diego, CA, October 1990.

IV. TESTING

4.1 SAFETY / OPERATING INSTRUCTIONS

Safety should always be of primary concern and rigorously following established procedures will minimize if not eliminate hazardous situations. Considerable effort has been expended over the years in developing well thought out procedures and the establishment of operating instructions (OI's) for the test facilities, launchers, instrumentation systems, and freon tube. These OI's not only discuss safety concerns but also specifically provide the standard operating procedures for the facility and its systems. Faithfully following these guidelines will result in a safe and successful test program. A hurried chaotic process is inherently unsafe and leads to errors which culminate in test objections not being accomplished.

When situations arise which are not adequately covered by the existing OI's these should be noted and included in periodic reviews and amendments to the instructions. These situations occur because new instrumentation and launcher systems are developed or procured and new test requirements mandate operations which had never before been attempted. Nevertheless, these experiences should be included in the OI's as soon as practical and while memories are fresh.

4.2 PRELIMINARY EVALUATIONS

Frequently it is necessary to conduct a preliminary evaluation of the models, sabots or instrumentation prior to the primary test program. These preliminary evaluations are normally conducted on an outdoor range, i.e., the Ballistic Experimentation Facility[4.1] (BEF). The desire to accomplish such tests in an unconfined environment arises from the inherent uncertainties associated with such tests and for protecting the facility and the instrumentation systems from unnecessary risks. Occasionally these preliminary tests must be done within the confines of an indoor range because that is where the required systems are and the impracticality of moving or operating these systems in an outdoor environment. Nevertheless these preliminary evaluations should be accomplished in a manner such that the attendant risks are minimized.

4.2.1 Models and Sabots

It is good practice to launch new model / sabot packages first on the outdoor range in order to evaluate the performance of the package. This includes the separation of the sabot petals from the model, the amount of separation at a distance equivalent to the stripper or blast chamber wall, the trajectory of the petals, and the structural integrity and trajectory of the model itself. Even model and sabot designs that have been used on previous occasions should be reevaluated prior to a follow on test entry. Sometimes

materials are substituted for in the manufacturing process or the machine tolerances are different. These small variations can and frequently do result in drastically different performance and cause unexpected problems during testing.

Numerous systems have been used over the years to evaluate model / sabot performance during launch and subsequent flight. These include muzzle X-rays, high speed cameras, radar, witness panels and others. As mentioned the primary purpose of the evaluation is to determine model and sabot integrity during launch, sabot separation, and component trajectories after launch. X-rays are frequently used at the muzzle to view the model / sabot package upon exit because of the debris cloud (smoke, gasses, etc.) usually accompanying the package. An example X-ray is shown in Fig. 4.1. This X-ray image illustrates an excellent launch, both model and sabot appear to be in perfect condition and the sabot is separating as designed. Such muzzle X-rays do not assist in evaluating how much separation is achieved at a given distance, i.e. blast chamber wall or stripper, or what the trajectory of the sabot components might be. One simple technique of evaluating these concerns is the placement of witness panels at desired distances. Figure 4.2 is a typical example of the information that can be obtained from these witness panels. This figure illustrates that the sabot petals have separated about 14 inches in 30 feet and would be trapped in the blast chamber of the facility; thereby , eliminating any potential damage to the instrumentation systems due to petal impacts. However, other components of the sabot (3 plugs) would likely make it through the stripper creating a possible hazard to the downrange systems.

Frequently high framing rate cameras are used to evaluate the performance of the model / sabot package during the initial portion of the flight. Although these cameras cannot view the package immediately upon exit from the muzzle, due to the debris cloud, the model and sabot petals can be viewed a few feet from the muzzle and this separation evaluated. This technique is especially useful for relatively large packages (several inches) and low velocities (less than 2000 ft / sec). Image resolution and motion blur can be a problem when a large field of view is being observed, especially for high velocity launches.

4.2.2 Test Conditions

Another purpose of these preliminary checkout tests is to determine the launch conditions required to achieve the desired test velocity. Although the corresponding launcher conditions are normally predicted as discussed in Section 3.4.1 it is desirable to confirm these predictions using the actual model / sabot package. This desirability arises from several variables which can significantly affect the expected muzzle velocity as determined from predictions or even from similar previous launches. For example variations in sabot tolerances can drastically alter the muzzle velocity because the start pressure can change significantly. The start pressure is the pressure on the base of the model or sabot when the package initially begins to move down the launch tube. If the package is a "loose fit" it can start to accelerate too early in the launch cycle and exit the muzzle before all of the energy in the propellant is expended. Quite often unburned

Figure 4.1 Typical Muzzle X-Ray of a Model / Sabot Package
(X-Ray Obtained in the AEDC Range G)
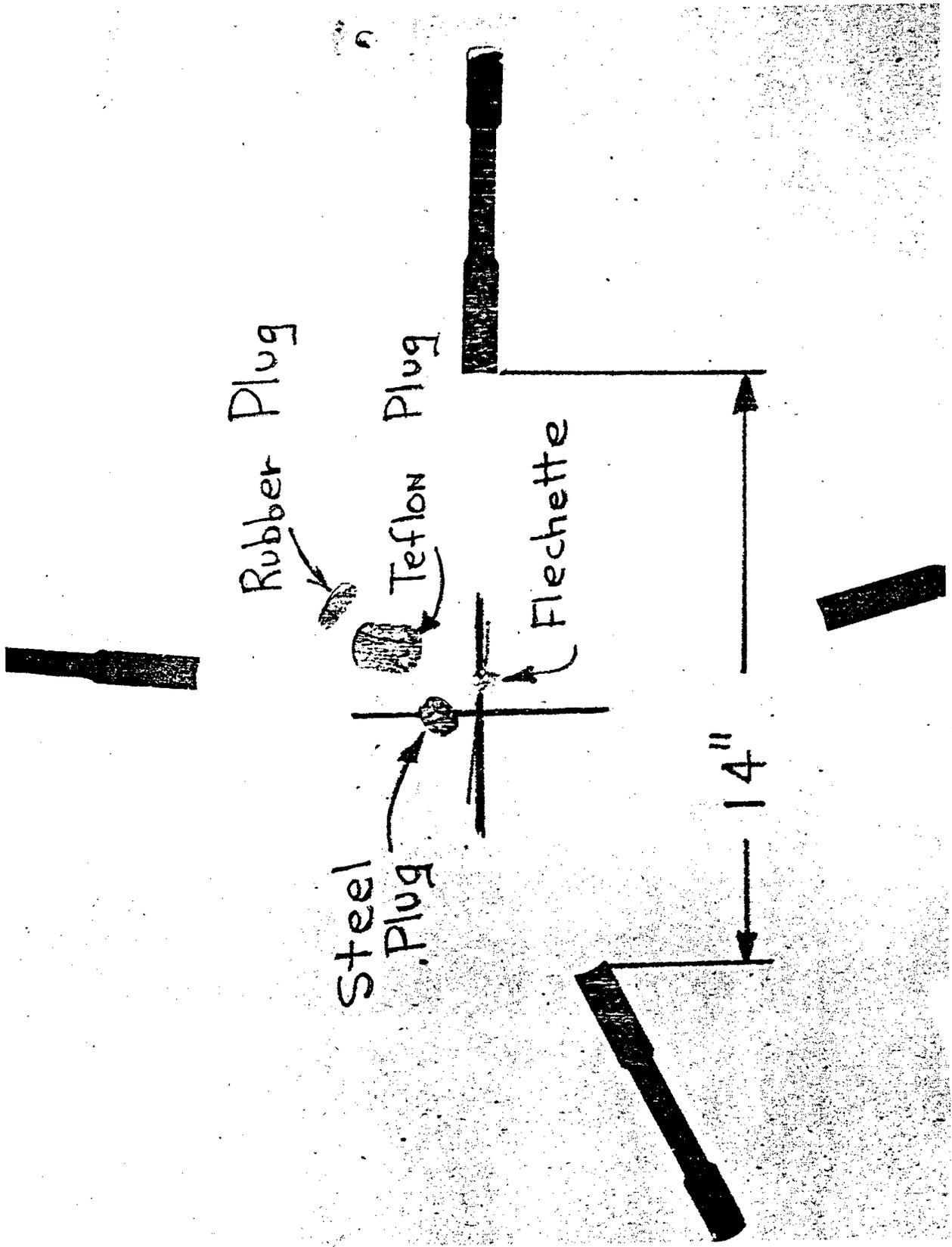
Figure 4.2 Sabot Separation Witness Card at 30 Feet (Fig. 11 of Ref. 4.2)

propellant is found in the blast chamber when this occurs and the resulting muzzle velocity is lower than expected. In practice designers usually attempt to tailor the start pressure in order to achieve maximum performance. Other variations such as launch tube wear, propellant conditions(damp or dry), diaphragm tolerances, and a host of other causes can affect the expected muzzle velocity.

This velocity determination has been accomplished on the outdoor range in the past using several different techniques, i.e. circuit break / make paper, multiple pulse X-rays, high speed framing cameras, digital CCD camera systems, and Doppler radar. All of these techniques have their advantages and depend on the resources available, i.e. funds, equipment, and man power. For example the circuit break / make paper technique (see Ref. 4.2) is a basic, simple, inexpensive system but is manpower intensive and is seriously affected by weather conditions (wind, rain, etc.) on the outdoor range. Whereas the Doppler radar unit is a more sophisticated system and initially more expensive. This system is also more versatile, see sample data in Fig. 4.3, and has a multitude of uses, i.e. muzzle velocities, in bore velocities, spin determination and long range elevated trajectory measurements[4.3].
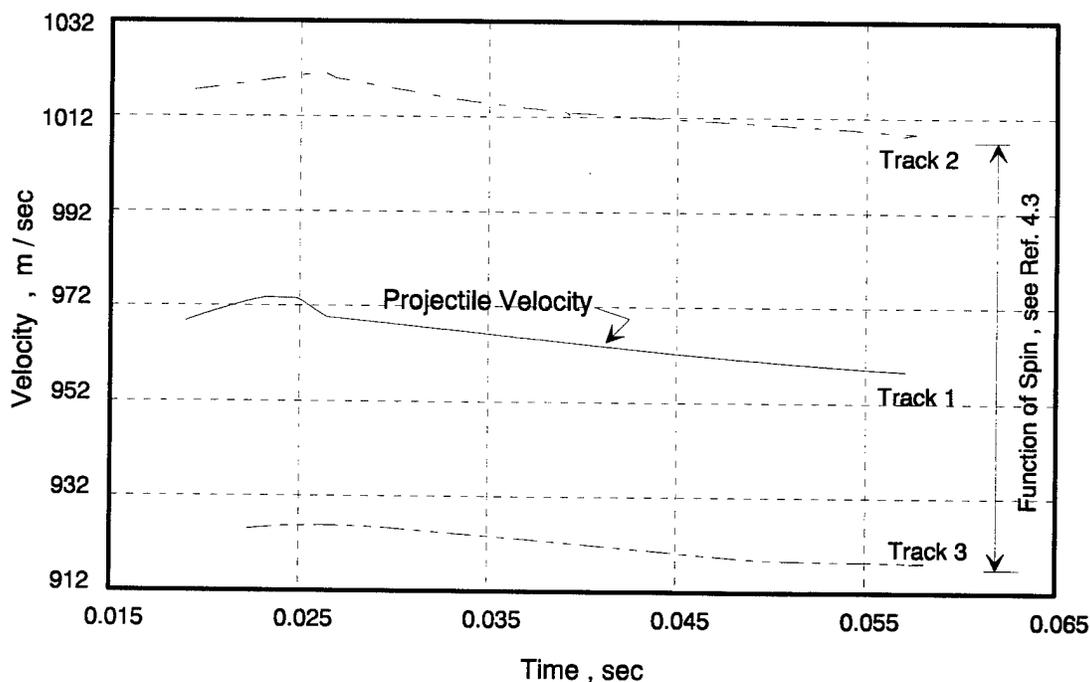
Figure 4.3 Doppler Velocity Tracks vs Time (25 mm Projectile)

The primary advantage of the photographic techniques (X-ray and cameras) in obtaining initial velocities is that the designer / test engineer can also simultaneously evaluate model / sabot integrity during launch. In practice even when the radar unit is

being utilized it is usually desirable to operate one or more of these photographic systems for this evaluation. Operating both types of systems when possible provides an independent check on velocity as well as a backup in case one system malfunctions. It can also permit the determination of the initial disturbances transmitted to the model during launch. This is often an important reason for conducting the preliminary outdoor tests in the first place. The model / sabot designer needs to insure that at least a certain amount of angular motion will be present for the trajectory analysis and coefficient extraction process to be successful. If adequate initial disturbances are not imparted to the model then augmentation may be required as discussed in Section 3.4.3.

Finally useful aerodynamic data can also be obtained during these outdoor tests if adequate preparation and thought are expended. In fact, organizations that do not have readily available access to an indoor free-flight facility can accomplish fairly sophisticated analysis on an outdoor range using the techniques described herein and in Refs. 4.4 and 4.5.

4.2.3 Instrumentation

Occasionally it is necessary to do preliminary testing in order to checkout, adjust, set delays, etc., for special instrumentation systems required for a particular tests. Normally this can not be accomplished on the outdoor range but must be done in the indoor facility because of lighting, protection from the weather, or the impracticality of moving the systems to an outdoor environment. For these occasions the general practice is to fire known, well behaved items, i.e. 20 or 30 mm target practice (TP) ammunition, through the systems for instrumentation evaluation. Once the instrumentation is deemed ready then the correct launcher is installed and the actual test items launched. Using the well behaved TP ammunition not only minimizes the risk of damage to the instrumentation systems but saves the test items for launching when the chances of success are the highest.

The process discussed above is also followed after periods of downtime in order to ensure that the basic shadowgraph system is in a state of readiness. After periods of extended downtime, due to calibration or holidays, camera shutters tend to stick, spark sources can collect moisture and become erratic, etc. A few checkout flights using well behaved and inexpensive projectiles can be useful in isolating these problems and getting the facility back in an operational status.

4.3 TESTS

The actual testing can be the shortest and most straight forward phase of the overall program as compared to the pretest and preparation or the post test analysis. However, this can be the phase which receives the most visibility. Often user representatives, management personnel, and contractor employees are present and their impressions of what they observe during this time forms the basis of their lasting memories of the

program. A deliberate professionally executed program which follows established procedures will provide a positive image and result in a safe and successful test program.

4.3.1 Test Plan

As a result of the pretest planning discussed in the previous section and the preliminary tests discussed above the test engineer is in a position to provide the operations crew with a test plan. This plan can be informal, but should include the information required by the crew to effectively and efficiently conduct the test. For example it should include:

1. proposed test matrix, i.e.
   a. expected velocities, number of shots
   b. launcher information, propellant, charge conditions, etc.

2. facility configuration, i.e.
   a. portable catcher requirement
   b. freon tube requirement, charge weight
   c. sabot stripper

3. instrumentation requirements, i.e.
   a. direct shadowgraph
   b. interferometry
   c. radar

4. any other information that is pertinent to the test program.

4.3.2 Documentation and Data Collection

The test engineer should ensure that the activities are adequately documented during the test process. Although much of this documentation has been computerized over the years personalized notes and observations can also be extremely valuable later when the trajectories are being analyzed. Also the information being recorded and saved in the computerized shot log must be checked for accuracy and completeness. An example of a daily computer log is shown as Fig. 4.4. As can be seen, shot date and time, facility atmospheric conditions, model measurements, launcher description, propellant type, and velocity achieved are all recorded. Some of this information, atmospheric conditions and model measurements, are passed to the image processing routine and subsequently used in the trajectory calculations. Immediately after the shot the hall and pit time information is recorded and also passed to the film reader routine. A sample print out of the time information is shown as Table 4.1 and will be discussed in more detail in Section V. The information in Fig. 4.4 and Table 4.1 and any notes the test engineer may have recorded along with all of the photographs, i.e. shadowgrams, direct photographs, holograms, etc., obtained represents the primary shot documentation during and immediately after the test.

```
***********************  ARF SHOT LOG  ******************************
SHOT NO: 95073104                               DATE: 7/31/95    TIME: 9:40
TITLE:  WAF/ISL
REMARKS:
*************************************************************************
TEMPS (deg F):    72.00  72.00  71.00  71.00  71.00  70.00  69.00  71.00
AIR PRESSURE:   1017.27 mb  TEMP:        21.60 deg C  REL HUMIDITY:      53.00 %
DENSITY:   1.201873 kg/m^3  VISC: 1.822x10^-5 N*s/m^2
*************************************************************************
MODEL NUM:          4
MODEL MASS:     86.000 gm  SABOT MASS:    490.500 gm  PACKAGE MASS:   576.500 gm
CG FROM NOSE:   59.120 mm  MODEL LENGTH:  114.355 mm  MODEL DIA:      18.954 mm
Ix :        45.9998 gm*cm^2  Iy:     879.4477 gm*cm^2  Iz:       879.4477 gm*cm^2
Ixy:        .      gm*cm^2
MODEL DESCRIPTION:         ALUMINIUM W/STEEL NOSE  THICK WAF
SABOT DESCRIPTION:         4 PIECE LEXAN W/ 2 PIECE POLY/STEEL PUSHER
*************************************************************************
GUN TYPE: 2.5IN        •  POWDER MASS:    400.00 gm  POWDER TYPE: GAU-8
GAS PRES:        .  psi  PISTON WT:        .  lb  BURST PR:          .   psi
EXPECTED V: 2200.00 ft/s  FREON:         0.00 gm  TWIST:          .  cal/rev
** RESULTS **************************************************************
V MUZZLE:   2063.62 ft/s  V MID:    1575.19 ft/s  V IMPACT:    1198.05 ft/s
MACH:          1.39       CD MID:     1.258
RE (DIA):   0.6003x10^6   RE (LTH):  3.6217x10^6
```

Figure 4.4 Example of Daily Shot Log Entry

All of the photographic results should be examined carefully by the test engineer to ensure that no damage occurred to the test item during the launching process. Generally speaking models that have been damaged in some way should be deleted from the analysis process. Retaining results obtained from damaged models could contaminate the final conclusions associated with the actual configuration of interest, (the undamaged models). Some test items are purposely altered during the launching process and the resulting data from such configurations are meaningful. For example, spin stabilized projectiles are designed to engage the rifling of the launch tube. Hence the rifling in the barrel cuts grooves into the projectile's rotating bands and frequently scores the cylindrical section of the projectile. Since this 'damage' is typical of the operational ammunition the data resulting from such trajectories are of importance. However, such variations from model to model may not be totally consistent and the final aerodynamic coefficients and derivatives may exhibit more apparent scatter than would have otherwise occurred for a saboted model.

Another problem the test engineer should be alert to is possible reflected shock waves off the walls of the facility. These can be evident for models which decelerate through Mach 1 during their flight. At this condition the near normal bow shock can reflect off the walls of the facility and impinge on the model. This reflected shock can then add an impulse to the model's motion. Such trajectories should then be treated as two separate flights. The first limited to that portion of the flight prior to the impingement of the reflected shock and the second after the impingement of the reflected shock. As will be discussed in Section V the shadowgraph images are digitized and the experimentally measured trajectories computed using the CADRA[4.7] system.

Table 4.1

Sample Hall and Pit Time Printout

AEROBALLISTIC RESEARCH FACILITY
SHOT NUMBER: 91 5 650   TIME: 12:17   DATE: 6/ 5/91   VMUZ: 7049.76   VMID: 4042.51   VIMP: 1720.45
MODEL DESCRIPTION: HART MODEL 13 850GRS 3331 4Kdg. 400 psi HEM. LLG 3

STATION NUMBER	DELAY TIME	HALL TIME	PIT TIME	F 1	RAW VELOCITY	F 2	SMOOTHED VELOCITY	DRAG COEF
1	0.01	247294.6	247293.5	*	0.00	*	6707.16	4.888
2	0.01	248130.3	248190.7	*	5770.65	*	6670.49	4.915
3	0.01	248965.3	248967.0	*	6206.18	*	6633.82	4.942
4	0.01	250609.7	250608.0	*	6075.35	*	6560.62	4.997
5	0.01	253944.7	253948.6	*	5991.98	*	6413.93	5.112
6	0.01	255616.6	255631.2	*	5962.14	*	6340.59	5.171
7	0.01	257274.0	257273.5		6012.66	*	6267.83	5.231
8	0.21	258108.8	258110.7	*	6375.60	*	6228.73	5.264
9	0.01	258946.2	258947.5	*	5769.90	*	6193.31	5.294
10	0.01	262288.6	262289.7	*	6007.86		6046.03	5.423
11	0.01	265674.5	265690.0	*	5967.98	*	5897.51	5.559
12	0.01	267336.5	267335.4	*	5944.24	*	5825.41	5.628
13	0.01	269054.8	269031.8	*	5903.85	*	5751.48	5.700
14	0.01	270741.1	270741.8		5841.68	*	5678.72	5.773
15	0.01	271575.4	271605.7	*	5888.63	*	5642.05	5.811
16	0.01	275017.8	275017.8		5858.90	*	5494.77	5.967
17	0.01	276755.6	276756.6		5850.61	*	5420.18	6.049
18	0.01	277639.0	277637.6	*	5622.28	*	5383.80	6.090
19	0.01	282186.5	282185.8		5459.71	*	5201.69	6.303
20	0.01	283969.3	283966.5	*	5567.56	*	5128.93	6.392
21	0.01	285888.2	285906.2	*	5141.82	*	5056.17	6.484
22	0.01	287788.7	287823.2	*	5197.12	*	4983.41	6.579
23	0.01	289710.5	289707.1	*	5344.59	*	4908.82	6.679
24	0.01	291711.5	291711.3		4908.60	*	4836.72	6.778
25	0.01	293765.9	293764.8	*	4946.55	*	4762.20	6.884
26	0.01	294795.6	294795.4		5009.03	*	4724.36	6.940
27	0.01	297984.2	297980.2	*	4653.77		4615.59	7.103
28	0.01	301312.2	301314.2	*	4503.12		4505.57	7.277
29	0.01	304699.0	304700.4	*	4452.95		4394.97	7.460
30	0.01	308370.9	308370.9		4132.16	*	4283.70	7.653
31	0.01	312144.7	312143.4	*	3975.47	*	4173.69	7.855
32	0.01	320111.5	320114.2	*	3827.43	*	3949.98	8.300
33	0.01	324345.1	324344.2		3525.69	*	3840.55	8.537
34	0.01	328718.5	328718.4		3294.61	*	3734.86	8.778
35	0.01	333310.7	333312.7	*	3187.30	*	3627.49	9.038
36	0.01	338131.1	338176.2	*	3004.98	*	3520.77	9.312
37	0.01	342777.0	342773.6	*	3351.61		3407.16	9.622
38	0.01	348229.5	348219.0	*	2758.33	*	3296.92	9.944
39	0.01	353571.1	353544.7	*	2817.96	*	3186.68	10.288
40	0.01	359061.1	359061.1		2716.60	*	3077.03	10.655
41	0.01	364737.1	364736.2		2646.44	*	2966.87	11.050
42	0.01	370633.5	370635.1	*	2545.10	*	2856.78	11.476
43	0.01	376743.7	376734.5	*	2448.88	*	2747.13	11.934
44	0.01	382747.3	382731.6	*	2501.52	*	2637.04	12.433
45	0.01	393754.9	99999.0	*	2267.53	*	2453.97	13.360
46	0.01	400465.0	400465.0		2244.39	*	2343.51	13.990
47	16.65	407286.6	407278.7	*	2198.70	*	2233.57	14.678
48	0.01	448197.0	448187.9	*	366.17	*	2123.70	15.438
49	0.01	99999.0	450502.5	*	6446.07	*	2014.27	16.276
50	0.12	429170.0	429189.7	*	0.00	*	1903.81	17.221

STA NO	5	10	15	20	25	30	35	40	AVE
TEMP	21.67	21.67	22.22	21.67	21.67	21.67	21.67	21.11	21.67

DIAMETER	MASS	REL HUM	BARO PRES	VEL TOL	SLOPE	INTERCEPT	COEF DRAG
0.3330	45.89	46.00	1019.30	100.000	-7.334	6707.16	8.110

Note: Stations at the far end of the range will take up to 3.3 micro sec's
longer to receive the common start pulse. This time delay has been
measured at each station and is compensated for in the data reduction.

When tests are accomplished in/on a facility which does not use a daily shot log of some type the test engineer is primarily responsible for documenting the process and maintaining an adequate record of the test. This can be the situation for some outdoor test environments; but, even here a standardized record should be maintained covering the equivalent information that is shown in Fig. 4.4. The importance of documentation can not be over stated because a lack of an adequate record can result in useless shots requiring repeat firings wasting resources and manpower.

REFERENCES

4.1 Buckley, P.R., et al, " Air Force Armament Laboratory Technical Facilities / Capabilities", AFATL-TR-85-55, September 1985.

4.2 Mayer, P.C., and Winchenbach, G.L., " Free Flight Range Tests of a High Density Armor Piercing Flechette Utilizing Yaw Cards", AFATL-TR-74-73, April 1974.

4.3 Whyte, R.H., Steinhoff, M., Siewert, J., and Hathaway, W.H., " Recent Experience in the Extraction of Aeroballistic Performance from Doppler Radar Data", paper presented at the 46th Meeting of the Aeroballistic Range Association, Minnetonka, Minn, September 1995.

4.4 West, K.O., " Yaw Card Range Test of a 30mm Frangible TP Projectile", AFATL-TR-76-5, January 1976.

4.5 Winchenbach, G.L. and West, K.O.," Free-Flight Range Test of the MK84, GBU-15 Cruciform Wing Weapon (CWW) at Mach Numbers of 0.5 to 1.2", AFATL-TR-78-85, March 1978.

4.6 Heinrici, U., and Winchenbach, G.L., " Description and Comparison of Photographic Instrumentation Systems Used in Some Free Flight Ranges", paper presented at the 32nd Meeting of the Aeroballistic Range Association, Karlsburg, Sweden, August 1981.

4.7 Yates, L.A., Chapman, G.T., and Row, Chang-Shik, "CADRA: A Comprehensive Aerodynamic Data Reduction System for Aeroballistic Ranges", paper presented at the 47th Meeting of the Aeroballistic Range Association, Saint Louis, France, October 1996.

V. TRAJECTORY DETERMINATION

5.1 IMAGE ANALYSIS

As the model travels downrange it passes the photographic stations and orthogonal images are obtained at each station as was illustrated in Fig.1.2. Each camera records the shadow of the model on the reflective screen as cast by the light from the associated spark units. Each image also includes the facility's reference wires and beads as shown in the typical shadowgraph of Fig. 5.1. At the present time film cameras are used as the primary recording medium and the time of flight, shot and station identification are also included on the film format as shown in Fig. 5.1. Recently the microdensitometer previously used to read the film, Ref. 5.1, has been replaced with the film scanner and image processing system shown in Fig. 5.2. Using this system the film images are scanned and the points of interest on each image are numerically coded and the range coordinates computed. Once the film images are digitized using the Ektron model 1412 digital imaging camera the digital image is then processed so that only the area of interest (projectile and reference beads) need be saved. The image processing and storage are then accomplished using a Macintosh Quadra 800 computer and peripherals with the CADRA interactive software system. The film scanning and CADRA system is described in detail in Ref. 5.2. Once the images are scanned and saved they may be retrieved as required for the actual film reading.

It is planned to replace the film cameras with solid state CCD cameras in the near future[5.3,5.4]. This plan calls for cameras with 1k x 1k pixel arrays in the up-range end of the ARF and 2k x 2k pixel arrays in the downrange portion of the facility. It is expected that some of these cameras will be installed during 1997 but that it will require several years to completely outfit the facility. Once this upgrade has been accomplished the digitized images will be transferred directly to the CADRA system for analysis and the film processing and film scanning will be bypassed. At present the film processing generally requires waiting overnight to see the film from the previous day's testing. Whereas the film scanning requires about 2 hours for a full range flight. This upgrade will therefore enable the test engineer to have access to the experimentally measured trajectories for analysis shortly after the launch, certainly on the same day.

Although the pixel arrays do not provide equal image resolution as film, the technique used in processing the electronically stored images utilizes the complete image in contrast to the previous film method where only specific points on the model's shadow were determined, i.e., nose, corners of the base, and spin pin. Both techniques require locating the reference beads since these represent the facility's axis system. As a result of utilizing
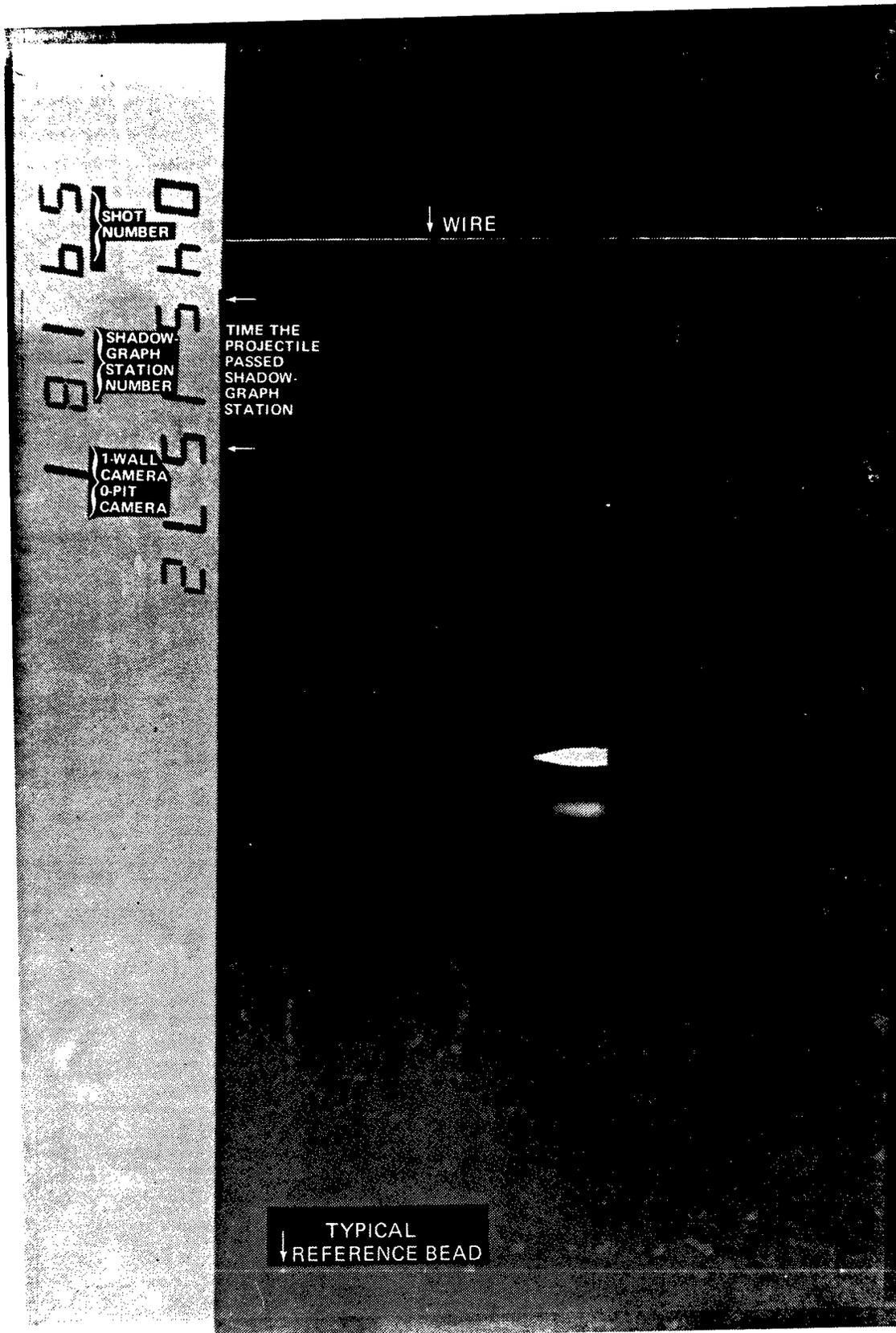
Figure 5.1 Typical Shadowgraph

58
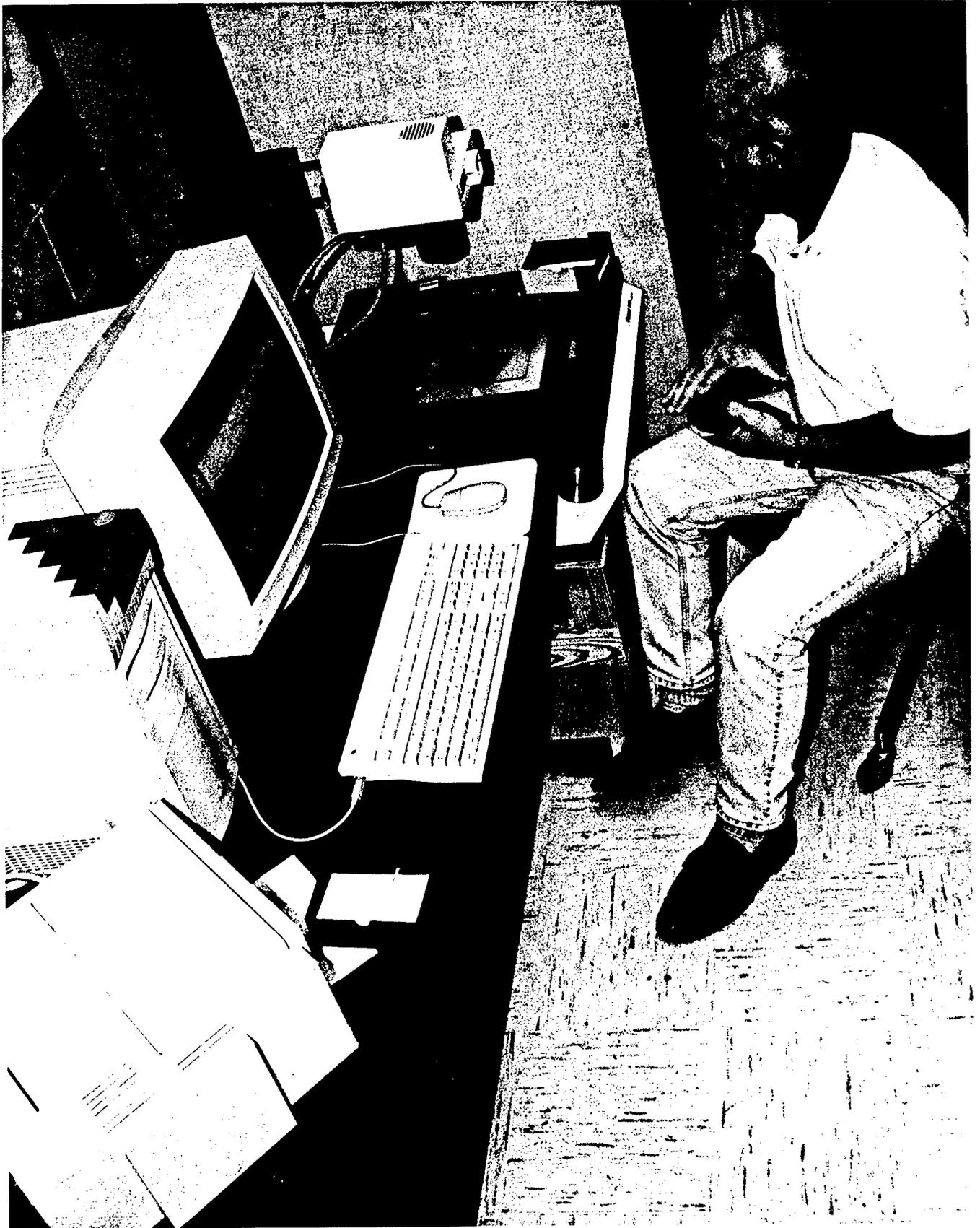
Figure 5.2 Film Scanner and Image Processing System

the complete image the precision to which the model's positions and attitudes are determined has actually increased even though the image resolution has decreased. This technique is illustrated using the following idealized sketch of a typical shadowgram.
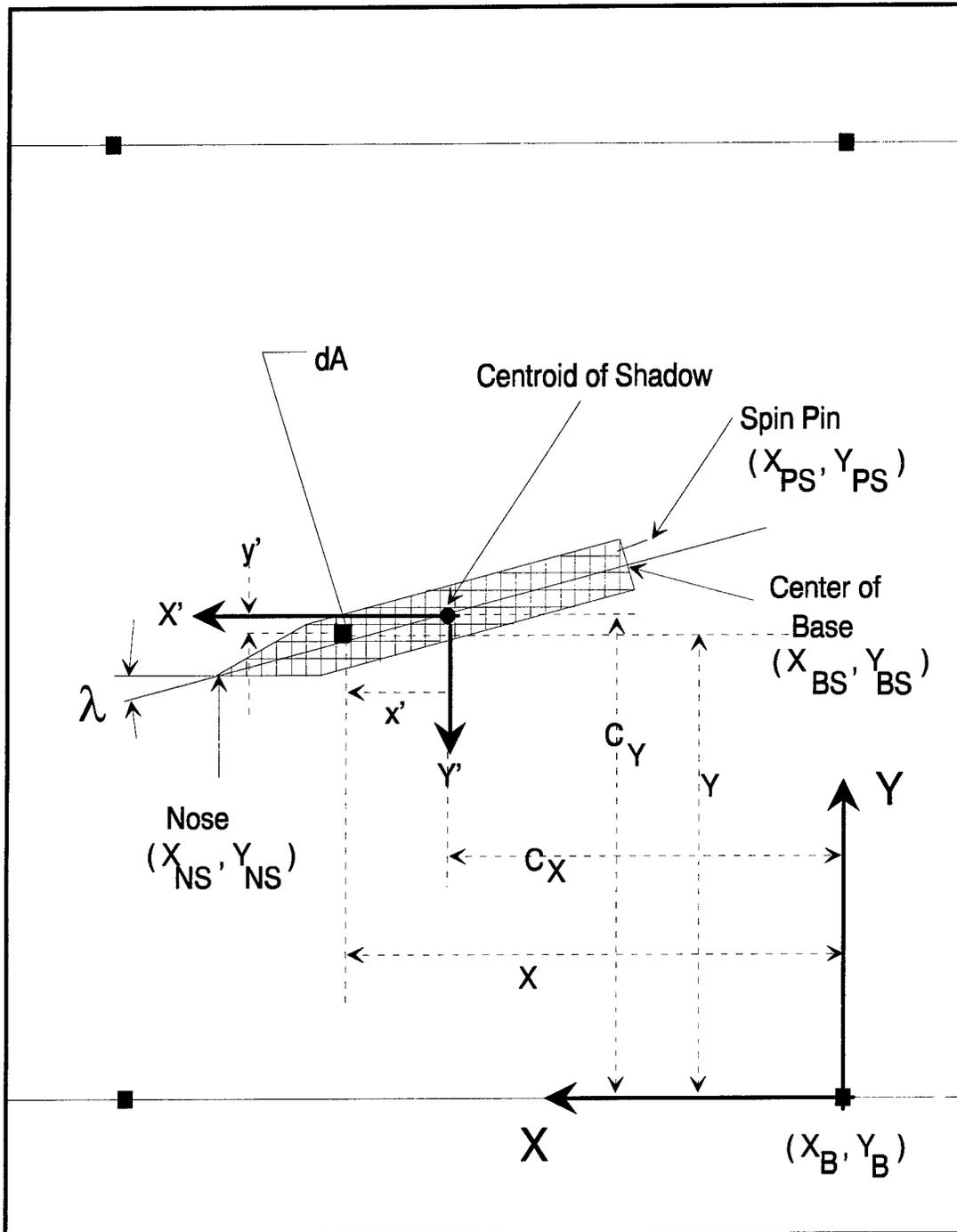
Figure 5.3 Idealized Sketch of a Typical Shadowgram

The equations for the centroid of the shadow are given by:

$$C_X = \frac{\int x\, f_n\, dA}{\int f_n\, dA} = \frac{\sum_0^N x\, f_n\, \Delta A}{\sum_0^N f_n\, \Delta A}$$

and

$$C_Y = \frac{\int y\, f_n\, dA}{\int f_n\, dA} = \frac{\sum_0^N y\, f_n\, \Delta A}{\sum_0^N f_n\, \Delta A}$$

$$\left. \right\} \quad 5.1$$

Where:

ΔA = area of one pixel

f_n = fraction of each pixel area filled by the model shadow

N = number of pixels in the shadow

Once the centroid of the shadow has been determined the angle λ can be computed by finding the axis for which the second moment of inertia of the shadow area is a minimum. Or,

$$\tan 2\lambda = -2\, I_{xys} / (\, I_{xs} - I_{ys}\,) \qquad\qquad 5.2$$

where,

$$I_{ys} = \int x'^2\, dA = \sum_1^N x'^2\, \Delta A$$

$$I_{xs} = \int y'^2\, dA = \sum_1^N y'^2\, \Delta A$$

$$I_{xys} = \int y'\, x'\, dA = \sum_1^N y'\, x'\, \Delta A$$

All that remains is to calculate the x,y coordinates of the nose and the center of the base. Both of these points lie on the line defined by the centroid and the angle λ and can be located by scanning along this line until the gray scale levels change rapidly indicating the limits of the projectile shadow. A more complete description of this technique can be found in Ref. 5.3.

5.2 POSITION AND ATTITUDE MEASUREMENTS

In order to calculate the model's position and attitude in space it is necessary to convert the planar measurements obtained from the images and discussed in the previous section to the three-dimensional geometry of the facility. This process will be described for a typical shadowgraph station as illustrated in Fig. 5.4. In this figure it should be recognized that the reference bead coordinates (X_{Bi} , Y_{Bi} , Z_{Bi}) and the spark gap locations (X_i , Y_i , Z_i) where i = H, P referring to the hall and pit planes respectively are known from calibrating the range as was discussed in Section 3.5.3 and Appendix 2.
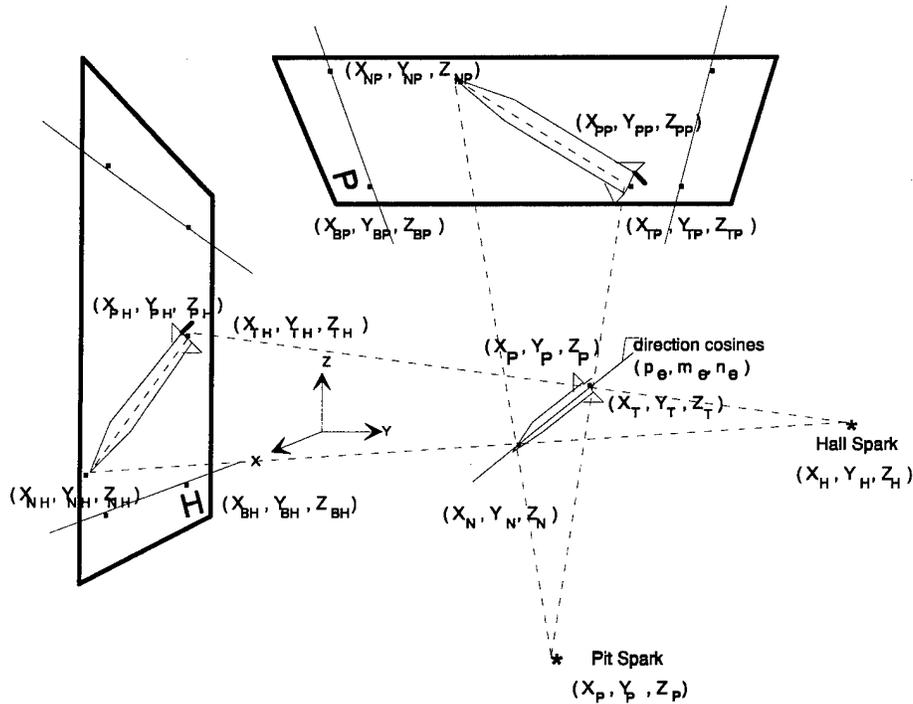
Figure 5.4 Projectile Attitude / Positioning Scheme

The three dimensional range coordinates of the model's shadow can be related to the image measurements of the previous section using the relationships shown in Table 5.1. Note that the hall screens are approximately 0.25 inches behind the beads on the reference system wires. Since the reference wires define the zero Y coordinate the range Y coordinate for all shadows on the hall screen are -0.25 inch. Since the overhead screen is about 0.25 inch above the beads the Z coordinates of all the overhead shadows are Z_i + 0.25.

Table 5.1
Relationship Between Film / Image and Range Coordinates

Point	Hall Image		Pit Image	
	Film / Image Coordinarte	Range Coordinate	Film / Image Coordinate	Range Coordinate
Reference Bead	X_B	X_{BH}	X_B	X_{BP}
	Y_B	Z_{BH}	Y_B	Y_{BP}
		$Y_{BH} = 0$		Z_{BP}
Nose	X_{NS}	X_{NH}	X_{NS}	X_{NP}
	Y_{NS}	Z_{NH}	Y_{NS}	Y_{NP}
		$Y_{NH} = -0.25$		$Z_{NP} + 0.25$
Center of Base	X_{TS}	X_{TH}	X_{TS}	X_{TP}
	Y_{TS}	Z_{TH}	Y_{TS}	Y_{TP}
		$Y_{TH} = -0.25$		$Z_{TP} + 0.25$
Spin Pin	X_{PS}	X_{PH}	X_{PS}	X_{PP}
	Y_{PS}	Z_{PH}	Y_{PS}	Y_{PP}
		$Y_{PH} = -0.25$		$Z_{PP} + 0.25$

Note that the hall screens are approximately 0.25 inchs behind the beads on the reference system wires. Since the reference wires define the zero y coordinate the range y coordinate for all shadows on the hall screens are -0.25 inch. Also note that the overhead screens are approximately 0.25 inch above the overhead reference wire.

5.2.1 Direction Cosines

The mathematical process of determining the direction cosines (m_e, n_e, p_e) of the model's principal axis becomes a problem of determining the intersection of two planes. These two planes are defined as shown in Fig. 5.4 or, plane 1 is specified by the hall spark location and the centerline of the model's shadow on the wall reflective screen (H screen in Fig. 5.4). Plane 2 is specified by the pit spark location and the centerline of the model's shadow on the ceiling reflective screen (P screen in Fig 5.4). It is assumed that the centerline of the model's shadow represents the projection of the model's principal axis on the reflective screens. For asymmetric configurations or even symmetric shapes that may project a shadow which is asymmetric, i.e. a missile with three fins, a template matching technique has been developed and is discussed in Ref. 5.2. Essentially that technique computes how the shadow of the model should appear on the reflective screens at various pitch, yaw and roll angles until the computed shadow matches the images obtained from the shadowgrams. However, for the illustrative discussion herein we will

assume a symmetrical shadow projection. It should also be noted that there are other methods of determining the direction cosines of the model's principal axis but the method of intersecting planes utilizes the model's complete shadow in identifying the angle λ as defined in Eq. 5.2.

The general equation for a plane can be written as,

$$PX + QY + RZ = 1 \qquad\qquad 5.3$$

where P, Q, R are the direction numbers of a line normal to the plane. If we apply Eq.5.3 to the plane associated with the horizontal plane (H screen) then using the nomenclature in Fig. 5.4 we can write the three relations below:

$$\left.\begin{array}{l} P_H X_{NH} + Q_H Y_{NH} + R_H Z_{NH} = 1 \\ P_H X_{TH} + Q_H Y_{TH} + R_H Z_{TH} = 1 \\ P_H X_H \;\; + Q_H Y_H \;\; + R_H Z_H \;\; = 1 \end{array}\right\} \quad 5.4$$

Equations 5.4 may be solved for P_H, Q_H, and R_H and written in matrix form as:

$$\begin{bmatrix} P_H \\ Q_H \\ R_H \end{bmatrix} = \begin{bmatrix} X_{NH} & Y_{NH} & Z_{NH} \\ X_{TH} & Y_{TH} & Z_{TH} \\ X_H & Y_H & Z_H \end{bmatrix}^{-1} \begin{bmatrix} 1 \\ 1 \\ 1 \end{bmatrix} \qquad 5.5$$

If we apply Eq. 5.3 to the vertical plane (P screen) then we can similarly write:

$$\begin{bmatrix} P_P \\ Q_P \\ R_P \end{bmatrix} = \begin{bmatrix} X_{NP} & Y_{NP} & Z_{NP} \\ X_{TP} & Y_{TP} & Z_{TP} \\ X_P & Y_P & Z_P \end{bmatrix}^{-1} \begin{bmatrix} 1 \\ 1 \\ 1 \end{bmatrix} \qquad 5.6$$

and solve for P_P, Q_P, and R_P.

Once the two planes are defined we need to find the line that is common to both planes. This line represents the principal axis of the model. To accomplish this we will define two points that lie on this line as (X_1, Y_1, Z_1) and (X_2, Y_2, Z_2). Then using Eq. 5.4 we can further write:

$$Q_H Y_1 + R_H Z_1 = 1 - P_H X_1$$
$$Q_P Y_1 + R_P Z_1 = 1 - P_P X_1 \qquad\qquad 5.7$$

$$Q_H Y_2 + R_H Z_2 = 1 - P_H X_2$$
$$Q_P Y_2 + R_P Z_2 = 1 - P_P X_2 \qquad\qquad 5.8$$

If we solve the two 5.7 equations for Y_1 , set equal and then solve for Z_1 we can obtain after some manipulation,

$$Z_1 = [(1 - P_P X_1)Q_H - (1 - P_H X_1)Q_P] / (Q_H R_P - Q_P R_H) \qquad 5.9$$

64

Now if we solve the two 5.7 equations for Z_1, set equal and solve for Y_1 we can similarly arrive at,

$$Y_1 = [(1 - P_H X_1)R_P - (1 - P_P X_1)R_H] / (Q_H R_P - Q_P R_H) \qquad 5.10$$

Duplicating these derivations for Eqs. 5.8 we get,

$$Z_2 = [(1 - P_P X_2)Q_H - (1 - P_H X_2)Q_P] / (Q_H R_P - Q_P R_H) \qquad 5.11$$

and

$$Y_2 = [(1 - P_H X_2)R_P - (1 - P_P X_2)R_H] / (Q_H R_P - Q_P R_H) \qquad 5.12$$

Substituting Eqs. 5.9 through 5.12 into the definitions of the direction numbers, m_n, n_n, and p_n (Eqs. 5.13),

$$\left. \begin{array}{l} m_n = Y_2 - Y_1 \\ n_n = Z_2 - Z_1 \\ p_n = X_2 - X_1 \end{array} \right\} \quad 5.13$$

one arrives at, after some manipulation, the relations for the direction numbers shown below.

$$m_n = - p_n [(R_P P_H - R_H P_P) / (Q_H R_P - Q_P R_H)]$$
$$n_n = - p_n [(Q_H P_P - Q_P P_H) / (Q_H R_P - Q_P R_H)]$$

If we selectively choose the two points lying on this line of intersection such that $X_2 - X_1 = 1$, or $p_n = 1$, then the direction cosines of the models principal axis is,

$$\left. \begin{array}{l} m_e = m_n / D_e \\ n_e = n_n / D_e \\ p_e = 1 / D_e \end{array} \right\} \quad 5.14$$

where

$$D_e \equiv (1 + m_n^2 + n_n^2)^{1/2}$$

Equations 5.14 are used to compute the direction cosines of the model's principal axis at each shadowgraph station after the model has traversed the instrumented range. It should be recognized that by selectively choosing the two points such that $X_2 - X_1 = 1$ we have assumed that the model's angle of attack will never be greater than 90 degrees or that the model can not tumble. This assumption has never been a problem in the past. However, if in the future a model is launched 'backwards' in order to obtain very high angle of attack data then this assumption might have to be removed from the derivation. The geometric principles used in this and the following derivations have been extracted from various text books, see for example Ref.5.5.

65

5.2.2 Position

Now that we have the projectile's orientation defined we need to determine the range coordinates of the projectile. For discussion purposes we will select the nose tip of the projectile as the point that we will determine. However, it should be understood that the method described can be used to determine the range coordinates of any point on the projectile including the spin pin or the centroid of the shadow as defined in Section 5.1. The range coordinates of the projectile's nose (X_N, Y_N, Z_N) are defined as the nearest point of intersection of the two lines connecting the hall spark coordinates (X_H, Y_H, Z_H) and the shadow of the nose on the hall screen (X_{NH}, Y_{NH}, Z_{NH}) and the pit spark location (X_P, Y_P, Z_P)and the shadow of the nose on the overhead screen (X_{NP}, Y_{NP}, Z_{NP}), see Fig. 5.4. Recognize that there is a point on each of these lines, (X_i ,Y_i , Z_i) where i = 1,2 respectively, such that the distance between these two lines is a minimum.

Using the general equation for a straight line, the following relationships can be written:

$$\frac{X_1 - X_H}{X_{NH} - X_H} = \frac{Y_1 - Y_H}{Y_{NH} - Y_H} = \frac{Z_1 - Z_H}{Z_{NH} - Z_H} \qquad 5.15$$

and

$$\frac{X_2 - X_P}{X_{NP} - X_P} = \frac{Y_2 - Y_P}{Y_{NP} - Y_P} = \frac{Z_2 - Z_P}{Z_{NP} - Z_P} \qquad 5.16$$

The distance between points 1 and 2 is defined as,

$$d = [(X_2 - X_1)^2 + (Y_2 - Y_1)^2 + (Z_2 - Z_1)^2]^{1/2} \qquad 5.17$$

If we let,

$$X_{NH} - X_H = A_1 \quad , \quad Y_{NH} - Y_H = B_1 \quad , \quad Z_{NH} - Z_H = C_1$$

and,

$$X_{NP} - X_P = A_2 \quad , \quad Y_{NP} - Y_P = B_2 \quad , \quad Z_{NP} - Z_P = C_2$$

Then Eqs. 5.15 and 5.16 can be rewritten as shown below:

$$\frac{X_1 - X_H}{A_1} = \frac{Y_1 - Y_H}{B_1} = \frac{Z_1 - Z_H}{C_1} \qquad 5.18$$

and

$$\frac{X_2 - X_P}{A_2} = \frac{Y_2 - Y_P}{B_2} = \frac{Z_2 - Z_P}{C_2} \qquad 5.19$$

Solving Eqs. 5.18 for Y_1 yields,

$$(X_1 - X_H) B_1 = (Y_1 - Y_H) A_1 \Rightarrow Y_1 = (B_1/ A_1) X_1 - D_1/ A_1 \qquad 5.20$$

where,
$$D_1 \equiv X_H B_1 - Y_H A_1$$

Similarly solving for Y_2, Eq. 5.19, one arrives at:
$$Y_2 = (B_2 / A_2) X_2 - D_2 / A_2 \; ; \; \text{where,} \; D_2 \equiv X_P B_2 - Y_P A_2 \qquad 5.21$$

Subtracting Eq. 5.20 from 5.21 we then get,
$$Y_2 - Y_1 = (B_2 / A_2) X_2 - (B_1 / A_1) X_1 + K \; ; \; \text{where,} \; K \equiv D_1 / A_1 - D_2 / A_2 \qquad 5.22$$

Following the same logic as outlined above, relations for Z_1, Z_2 and $Z_2 - Z_1$ can also be derived from Eqs. 5.18 and 5.19. The resulting equations are listed below:
$$Z_1 = (C_1 / A_1) X_1 - E_1 / A_1 \; ; \; \text{where,} \; E_1 \equiv X_H C_1 - Z_H A_1 \qquad 5.23$$
$$Z_2 = (C_2 / A_2) X_2 - E_2 / A_2 \; ; \; \text{where,} \; E_2 \equiv X_P C_2 - Z_P A_2 \qquad 5.24$$
$$Z_2 - Z_1 = (C_2 / A_2) X_2 - (C_1 / A_1) X_1 + L \; ; \; \text{where,} \; L \equiv E_1 / A_1 - E_2 / A_2 \qquad 5.25$$

Substituting Eqs. 5.22 and 5.25 into Eq. 5.17 the distance d can be expressed as
$$d = \{(X_2 - X_1)^2 + [(B_2/A_2)X_2 - (B_1/A_1)X_1 + K]^2 + [(C_2/A_2)X_2 - (C_1/A_1)X_1 + L]^2\}^{1/2} \qquad 5.26$$

Now if we expand the terms in Eq. 5.26, collect like terms, take the partial derivatives of d with respect to both X_1 and X_2, set these partial derivatives equal to zero, we can arrive at the two relations shown below:
$$H X_1 - J X_2 - G = 0 \qquad 5.27$$
$$M X_2 - J X_1 + S = 0 \qquad 5.28$$
where,

$$H = 1 + (B_1/A_1)^2 + (C_1/A_1)^2$$
$$J = 1 + (B_2 B_1)/(A_2 A_1) + (C_2 C_1)/(A_2 A_1)$$
$$G = K(B_1/A_1) + L(C_1/A_1)$$
$$M = 1 + (B_2/A_2)^2 + (C_2/A_2)^2$$
$$S = K(B_2/A_2) + L(C_2/A_2)$$

Solving Eqs. 5.27 and 5.28 for X_2 and X_1 we arrive at:
$$X_2 = (SH - JG) / (J^2 - MH) \qquad 5.29$$
$$X_1 = (JX_2 + G) / H \qquad 5.30$$

Once we have determined X_2 and X_1 we can substitute these back into Eqs. 5.20, 5.21 and Eqs. 5.23, 5.24 to compute Y_1, Y_2 and Z_1, Z_2 respectively. These are the coordinates of the two points on lines 1 and 2 which represent the closest point of intersection. We now assume that the range coordinates of the nose are halfway between the two points. Or
$$\left.\begin{array}{l} X_N = (X_2 - X_1) / 2 \\ Y_N = (Y_2 - Y_1) / 2 \\ Z_N = (Z_2 - Z_1) / 2 \end{array}\right\} \qquad 5.31$$

We can now compute the range coordinates of the model's nose, or any other point on the body of the projectile, in terms of the measured shadow coordinates and the calibrated spark gap and reference bead coordinates.

5.2.3 Roll Orientation

When measuring the roll orientation of a projectile in range coordinates it is usually necessary to modify the model in some manner. Normally this modification consists of inserting a reference point, i.e. spin pin, into the base of the projectile. This spin pin provides a radial reference location from which the model's roll orientation can be determined as will be demonstrated in this section. In order to minimize the roll measurement error the spin pin should be positioned radially as far from the center of the base (or model's centerline) as practical. Trailing edge fin tabs are sometimes used in place of spin pins on finned models because of this requirement. The error in the roll orientation measurements as a function of the distance (L) between the model's centerline and the spin pin is illustrated in Fig. 5.5.

$$\phi_E = \text{Arctan} \, (\, 2 \, E_M \, / \, L \,)$$

Assumes a position measuring accuracy (E_M) of 0.05 cm

(x-axis: L , Distance Between Center of Base and Spin Pin, cm)

(y-axis: ϕ_E , Error in Roll Orientation, Deg)
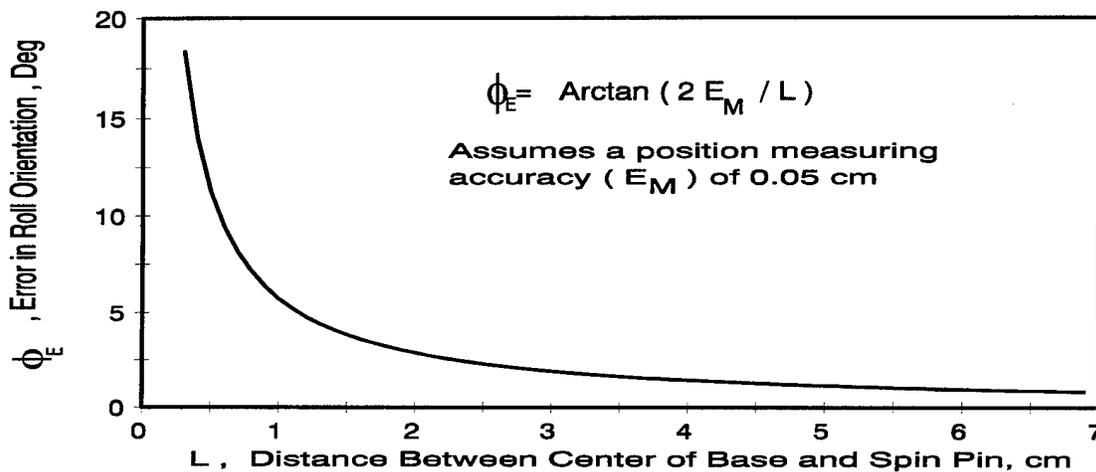
Figure 5.5   Accuracy of Roll Orientation Measurements

The curve shown in Fig. 5.5 represents a worst case scenario since it assumes a measurement error (E_M) of 0.05 cm in both the location of the spin pin and the center of the base. The centerline of the model is computed using the complete shadow image as discussed in Section 5.2; hence, the precision to which the range coordinates of the center of the base is determined is significantly better than that of locating a point. Nevertheless, the curve does demonstrate the importance of positioning the spin pin as far from the model's centerline as practical.

It should be noted that, in the past, frequently two spin pins were used in determining the roll orientation. Essentially the advantage of using two spin pins was to double L in the figure above. The disadvantage of using two spin pins was in identifying which pin was which. In order to expedite that identification, spin pins of differing diameters were employed. However, because of flow turbulence in the model's wake, trailing shock waves, etc. it was often difficult to correctly differentiate between the spin pins and large errors in the computed roll orientations resulted. Since the incorporation of CADRA[5.2] as the image processing system only one spin pin has been utilized and the technique of

determining the roll orientation using only one spin pin will be described herein. The process would be the same if two spin pins were used except the range coordinates of the center of the base would be replaced with the coordinates of the second pin.

The range coordinates of the spin pin and the center of the base are assumed to have been determined using the methods described in the previous sections. The coordinates of these two points are therefore:

$$(X_P , Y_P , Z_P) \equiv \text{Spin Pin}$$
$$(X_T , Y_T , Z_T) \equiv \text{Center of Base(Tail)}$$

The direction cosines of the vector connecting the spin pin with the center of the base are defined as shown below:

$$\left. \begin{array}{l} m_p = (Y_P - Y_T) / D_P = \cos \beta \\ n_p = (Z_P - Z_T) / D_P = \cos \gamma \\ p_p = (X_P - X_T) / D_P = \cos \mu \end{array} \right\} \quad 5.32$$

Where the distance between the pin and the centerline of the body is,

$$D_P = \sqrt{ (X_P - X_T)^2 + (Y_P - Y_T)^2 + (Z_P - Z_T)^2 }$$

and the angles β, μ, and γ are defined on the sketch below.

69
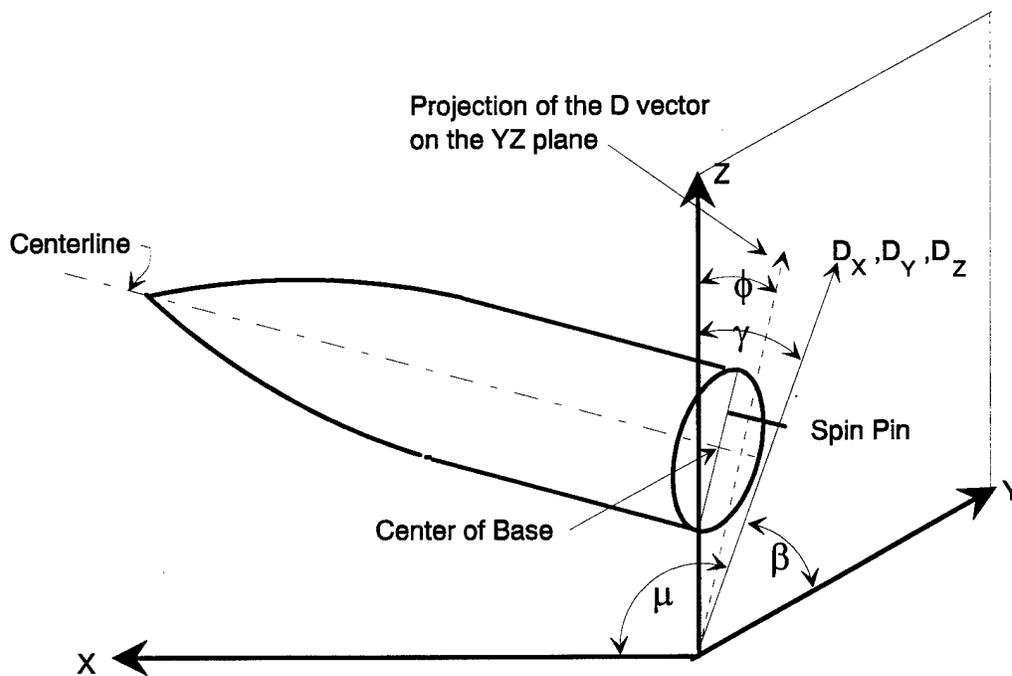
If we assume that the length of the D vector defined by the centerline of the body and the tip of the spin pin is unity, then the coordinates of the end point are D_X, D_Y, D_Z. Then the projection of the vector endpoints on the Y-Z plane is at X=0, $Y=D_Y$, and $Z=D_Z$. Where, $D_Y = \cos \beta = m_p$ and $D_Z = \cos \gamma = n_p$. The angle ϕ shown in the sketch is the angle of the D vector projected on the Y-Z plane. Then,

$$\tan \phi = D_Y / D_Z = m_p / n_p$$

or

$$\phi = \tan^{-1} (m_p / n_p) \qquad\qquad 5.33$$

Equation Eq. 5.33 is the relationship used to determine the model's roll orientation at each of the shadowgraph stations.

5.2.4 Center-of-Gravity

In Section 5.2.2 the model's nose was chosen to illustrate the method used to determine the range coordinates of specific points on the body. However, what the data reduction routines require are the range coordinates of the model's center-of -gravity. This is the point about which the equations of motion have been derived and therefore is the point for which the X,Y, Z position measurements are required. One of the pretest measurements as discussed in Section 3.5.1 was the distance, L_{cg}, between the nose and the center-of gravity of the model. This measurement in conjunction with the range coordinates of the nose as obtained using Eqs. 5.31 and the direction cosines from Eqs. 5.14 is used to compute the range coordinates of the model's center-of-gravity. These relationships are shown below:

$$
\left.
\begin{aligned}
X_{cg} &= X_N - L_{cg} (p_e) \\
Y_{cg} &= Y_N - L_{cg} (m_e) \\
Z_{cg} &= Z_N - L_{cg} (n_e)
\end{aligned}
\right\} \qquad 5.34
$$

The range coordinates of the model's center-of gravity, X_{cg}, Y_{cg}, Z_{cg}, are also determined at each shadowgraph station and provided to the data reduction routines for analysis of the aerodynamic coefficients and derivatives.

5.3 TIME OF FLIGHT MEASUREMENTS

The present chronograph system provides the required times of flight as the projectile traverses the instrumented range. Event times corresponding to each spark source discharge, hall and pit, are obtained to a resolution of ± 0.01 μsec by electronic chronographs at each of the 50 shadowgraph stations. The chronographs at each station operate under the control of the sequencer and in conjunction with the IR detection system and the spark gap assembly. The timing system in all chronographs is synchronized to a master 10 Mhz clock located in the control console. The sequencer provides the pulses listed below to the chronographs at the following times in the firing sequence:

      (1) -3.5 seconds, solenoid operated camera shutters open

(2) -2.0 seconds, clear (resets all chronograph counters to zero)

(3) -1.5 seconds, start (counters synchronized to master 10 Mhz clock)

(4) -1.0 seconds, fire (fire pulse sent to launcher)

(5) +3.5 seconds, solenoid operated camera shutters closed

(6) +10.5 seconds, strobe (accumulated times transferred and strobed on film)

When the projectile is detected in the vicinity of a shadowgraph station a 15-volt pulse initiates the discharge of the capacitor. A light sensing diode located inside each of the spark gap cavities senses the discharge and subsequently stops the chronographs for both the hall and pit counters. This results in the total elapsed time from when the common start pulse was sent to the arrival of the projectile at the shadowgraph station. A sample printout of the accumulated times for both the hall and pit cameras were shown previously, see Table 4.1. The hall and pit times are averaged to obtain the time of flight which is provided to the data reduction routines along with the position-attitude data as discussed in the preceding section.

Some of the other data that were listed in Table 4.1 should be mentioned. For example the raw velocity profile is computed using the averaged hall and pit times and the nominal distances between stations as listed in Appendix 1. This raw velocity profile is also 'fitted' using a polynomial least squares curve fit and the resulting smoothed velocity profile also shown. These velocity profiles are provided in order to assist the facility's operational crew and test engineer in an immediate evaluation of that particular flight and are not used in the final data analysis routines. Also included in Table 4.1 is a flag (F1) indicating whether or not the hall and pit times are within 1 μsec of each other. Variations in these times greater than 1 μsec should be examined by the operations crew and the appropriate adjustments made. The column of drag coefficients is determined from the smoothed velocity profile and is presented as a quick look evaluation mechanism and not as a final determination of the drag coefficient.

5.4 TRAJECTORY OUTPUT

The final trajectory data determined using the techniques previously discussed are provided to the aerodynamic data analysis routines as computed using CADRA[5.2]. A sample raw data file is shown as Table 5.2. The time of flight data were measured directly as discussed in the previous section where the time at the first station was subtracted from each of the following times yielding a time profile with zero time at the first station. The x,y,z position columns were obtained using Eqs. 5.34 and the roll orientation, ϕ, was computed from Eq. 5.33. The fixed plane angles are derived from the direction cosines, (m_e, n_e, p_e), as shown in Eqs. 5.14 and the fixed plane identities as listed in Section 2.4.1, see Eqs. 2.8. Or,

$$\sin \theta = -n_e \quad \text{and} \quad \sin \psi = m_e / (m_e^2 + p_e^2)^{1/2} \qquad 5.35$$

This now completes the methodology of determining the experimentally measured trajectories which are provided to the analysis routines for extraction of the aerodynamic parameters.

Table 5.2

Raw Trajectory Data From CADRA

950704 ISL/WAF
Range data file saved in S950704.xyz
Average Reynolds Number = 2050000;   Average Mach Number = 1.48

Station	time	V(m/sec)	x(m)	y(m)	z(m)	-sin(ψ)	sin(θ)	ϕ(°)
1	0.0000000	618.26	2.12497	1.41345	0.73105	0.10361	-0.15549	226.66
2	0.0025025	615.98	3.66820	1.41971	0.73672	-0.07315	-0.18116	181.90
3	0.0050034	613.71	5.20546	1.42374	0.73858	-0.19982	-0.07842	147.92
4	0.0099451	609.29	8.22347	1.42528	0.74674	-0.05133	0.18431	30.82
5	-0.2514225	0.00	14.28941	1.43166	0.77003	0.00278	-0.18781	151.52
6	0.0251753	596.05	17.39730	1.43791	0.77688	-0.17858	0.02295	342.49
7	0.0302340	591.78	20.39437	1.43961	0.78392	0.05431	0.17573	168.58
8	0.0328044	589.63	21.91187	1.43994	0.79007	0.16627	0.08201	92.74
9	0.0354859	587.41	23.48780	1.44302	0.79432	0.16190	-0.07419	341.13
10	0.0459116	578.93	29.55916	1.45214	0.81134	-0.11680	0.13258	345.73
11	0.0566330	570.45	35.70624	1.46220	0.82884	0.06102	-0.15324	286.38
12	0.0619041	566.37	38.69989	1.46673	0.83496	-0.16408	-0.01770	113.81
13	0.0673124	562.25	41.74600	1.47039	0.83913	0.01794	0.17214	285.94
14	0.0727530	558.17	44.79242	1.47272	0.84591	0.15227	-0.04873	88.69
15	0.0754616	556.15	46.30227	1.47567	0.85318	0.06332	-0.13776	357.28
16	0.0865332	548.07	52.40311	1.48547	0.86514	0.02475	0.15914	333.02
17	0.0921448	544.07	55.46419	1.48800	0.87129	0.15005	-0.04899	145.67
18	0.0949342	542.10	56.98063	1.49013	0.87708	0.03830	-0.10338	73.39
19	0.1091995	532.25	64.62859	1.49987	0.88627	0.15391	0.05611	296.69
20	0.1150409	528.32	67.72624	1.50745	0.89362	0.01094	-0.16405	145.54
21	0.1207103	524.56	70.71324	1.51155	0.89643	-0.12654	0.03632	339.91
22	0.1264541	520.80	73.71564	1.50739	0.90060	0.08501	0.12370	166.66
23	0.1323776	516.98	76.79142	1.52084	0.90080	0.08317	-0.10487	7.21
24	0.1382248	513.27	79.80318	1.52611	0.90757	-0.11228	-0.04451	210.44
25	0.1442620	509.49	82.89021	1.52940	0.90714	0.01446	0.14294	47.99
26	0.1472299	507.65	84.40366	1.52956	0.90960	0.12048	0.09482	333.54
27	0.1562597	502.14	88.96892	1.53878	0.91372	-0.08002	-0.09976	144.69
28	0.1654281	496.67	93.55601	1.54535	0.91592	0.06102	0.12929	295.23
29	0.1746733	491.27	98.13047	1.55271	0.91964	-0.00966	-0.12632	113.88
30	0.1840232	485.93	102.71127	1.55765	0.91537	-0.00296	0.12628	285.85
31	0.1935652	480.59	107.32884	1.56425	0.92208	0.03112	-0.12796	113.04
32	-0.0922876	0.00	0.00000	0.00000	0.00000	0.00000	0.00000	180.00
33	0.2225252	465.10	121.05094	1.58288	0.91885	-0.07198	0.12088	339.86
34	0.2322087	460.14	125.54861	1.59135	0.91409	0.11390	-0.09023	159.34
35	0.2422016	455.13	130.12985	1.59589	0.91235	-0.11643	0.07853	358.38
36	0.2524416	450.11	134.77364	1.60659	0.90783	0.13468	-0.08008	160.02
37	0.2625836	445.24	139.32494	1.61151	0.90246	-0.13006	0.07177	348.46
38	0.2726660	440.51	143.79599	1.61415	0.89701	0.15049	-0.05835	185.87
39	0.2832808	435.64	148.44504	1.62340	0.88753	-0.14166	0.06864	342.70
40	0.2938210	430.90	153.01378	1.62996	0.88074	0.16352	-0.07236	166.57
41	0.3045064	426.20	157.59068	1.63824	0.87054	-0.13382	0.08178	354.85
42	0.3153282	421.55	162.17097	1.64027	0.86018	0.15472	-0.09490	152.74
43	0.3263592	416.91	166.78352	1.64999	0.84774	-0.12224	0.12451	322.49
44	0.3374380	412.35	171.35765	1.65641	0.83529	0.12631	-0.12955	144.50
45	0.3561066	404.89	178.94235	1.66385	0.81138	0.18168	-0.01659	206.80
46	0.3675855	400.43	183.53200	1.67269	0.79490	-0.16948	0.05072	347.20
47	-0.4100693	0.00	0.00000	0.00000	0.00000	0.00000	0.00000	180.00
48	0.3906884	391.76	192.59471	1.68348	0.75577	-0.13874	0.12300	347.60
49	-0.0101338	0.00	0.00000	0.00000	0.00000	0.00000	0.00000	180.00
50	0.4147032	383.13	201.77632	1.69648	0.71092	-0.06531	0.17812	318.64

REFERENCES

5.1 Lucas, B.F., and Winchenbach, G.L., "An Advanced Reader for Free-Flight Spark Range Shadowgraph Film", paper presented at the 31st Meeting of the Aeroballistic Range Association, California Institute of Technology, 7-8 October 1980.

5.2 Yates, L.A.,"A Comprehensive Automated Aerodynamic Reduction System for Ballistic Ranges", WL-TR-96-7059, October 1996.

5.3 Holt, D.M., and Winchenbach, G.L.," An Electronic Shadowgraph Station and Control System", AIAA paper 88-2061 presented at the 15th Aerodynamic Testing Conference, 18- 20 May 1988, San Diego CA.

5.4 Winchenbach, G.L., et al, "An Electronic Imaging System for the Aeroballistic Research Facility", AIAA paper 92-3932 presented at the 17th Aerospace Ground Testing Conference, 6-8 July 1992, Nashville TN.

5.5 Middlemiss, R.R.,"Analytic Geometry", Mc Graw Book Company, Inc., NewYork and London, 1945.

(This page is blank)

74

VI. TRAJECTORY ANALYSIS

Trajectory analysis as referred to in free-flight testing is the process by which the aerodynamic coefficients and derivatives are obtained from the experimentally measured trajectory. This process consists of fitting the theoretical equations of motion to the experimental position-attitude-time measurements assuming that the aerodynamic coefficients and derivatives are unknowns in the process. There are various techniques that have been used to accomplish this process. The two techniques to be described herein are generally referred to as 'Linear Theory' and 'Numerical Integration'.

6.1 LINEAR THEORY

When Charters[1.1] first began to extract aerodynamic coefficients and derivatives from free-flight spark range data at BRL in the 1940's computer technology was in its infancy. This lack of computer power necessitated that the equations of motion be derived in a manner such that closed form solutions could be written from the differential equations. These closed form solutions were then used in the fitting process to determine the associated aerodynamics. In fact in those early days the fitting process usually consisted of analog computer techniques or frequently graphical methods of extracting the aerodynamics. In writing these closed form solutions it was necessary to make various assumptions which will be highlighted in the following sections. The two primary assumptions inherent in these derivations are symmetry and linear aerodynamics. Linear aerodynamics means that derivatives of the aerodynamic moment and force coefficients with respect to the angle-of-attack are constants, i.e., C_m vs α can be represented as a straight line. This assumption of linearity also means that small angles are usually assumed.

The various linear theory techniques discussed herein were developed by numerous individuals. However, the two people primarily associated with these techniques are Dr. Charles Murphy[6.1, 6.2] and Dr. John D. Nicolaides[6.3, 6.4]. Many of the derivations and much of the discussion in the following sections were extracted from these and other references, i.e., also see Refs. 6.5 and 6.6. These linear theory techniques provide insights into the free-flight dynamics that cannot be achieved using the complex numerical integration methods that will be discussed later in Section 6.3. Linear theory is also typically used to provide the initial estimates of the aerodynamic coefficients and derivatives required by the numerical integration methods. For many test configurations and conditions where the inherent assumptions, required in deriving the linear theory equations of motion, are not severely violated these techniques provide very accurate estimates of the resulting aerodynamics.

6.1.1 Drag

The total aerodynamic drag coefficient, C_D, is obtained from an analysis of the

distanced traveled, x, verses time measurements. The total drag coefficient is defined as $C_D = D / (1/2) \rho V^2 A$ and applying Newton's second law, $D = - m_a a$, the following relationship can be written:

$$C_D = - (2 m_a / \rho A V^2) a$$

Since the deceleration, a, can be expressed as $V (dV / dx)$ the above relationship becomes,

$$C_D = - (2 m_a / \rho AV) dV/dx \qquad\qquad 6.1$$

If the functional dependence between t and x is assumed to be a cubic polynomial, i.e.

$$t = c_0 + c_1 x + c_2 x^2 + c_3 x^3$$

then

$$(dt /dx) = (1/V) = c_1 + 2c_2 x + 3c_3 x^2 \qquad\qquad 6.2$$

and

$$(dV/dx) = - (2c_2 + 6c_3 x) / (c_1 + 2c_2 x + 3c_3 x^2)^2 \qquad\qquad 6.3$$

Substituting Eqs. 6.2 and 6.3 into Eq. 6.1 produces the following equation:

$$C_D = (2 m_a / \rho A) [(2c_2 + 6c_3 x) / (c_1 + 2c_2 x + 3c_3 x^2)] \qquad\qquad 6.4$$

Equation 6.4 is the common linear theory relationship used in computing the total drag coefficient. The process is to least squares fit the measured time and distance traveled data using the cubic polynomial as shown. Once the coefficients (c_i's) of the polynomial have been determined they are substituted into Eq. 6.4 and the C_D evaluated at the midrange x location.

Occasionally the analyst is provided velocity data in lieu of time vs distance. This can come from velocity screens where the Δt and Δx measurements are used to compute average velocities between screens. The total drag coefficient can be determined from these measurements using the familiar relation:

$$V = V_0 e^{-Kx} \qquad \text{where,} \quad K = C_D \rho A / 2 m_a \qquad\qquad 6.5$$

or,

$$\ln (V / V_0) = -Kx \qquad\qquad 6.6$$

Graphically this can be described as plotting V / V_0 on a log scale vs x (semi-log paper) and fitting the measurements with a straight line as shown on the following sketch.

x , distance
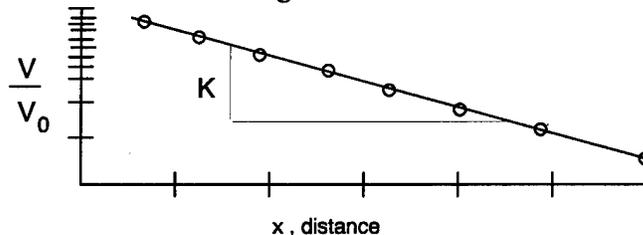
The slope of the straight line is K, see Eq. 6.6, thus $C_D = K (2 m_a / \rho A)$. The term "ballistic coefficient", β, is frequently used and this is generally defined as the projectile weight divided by $C_D A$, or

$$\beta = g m_a / C_D A$$

Equation 6.5 is frequently used in estimating the velocity of an object as a function of distance when the drag coefficient is assumed to be known. This relation provides

accurate velocity estimates even when relatively large distances are involved or large decelerations are present. For those cases where the velocity decay is small, less than 10 percent, Eq. 6.1 is frequently used directly. Historically Eq. 6.1 was used because of the simplicity of plotting velocity vs distance, drawing a straight line through the data, computing the slope of the line and calculating C_D assuming that $dV/dx = \Delta V/\Delta x$. This could be accomplished graphically with ease and precision even prior to the advent of computer technology, see sketch below.

x , distance
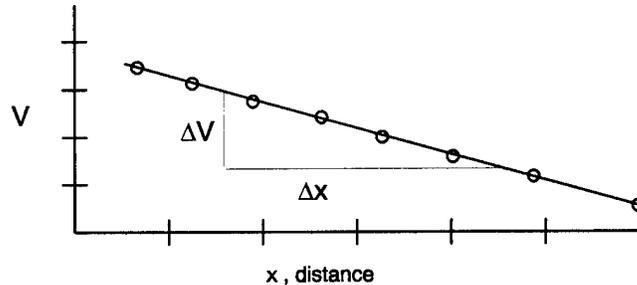
All of the techniques mentioned above result in the estimate of the total drag coefficient of the free-flight object. If that object is flying at a non-zero angle-of-attack, normally an oscillatory angular motion is present and possibly trimmed, then the measured C_D is affected (usually increased) by this non-zero angle-of-attack flight condition. This change in C_D caused by the object's angle-of-attack can be estimated and the total drag coefficient adjusted yielding the zero angle-of-attack drag coefficient, C_{D0}. This process will be described in Section 6.2.1.

6.1.2 Roll

The analysis of the missile's rolling motion is accomplished using the measured roll orientation, ϕ, and x data. Since the roll moment is defined as $C_l = l / (1/2) \rho V^2 A d$ and the rotational equivalent of Newton's second law is $l = I_x \ddot{\phi}$, it follows that:

$$I_x \ddot{\phi} = (1/2) \rho V^2 A d C_l \qquad 6.7$$

If we assume that C_l is comprised of a driving moment, due to fin cant, and a roll damping moment, caused by skin friction and the paddle wheel effect of the fins, then C_l can be expanded as,

$$C_l = \delta C_{l\delta} + (\dot{\phi} d / 2V) C_{lp} \qquad 6.8$$

Substituting Eq. 6.8 into 6.7 yields:

$$I_x \ddot{\phi} = (1/2) \rho V^2 A d [\delta C_{l\delta} + (\dot{\phi} d / 2V) C_{lp}] \qquad 6.9$$

Since we have both ϕ and time measurements a closed form solution to Eq. 6.9 could be written and in conjunction with a curve fitting process the unknown aerodynamic coefficients $C_{l\delta}$ and C_{lp} determined. This closed form solution would require assuming that the coefficients of the differential equation are constant. As a result of this assumption the velocity of the missile would also be assumed to be constant, or $C_D = 0$. This very restrictive assumption can be relaxed by changing the independent variable in

77

Eq. 6.9 from time to distance. This will permit the velocity to vary and hence C_D to be non-zero. Eventually however, we will be required to assume that C_D is a constant. Nevertheless, it is believed that this is a prudent change of variables and is accomplished as shown below. Since

$$\dot{\phi} = d\phi/dt = (d\phi/dx)(dx/dt) = V \phi'$$

then $\ddot{\phi}$ can be expressed as,

$$\ddot{\phi} = \phi'' V^2 + V' \dot{\phi}$$

Substituting the above relationships for $\dot{\phi}$ and $\ddot{\phi}$ along with V' as obtained from Eq. 6.1 into Eq. 6.9 and collecting like terms, one can arrive at the following differential equation:

$$\phi'' + K_p \phi' - K_\delta = 0 \qquad\qquad 6.10$$

where
$$K_p = -(\rho A/ 2m_a)[C_D + (d^2 m_a/ I_x) C_{lp}]$$

and
$$K_\delta = (\rho A d / 2I_x) \delta C_{l\delta}$$

Assuming that K_p and K_δ in Eq. 6.10 are constants, or C_D, C_{lp}, and $C_{l\delta}$ are constants, the two roots of the characteristic equation are zero and $- K_p$. The particular solution is $(K_\delta / K_p) x$ and after some manipulation the solution of Eq. 6.10 can be written as shown below:

$$\phi = \phi_0 + (K_\delta / K_p) x + C (e^{-K_p X} -1) \qquad\qquad 6.11$$

The unknowns in Eq. 6.11 which require determination are ϕ_0, K_δ, K_p and the constant C. Because K_p appears in a nonlinear fashion, the process of fitting the above equation to the measured ϕ and x data requires using a differential corrections technique. This is the same process used in fitting the oscillatory pitch and yaw motions, see Appendix 5. Historically this complexity was eliminated by approximating the $e^{-K_p X}$ term with the first four terms of the infinite series expansion, i.e.,

$$e^{-K_p X} = 1 - K_p x + (1/2) K_p^2 x^2 - (1/6) K_p^3 x^3$$

Substituting this expansion into Eq. 6.11 and collecting like terms, one arrives at the equation shown below:

$$\phi = \phi_0 + \phi_1 x + \phi_2 x^2 + \phi_3 x^3 \qquad\qquad 6.12$$

where,
$$\phi_1 = (K_\delta / K_p) - C K_p$$

$$\phi_2 = (1/2) C K_p^2$$

$$\phi_3 = -(1/6) C K_p^3$$

78

The unknown ϕ_i's in Eq. 6.12 can now be determined using a simple least squares fitting process. Then C_{lp} and $\delta C_{l\delta}$ are determined using the ϕ_1, ϕ_2, and ϕ_3 relations (Eqs. 6.12) in conjunction with the K_p and K_δ definitions (Eqs. 6.10) arriving at:

$$C_{lp} = (I_x / d^2 m_a)[(6 \phi_3 m_a / \phi_2 \rho A) - C_D]$$

and
$$\delta C_{l\delta} = (2I_x / \rho A d) [2 \phi_2 - (3 \phi_3 \phi_1/ \phi_2) \qquad\qquad 6.13$$

Both Eqs. 6.10 and 6.13 demonstrate that prior to computing the roll damping derivative, C_{lp}, the drag coefficient must be known.

6.1.3 Pitch and Yaw

The differential equation governing the angular oscillatory motion of a slightly asymmetric missile as a function of distance traveled has been rigorously derived in Refs. 6.1 to 6.4 and is not repeated herein. However, this differential equation is shown below:

$$(\beta + i\alpha)'' + (H - iP) (\beta + i\alpha)' - (M + iPT) (\beta + i\alpha) = iA_T\, e^{i\int p\,dx} \qquad 6.14$$

where
$$H = (\rho A/2m_a) [C_{N\alpha} - 2C_D - k_t^{-2}(C_{mq} + C_{m\dot\alpha})] \qquad\qquad 6.15$$

$$M = (\rho A/2m_a d) k_t^{-2} C_{m\alpha} \qquad\qquad 6.16$$

$$T = (\rho A/2m_a) [C_{N\alpha} - C_D + k_a^{-2} C_{np\alpha}] \qquad\qquad 6.17$$

$$P = (I_x / I_y) p \qquad\qquad 6.18$$

$$A_T = (\rho A/2m_a d) \{k_t^{-2}(C_{mo} + iC_{no}) + Pd[(I_x / I_y) -1](C_{Yo}+ iC_{Zo})\} \quad 6.19$$

Also k_a and k_t are the nondimensionized axial and transverse radiuses of gyration respectively, or

$$k_a = (I_x / m_a d^2)^{1/2} \quad\text{and}\quad k_t = (I_y / m_a d^2)^{1/2}$$

The closed form solution to Eq. 6.15 assuming that H, M, T, P, A_T and the roll rate, p, are all constant can be immediately written as shown below:

$$\beta + i\alpha = K_P \exp[(\mu_P + i\phi_P')x] + K_N \exp[(\mu_N + i\phi_N')x] + K_T \exp(ipx) \qquad 6.20$$

Equation 6.20 is frequently referred to as the 'tricyclic equation of motion' because it can be graphically represented by three rotating vectors in the complex $\beta + i\alpha$ plane, as illustrated in the sketch below.

sketch looking downrange
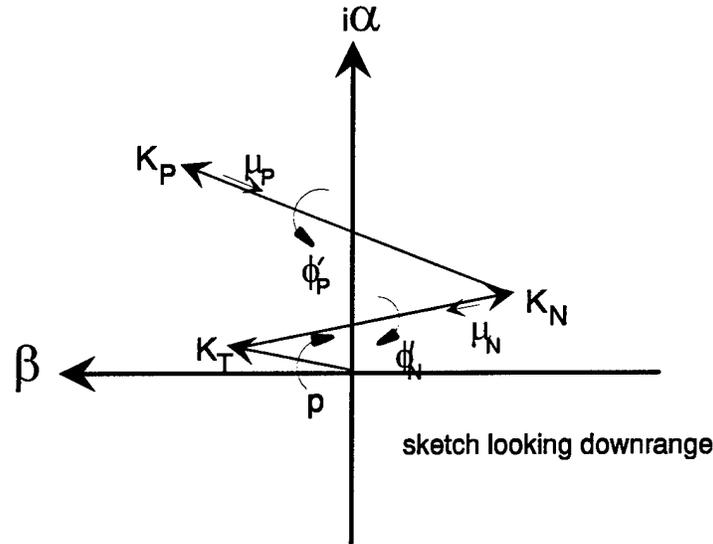
This sketch demonstrates that the trim vector, K_T, has a constant amplitude and rotates at the spin rate, p. The nutational vector, K_N, rotates with a rate of ϕ_N' and changes amplitude at a rate of μ_N. Likewise, the precessional vector rotates at a rate of ϕ_P' and changes amplitude at a rate of μ_P. Note that if the μ's are negative both vectors decrease in amplitude and the motion damps. By definition $(\mu_N + i\phi_N')$ and $(\mu_P + i\phi_P')$ are the roots of Eq. 6.14. Also, the assumption that H, M, and T are constant necessitates that the aerodynamic coefficients are linear with angle-of-attack and hence the name 'Linear Theory'.

This 'Linear Theory' technique of analyzing the angular motion of a missile in free-flight requires that the measured $\beta + i\alpha$ data be fitted as a function of distance traveled, x, and determine K_N, K_P, K_T, μ_N, μ_P, ϕ_N', and ϕ_P' in Eq. 6.20 assuming that they are the unknowns in the process. This fitting process is derived and discussed in Appendix 3. Therefore, in this section we will proceed as if the K_i's, μ_i's, and ϕ_i's have already been determined .

We can relate the determined μ_i's and ϕ_i's to the aerodynamic coefficients as defined in the constants, Eqs. 6.15 to 6.18, of the differential equation, Eq. 6.14, by analyzing the roots of the characteristic equation using the operator method. Or,

$$D^2 + (H - iP) D - (M + iPT) = 0$$

then the roots are ,

$$D_{1,2} = (1/2) [- (H - iP) \pm \sqrt{(H - iP)^2 + 4(M + iPT)}] \qquad 6.21$$

By adding the two roots we can obtain,

$$D_1 + D_2 = - (H - iP) \qquad 6.22$$

and by multiplying the two roots,

$$D_1 D_2 = - (M + iPT)$$ 6.23

By using the definition of the roots we can also write,

$$D_1 + D_2 = (\mu_N + \mu_P) + i(\phi_N' + \phi_P')$$ 6.24

and

$$D_1 D_2 = \mu_N \mu_P - \phi_N' \phi_P' + i(\phi_N' \mu_P + \phi_P' \mu_N)$$ 6.25

If we now equate the real and imaginary parts of Eq. 6.22 with the real and imaginary parts of Eq. 6.24, after some manipulation and using Eqs. 6.16 through 6.19 we can arrive at the following equations:

$$- (2m_a / \rho A)(\mu_N + \mu_P) = C_{N\alpha} - 2C_D - k_t^{-2} (C_{mq} + C_{m\dot\alpha})$$ 6.26

and

$$p = (I_y / I_x) (\phi_N' + \phi_P')$$ 6.27

Likewise if we equate the real and imaginary parts of Eq. 6.23 and 6.25, and using Eqs. 6.15 through 6.18, after manipulation we obtain:

$$(\phi_N' \phi_P' - \mu_N \mu_P) (2I_y / \rho A d) = C_{m\alpha}$$ 6.28

and

$$(\phi_N' \mu_P + \phi_P' \mu_N) / (\phi_N' + \phi_P')(\rho A / 2m_a) = C_D - C_{N\alpha} - k_a^{-2} C_{np\alpha}$$ 6.29

Equations 6.26 through 6.29 illustrate that the aerodynamic coefficients and derivatives are a function of the 'fitted' μ_i's and ϕ_i's of Eq. 6.20. The drag coefficient would be provided using the techniques of Section 6.1.1 and the normal force derivative, $C_{N\alpha}$, using the method discussed in the next section. Eqs. 6.26, 6.28, and 6.29 would then be used to determine $C_{mq} + C_{m\dot\alpha}$, $C_{m\alpha}$, and $C_{np\alpha}$. It is of interest to note that the spin rate, p, of Eq. 6.27 is a function of the nutational and precessional frequencies. For this reason the spin rate is not treated as an unknown in Eq. 6.20. It should also be noted that normally the product of the damping rates, $\mu_N \mu_P$, in Eq. 6.28 is assumed negligible and the pitching moment, $C_{m\alpha}$, is written only as a function of the frequencies. This was a particularly useful simplification in the days when graphical techniques were used. Although this product is very small and ignoring it results in a negligible error to $C_{m\alpha}$ there is really no reason why this assumption still persists.

Most linear theory routines in use today have been modified from that shown as Eq. 6.20 by allowing the nutational and precessional frequencies to be linear functions of distance. These are assumed to be,

$$\phi_P' = \phi'_{P0} + \phi_P'' x \qquad \text{and} \qquad \phi_N' = \phi'_{N0} + \phi_N'' x$$ 6.30

If we substitute Eqs. 6.30 into Eq. 6.27 the spin rate also becomes a linear function of x. Or,

$$p = (I_y / I_x) [\phi'_{N0} + \phi'_{P0} + (\phi_N'' + \phi_P'') x] \qquad 6.31$$

The aerodynamic coefficients, $C_{m\alpha}$ and $C_{np\alpha}$, as defined by Eqs. 6.28 and 6.29 then become functions of x and are normally evaluated at the midrange (x_{mr}) location using Eqs. 6.30. This variable frequency expansion to the classic 'Linear Theory' technique is a powerful tool and is often utilized by the analyst as a first order approximation in accounting for nonlinear and variable roll effects in the experimentally measured motion profiles. Notice that the variable frequencies do not affect the computation of $C_{mq}+C_{m\dot\alpha}$ from Eq. 6.26. However, if the wavelength of the motion is not well matched during the fitting process this will usually result in significant errors in the fitted damping rates, μ_i's, and hence cause significant errors in the computed $C_{mq}+C_{m\dot\alpha}$ values. Therefore the use of this variable frequency expansion helps to ensure that the errors in the computed aerodynamics are minimized.

It should be recognized that the inclusion of these variable frequencies is strictly an intuitive approach and does not represent an actual mathematical solution to the differential equation. In fact, the variable spin rate and the variable frequencies violate the assumption that H, M, P, T, and p are all constant when writing the closed form solution to the differential equation.

Some linear theory routines have also been modified to permit the trim vector to change magnitude by including a damping rate, μ_T, on the trim term of Eq. 6.20. This extension of the classic 'Linear Theory' can also be useful, especially in analyzing free-flight trajectories for missiles which may be approaching a spin-yaw resonate condition, $p \rightarrow \phi_N'$. When this condition occurs the aerodynamic trim increases in amplitude as shown in the sketch below.
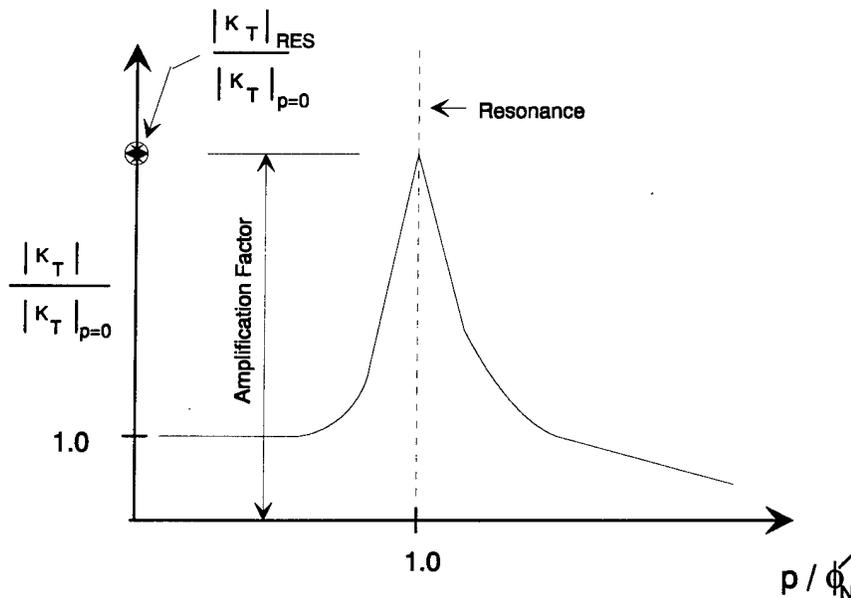
This increase in amplitude is described by the amplification factor, AF, and can be shown to be defined by the relationship below:

$$AF \approx -(m_a d / I_y \phi_N') C_{m\alpha} / [C_{N\alpha} - (m_a d^2 / I_y) (C_{mq} + C_{m\dot{\alpha}})] \qquad 6.32$$

For most missile configurations this amplification factor turns out to be a value between 8 and 14. Because of this amplification effect the inclusion of a damping rate on the trim term of Eq. 6.20 can sometimes assist in fitting the tricyclic equation of motion to the experimentally measured trajectories. If the model actually passes through resonance where the trim initially grows and then decreases a simple damping rate added to the trim term will not appreciably aid the fitting process. Other problems associated with this resonance condition can also arise when fitting the angular motion. For example by definition this condition means that both the nutational and trim vectors are rotating in the same direction at about the same rate. Mathematically this motion can be described by a single vector rotating at near resonance and the fitting routine can and frequently does diverge because of the absence of a unique solution. Nevertheless, various analysts have taken considerable liberties with the classic 'Linear Theory' over the years and one should be alert for these modifications.

6.1.4 Swerve

In contrast to the rigorous derivation for the angular motion in Refs. 6.1 to 6.4 here we will do an intuitive derivation of the swerving motion starting with Newton's second law, $a = F/m_a$ (see Ref. 6.1 for a complete derivation). We will use the complex nomenclature similar to Eq. 6.15, or $a = (\ddot{y} + i\ddot{z})$, then

$$(\ddot{y} + i\ddot{z}) = (1/2) \rho A V^2 C_F / m_a \qquad 6.33$$

The force coefficient , C_F, can be expanded as a function of the lift force coefficient, C_L, and a trim force which rotates with the spin rate, or

$$C_F = C_L + (C_{Y0} + iC_{Z0}) e^{ipx} \qquad 6.34$$

The C_L coefficient is further expanded as $C_{L\alpha}(\beta + i\alpha)$ and substituting this and Eq. 6.34 into Eq. 6.33 we obtain:

$$(\ddot{y} + i\ddot{z}) = (\rho A / 2m_a) V^2 [C_{L\alpha}(\beta + i\alpha) + (C_{Y0} + iC_{Z0}) e^{ipx}] \qquad 6.35$$

If we now use the change of variables technique as was done for the roll equation, Eq. 6.9, Eq. 6.35 can be written as,

$$(y + iz)'' = (\rho A / 2m_a) [C_{L\alpha}(\beta + i\alpha) + (C_{Y0} + iC_{Z0}) e^{ipx}] \qquad 6.36$$

Now if we substitute Eq. 6.20 for $(\beta + i\alpha)$, collect like terms, integrate twice by parts, and evaluate from 0 to x, after some manipulation we can arrive at the equation shown below:

$$(y + iz) = (\rho A / 2m_a)\{C_{L\alpha} [\phi_N^{-2}(K_N \exp\phi_N x) + \phi_P^{-2}(K_P \exp\phi_P x) - (K_N \phi_N^{-1} + K_P \phi_P^{-1}) x$$

$$- (K_N \phi_N^{-2} + K_P \phi_P^{-2})] + (K_T C_{L\alpha} + C_{Y0} + iC_{Z0})(p^{-2})[1 - \cos px + i(px - \sin px)]\}$$

$$+ (y + iz)'_0 x + (y + iz)_0 \qquad\qquad 6.37$$

Where: $\phi_P = \mu_P + i\phi_P'$, $\phi_N = \mu_N + i\phi_N'$ and,

$(y + iz)'_0$ = initial velocities in the y and z directions

$(y + iz)_0$ = initial displacements in the y and z directions

In arriving at the above equation it was also necessary to assume that ϕ_P ,ϕ_N and p were not equal to zero.

Equation 6.37 is fit to the measured position data, y + iz, assuming that $C_{L\alpha}$, C_{Y0} , C_{Z0} and the initial velocities and displacements are unknown. Note that the K_i's, ϕ_i's, and p are assumed to be known and provided by the analysis discussed in the preceding section. It should be noted that for spin stabilized projectiles it is normally assumed that K_T, C_{Y0}, and C_{Z0} are zero and Eq. 6.37 is somewhat simplified.

6.2 QUASI-NONLINEAR ANALYSIS

The linear aerodynamics assumption required in writing closed form solutions to the differential equations have placed certain restrictions on these analysis techniques. These restrictions have been recognized by many researchers and various quasi-nonlinear methods have been proposed by several individuals, see Refs. 6.7 to 6.10. All of these quasi-methods attempt to take the aerodynamic coefficients and derivatives obtained using the linear theory techniques and infer from those estimates what the nonlinear effects are. Murphy, Refs. 6.1, 6.7, and 6.10, has developed methods which assume certain forms of the nonlinear aerodynamics and these will be described in the following sections. These methods are easily applied by the analyst and have been shown to produce very good results. It is not our purpose herein to derive all of these nonlinear methods; however, we will attempt to provide the reader with the general processes involved in arriving at the quasi-nonlinear techniques.

6.2.1 Drag

The determination of the total drag coefficient, C_D, was discussed in Section 6.1.1. As was noted in that section, C_D is a function of the angle-of-attack history experienced by the model as it traverses the instrumented range. Therefore, the total drag coefficient is an

average value corresponding to an effective angle of attack experienced during the model's flight. It is assumed that C_D can be represented as a quadratic function of this effective angle-of-attack, or

$$C_D = C_{D0} + C_{D2}\, \overline{\delta}^2 \qquad\qquad 6.38$$

Then from Ref. 6.7, $\qquad \overline{\delta}^2 = [1/(x_2 - x_1)] \int_{x_1}^{x_2} \delta^2\, dx \qquad\qquad 6.39$

where, $\qquad\qquad \delta = \alpha + \beta$

C_{D0} = zero angle-of-attack drag

C_{D2} = quadratic slope term

The effective angle-of-attack squared term, $\overline{\delta}^2$, is normally obtained from a fit of the angular motion by integrating Eq. 6.21 for δ and accomplishing the summation indicated by Eq. 6.39. It should be recognized that the same portion of the flight used to determine C_D must also be used to accomplish the angular motion fit and hence the $\overline{\delta}^2$ calculation.

The process of determining the zero angle-of-attack drag coefficient, C_{D0}, and the quadratic drag term, C_{D2}, then consists of plotting the determined C_D values as a function of the respective $\overline{\delta}^2$ as illustrated in the sketch below.
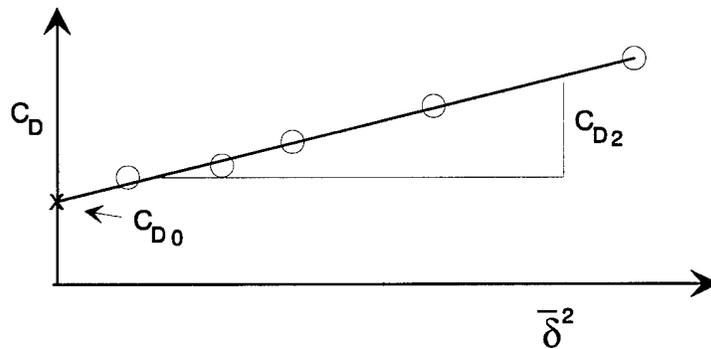
As can be inferred from the above sketch this process requires several flights of the identical configuration at each test condition. Normally, once the C_{D2} term is determined from the group of flights at each test condition, the C_{D0} term is computed for each flight by using the transpose of Eq. 6.38, or

$$C_{D0} = C_D - C_{D2}\, \overline{\delta}^2 \qquad\qquad 6.40$$

Obviously the higher the angles-of-attack experienced by the projectile during flight the more critical an accurate determination of C_{D2} becomes. If C_{D2} cannot be determined because of too few data points or relatively small angles-of-attack it can be estimated using Eq. 6.41 below (see derivation in Section 7.1).

$$C_{D2} \approx C_{X2} + C_{N\alpha} \qquad\qquad 6.41$$

As shown in the derivation of Section 7.1 this relation assumes small angle theory and that both C_D and C_X can be represented as a quadratic expansion. The technique outlined above for determining C_{D0} and C_{D2} from the total drag measurements has proven over the years to be quite adequate for most configurations, see Ref. 6.11.

6.2.2 Pitching Moment and Normal Force

Again what is required is to determine an effective angle-of-attack for the pitching moment derivative, $C_{m\alpha}$,and the normal force derivative, $C_{N\alpha}$, in a similar manner as was accomplished in the previous section for the drag coefficient. These effective angles-of-attack will correspond to the polynomial expansions and hence are a function of the assumed nonlinearities. This process will be illustrated herein by deriving the effective angle-of-attack for an assumed cubic pitching moment. The process is identical for a fifth order expansion as shown in Ref. 6.7 and 6.10. The cubic expansion is chosen here for the pitching moment because it represents the expansion which is most frequently used to analyze free-flight data. Even though nonlinearities are frequently found in free-flight spark range data, the angles-of-attack are normally below 20 degrees and higher order nonlinearities are not prevalent. Nevertheless analysts should recognize that higher order expansions may be required and utilize the corresponding effective angle-of-attack parameters as derived in Refs. 6.7 and 6.10.

If we assume that the pitching moment can be represented as a cubic expansion of the angle-of-attack, then

$$C_m = C_{mo} + C_{m\alpha o}\, \alpha + C_{m\alpha 3}'\, \alpha^3 \qquad 6.42$$

and the derivative with respect to α, becomes,

$$C_{m\alpha} = C_{m\alpha o} + C_{m\alpha 3}\, \alpha^2 \quad \text{where, } C_{m\alpha 3} \equiv 3\, C_{m\alpha 3}' \qquad 6.43$$

The technique requires a determination of the effective angle-of-attack squared, δ_e^2, which will correspond to α^2 in Eq. 6.43. This determination is shown below.

If we rewrite Eq. 6.14 assuming zero damping and zero trim, we see that

$$(\beta + i\alpha)'' + (-iP)(\beta + i\alpha)' - (M)(\beta + i\alpha) = 0 \qquad 6.44$$

With the assumed cubic expansion of C_m , M in Eq. 6.44 becomes

$$M = M_0 + M_2\, \delta_e^2 \qquad 6.45$$

where

$$M_0 = (\rho A / 2m_a d)\, k_t^{-2}\, C_{m\alpha o}$$

and

$$M_2 = (\rho A / 2m_a d)\, k_t^{-2}\, C_{m\alpha 3}$$

The solution to Eq. 6.44 can be written similarly to Eq. 6.20, or

$$\beta + i\alpha = K_P \exp(i\phi_P'\, x) + K_N \exp(i\phi_N' x) \qquad 6.46$$

The derivatives with respect to x can therefore be written as shown below:

$$(\beta + i\alpha)' = K_P\, i\phi_P'\, \exp(i\phi_P'\, x) + K_N\, i\phi_N'\exp(i\phi_N'x) \qquad 6.47$$

and
$$(\beta + i\alpha)'' = - K_P (\phi_P')^2 \exp(i\phi_P' x) - K_N (\phi_N')^2 \exp(i\phi_N'x) \qquad 6.48$$

In Ref. 6.7, Murphy defines δ^2 as $\equiv (\beta + i\alpha)(\overline{\beta + i\alpha})$ and accomplishing the indicated multiplication using Eq. 6.46 one obtains,
$$\delta^2 = K_N^2 + K_P^2 + K_N K_P [\exp i(\phi_N' - \phi_P')x + \exp i(\phi_P' - \phi_N')x] \qquad 6.49$$

If Eqs. 6.46 through 6.49 are substituted into Eq. 6.44 and like terms collected one can arrive at the lengthy relationship shown below:
$$K_N (\exp i\phi_N')[- \phi_N'^2 + P\phi_N' - M_0 - M_2 (K_N^2 + 2K_P^2)]$$
$$+ K_P (\exp i\phi_P')[- \phi_P'^2 + P\phi_P' - M_0 - M_2 (2K_N^2 + K_P^2)]$$
$$- M_2 \{ K_N^2 K_P[\exp i(2\phi_N - \phi_P)] + K_N K_P^2 [\exp i(2\phi_P - \phi_N)]\} = 0 \qquad 6.50$$

The third term containing the mixed frequencies in Eq. 6.50 is neglected; and, since K_N and K_P cannot be zero the quantities within the brackets must be zero. Or
$$- \phi_N'^2 + P\phi_N' = M_0 + M_2 (K_N^2 + 2K_P^2) \qquad 6.51$$
$$- \phi_P'^2 + P \phi_P' = M_0 + M_2(2K_N^2 + K_P^2) \qquad 6.52$$

If we define $\delta_{e2}^2 \equiv K_N^2 + 2K_P^2$ and $\delta_{e1}^2 \equiv 2K_N^2 + K_P^2$ and solve both Eqs. 6.51 and 6.52 for P and set equal to each other we can show that,
$$\phi_N' \phi_P' = M_0 + M_2 [(\phi_P' \delta_{e2}^2 - \phi_N' \delta_{e1}^2) / (\phi_P' - \phi_N')] \qquad 6.53$$

Since Eq. 6.53 is equivalent to Eq. 6.45, δ_e^2 must be defined as:
$$\delta_e^2 = (\phi_P' \delta_{e2}^2 - \phi_N' \delta_{e1}^2) / (\phi_P' - \phi_N') \qquad 6.54$$

Finally, if the definitions of δ_{e1}^2 and δ_{e2}^2 are substituted into Eq. 6.54 the effective angle-of-attack squared can be written as shown below:
$$\delta_e^2 = K_N^2 + K_P^2 + [(\phi_N' K_N^2 - \phi_P' K_P^2) / (\phi_N' - \phi_P')] \qquad 6.55$$

What Eq. 6.55 represents is an equivalent angle-of-attack squared parameter consistent with a cubic pitching moment expansion. In practice how this would be utilized is similar to the drag analysis of the previous section. For example the determined $C_{m\alpha}$ values as obtained by fitting Eq. 6.20 and using Eq. 6.28 are plotted as a function of δ_e^2 as illustrated in the sketch below.
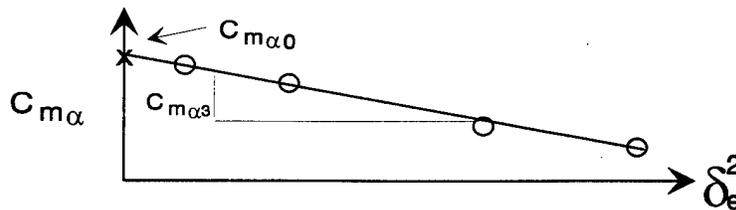
The midrange values for K_N, K_P, ϕ_N', and ϕ_P'(if the variable frequencies are utilized, see Eq. 6.30) are used in computing δ_e^2. By using the midrange values we are accounting for the damping in the system thus relaxing somewhat the assumption of zero damping when we derived the relationship for δ_e^2. Again it is obvious that several flights of the same configuration at similar test conditions must be available to accurately determine the $C_{m\alpha o}$ and $C_{m\alpha 3}$ terms using this technique. If, once the $C_{m\alpha}$ vs δ_e^2 plot has been

accomplished, the plotted data cannot be represented by a linear function then a higher order nonlinearity must be assumed. Murphy has derived these various higher order effective amplitudes in various references, see for example Ref. 6.7.

A similar process is again applied to the measured normal force derivatives, $C_{N\alpha}$, data. Although not derived herein, the effective amplitude parameter assuming a cubic polynomial expansion that results from this process is shown below.

$$\delta_{es}^2 = K_N^2 + K_P^2 + [K_N^2 K_P^2(\phi_N'^4 + \phi_P'^4) / (K_P^2 \phi_N'^4 + K_N^2 \phi_P'^4)] \qquad 6.56$$

Again plotting $C_{N\alpha}$ vs δ_{es}^2 yields both $C_{N\alpha o}$ and $C_{N\alpha 3}$,see sketch below.
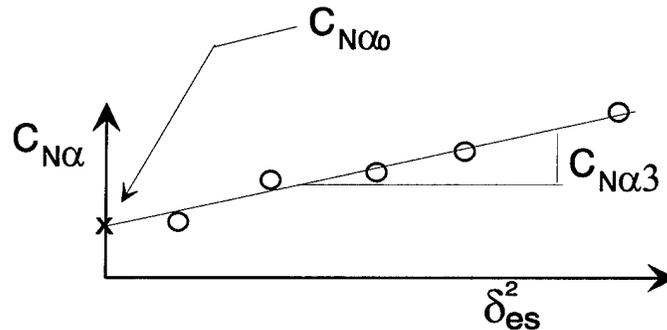
These quasi-nonlinear techniques for C_D, (previous section), $C_{m\alpha}$ and $C_{N\alpha}$ are relatively straight forward and easy to apply once the aerodynamic coefficients have been determined and the effective amplitude parameters calculated. This process has been shown to provide good results with the primary disadvantage being the number of flights required to adequately determine both the zero angle-of-attack coefficients and their respective nonlinear terms. Also, when large nonlinearities are present the very nature of 'Linear Theory' means that the fits to the experimentally measured trajectories will not be within the measuring capability of the facility. These fits will normally result in residuals that display a definite sinusoidal variation. Hence, these poor quality fits to the measured motions are not conducive to establishing a positive feeling for the accuracy of the final results. Therefore, even though the final results may be quite good it can be difficult to appreciate the quality of results in light of the poor fits to the measured motions.

6.2.3 Damping and Magnus

As defined previously, the damping derivatives being extracted from free-flight trajectory measurements are in actuality the combination of $(C_{mq} + C_{m\dot\alpha})$. Analysts have become lax in their identification of these derivatives and quite frequently refer to the combination as C_{mq} only. This simplification is often used in writing the equations of motion and in tabulating and presenting results. This abbreviated nomenclature was used in Section 2.3 and will be used again in this section but with the understanding that it refers to the combined damping-in-pitch derivatives.

Murphy, Ref. 6.1, again derives an effective angle-of-attack associated with the determined C_{mq} values similar to the process previously discussed. This expansion has the form shown below:

$$C_{mq} = C_{mqo} + C_{mq2} \Delta \qquad\qquad 6.57$$

where

$$\Delta = -(I_y / I_x) [(\phi_N' + \phi_P') / (\phi_N' - \phi_P')] (K_N^2 - K_P^2)$$

Although Δ has the units of degrees^2 (or rad^2) it can take on negative values depending on the magnitudes of the nutational and precessional vectors. Because negative values of Δ can be disconcerting to the analyst an alternate approach is frequently used to evaluate potential nonlinear effects associated with C_{mq}. This alternate approach is also used for the Magnus moment derivative, $C_{np\alpha}$, as well. The effective amplitudes squared for the nutational and precessional damping rates turns out to be δ_{e1}^2 and δ_{e2}^2, as previously defined. Or,

$$\delta_{e2}^2 \equiv K_N^2 + 2K_P^2$$
$$\delta_{e1}^2 \equiv 2K_N^2 + K_P^2$$

The process then becomes plotting the nutational damping rate vs δ_{e2}^2 and the precessional damping rate vs δ_{e1}^2 as shown in the sketch below.
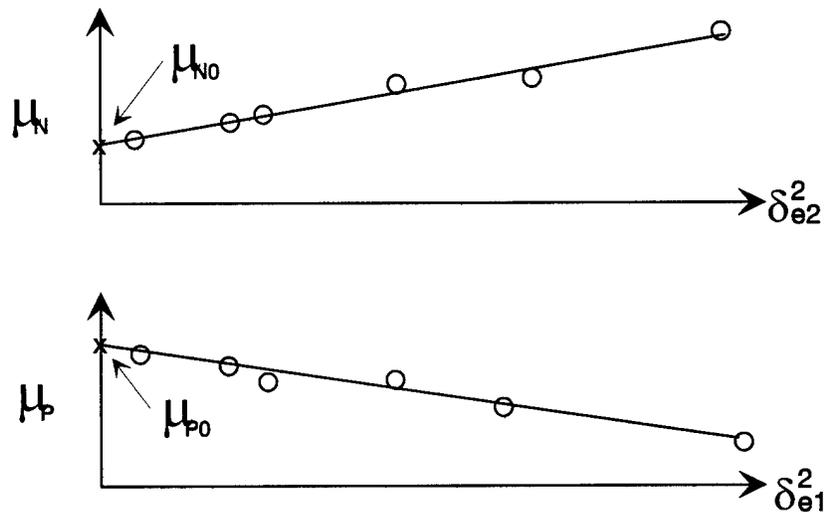
The two zero angle-of-attack damping rates, μ_{P0} and μ_{N0}, are then substituted into Eq. 6.26 to calculate $(C_{mq}+C_{m\dot\alpha})_0$ and into Eq. 6.29 to calculate $C_{np\alpha o}$. This process eliminates the concern associated with the sign of Δ as previously mentioned; but, does not easily lend itself to determining the higher order nonlinear coefficients.

It may appear to the reader that these quasi-nonlinear techniques are somewhat desperate attempts at eliminating the severe assumptions of linear aerodynamics in the derivations of the equations of motion. Although there may be some truth in this, these quasi-nonlinear techniques have proven to be extremely useful over the years and have provided very good estimates for both the zero angle-of-attack coefficients as well as the

nonlinear terms. A good example of the application of these techniques are provided in Ref. 6.12. As mentioned previously the primary disadvantage has been the large number of flights required to accurately determine the nonlinearities.

6.3 NUMERICAL INTEGRATION

Linear Theory and the associated quasi-nonlinear techniques discussed in the previous sections were developed in the manner discussed primarily because of a lack of computer power during the period of 1940 through the 60's. Because of this lack of computer power closed form solutions of the differential equations were required in order to extract the aerodynamic coefficients and derivatives. This changed considerably in 1970 when Chapman and Kirk published a method of data analysis they called parametric differentiation[6.13]. Since the differential equations were used directly by numerically integrating the equations and comparing the resulting motions with the experimental measurements, many of the assumptions required by the linear theory techniques were no longer necessary. This numerical integration (NI) method has developed to the point where typically all of the differential equations describing the motions in the x,y,z directions along with the angular motions,θ ,ψ, and ϕ are simultaneously fitted for multiple flights. These differential equations, both fixed plane and body fixed, have been presented in Section 2.2.2 and will not be repeated here.

This NI technique also permits the aerodynamic coefficients and derivatives to be functions of the angle-of-attack, Mach number, and roll orientation or roll rate, see for example the aerodynamic expansions shown in Section 2.3. In fact, the primary restriction on this technique is the analyst's ability and ingenuity in mathematically modeling the aerodynamic variations. Since the assumptions of linear aerodynamics with angle-of-attack are no longer required this technique is frequently referred to as nonlinear analysis. This technique has been described in great detail in various references, see Refs. 2.2 to 2.5 and 6.13; therefore, only a simple explanatory example will be described herein.

6.3.1 Drag Example

We will rewrite Eq. 6.1 as shown below:

$$\ddot{x} = - (\rho A / 2m_a) (\dot{x})^2 C_D \qquad\qquad 6.58$$

Now if we expand the total drag coefficient to be a function of angle-of-attack and velocity as,

$$C_D = C_{D0} + C_{D2} \varepsilon^2 + C_{DV} (\dot{x} - V_{REF}) \qquad\qquad 6.59$$

we obtain,

$$\ddot{x} = K(\dot{x})^2 [C_{D0} + C_{D2} \varepsilon^2 + C_{DV} (\dot{x} - V_{REF})] \qquad\qquad 6.60$$

where $\qquad K = - (\rho A / 2m_a)$

$\qquad\qquad \varepsilon^2 = \sin^2 \overline{\alpha}$,(see Eq. 2.14)

$\qquad\qquad V_{REF}$ = reference velocity

The drag expansion shown in Eq. 6.59 permits the total drag to be a quadratic function of the angle-of-attack with a linear variation of velocity about a reference value.

The problem now is to determine the unknown C_{D0}, C_{D2}, and, C_{DV} coefficients of the expansion by matching the theoretical trajectory as defined by Eq. 6.60 to the experimentally measured time, t, and distance, x, data. It is also assumed that the angle-of-attack history is available. If we define the partial derivatives, P_i, as follows:

$$P_1 \equiv \partial x / \partial C_{D0} \;,\; P_2 \equiv \partial x / \partial C_{D2} \;,\; P_3 \equiv \partial x / \partial C_{DV} \;, \text{and}$$
$$P_4 \equiv \partial x / \partial x_0 \;,\; P_5 \equiv \partial x / \partial \dot{x}_0 \qquad\qquad 6.61$$

We will also assume that the order of differentiation can be reversed, or

$$\partial / \partial C_i (d^2 x / dt^2) = d^2 / dt^2 (\partial x / \partial C_i) = \partial \ddot{x} / \partial C_i = \ddot{P}_i$$

and similarly,

$$\partial / \partial C_i (dx / dt) = d / dt (\partial x / \partial C_i) = \partial \dot{x} / \partial C_i = \dot{P}_i$$

Using the above relationships in conjunction with Eq. 6.60 we can write:

$$\ddot{P}_1 = \partial \ddot{x} / \partial C_{D0} = K\dot{x}[\, 2C_{D0} + 2C_{D2}\,\varepsilon^2 + C_{DV}(3\dot{x} - 2V_{REF})] \,(\partial \dot{x} / \partial C_{D0}) + K\dot{x}^2$$

After expanding, collecting like terms, and simplifying we arrive at:

$$\ddot{P}_1 = K(\dot{x}_0)^2 \,[(\,1 + 3\,C_{DV0}\,\dot{P}_1) + 2\dot{P}_1(C_{D0} + C_{D2}\,\varepsilon^2 - C_{DV}\,V_{REF})_0\,] \qquad 6.62$$

Where the subscripted, 0, terms imply that the quantity was evaluated with the given coefficients, either initial guesses or corrected values, after each iteration. Likewise the remaining partials can be derived and the resulting relations are shown below:

$$\ddot{P}_2 = K(\dot{x}_0)^2 \,[(\varepsilon^2 + 3\,C_{DV0}\,\dot{P}_2) + 2\dot{P}_2(C_{D0} + C_{D2}\,\varepsilon^2 - C_{DV}\,V_{REF})_0\,] \qquad\qquad 6.63$$

$$\ddot{P}_3 = K(\dot{x}_0)^2 \,\{[(\,\dot{x} - V_{REF})_0 + 3\,C_{DV0}\,\dot{P}_3] + 2\dot{P}_3(C_{D0} + C_{D2}\,\varepsilon^2 - C_{DV}\,V_{REF})_0\,\} \;\; 6.64$$

$$\ddot{P}_4 = K(\dot{x}_0)^2 \,[(\,3\,C_{DV0}\,\dot{P}_4) + 2\dot{P}_4(C_{D0} + C_{D2}\,\varepsilon^2 - C_{DV}\,V_{REF})_0\,] \qquad\qquad 6.65$$

$$\ddot{P}_5 = K(\dot{x}_0)^2 \,[(\,3\,C_{DV0}\,\dot{P}_5) + 2\dot{P}_5(C_{D0} + C_{D2}\,\varepsilon^2 - C_{DV}\,V_{REF})_0\,] \qquad\qquad 6.66$$

Equation 6.60 is numerically integrated utilizing the initial guesses for the unknown coefficients of the drag expansion and the estimated initial conditions (x_0 and $\dot{x}_0$). Equations 6.62 through 6.66 are also numerically integrated such that the partial derivatives with respect to each of unknown coefficients are evaluated. The method of differential corrections is then used to obtain the corrections to each of the initial guesses. This method consists of expanding the calculated value of $x_{i,cal}$ about a given set of coefficients in a Taylor series, or

$$x_{i,cal} = x_{i,calo} + \sum_{j=1}^{N} \partial x_i / \partial C_j \big|_i \; \Delta C_j \; + \text{higher order terms} \qquad 6.67$$

91

Note that the higher order terms are neglected, N is the total number of unknowns, and that the subscript, 0, again indicates that the term is evaluated using the given set of values, either initial guesses or updated values after each iteration.

The sum of the squares of the residuals can be written as,

$$RSQ = \sum_{i=1}^{NP} (x_i - x_{i,cal})^2 \qquad 6.68$$

The subscript i denotes the i-th measurement and NP the total number of measurements. If we substitute Eq. 6.67 into 6.68, taking the derivative of RSQ with respect to each of the unknown coefficients(C_k) and setting equal to zero, we can arrive at the following equation:

$$C = (A_{jk})^{-1} B_k \qquad 6.69$$

where,

$$A_{jk} = \sum_{i=1}^{NP} \partial x_i / \partial C_j |_o (\partial x_i / \partial C_{ko})$$

and,

$$B_k = \sum_{i=1}^{NP} (x_i - x_{i,calo}) (\partial x_i / \partial C_k) |_o$$

The C matrix in Eq. 6.69 represents the corrections to be added to each of the unknowns to be determined, including the initial conditions x_0 and $\dot{x}_0$. Once these corrections are added to the initial estimates then these new estimates are substituted back into Eq. 6.60 and 6.62 through 6.66 and the process repeated until convergence is achieved. Convergence is defined as when the change in the sum of the residuals squared is less than a small predetermined value. This small predetermined value is set by the analyst depending on the precision deemed necessary.

Several aerodynamic modeling investigations have been accomplished over the years using the very routine described in this section. These investigations have included both drag and roll expansions using various polynomials and splines, see Refs. 6.14 and 6.15.

6.3.2 Maximum Likelihood Method

In the simple drag example shown in the previous section the data correlation technique was basic least squares. When simultaneously fitting multiple sets of equations of motion such as those listed in Section II to experimental data containing different levels of measurement noise basic least squares cannot be used. There does exist various correlation techniques which can handle this situation, i.e, weighted least squares, WLS, and the maximum likelihood method, MLM, along with others. An error matrix containing the known measurement noise is incorporated into the least squares theory to account for the different levels of measurement noise. Whereas, the MLM can determine the error matrix along with the unknown parameters in the equations of motion. The

correlation technique we have chosen for fitting the fixed plane and body fixed equations of motion shown in Section II is a hybrid of both WLS and MLM. This technique is referred to as a hybrid because although the likelihood function is maximized the error matrix is assumed known. This simplification to the standard MLM approach is justified because after analyzing numerous free-flight trajectories the facility's measurement error levels are known to a high degree. This modified MLM is an iterative procedure which adjusts the unknown aerodynamic coefficients until the theoretical equations of motion match the experimental data.

The mathematical treatment is a sensitivity analysis where the partial differential equations form a basis of quasi-linearization. These are derived by differentiating the equations of motion with respect to each of the unknown coefficients and derivatives as was done in the preceding simple drag example. Again the sensitivity equations are integrated in parallel with the equations of motion to yield the sensitivity coefficients (partial derivatives) which reflect the sensitivity of the computed solution with respect to each of the unknown parameters. The differential corrections procedure in conjunction with the Taylor series expansion is again used to form the relationship between residuals, corrections to the unknowns, and partial derivatives. The likelihood function is then defined as,

$$L = [1 / (2\pi)^{1/2} |S|^{1/2}] \exp[(-1/2) \sum_{}^{N} R^T S^{-1} R] \qquad 6.70$$

where,

   N = number of data points
   S = covariance matrix of measurement noise
   R = residuals after corrections have been made

The application of this likelihood function in the trajectory matching process eliminates the inherent assumption in least squares that the magnitude of the measurement noise must be consistent between dynamic parameters, irrespective of units. This is achieved through the covariance matrix which contains the information concerning the measurement precision. The likelihood function also has the property of asymptotically approaching the solution as compared to least squares which approaches the solution parabotically. A good discussion of data correlation techniques can be found in Ref. 6.16 and many texts.

6.4 DATA ANALYSIS SOFTWARE SYSTEM

The software system developed for analyzing free-flight trajectory data and extracting the aerodynamic coefficients and derivatives is the Aeroballistic Research Facility Data Analysis System (ARFDAS). This system is illustrated in the Fig. 6.1 below and described in detail in Refs. 2.2 to 2.4.
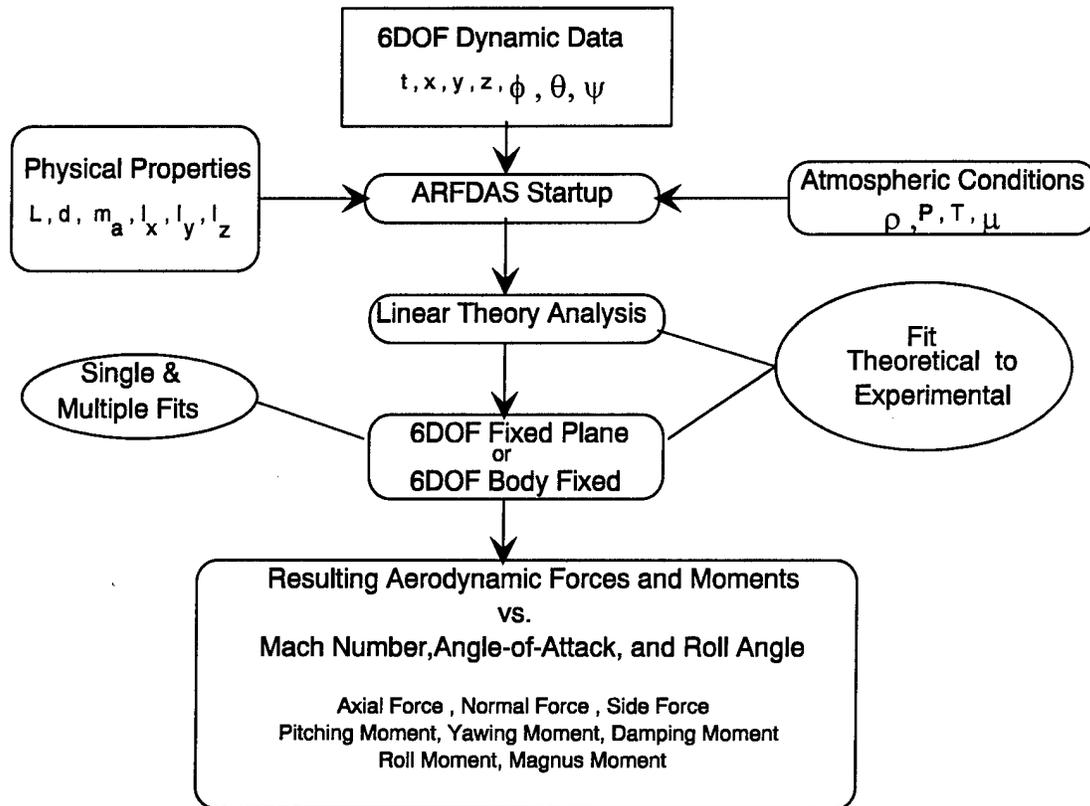
Figure 6.1 Aeroballistic Research Facility Data Analysis System (ARFDAS)

This software system uses the experimental trajectories, CADRA output - see Section 5.4, along with the model's physical characteristics and the atmospheric conditions in the facility and accomplishes a preliminary screening of the raw trajectory data. The system then does linear theory fits consistent with the process as described in Section 6.1 and provides these results to the appropriate NI routine for a nonlinear analysis. Once each of the experimental trajectories have been analyzed separately this routine can then be used to fit multiple trajectories.

Obviously only similar configurations at nearly the same test conditions should be simultaneously analyzed. The techniques as described herein can be a complex and lengthy process requiring considerable computer power. This is especially true when multiple sets of equations are utilized such as the fixed plane or body fixed equations of motion as outlined in Section 2.2.2. Obviously, not all of the associated coefficient expansion terms, as shown in Section 2.3, are determined from each experimentally measured trajectory. The analyst requires considerable experience in determining which of the potential aerodynamic expansions are likely to affect the motions of the configuration being tested. Usually this requires fitting the trajectories several times with different combinations of the unknowns being examined. Although at first glance this may appear to be an impossible task, the selection of the correct combination of unknowns becomes quite manageable and logical with experience.
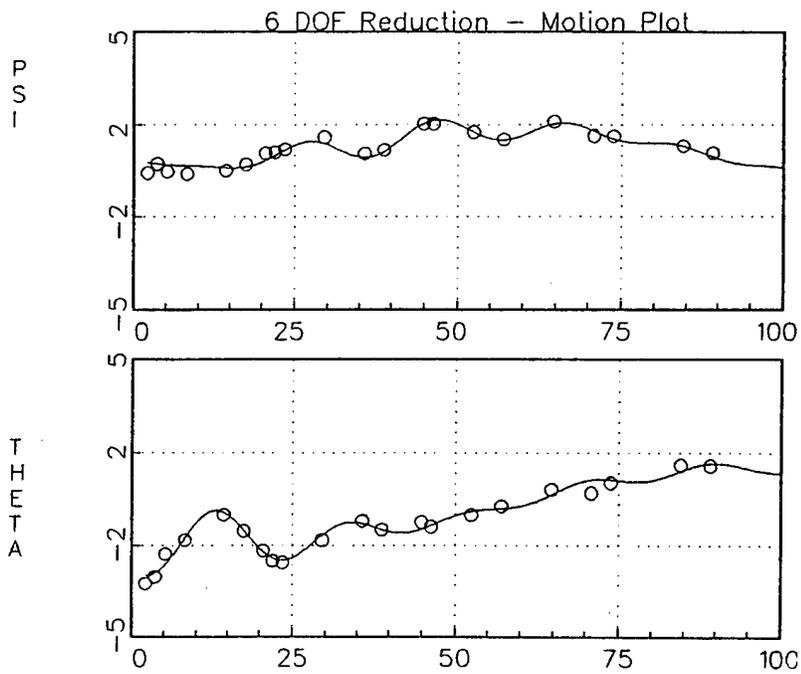
a. Body Fixed Analysis (asymmetric body)
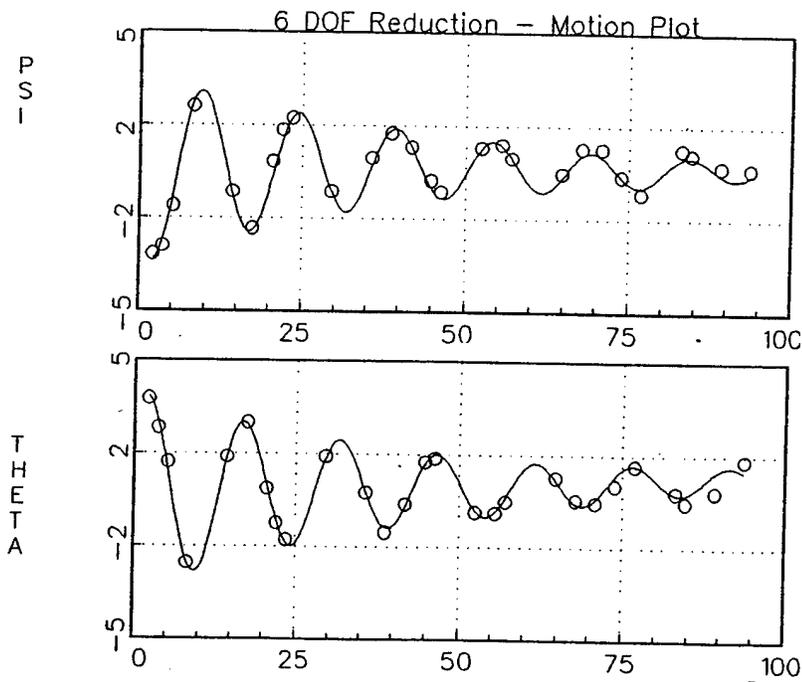
b. Fixed Plane Analysis (symmetric body)

Figure 6.2 Typical Angular Motion Theoretical Fits
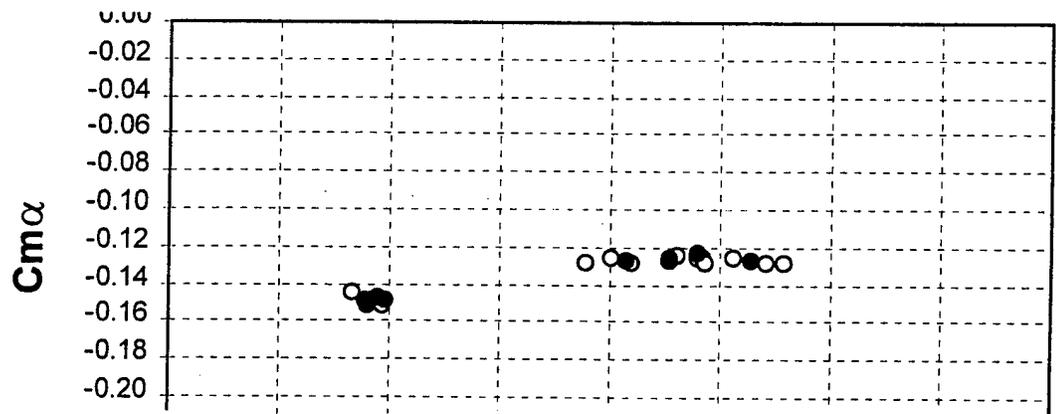
a. Pitching Moment Derivative
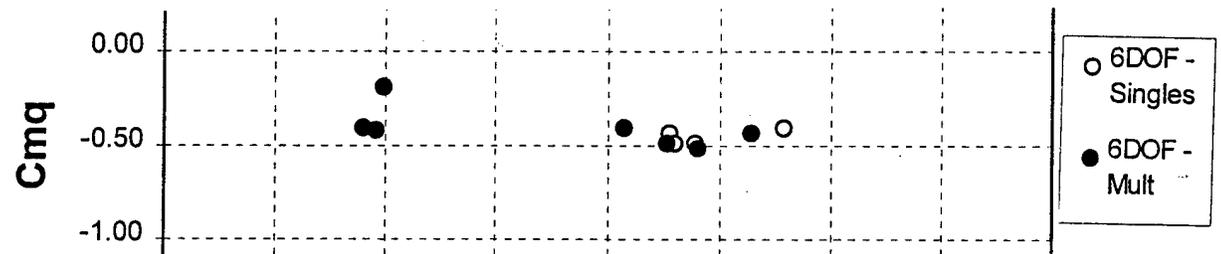
b. Pitch Daming Derivative
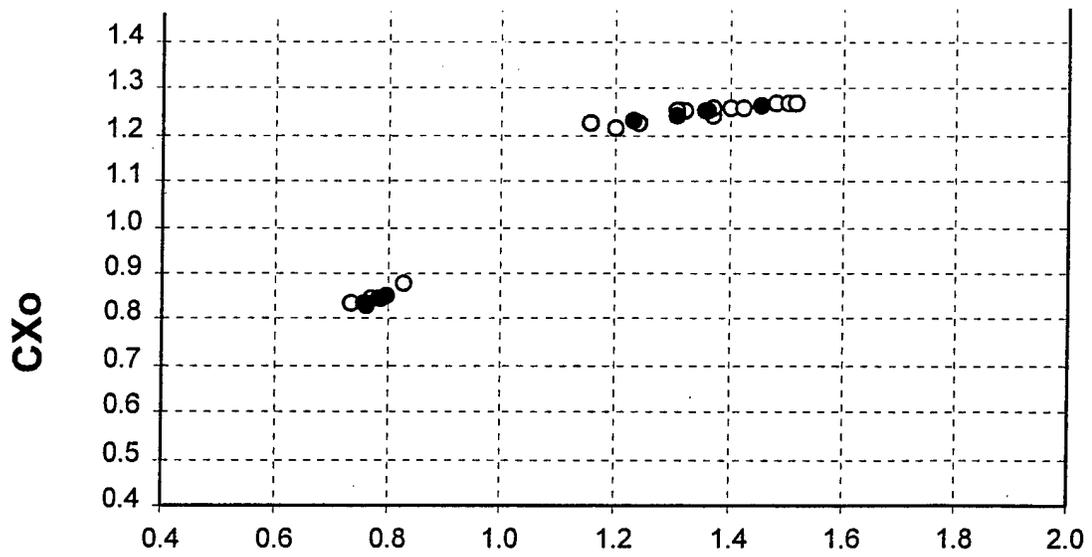
c. Axial Force

Mach No.

Figure 6.3 Example of Aerodynamic Results
(Blunt Planetary Probe)

Examples of typical NI curve fits to experimental angular motions are shown in Fig. 6.2. These fits were accomplished using ARFDAS and demonstrate both body fixed and fixed plane analyses. Many such fits for the angular as well as roll and swerve motions are presented in various papers and data reports, see Appendix 6. Examples of some aerodynamic results from a planetary probe configuration are also shown in Fig. 6.3. These results were obtained from analyses of single trajectories as well as multiple flights and are shown here only for illustrative purposes.

REFERENCES

6.1 Murphy, C. H.," Free-Flight Motion of Symmetric Missiles", BRL Report No. 1216, Aberdeen Proving Ground, Maryland, July 1963.

6.2 Murphy, C. H.," Data Reduction for the Free-Flight Spark Ranges", BRL Report No. 900, Aberdeen Proving Ground, Maryland, February 1954.

6.3 Nicolaides, J. D.,"Free-Flight Dynamics", University of Notre Dame, South Bend, Indiana, 1967.

6.4 Nicolaides, J. D.,"On the Free-Flight Motion of Missiles Having Slight Configurational Asymmetries", BRL Report No. 858, Aberdeen Proving Ground, Maryland, June 1953.

6.5 Etkin, Bernard,"Dynamics of Flight", John Wiley and Sons,Inc., New York,1959.

6.6 Wilie, C. R.,"Advanced Engineering Mathematics", McGraw-Hill Book Company, Inc., New York, 1960.

6.7 Murphy, C. H.," The Measurement of Non-Linear Forces and Moments by Means of Free-Flight Tests", BRL Report No. 974, Aberdeen Proving Ground, Maryland, February 1956.

6.8 Rasmussen, M. L.,"Determination of Nonlinear Pitching-Moment Characteristics of Axially Symmetric Models from Free-Flight Data", NASA TND-144, February 1960.

6.9 Lietmann, G.,"Nonlinear Equations of Motion of Spin-Stabilized Missile Solved by a Perturbation Method", NAVORD 3364, August 1954.

6.10 Murphy, C. H.,"On the Quasi-Linear Substitution Method for Missile Motion Caused by Strongly Nonlinear Static Moment", BRL MR No. 1466, Aberdeen Proving Ground, Maryland, April 1963.

6.11 Madagan, A.N.,"An Investigation of the Method Used in Free-Flight Hypersonic Testing for Reducing Total Drag Coefficient to Zero-Lift Drag Coefficient", M.S. Thesis, University of Tennessee Space Institute, June 1968.

6.12 Winchenbach, G.L., and Watt, R.M.,"Free-Flight Range Tests of a 25-mm Shell with the M505A3 Fuze", AFATL-TR-71-62, Eglin AFB, Florida, April 1971.

6.13 Chapman,G.T., and Kirk, D.B.,"A Method for Extracting Aerodynamic Coefficients from Free-Flight Data", AIAA Journal, Vol. 8, April 1970, pp 753-757.

6.14 Sabot, S.M., Winchenbach, G.L., and Chapman, G.T."Comparison of Various Drag Coefficient Expansions Using Polynomials and Splines", Journal of Spacecraft and Rockets, Vol. 23, Number 3, May-June 1986, pp 259-263.

6.15 Kim, Y.H., and Winchenbach, G.L.,"Roll Motion of a Wraparound Fin Configuration at Subsonic and Transonic Mach Numbers", Journal of Guidance, Control, and Dynamics, Vol. 9, Number 2, March-April 1986, pp 253-255.

6.16 Hathaway, W.H., "Analysis of the Free-Flight Aerodynamics of Non-Symmetric Bodies from Ballistic Spark Range Data", M.S. Thesis, University of Vermont, February 1976.

VII. AERODYNAMIC ANALYSIS

Once the aerodynamic coefficients and derivatives have been determined from the experimental trajectories additional analysis is normally required in order to determine the missile's center-of-pressure, gyroscopic stability factor, dynamic stability and other aerodynamic parameters. Also in order to compare these results with data obtained from previous tests, the moment data may require shifting to a different reference location. The purpose of this section is to develop some of the relationships used for these purposes.

7.1 AERODYNAMIC DRAG

The relationships between the aerodynamic drag, axial force, lift and normal force are illustrated in the sketch below.
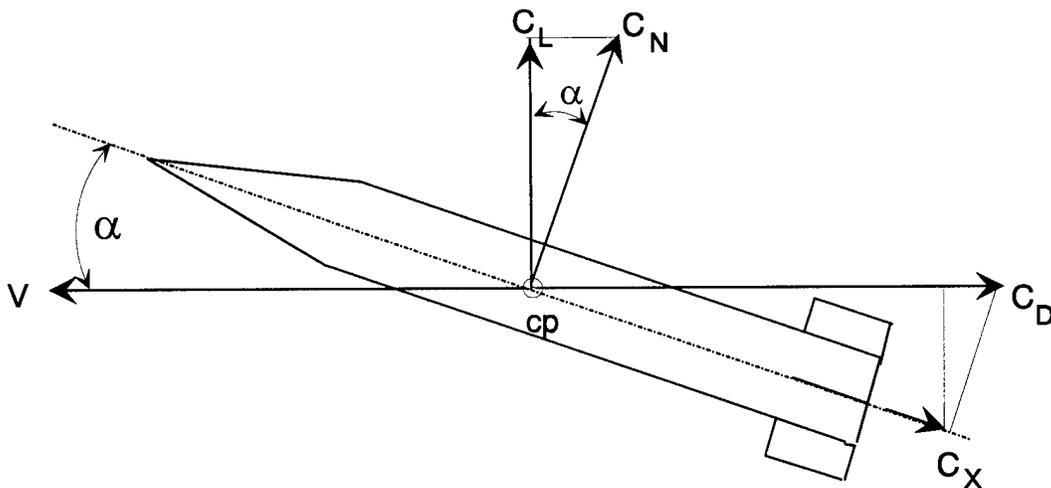
From the sketch:

$$C_D = C_X \cos \alpha + C_N \sin \alpha \qquad 7.1$$

$$C_L = C_N \cos \alpha - C_X \sin \alpha \qquad 7.2$$

If we assume that both C_D and C_X can be expanded as a quadratic polynomial in α, then Eq. 7.1 becomes,

$$C_{D0} + C_{D2} \alpha^2 = (C_{X0} + C_{X2} \alpha^2) \cos \alpha + C_{N\alpha} \alpha \sin \alpha \qquad 7.3$$

Now if we apply small angle theory, $\cos \alpha \approx 1$ and $\sin \alpha \approx \alpha$, and recognizing that C_{X0} is equal to C_{D0} then Eq. 7.3 can be rewritten and simplified to obtain,

$$C_{D2} \approx C_{X2} + C_{N\alpha} \qquad 7.4$$

This relationship is occasionally used to estimate C_{D2} when insufficient data are available to determine it from other sources. The C_{X2} term is normally small (≈ 1) compared to $C_{N\alpha}$ which can take on values of 2 to 3/rad for spin stabilized projectiles, cones, and other non finned missile configurations to values as high as 8 -12 for finned configurations. Another common relationship can be obtained from Eq. 7.2. Again

assuming small angle theory and taking the derivative with respect to α, one obtains the relations shown:

$$C_{N\alpha} \approx C_{L\alpha} + C_{X0} \qquad\qquad 7.5$$

or
$$C_{X0} = C_{D0} \approx C_{N\alpha} - C_{L\alpha} \qquad\qquad 7.6$$

7.2 STABILITY

7.2.1 Static

The static stability criteria for any system is defined as the tendency to restore itself to its original state once a disturbance has been input to the system. The classic examples are the ball on a hill and the ball in the valley, see below.
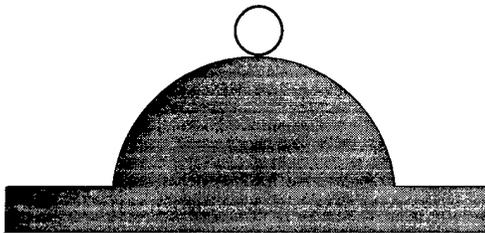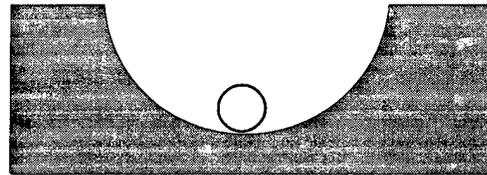
a. Statically Unstable   **b. Statically Stable**

Here if the ball in sketch 'a' above is disturbed from its point of rest the ball continues to deviate from its initial position; hence, the system is statically unstable. However, when the ball in sketch 'b' is disturbed it will tend to return to its initial position and after oscillating back and forth will again come to rest. This system is defined as statically stable. This analogy when applied to an object in flight implies that the forces and moments acting on that body tend to return the angle-of-attack to the trim angle once the object has been disturbed. There are two distinct techniques by which static stability can be provided to a free-flight object. These are typically referred to as aerodynamic and gyroscopic stability.

7.2.1.1 Aerodynamic

Aerodynamic static stability is illustrated in the sketch below.
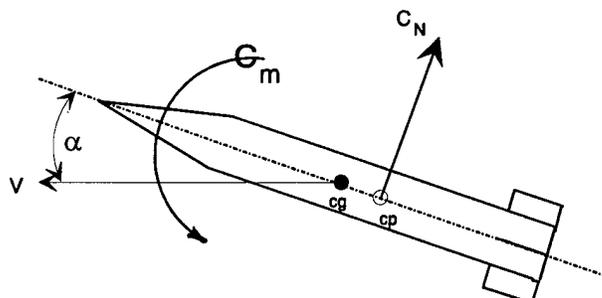
This sketch indicates that at an angle-of-attack the resulting normal force creates a moment about the missile's center-of-gravity which tends to return the angle-of-attack back to zero. Therefore the missile's static stability can be decreased or increased by shifting the center-of-gravity (forward shift provides more stability) or by changing the magnitude and/or the location of the resulting normal force. This alteration of the normal force is exactly what the addition of fins provide to the static stability of the missile. Note that if the fins were forward of the center-of-gravity (i.e. canards) they would provide a destabilizing moment to the missile.

The derivative of the pitching moment with respect to α, $C_{m\alpha}$, is often referred to as the static stability derivative because the sign of the derivative defines whether or not the missile possesses aerodynamic static stability. If the sign of $C_{m\alpha}$ is negative the missile is statically stable. This is true for symmetrical as well as asymmetric configurations; however, the normal convention used by aircraft designers for the yawing moment derivative, $C_{n\beta}$, is reversed. Therefore if the sign of $C_{n\beta}$ is positive the aircraft possesses static stability in the yaw plane. Note that this arbitrary sign change is not reflected in the aerodynamic expansions for the body fixed equations of motion as shown in Section 2.3.1. and both $C_{m\alpha}$ and $C_{n\beta}$, as used herein, require negative values for static stability to exist in the pitch and yaw planes.

7.2.1.2 Gyroscopic

Missiles or projectiles which are inherently aerodynamically unstable, i.e. the normal force creates a destabilizing moment, can be stabilized with spin. For this condition the spin rate must be high enough to develop a gyroscopic moment which overcomes the aerodynamic instability and the missile is said to be gyroscopically stable. This is typically the case for most gun launched projectiles (handguns, rifles, cannons, etc.) where the rifling of the barrel provides the required spin to the projectile.

In describing this condition ballisticians have developed a gyroscopic stability factor, S_g, which is obtained from the roots of the linear theory equation of motion, Eq. 6.21. The boundary of the stability limits is defined as the condition where both μ_N and μ_P are zero. Therefore from Eqs. 6.15 and 6.26 it can be seen that,

$$\mu_N + \mu_P = - H = 0$$

Likewise from Eqs. 6.17 and 6.29,

$$(\phi_P' \mu_N + \mu_P \phi_N') / (\phi_P' + \phi_N') = - T = 0$$

Substituting zero for both H and T into Eq. 6.21 yields Eq. 7.7 below:

$$\phi_N', \phi_P' = (1/2) P \pm (1/2) (P^2 - 4M)^{1/2} \qquad\qquad 7.7$$

If we now substitute Eq. 6.18 into Eq. 7.7 above we can obtain,

$$\phi_N', \phi_P' = (I_x p / 2 I_y) \pm (1/2) [(I_x p / I_y)^2 - 4M]^{1/2} \qquad\qquad 7.8$$

We will now define the gyroscopic stability factor as,

$$S_g \equiv (I_x\, p\, /\ I_y)^2 / 4M \qquad\qquad 7.9$$

Using this definition Eq. 7.8 can be rewritten as,

$$\phi_N{}',\, \phi_P{}' = (I_x\, p\, /\ 2\, I_y)[\ 1\ \pm\ (1 - 1\, /\ S_g)^{1/2}\ ] \qquad\qquad 7.10$$

Eq. 7.10 demonstrates that if the frequencies are to be real numbers, S_g, must always be greater than 1. Hence if a missile is to be gyroscopically stable $S_g > 1$. The form of S_g as shown in Eq. 7.9 is not a very useful relationship for computing; therefore, if we substitute Eq. 6.16 into Eq. 7.9 we can arrive at the equation shown below:

$$S_g \equiv (\ 2 I_x{}^2\, p^2\ )\ /\ (\ I_y\, \rho\, \pi\, d^3\, C_{m\alpha}\ ) \qquad\qquad 7.11$$

Note that $k_t{}^{-2}$ in Eq. 6.16 can be written as,

$$k_t{}^{-2} = m_a\, d^2\ /\ I_y \qquad\qquad 7.12$$

Equation 7.11 is the relationship typically shown or used when discussing the level of the gyroscopic stability of a spin stabilized configuration.

7.2.2 Dynamic

Dynamic stability is defined as the condition where a system is perturbed and the ensuing oscillatory motion has a tendency to either decrease(damp) or increase(undamp). Note that this definition assumes that static stability is present, otherwise the oscillatory motion would not occur. This static stability criteria can be provided by either the aerodynamic or gyroscopic moments as previously defined. Some analysts and test engineers feel that dynamic stability is a somewhat complicated system parameter to describe and define. This section will attempt to provide a simple derivation of the dynamic stability criteria and hopefully put at ease those who feel uncomfortable about this very important aerodynamic effect.

Again we will begin by using some previously derived relations, see the previous section and/or Section 6.1.3.

$$\mu_N + \mu_P = -\, H \qquad\qquad 7.13$$
$$(\ \phi_P{}'\mu_N + \mu_P\, \phi_N{}')\ = -\, PT \qquad\qquad 7.14$$
$$(\phi_P{}' + \phi_N{}') = P \qquad\qquad 7.15$$

Solving Eqs. 7.13 and 7.14 for μ_N and μ_P we arrive at,

$$\mu_N = (\ PT - \phi_N{}'\, H\ )\ /\ (\phi_N{}' - \phi_P{}')$$

and

$$\mu_P = (\ PT - \phi_P{}'\, H\ )\ /\ (\phi_P{}' - \phi_N{}')$$

Using Eq. 7.15 the two equations above can be written as shown below:

$$\mu_N = -\ (\ \phi_N{}'\, H - PT)\ /\ (2\phi_N{}' - P) \qquad\qquad 7.16$$

and

$$\mu_P = -\ (\ \phi_P{}'\, H - PT)\ /\ (2\phi_P{}' - P) \qquad\qquad 7.17$$

Equation 7.17 can now be expanded by adding and subtracting a like term, or

$$\mu_P = - [(\phi_P' H - PT) / (2\phi_P' - P)] + [(1/2) HP / (2\phi_P' - P)] - [(1/2) HP / (2\phi_P' - P)]$$

After simplifying we arrive at,

$$\mu_P = - (1/2)[H - P(2T - H) / (2\phi_P' - P)]$$

or,
$$\mu_P = - (1/2)[H - P(2T - H) / (\phi_P' - \phi_N')] \qquad 7.18$$

Likewise for Eq. 7.16, or

$$\mu_N = - (1/2)[H + P(2T - H) / (\phi_P' - \phi_N')] \qquad 7.19$$

Equations 7.18 and 7.19 shows that $\mu_N + \mu_P = - H$, which agrees with Eq. 7.13. Also that for zero spin, P=0,

$$\mu_N = \mu_P = - (1/2)H$$

As the spin rate increases

$$\mu_P = - (1/2)(H - \Delta)$$
$$\mu_N = - (1/2)(H + \Delta)$$

where

$$\Delta = P(2T - H) / (\phi_P' - \phi_N') \qquad 7.20$$

Now if we substitute Eq. 7.10 for ϕ_P' and ϕ_N' into Eq. 7.20 we can show that,

$$\Delta = - (2T - H) / (1 - 1 / S_g)^{1/2}$$

or
$$\Delta = - H(2T/H - 1) / (1 - 1 / S_g)^{1/2}$$

The above derivation illustrates that nutational and precessional damping rates, μ_N and μ_P, can be represented as functions of spin (P) as shown in the sketch below.
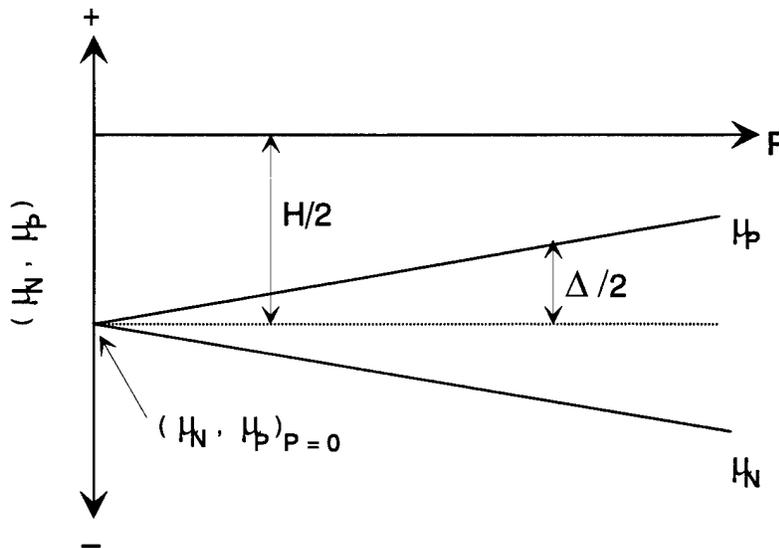
If the missile is always dynamically stable then both μ_N and $\mu_P < 0$ and from the sketch it is obvious that $\Delta/2 \le H/2$, or $\Delta \le H$. Therefore:

$$\Delta = - H(2T/H - 1) / (1 - 1 / S_g)^{1/2} \le H$$

or

$$(2T/H - 1) / (1 - 1 / S_g)^{1/2} \ge 1 \qquad 7.21$$

Now if we define the dynamic stability parameter S_d, as shown below:

$$S_d \equiv 2T / H \qquad 7.22$$

Substituting this definition back into Eq. 7.21 yields,

$$(S_d - 1)^2 \ge 1 - 1 / S_g$$

or

$$S_d \ge 1 \pm (1 - 1 / S_g)^{1/2} \qquad 7.23$$

Equation 7.23 effectively maps the dynamic stability bounds of any missile configuration as illustrated in Fig. 7.1
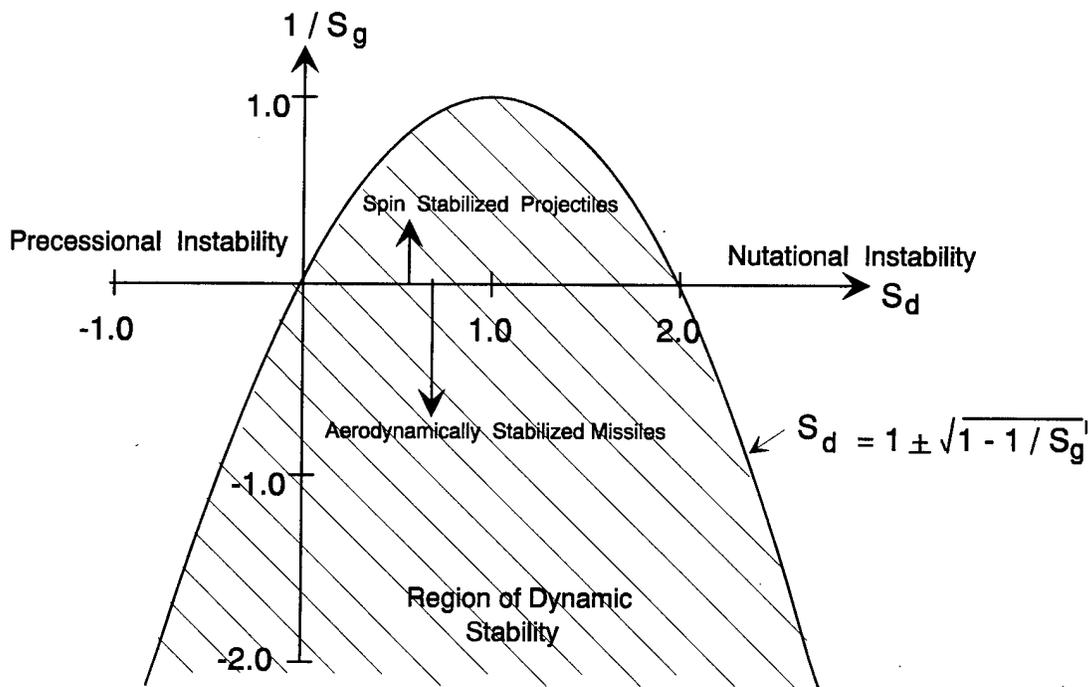
Figure 7.1 Dynamic Stability Criteria

The area above the S_d axis represents all gyroscopically stabilized projectiles, i.e. $S_g \ge 1$; likewise, the area below the S_d axis represents all other missile configurations. Once the missile's aerodynamics are known, either from testing or predictions, then S_g can be computed using Eq. 7.11 and S_d obtained from the relationship shown below.

$$S_d = 2(C_{N\alpha} - C_D + k_a^{-2} C_{np\alpha}) / [C_{N\alpha} - 2C_D - k_t^{-2}(C_{mq} + C_{m\dot\alpha})] \qquad 7.24$$

Equation 7.24 was obtained by substituting Eqs. 6.15 and 6.17 into Eq. 7.22.

Plotting $1/S_g$ vs S_d as indicated by Fig. 7.1 provides the analyst or missile designer with an estimate of the configuration's stability characteristics. This figure also illustrates where a precessional or nutational instability (μ_P or $\mu_N > 0$) would fall on the stability criteria chart. Obviously if the aerodynamics are nonlinear with angle-of-attack this evaluation may be required over a range of amplitudes. It would not be unusual to find that a missile is dynamically stable for some angles-of-attack and unstable at others. Frequently these conditions lead to angular motion patterns that develop into limit cycles. Also, occasionally analysts use terms such as 'Magnus instability' and this would simply be an instability caused by a Magnus moment derivative, $C_{np\alpha}$, of such a magnitude as to cause S_d to be outside the stability bounds as defined by Eq. 7.24. Since $C_{np\alpha}$ is an out of plane moment (perpendicular to the plane of the angle-of-attack) this moment is quite often the cause of such dynamic instabilities. Some configurations may exhibit out of plane moments which are not functions of spin, i.e. wrap around fin configurations[7.1,7.2]. For these configurations the $C_{np\alpha}$ term in Eq. 7.24 is replaced with a $C_{n\alpha}$ term and this out of plane moment can also be a source of dynamic problems, see Ref. 7.1.

7.3 OTHER USEFUL RELATIONS

7.3.1 Center-of-Pressure

The definition of the center-of-pressure is the point on the body where the resultant aerodynamic forces can be assumed to act. Therefore if we repeat the sketch shown in Section 7.2.1.1 the normal force, N, would be acting through the center-of-pressure, see the sketch below.
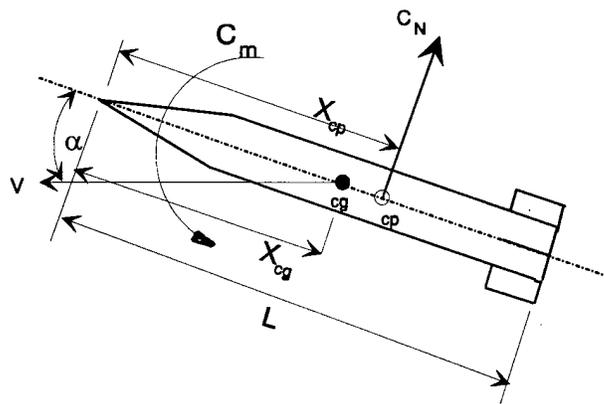
The center-of pressure can therefore also be defined as the point where the resultant aerodynamic moment is zero. In order to compute this point from the determined $C_{N\alpha}$ and $C_{m\alpha}$ data we start by writing the moment transfer equation, or

$$m_A = m_B + F x \qquad\qquad 7.25$$

This relation says that any moment about point A is equal to the moment about any other point B plus the force times distance between points A and B. Therefore if we let point A be the center-of-gravity(cg) , point B the center-of -pressure(cp), N the normal force, and x the distance between the cg and cp, then Eq. 7.25 can be rewritten as shown:

$$m_{cg} = m_{cp} + N (x / L) L$$

Expanding x as $x_{cg} - x_{cp}$, substituting the definitions for the force and moment coefficients, and note that $m_{cp} = 0$, the above equation can be written as:

$$x_{cp} / L = (x_{cg} / L) - (C_m / C_N)(d / L) \qquad\qquad 7.26$$

Equation 7.26 is the relationship used to compute the center-of-pressure location from force and moment coefficient data as obtained in a wind tunnel; where, the (x_{cg} / L) term is the moment reference location for that wind tunnel data. If the force and moment derivatives had been obtained instead of the coefficients, i.e. free-flight data, then Eq. 7.26 could be similarly written as:

$$x_{cp} / L = (x_{cg} / L) - (C_{m\alpha} / C_{N\alpha})(d / L) \qquad\qquad 7.27$$

It should be noted that the distance between the center-of-gravity and the center-of-pressure, $x_{cg} - x_{cp}$, is referred to as the missile's static margin.

7.3.2 Moment Reference Shift

In contrast to the aerodynamic forces, the moments are a function of the moment reference position. For free-flight data this is normally the model's cg location, at least during the trajectory analysis process. However, for wind tunnel data the moment reference location may be any position which is convenient for the model / balance installation. Therefore similar configurations may be tested at various times and facilities using different moment reference locations. In order to compare the results from these different tests the moment data must be shifted to a common reference location. Typically this common reference location might be the actual cg location for the full scale vehicle.

In order to accomplish this shift we will again start with Eq. 7.25. Substituting the force and moment definitions into this equation the following relationship can be written:

$$C_{mB} = C_{mA} - C_N [(x_A / L) - (x_B / L)] (L / d)$$

Again C_{mA} is the moment about the cg; however, now C_{mB} is the moment about an arbitrary common reference location, then

$$C_{mREF} = C_{mcg} - C_N [(x_{cg} / L) - (x_{REF} / L)] (L / d) \qquad\qquad 7.28$$

The corresponding relationship for the derivatives is therefore,

$$C_{m\alpha REF} = C_{m\alpha cg} - C_{N\alpha} [(x_{cg} / L) - (x_{REF} / L)] (L / d) \qquad\qquad 7.29$$

Equations 7.28 and 7.29 are the relationships used to shift the moment data to any other reference location and thereby compare results obtained from different facilities or at different times.

7.3.3 Normal Force Relation

As was shown in Section 6.1.4 the normal force derivative can be obtained from an analysis of the swerving motion. However, for cases where the model / projectile does not exhibit any significant swerving motion, i.e. a heavy model and/or one which has very small angular motions, the accuracy of the determined $C_{N\alpha}$ values may be suspect. For these cases another method of determining $C_{N\alpha}$ exists but which requires the moment data to be available for two different reference locations.

Rewriting Eq. 7.29 for two arbitrary reference locations, A and B, one can obtain Eq. 7.30 as shown below:

$$C_{N\alpha} (L / d) = (C_{m\alpha A} - C_{m\alpha B}) / [(x_A / L) - (x_B / L)] \qquad 7.30$$

This equation can be illustrated graphically as shown in the sketch below.
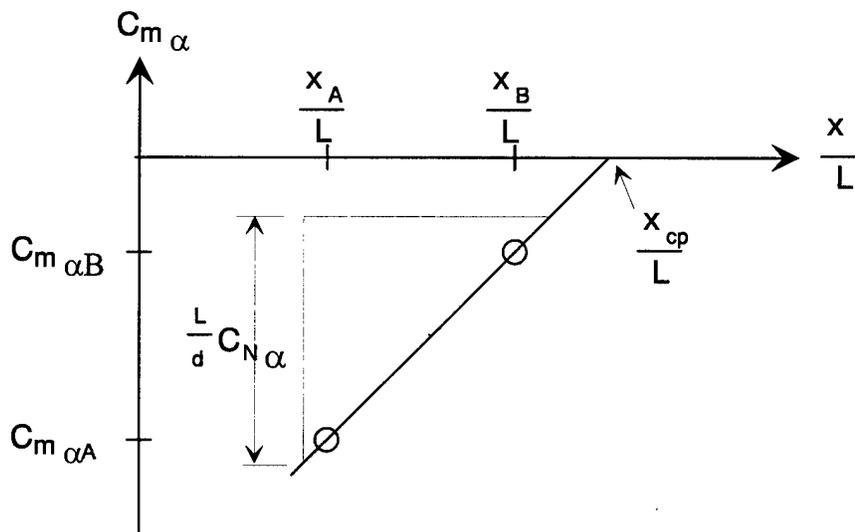
This sketch shows that the normal force derivative can be determined from the slope of $C_{m\alpha}$ vs x/L. In application this method consists of launching models with different cg locations at the same Mach numbers, determining their respective pitching moment derivatives, and computing $C_{N\alpha}$ from the indicated slope using Eq. 7.30. Since the pitching moment derivative can be determined very accurately even from relatively small angular motions this method can provide good estimates for the normal force when the results obtained by fitting the swerving motion are questionable.

7.4 DISPERSION

Frequently there is confusion over the definitions of dispersion and accuracy and as a result these terms can be misused. Simply put dispersion is the measure of the distribution of impacts whereas accuracy is a measure of the difference between the center of the dispersion distribution and the aim point. These definitions are illustrated in the sketches shown in Fig. 7.2.

a. High Dispersion, Inaccurate

b. High Dispersion, Accurate

c. Low Dispersion, Inaccurate

d. Low Dispersion, accurate
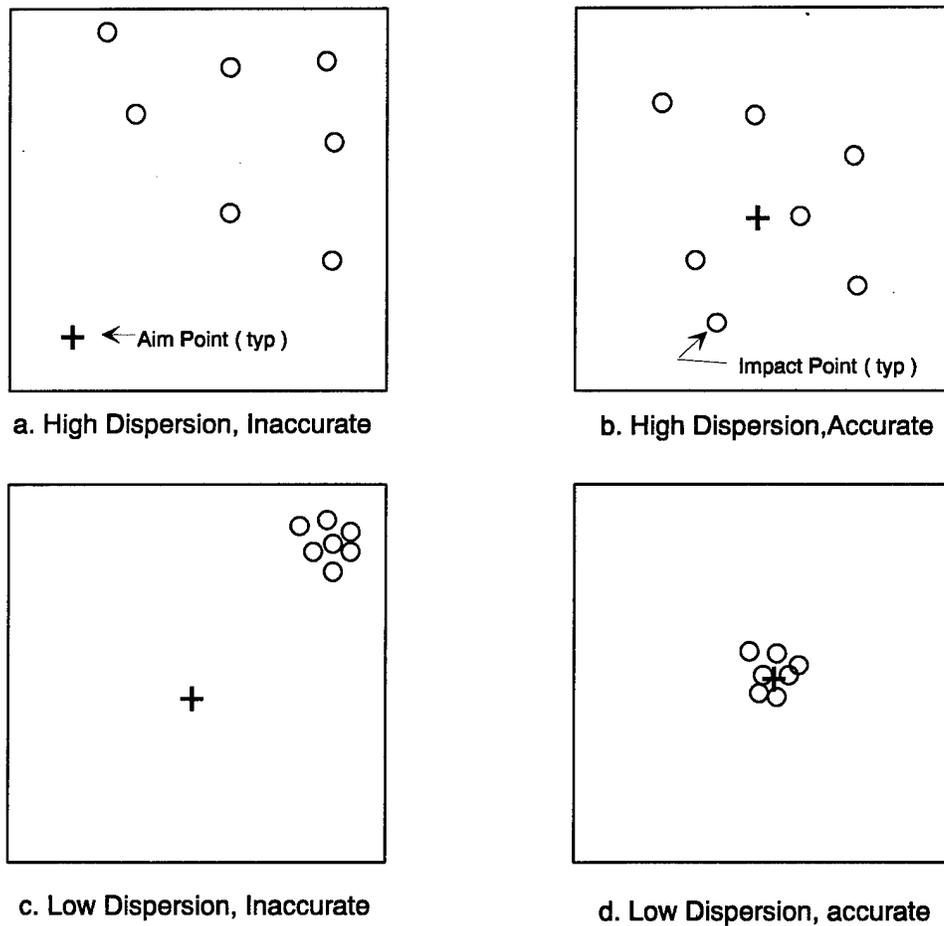
Figure 7.2 Illustration of Dispersion and Accuracy

Dispersion can be a function of a multitude of parameters associated with the launcher, projectile, and platform. Hence optimizing the dispersion can be a very complex task. However, accuracy can normally be achieved by adjusting the sighting system. For example a rifle possessing low dispersion can be 'sighted in' with a minimum number of shots, sometimes only one, by simply adjusting the sights to the impact points.

Since dispersion can be a critical performance parameter for any weapon system or munition, i.e. number of projectiles on target or probability of hit for a given munition, it is normally specified as an angular measurement (milliradians) and experimentally measured to ensure it is within specifications. Caution must be used in accomplishing these measurements because the apparent dispersion can be a function of the distance over which the measurements are obtained. This is especially true if the dispersion measurements are obtained over a relatively short flight distance such as a 1000 calibers or less, as will be shown in the following section. Generally the longer distance over which the measurements are taken the better, i.e. several thousand calibers should be the goal.

7.4.1 Predictions

It is difficult at best to compute the dispersion of a complete weapon system. However, the dispersion associated with the aerodynamic forces acting on a free-flight object can be reasonably estimated. If we start with Eq. 6.36 and neglect trim the swerving motion is only a function of the lift force derivative and the angular motion, or:

$$(y + iz)'' = (\rho A / 2\, m_a) [C_{L\alpha}(\beta + i\alpha)]$$

This relation is an oscillatory function with range; however, if the body is dynamically stable(i.e. the motion damps) this relation tends to degenerate into a straight line at extended ranges. Since the first maximum angle-of-attack will also be the largest angle-of attack experienced during the flight this straight line will not be parallel to the bore sight line. This deviation from the bore sight line is called 'aerodynamic jump', (A.J.), and is defined mathematically as shown below:

$$\text{A.J.} \equiv (y + iz) / x = \lim_{x \to \infty} (1/x)(\rho A/2m_a)\, C_{L\alpha} \int_0^x \int_0^x (\beta + i\alpha)dxdx \qquad 7.31$$

From Eq. 6.14, assuming $A_T = 0$, we can write

$$(\beta + i\alpha) = [(\beta + i\alpha)'' + (H - iP) (\beta + i\alpha)'] / (M + iPT)$$

Now if this equation is substituted into Eq. 7.31 and integrated by parts twice we can obtain,

$$\text{A.J.} = \lim_{x \to \infty}(\rho A/2m_a)[C_{L\alpha}/(M + iPT)]\{(1/x)(\beta + i\alpha)' - (x/x)(\beta + i\alpha)_0'$$

$$+ [(1/x)(\beta + i\alpha) - (x/x)(\beta + i\alpha)_0] (H - iP)\}$$

Taking the indicated limit we obtain,

$$\text{A.J.} = [(\rho A/2m_a)\, C_{L\alpha}/(M + iPT)]\{- (\beta + i\alpha)_0' - (\beta + i\alpha)_0 (H - iP)\}$$

where

$$(\beta + i\alpha)_0' \approx q_0 \text{ , initial angular cross rate}$$
$$(\beta + i\alpha)_0 \approx \delta_0 \text{ , initial angular displacement}$$

If we neglect the density squared terms, i.e. $\rho^2 \approx 0$, and assume that PT is small compared to M (M is in the C_L plane where PT is the side moment), then

$$\text{A.J.} = (C_{L\alpha}/M)\{-(\rho A/2m_a)\,q_0 + i(\rho A/2m_a)\,P\delta_0\}$$

Substituting Eq. 6.16 for M, Eq. 6.18 for P, and Eq. 7.12 for k_t^{-2} we finally arrive at the relation shown below:

$$\text{A.J.} = (d\,C_{L\alpha}/C_{m\alpha})\{-(I_y\,q_0/d^2 m_a) + i(I_x\,p\delta_0/d^2 m_a)\} \qquad 7.32$$

Equation 7.32 can be used to estimate the dispersion caused by the aerodynamic lift force derivative at extended ranges. Note that this relationship does not include the oscillatory portion of the swerve caused by the transient angular motion. Also recognize that this equation ignores the dispersion due to trim. For bodies with near zero spin containing aerodynamic or mass asymmetries the resulting aerodynamic trim can cause large dispersions since this trim force is always oriented in the same direction. However, this trim dispersion can be negated by purposely causing the model to spin thereby changing the orientation of the trim vector.

If the spin rate becomes very large, i.e. spin stabilized projectiles, Eq. 7.32 can be used to compute the aerodynamic jump caused by the in-bore clearances of the launch tube. For this condition the initial cross rate(q_0)can be assumed to be equal to $ip\delta_0$ where now δ_0 is the angle in the launch tube due to gun clearances. Therefore Eq. 7.32 can be written as,

$$\text{A.J.} = -i\,C_{L\alpha}\,\delta_0\,p(I_y - I_x)/(C_{m\alpha}\,d\,m_a) \qquad 7.33$$

The angle due to gun clearances, δ_0, can be easily computed as shown in the sketch below.
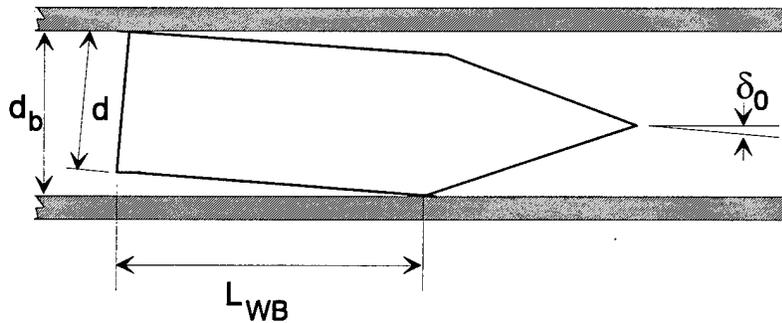
Or,

$$\delta_0 = (d_b - d)/L_{WB} \qquad 7.34$$

where: d_b = diameter of the barrel

         d = diameter of the projectile

        L_{WB} = length of the projectile's wheel base

The wheel base length can sometimes be difficult to estimate since most projectiles do not have easily defined points of contact. For example the model's base may be boat-tailed with a rotating band present and the nose section may consist of an ogive shape. Nevertheless L_{WB} can be estimated and Eq. 7.33 in conjunction with 7.34 has been successfully used to compute the dispersion of numerous configurations of various sizes and shapes of ammunition. The reader should refer to Ref. 6.1 for a much better treatment of aerodynamic jump.

7.4.2 Measurements

When experimentally measuring dispersion several factors should be remembered and considered. Some of these are outlined below.

a. The measurements should be obtained at a far enough distance such that the transient angle-of-attack effects have dampened out. As mentioned previously this should normally be several thousand calibers.

b. The measurements are obtained with respect to the center of the impact pattern, not the aim point.

c. The launcher and mounting system should not be altered in any way during the tests. If it is absolutely necessary to move the gun or mounts the resulting dispersion data must be corrected in some manner, i.e. the data could be corrected using the before and after aim point. However, it is preferable to start a new statistical base based on the new impact pattern.

d. If the muzzle velocities vary significantly during the tests, the data must be corrected for gravity drop.

e. Each projectile configuration will have its own dispersion pattern. Therefore enough rounds of each configuration should be fired to obtain a statistical base for that configuration.

Although the individual measurements are normally presented in mils, the dispersion pattern is frequently described as circular error probable, CEP. The CEP of the dispersion pattern is defined as the radius of the circle in which 50 percent of the rounds will impact. Usually, with only minimal effort, dispersion measurements can be obtained in the free-flight spark range at the same time the aerodynamic tests are ongoing. Frequently this is not accomplished either because it is believed that the data would not be representative of the actual configuration or because something was done during testing in order to excite the angular motion. Nevertheless the test engineer should note that this data can be obtained at very small additional expense and effort if it is required and appropriate for his particular tests.

REFERENCES

7.1 Winchenbach, G. L ., Buff, R. S., Whyte, R. H., and Hathaway, W, H.,"Subsonic and Transonic Aerodynamics of a Wraparound Fin Configuration", AIAA Paper 85-0106, January 1985.

7.2 Abate, G. L., and Winchenbach, G. L.,"Aerodynamics of Missiles with Slotted Fin Configurations", AIAA Paper 91-0676, January 1991.

VIII. FUTURE REQUIREMENTS

It is always dangerous in attempting to predict what the future might bring to any line of endeavor. However, it is somewhat less hazardous here since each of the technologies discussed have efforts already on-going and some have been in consideration for several years. Other than the interesting aerodynamic issues a researcher can be involved with there are also three primary support technologies which are always of interest to the ballistician. These three areas are advanced instrumentation systems, improved launchers and launch techniques, and new theoretical and trajectory analysis algorithms. A brief discussion of the on-going efforts in these three areas will be presented in this section.

8.1 INSTRUMENTATION

8.1.1 Flow Field Visualization and Measurements

Over the years the study of basic fluid flow physics has required the development of flow visualization techniques. These have included smoke generation, shadowgraph and schlieren photography along with relatively complex interferometry techniques. The aerodynamist is also constantly attempting to relate changes / variations in the measured aerodynamic coefficients and derivatives with observable phenomenon occurring in the flow about the body. For these reasons and others, flow visualization is of interest to the researcher. Recently with the development of computational fluid dynamics (CFD) codes a requirement to be able to validate these codes with experimental data has arisen. Although surface pressure and non-obtrusive velocity data can be obtained in the wind tunnel, non-obtrusive pressure and density measurements in the far flow fields or wake can be difficult if not impossible to obtain.

In order to obtain basic non-obtrusive measurements an effort was initiated in the early 1990's to develop a multiview holographic interferometry system, and the corresponding data analysis algorithms for mapping the flow field density [8.1,8.2]. These flow field density maps would then be used to assist in validating the corresponding CFD predictions or to develop advanced CFD turbulence models, etc. A schematic of the holocamera developed for this purpose [8.1] is presented in Fig. 8.1 and was positioned in the up-range end of the ARF. Several basic model configurations were flown through this holocamera and 6 different views obtained (see interferograms in Fig. 8.2). These images were then passed into the phase shift interferometry algorithm [8.2] for analysis. Although this algorithm was successfully demonstrated using generated data the existence of experimental noise (primarily Laser speckle) in the images caused the phase map unwrapping process to fail.

It is believed that the primary source of the Laser speckle comes from the scatter plates in the holocamera, see Fig. 8.1. In fact, preliminary bench tests [8.2] using a mirror in place of a scatter plate tended to confirm this belief. As a result, an effort to continue development of this technique is currently in progress. The initial approach will be to
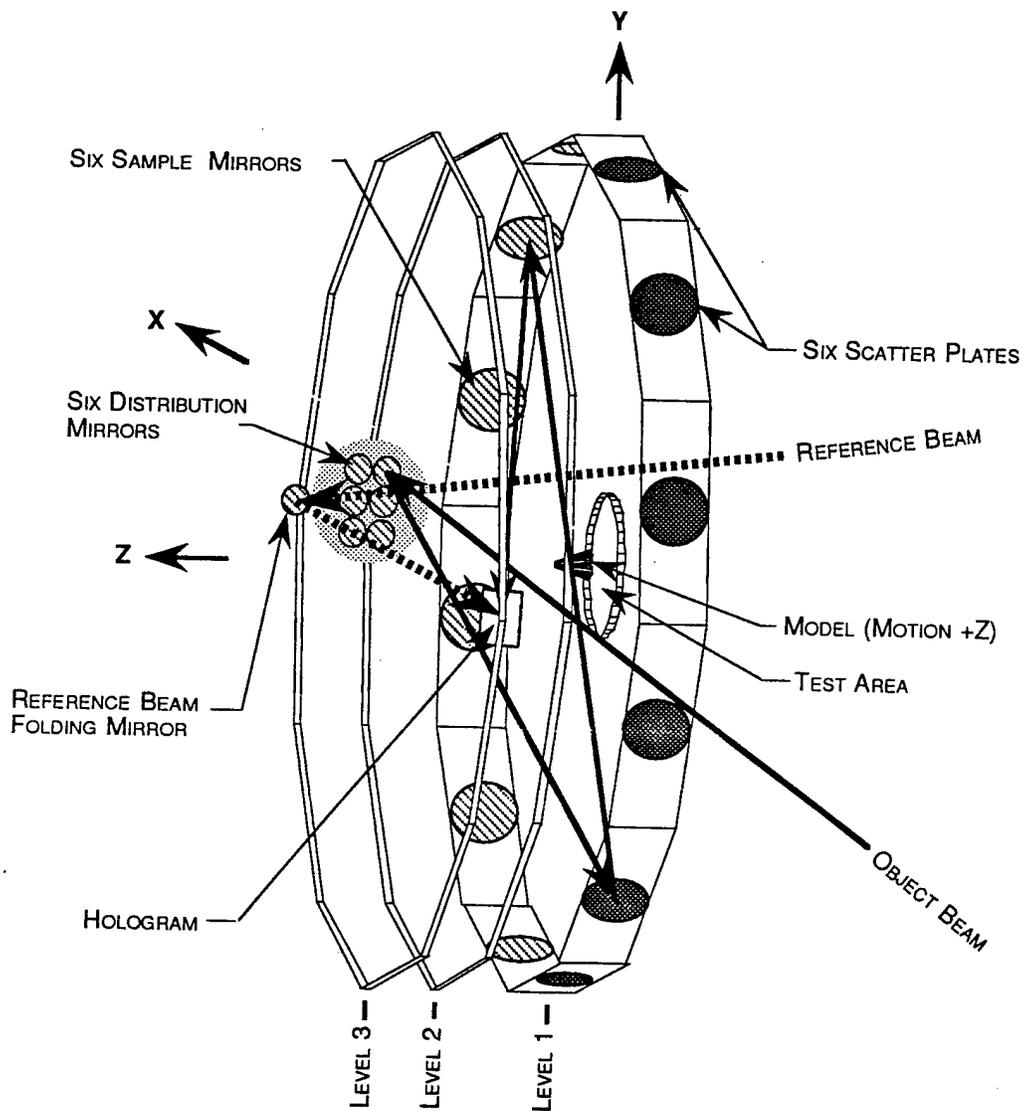
Figure 8.1 Three Dimensional Layout of the Holocamera
(Fig. 2 from Ref. 8.1)

replace one of the scatter plates with a first surface mirror and obtain a holographic interferogram of a free-flight object. This interferogram will be duplicated 5 times and the corresponding 6 images passed into the phase shift interferometry algorithm for analysis and evaluation. Assuming that a successful result will be achieved the remaining scatter

plates in the holocamera will be replaced with similar mirrors. This would then complete a system which would be capable of determining the flow field densities about free-flight missile configurations and provide heretofore unobtainable data for analysis and comparison with theoretical predictions.
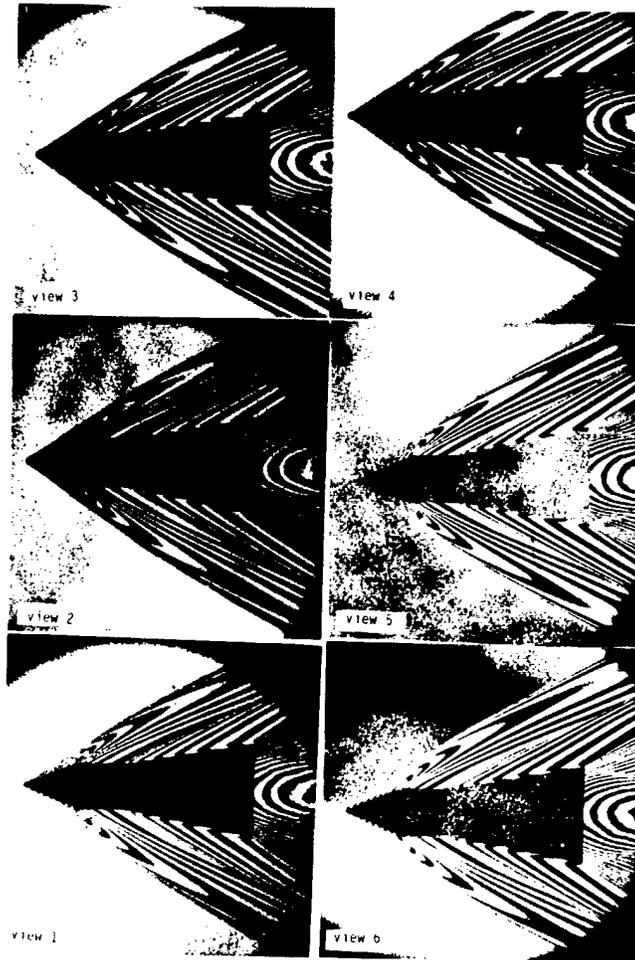
Figure 8.2 Six Simultaneous Interferograms of a Cone Cylinder Flare Configuration at Mach 3. (Fig.13 from Ref. 8.1)

8.1.2 Electronic Imaging

As was discussed in Section 5.1, also see Ref. 5.4, it has been planned for some time to convert the existing film based system in the ARF to an electronic imaging system based on modern charge coupled device (CCD) technology. The first part of this conversion was the procurement of the Ektron film scanner and the development of the associated image processing system (CADRA)[5.2]. Now that the image processing system is operational and used on a daily basis the primary task still requiring completion is the procurement and installation of the CCD cameras. The cameras chosen for this installation are EG&G, Optoelectronics-Reticon, high resolution devices. It is planned to

115

install 1k x 1k pixel array cameras in the up-range end of the facility and 2k x 2k devices in the down-range section of the ARF. It is believed that the higher resolution is required down-range for two reasons. First the cross sectional dimensions of the facility are larger down-range and secondly, because of potential projectile dispersion, the area to be viewed is significantly larger. The network connecting the cameras to the control room, data collection and analysis system has been designed and will incorporate an ethernet interface and protocol. A schematic of the electronic shadowgraph system including the existing film scanner is included in Fig. 8.3.
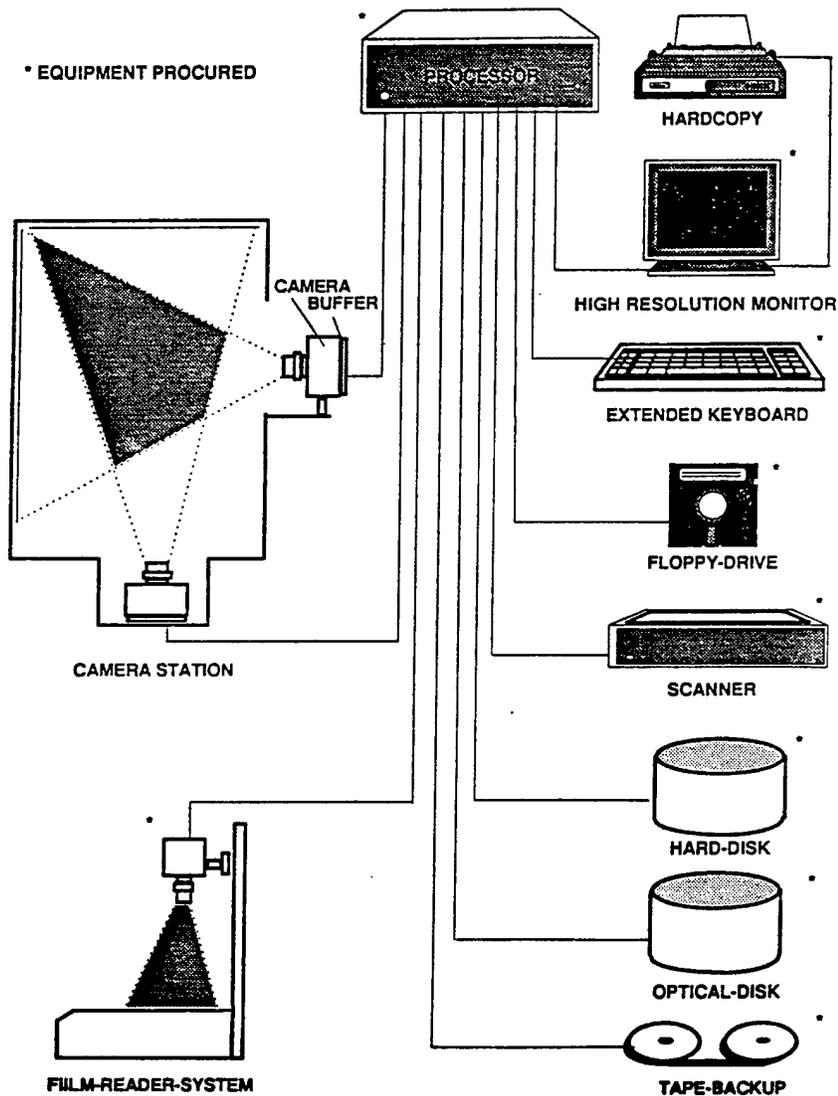
Figure 8.3 Schematic of Electronic Shadowgraph System
(Fig. 5 from Ref. 5.4)

Once this system has been installed the complete process from test firing to having the trajectories ready for analysis will be minutes instead of days as is presently required. The film scanning and digitization is the single most manpower intensive operation at the present time and this along with film handling and processing will be completely eliminated with the installation of the electronic cameras. However, because of limited resources, it is contemplated that completion may require several years to procure the 100 cameras required to outfit the facility.

8.1.3 On-Board Instrumentation

On-board instrumentation techniques have been used in aerodynamic testing for many years especially for the development of manned vehicles or relatively large unmanned systems. Objects as small as artillery rounds or sounding rockets [8.3,8.4] have also utilized on-board instrumentation; however, such packages have not been used extensively for test items in the 20-30 mm diameter range. This is primarily due to the relatively small volumes available for packaging the desired instrumentation and the problems associated with recovering the data. Historically, two different approaches to recovering the data have been used. The first is to transmit the data to a receiving station while the test item is in flight. This approach requires the model to not only carry the desired sensor(s) but a miniaturized transmitter and antenna as well. The second approach is to record the data on-board and to recover the test item and remove the stored data. This approach requires a miniaturized recording device that must survive the flight termination event and also be recoverable. Although both techniques have been successfully used in the past neither has been particularly beneficial to free-flight testing of subscale items.

This may change in the very near future with the development of a family of hardened subminiature sensor and telemetry packages. Such a family of on-board instrumentation is presently being developed by the U.S Army [8.5]. It is hoped that this technology demonstration program will develop instrumentation for the continuous measurement of projectile attitude, pressure, temperature, accelerations and other flight data at reasonable costs. If this program is successful it could revolutionize free-flight aerodynamic testing as we know it and open numerous horizons heretofore unimaginable.

8.2 LAUNCH TECHNIQUES

8.2.1 Launchers

Ballistic researchers / practitioners are always interested in improving the existing launchers and developing new launch techniques. This interest stems from the desire to launch larger and heavier packages at higher and higher velocities or to subject existing packages to reduced in-bore acceleration loads. There is always the need to expand the existing operational envelopes into regions unobtainable in the past. Also, if the in-bore accelerations can be reduced while maintaining the muzzle velocity, relatively fragile model / sabot packages can be launched and still survive the launch loads. In general these are the considerations which led to the development of two-stage light gas guns

for use in various laboratories and initially spurred the interest in other more advanced concepts, i.e., electromagnetic launchers, ram accelerators, etc.

During a preliminary study into the possibility of weaponizing a two-stage light gas gun a rather unique two-stage firing cycle was discovered [8.6]. In contrast to the conventional two-stage light gas gun this new launcher(wave gun) employed a very light piston in a short pump tube (low volume) containing a light gas, i.e. hydrogen or helium, at relatively high pressures. These conditions permitted the piston to oscillate in the pump tube prior to the rupture of the diaphragm and the resulting acceleration of the model / sabot package down the launch tube. This firing cycle potentially can minimize the in-bore accelerations for a given muzzle velocity. Also portions of the existing two-stage light gas gun hardware could be used with only minor changes. Therefore this appears to be an attractive technique for use in free-flight experimental / research facilities. A comparison of the two types of cycles are shown in Fig. 8.4.
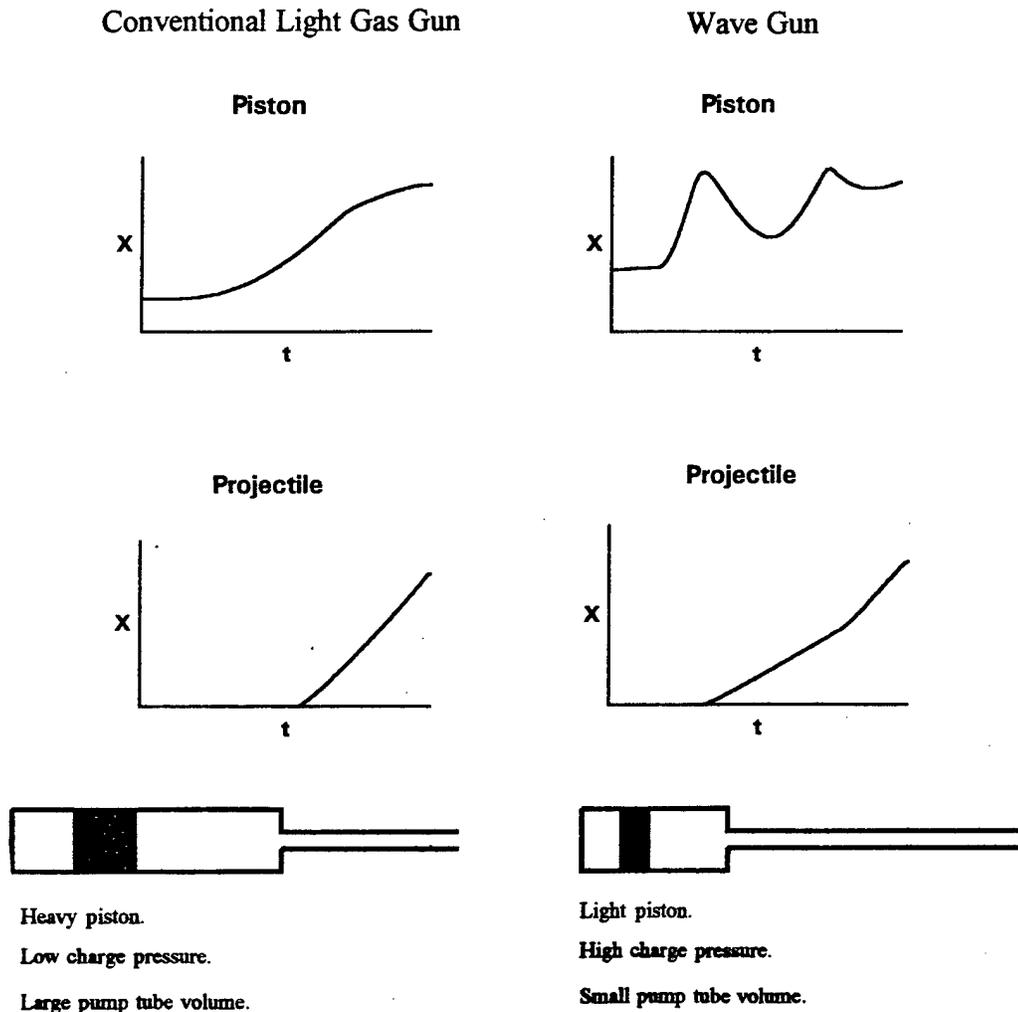
Figure 8.4 Firing Cycles for a Conventional Two-Stage Light Gas Gun and a Wave Gun

118

A recent investigation was conducted to develop a mathematical model of a wave gun and validate this model with some experimental tests [8.7]. That investigation was successful leaving two questions still to be determined. First, does the wave gun firing cycle illustrated in Fig. 8.4 possess enough advantages over the conventional two-stage light gas gun to justify the required modifications. Secondly, what are the optimum dimensions of the necessary hardware modifications, i.e., pump tube and piston. An effort is on-going to answer these questions and depending on the results the existing two-stage light gas gun [8.8] will either be modified or maintained in its present configuration.

8.2.2 Sabot Design

As mentioned in Section 3.3, at the present time the designer does not have access to a user friendly sabot design software package. There are several existing finite element software packages which have been successfully used for point designs, however, they could not be described as user friendly. Typically they require highly trained and experienced analysts and have been developed to handle a multitude of diverse and generalized design problems. What is required for the ballistics researcher is an easily used code and design process developed solely for sabots. This requirement was recognized and an on-going effort established in an attempt to provide the designer with such tools, see Ref. 8.9. This reference describes the on-going program and also contains an excellent bibliography of sabot technology. Essentially the final output of the effort will be a design code which will contain a finite element routine specifically written for sabots and simple closed form solution routines based on past point designs. The approach will be to develop several basic sabot designs using these codes which are expected to fail under certain launch conditions. These designs will then be built and tested at conditions in and around the expected failure conditions. The results of these tests will provide the required data to evaluate the design codes.

In conjunction with the effort described above a simple mechanism to evaluate the mechanical properties of various materials commonly used in sabot construction will also be constructed and evaluated, see sketch below.

119
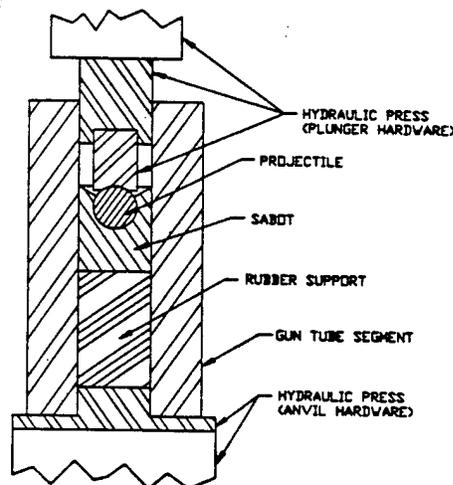
It is suspected that the material properties of some of these materials, i.e., polycarbonates, may vary significantly from batch to batch or with different manufacturers. There is also considerable concern that the material properties may change over time. Hence sabots constructed in the past and that were successful may fail at identical test conditions in the future. That certainly is a designer's nightmare and this simple testing apparatus may be sufficient to guard against that possibility.

Undoubtedly there will be several publications, papers and reports, documenting the results of this on-going effort in the relatively near future. It is hoped that this work and the associated publications will take some of the art out of sabot design and put it on a firm scientific basis.

8.3 TRAJECTORY ANALYSIS

8.3.1 Aerodynamic Modeling

Considerable progress has been made in modeling the aerodynamic coefficients and derivatives as functions of angle of attack, Mach number, and roll orientation during the past, see the discussions on the quasi-nonlinear analysis and numerical integration in Sections 6.2 and 6.3 and the references at the end of Section VI. All of these existing techniques assume that aerodynamic parameters can be expanded as predetermined mathematical functions, normally polynomials (see the expansions presented in Section 2.3). The analysis routines then determine the coefficients of these assumed functions such that the theoretical equations of motion best match the experimentally measured motions. For a great majority of the test flights this process works exceptionally well and the resulting aerodynamics adequately describes the experimental motion profiles.

However, there are configurations of interest where these predetermined mathematical functions do not adequately describe the aerodynamics. For example any configuration which possesses small angle-of-attack (-3 to + 3 degs) nonlinearities cannot be adequately modeled with polynomials since these functions inherently describe nonlinearities which increase with increasing angle-of-attack. Therefore any polynomial which would adequately describe a small angle-of-attack nonlinearity would greatly exaggerate the nonlinearities at the higher angles. Also, these functions can pose serious restrictions for almost any configuration at very high angles-of-attack (angles greater that 30 degs). Finally this existing process imposes a heavy burden on the analyst in selecting the correct form of the predetermined mathematical functions and requires considerable experience in recognizing which of the aerodynamic expansions are likely required to successfully describe the experimentally measured motions.

Considering the above comments the free-flight trajectory analyst is always vigilant in looking for advanced mathematical modeling techniques or processes which could alleviate the necessity of assuming a known form for the various nonlinearities. Recently three such techniques were investigated and discussed in Ref. 5.2. These three techniques were identified as splines, the Mook technique, and the Mook-Taylor series technique.

The splines investigated in Ref. 5.2 utilized continuous piecemeal linear functions. However, this technique would not be restricted to linear functions and higher order polynomials could be splined together in a similar manner. Essentially this process would describe the nonlinear aerodynamics as a series of short line segments where the analyst could select the interval for the knot locations, i.e., every degree or so. In the Mook technique no mathematical model for the aerodynamic parameters are specified and the aerodynamic coefficients and derivatives are computed at each experimentally measured data point. Therefore this technique provides the aerodynamics as a function of time not angle-of-attack, Mach number, or roll orientation. In the Mook-Taylor series technique the Mook terms represent the Taylor series corrections.

All of the above data correlation techniques have been coded into the CADRA software package along with the conventional polynomial expansions. But, other than what was done in Ref. 5.2, a detailed and systematic study of the various options have not been accomplished to date. Presently what is required is a pressing reason and need to accomplish such a detailed investigation. A set of experimental data which cannot be adequately analyzed using the conventional polynomial expansions would provide this reason and need.

If one of these or any other advanced data correlation technique proves successful in the future it is believed that it would be incorporated into the existing ARFDAS routine, see Fig. 6.1, instead of replacing the existing system. The idea being that the trajectory analysis would proceed exactly the same as now using the polynomial expansions for the aerodynamics. However, the last step would then be to pass these results into the new technique as the initial starting point for the advanced data correlation routine and accomplish one additional level of analysis. This last step may prove not to be necessary for all configurations but would be available for those that required a more general aerodynamic model.

8.3.2 AUTOMATION

At the present time free-flight data collection and trajectory analysis requires a considerable amount of hands-on interaction of the facility operators and analysts and are manpower intensive. This hands-on interaction starts with the film handling, i.e., loading film into cassettes, removing exposed film from the cassettes, film processing, and film scanning and digitization into the CADRA software system. The final completion and installation of the electronic shadowgraph system as described in Section 8.1.2 will eliminate these manpower intensive operations. In fact once the electronic cameras are installed the CCD images will be available for trajectory computations immediately after the test flight is terminated. The CADRA system has an automatic image scanning routine already imbedded in the software. This automatic image scanning routine has been checked out using ideally generated images but has not been utilized for experimentally obtained images. This automatic routine requires that the reference points in the images be somewhat consistently positioned each time an image at a given shadowgraph station is obtained. At the present time the film cannot be manually

positioned on the scanner with enough precision and consistency for the automatic routine to locate the reference points. However, when the CCD images arrive for scanning they will be consistently positioned and the automatic routine can be utilized. This not only means that the images are available for immediate analysis but that within minutes after the test flight the experimental trajectory will be available for analysis and extraction of the aerodynamic coefficients and derivatives.

In the past few years considerable effort has also been expended in automating much of the trajectory analysis process, see for example Ref. 8.10. This reference describes an expert system based on artificial intelligence (AI) techniques. It is believed that a similar system in conjunction with the automatic image processing and trajectory computation routines would permit real time trajectory analysis and the determination of the aerodynamic coefficients and derivatives for many if not most of the test configurations. Certainly this could be accomplished for most configurations within a hour or two of the test flight and allow the user and test engineer to consider these results prior to launching the next test model.

Continuing this process of automating the data collection and trajectory analysis process is an absolute necessity in the future. The benefits which will be derived from this process include:
   (1) the elimination of potential human errors which presently exist in the existing manpower intensive operations
   (2) reduced man-hours required, i.e., film handling, processing, scanning
   (3) reduced material resources required, i.e., film, processing chemicals
   (4) immediate availability of aerodynamic data for programmatic decisions
   (5) improved facility efficiency (more tests in less time)
   (6) improved user perceptions associated with perceived outdated processes and techniques
Automation is the key to the future viability of free-flight spark ranges. Such facilities have and should continue to provide a unique role in aerodynamic testing but like any other tool they must be maintained and improved to meet future requirements.

REFERENCES

8.1 Anderson, R.C., "Six View Holographic Interferometer", WL-TR-96-7034, April 1996.

8.2 Trolinger, J.D., Millerd, J., and Gran, M., "Development of an Interferometry / Tomography Data Reduction System", WL-TR-96-7023, February 1996.

8.3 Burdeshaw, M.R., and Clay, W.H., "Subminiature Telemetry Tests Using Direct Fire Projectiles", BRL-MR-3893, February 1991.

8.4 Brown, T.G., et al, "Flight Testing of a 2.75-inch Rocket; M257 Illuminating Warhead with MK66, Mod 2 Rocket Motor", ARL-MR-297, March 1996.

8.5 D'Amico, W.P., Burke, L.W., Faulstieh, R.J., and Hooper, A., "The Hardened Subminiature Technology and Sensor System Technology Demonstration Phase", ARL-TR-1206, October 1996.

8.6 Dahm, T.J., and Randall, D.S., "The Wave Gun Concept for a Rapid Fire Hypervelocity Weapon", paper presented at the 1984 JANNAF Propulsion Meeting, New Orleans, LA, 8 February 1984.

8.7 Hugenroth, J.J., and Courter, R.W., "Wave Gun Optimization", paper presented at the 47th meeting of the Aeroballistic Range Association, Saint-Louis, France, October 1996.

8.8 Swift, H.F., McDonald, J.W., and Chelekis, R.M., "Description and Capabilities of a Two-Stage Light Gas Launcher", paper presented at the 35th meeting of the Aeroballistic Range Association, Meppen, Germany, September 1984.

8.9 Swift, H.F, et al, "Modern Advances in Sabot Technology for Ballistic Research", WL-TR-96-7014, December 1994.

8.10 Hathaway, W.H., Steinhoff, M., and Whyte, R.H., "Expert System for Ballistic Range Data Analysis", WL-TR-93-7073, October 1993.

(This page is blank)

APPENDIX 1

LOCATION OF INSTRUMENTATION IN THE
AEROBALLISTIC RESEARCH FACILITY

ARF INSTRUMENTATION LOCATIONS

WINDOW NUMBER	NOMINAL X-DISTANCE FT	INSTRUMENTATION	WINDOW NUMBER	NOMINAL X-DISTANCE FT	INSTRUMENTATION
1	0.0	INTERFEROMETER 1	34	165.0	
2	5.0	S.G. STA. 1	35	170.0	S.G. STA. 16, T.C. 3
3	10.0	S.G. STA. 2, T.C. 1	36	175.0	
4	15.0	S.G. STA. 3	37	180.0	S.G. STA. 17
5	20.0	INTERFEROMETER 2	38	185.0	S.G. STA. 18
6	25.0	S.G. STA. 4	39	190.0	
7	30.0		40	195.0	MULTI. SPARK 3
8	35.0	DIRECT S. G. STA.	41	209.8	S.G. STA. 19
9	40.0	A.C. CONTROL	42	214.8	RELATIVE HUMIDITY
10	45.0	S.G. STA. 5	43	219.8	S.G. STA. 20
11	50.0		44	224.8	
12	55.0	S.G. STA. 6	45	229.8	S.G. STA. 21
13	60.0		46	234.8	
14	65.0	S.G. STA. 7	47	239.8	S.G. STA. 22
15	70.0	S.G. STA. 8	48	244.8	
16	75.0	S.G. STA. 9	49	249.8	S.G. STA. 23, A.C. CON.
17	80.0		50	254.8	
18	85.0	MULTI. SPARK 1	51	259.8	S.G. STA. 24, T.C. 4
19	90.0	T.C. 2	52	264.8	
20	95.0	S.G. STA. 10	53	269.8	S.G. STA. 25
21	100.0		54	274.8	S.G. STA. 26
22	105.0		55	279.8	
23	110.0		56	284.8	
24	115.0	S.G. STA. 11	57	289.8	S.G. STA. 27
25	120.0		58	294.8	
26	125.0	S.G. STA. 12	59	299.8	
27	130.0		60	304.8	S.G. STA. 28
28	135.0	S.G. STA. 13	61	309.8	
29	140.0		62	314.8	
30	145.0	S.G. STA. 14	63	319.9	S.G. STA. 29
31	150.0	S.G. STA. 15	64	324.9	
32	155.0		65	329.9	
33	160.0	MULTI. SPARK 2	66	334.9	S.G. STA. 30

ARF INSTRUMENTATION LOCATIONS

WINDOW NUMBER	NOMINAL X-DISTANCE FT	INSTRUMENTATION	WINDOW NUMBER	NOMINAL X-DISTANCE FT	INSTRUMENTATION
67	339.9	T.C. 5	100	505.1	
68	344.9		101	510.1	
69	349.9	S.G. STA. 31 , A.C. CON.	102	515.1	S.G. STA. 41
70	354.9		103	520.1	
71	359.9		104	525.1	
72	365.0	MULTI. SPARK 4	105	530.1	S.G. STA. 42
73	370.0		106	535.1	
74	375.0		107	540.1	
75	380.0	S.G. STA. 32	108	545.1	S.G. STA. 43
76	385.0		109	550.1	A.C. CONTROL
77	390.0		110	555.1	
78	395.0	S.G. STA. 33	111	560.1	S.G. STA. 44
79	400.0		112	565.1	
80	405.0		113	570.1	MULTI. SPARK 5
81	410.0	S.G. STA. 34	114	575.1	
82	415.0		115	580.2	T.C. 7
83	420.0		116	585.2	S.G. STA. 45
84	425.0	S.G. STA. 35	117	590.2	
85	430.0		118	595.2	
86	435.1		119	600.2	S.G. STA. 46
87	440.1	S.G. STA. 36	120	605.2	
88	445.1		121	610.2	
89	450.1	A.C. CONTROL	122	615.2	S.G. STA. 47
90	455.1	S.G. STA. 37	123	620.2	
91	460.1		124	625.1	
92	465.1		125	630.1	S.G. STA. 48
93	470.1	S.G. STA. 38	126	635.1	
94	475.1		127	640.1	
95	480.1		128	645.1	S.G. STA. 49
96	485.1	S.G. STA. 39	129	650.1	
97	490.1		130	655.1	A.C. CONTROL
98	495.1		131	660.1	S.G. STA. 50
99	500.1	S.G. STA. 40 , T.C. 6			

NOTE; T.C. # IS THERMOCOUPLE # - RANGE TEMP.
S.G. STA. # IS SHADOWGRAPH STATION #

(This page is blank)

128

APPENDIX 2

FACILITY CALIBRATION TECHNIQUE

(Extracted from Ref. 3.13)

A 2.1 BASIC CONCEPT

When developing the calibration technique several features appear advantageous. It was hoped that most if not all of these features could be incorporated into the final technique. These features were:
  a. no surveying should be required,
  b. technique to be accomplished by the normal operating crew,
  c. the range coordinates of all reference beads and spark source orifices (100 of each, two at each of the 50 shadowgraph stations) should be simultaneously determined,
  d. technique should require a minimum of range downtime,
  e. a minimum of special hardware and fixtures should be required.
Working with these considerations in mind the technique discussed herein was developed.

Early in the development process it was recognized that if shadowgrams of points in space with known range coordinates could be obtained that these would represent an ideal source of range calibration. The logic being that once these shadowgrams were obtained the range coordinates of the shadows of the known points could be determined with respect to the reference system which would likely contain errors. If the range coordinates of the reference system beads were not in error then the vectors connecting the shadows to the associated known points in space would intersect at the spark source orifice. This is obvious since the rays casting the shadows all originated at the orifice. Therefore if the range coordinates of a reference bead were in error, as likely they would be, the vectors connecting the shadows to the associated known points would not intersect. It was also recognized that the error (other than film reading) in the shadow of the known point is equal to the error in the range coordinates of the reference system bead. Note that the shadow coordinates are obtained with respect to the reference bead. Therefore if the range coordinate of the reference bead are varied until the vectors, defined by the shadows and the associated known points in space, intersect then these new coordinates are the true range coordinates of the reference bead and the point of intersection is the spark source orifice location. Actually, since film reading errors are also present the above process amounts to minimizing a circle of intersection of the vectors and assuming that the center of this circle corresponds to the spark source orifice.

A 2.2 DETERMINATION OF KNOWN POINTS

The above discussion illustrates that, using this approach, the problem of range calibration reduces to a problem of positioning points in space whose range coordinates are known. However, this also can be a serious problem especially when surveying is undesirable and it is wished to calibrate all shadowgraph stations simultaneously. The method selected for obtaining points with known coordinates consisted of a Kevlar® wire with beads positioned precisely 1.524 meters (5 ft) apart strung the entire length of the instrumented range. This wire was adjusted such that one bead was in the field of view of both cameras at each of the 50 shadowgraph stations. This calibration wire had been

constructed while under 3.63 Kgm (8 lb) of tension using an Invar® tape calibrated every 1.524 meters. When hanging in the range the calibration wire was fixed at the up-range end and the downrange end was passed over a near frictionless pulley with the same weight attached. The calibration wire with the beads attached, the calibrated tape, and the support system at both ends are all of the special hardware required.

With this calibration wire in place shadowgrams are obtained at all 100 cameras (two at each of the 50 shadowgraph locations). The calibration wire is then moved to another location both cross range and vertically and the process of obtaining shadowgrams at each of the 50 locations repeated. This process is accomplished for several different positions of the calibration wire. Three sets of shadowgrams are to be used to calibrate the reference bead and spark source orifice locations and the remaining sets of shadowgrams will be used to get a statistical base for determining the measurement precision. The positions of the shadows of the beads on the calibration wire are then read and numerically coded as if they were test items in flight. Using the resulting measured range coordinates of the calibration beads the actual range coordinates of the calibration beads are determined statistically by using the known physical state of the calibration wire. This known physical state consists of the facts listed below:
a. the cross-range coordinates (y) plotted vs the down-range coordinates (x) define a straight line,
b. the vertical-range coordinates (z) plotted vs x define the equation of a catenary,
c. initially the arc length between beads on the calibration wire was 1.524 meters.
The mathematical treatment as discussed in the following sections permits the calibration wire to stretch or contract assuming it occurs linearly over the entire length of the range.

A 2.2.1 CROSS-RANGE COORDINATES

The actual y (cross-range) coordinate of each calibration bead is determined statistically by least squares fitting a straight line to the measured y and x coordinate data. These measured y and x coordinates were obtained using a previous range calibration or initial estimates for the spark source orifice and reference bead locations.
Once this fit has been obtained, the theoretical y coordinate corresponding to each measured y coordinate represents the best statistical estimate of the actual cross-range coordinate for each bead location. It should be noted that when the calibration shadowgrams are obtained some care should be exercised to ensure that the calibration wire is nominally parallel to the range reference system. By insuring that the wires are nominally parallel, large errors in the measured x coordinates can be tolerated during the fitting process and still only insignificant errors in the theoretically determined y coordinates will result. Also , when the calibration shadowgrams are obtained the heating / air conditioning system must be turned off in order minimize the effects of air currents on the calibration wire. This ensures that the wire hanging under its own weight describes a vertical plane and the straight line assumption is valid. Since the technique of least squares fitting a straight line to data points is common place it is not elaborated on here.

131

A 2.2.2 VERTICAL-RANGE COORDINATES

Two different statistical approaches of determining the actual z (vertical) coordinate of each calibration bead were investigated. These two approaches consisted of fitting the measured z and x coordinates by either assuming that z was a parabolic function of x, or that z was a hyperbolic cosine function of x. The actual equation of a wire hanging under its own weight (the shape of which is called a catenary) is a hyperbolic cosine function but the fitting process is somewhat more complex than the parabola. It is also well known that a parabola is an excellent approximation to the equation of a catenary when the sag is small. Both of these methods were therefore evaluated by fitting the measured z and x coordinates of a typical calibration wire and comparing results. The maximum difference between the two theoretical curves as determined from these fits was 0.34×10^{-6} meters and the average difference was 0.14×10^{-6} meters. Since these differences are a couple orders of magnitude smaller that our measuring capability it was assumed that both methods were essentially identical and the simpler parabolic function was used in the calibration routines.

Again, once the fit has been obtained the theoretical z coordinate corresponding to each measured z coordinate represents the best statistical estimate of the actual vertical coordinate of each of the calibration beads. The technique of least squares fitting a quadratic (parabola) is also common place and will not be discussed here.

Here it should be noted that the primary reason why Kevlar$^{®}$ is used for the calibration wire is because its weight is minimal for the strength characteristics it possesses. The total sag experienced over the 201 meters, even with the beads in place, only amounts to 0.40 meters. This permits relatively large errors in the measured down-range coordinates without significantly affecting the statistical estimate of the actual z coordinate for each calibration bead.

A 2.2.3 DOWN-RANGE COORDINATES

The actual x (down-range) coordinate of each calibration bead is also determined statistically by a least squares fitting technique to the measured x coordinates. Since this fitting technique is somewhat unique it will be described in some detail herein. If we initially assume that the first measured x location is precise (this assumption will be relaxed later) and use the known arc lengths between the calibration beads the calibration bead locations are computed using the differential relationship shown below:

$$ds^2 = dx^2 + dz^2 \qquad A2.1$$

where s = known arc length.
Also we know from the previous section that z is a quadratic function of x, or:

$$z = C_1 x^2 + C_2 x + C_3 \qquad A2.2$$

and the constants C_1, C_2, and C_3 have previously been determined during the fitting process. Then Eq. A2.1 can be rewritten as shown:

$$s = \int_{x_0}^{x} (a\,x^2 + b\,x + c)^{1/2}\, dx \qquad\qquad \text{A2.3}$$

where, $\quad a = 4C_1^2 \quad , \quad b = 4\,C_1\,C_2 \quad , \quad c = C_2^2 + 1$

Integrating Eq. A2.3 we obtain,

$$s = [(2ax+b)X^{1/2}\,/\,4a]\,[(4ac-b^2)\,/\,8a][a^{-1/2}\,\ln\,(X^{1/2} + x\,a^{1/2} + b\,a^{-1/2}/\,2)]\,\Big|_{x_0}^{x} \qquad \text{A2.4}$$

note that, $\quad X \equiv ax^2 + bx + c$

Since everything in Eq. A2.4 is known except the down-range coordinate (x) associated with each known arc length , Eq. A2.4 is solved iteratively for each of these corresponding values. These computed values of x will likely be in error since the first x coordinate was arbitrarily set equal to the measured x coordinate of the first calibration bead. Also, the calibration wire may have stretched or contracted since the beads were positioned on the wire. However, the down-range distances between these calibration beads are now known as accurately as the arc lengths were known when the wire was constructed.

In order to understand the method of determining the actual x coordinate of each calibration bead, visualize a scale containing the computed x coordinates positioned alongside the measured x coordinates of each calibration bead. Slide this scale containing the computed x coordinates back and forth and permit the scale to stretch or contract until the scale best matches the measured x coordinates. The final position of the x coordinates on the scale now represents the best statistical estimate of the actual down-range coordinate at each of the measured calibration bead locations.

In describing this mathematically refer to the sketch below:
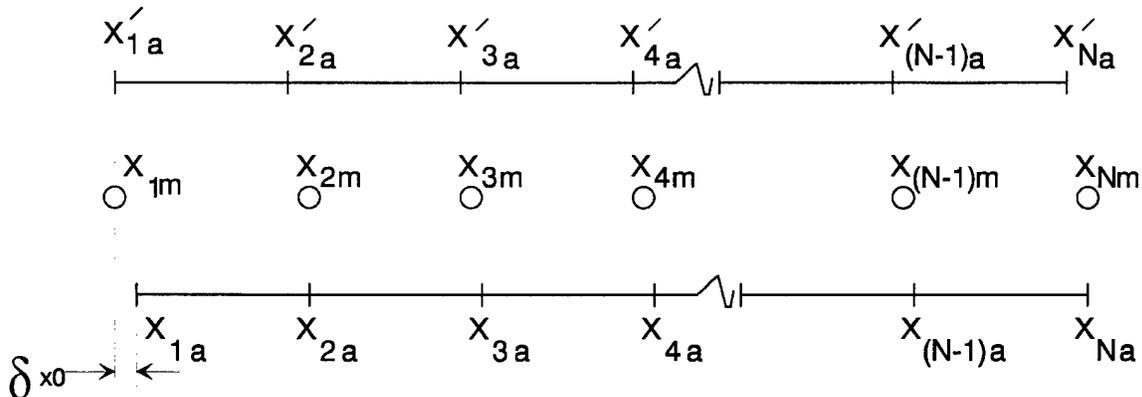
where, N = number of data points

x_{im} = measured x coordinates

x'_{ia} = computed x coordinates using known arc length

x_{ia} = actual x coordinates determined statistically from least squares fit

s_f = stretch factor between the x'_{ia} scale and the x_{im} coordinates

δ_{x0} = zero shift between the x'_{ia} and x_{ia} scales

The relation relating the two scales can be written as follows:

$$x_{ia} = x'_{ia} + \delta_{x0} + s_f x_{im} \qquad \text{A2.5}$$

If we define a delta x as,

$$\Delta x_i = x_{ia} - x_{im} \qquad \text{A2.6}$$

then substituting Eq. A2.6 into A2.5 and rearranging we can obtain the equation below:

$$\Delta x_i = x'_{ia} + \delta_{x0} + x_{im}(s_f - 1) \qquad \text{A2.7}$$

In order to minimize the sum of Δx_i^2, the following relation is used,

$$\partial / \partial \delta_{x0} \sum_{i=1}^{N} [x'_{ia} + \delta_{x0} + x_{im}(s_f - 1)]^2 = 0 \qquad \text{A2.8}$$

Equation A2.8 can be simplified to,

$$\delta_{x0} = - A - B(s_f - 1) \qquad \text{A2.9}$$

where,

$$A \equiv (1/N) \sum_{i=1}^{N} x'_{ia} \quad , \quad \text{and} \quad B \equiv (1/N) \sum_{i=1}^{N} x_{im}$$

Now if we substitute Eq. A2.9 into A2.7 we obtain,

$$\Delta x_i = x'_{ia} - A + B - x_{im} + s_f (x_{im} - B) \qquad \text{A2.10}$$

Again, in order to minimize the sum of Δx_i^2,

$$\partial / \partial s_f \sum_{i=1}^{N} [x'_{ia} - A + B - x_{im} + s_f (x_{im} - B)]^2 = 0 \qquad \text{A2.11}$$

Equation A2.11 can now be solved for the stretch factor and after some manipulation the following relation obtained:

$$s_f = [(NAB - \sum_{i=1}^{N} x_{im} x'_{ia}) / (\sum_{i=1}^{N} x_{im}^2 - N B^2)] + 1 \qquad \text{A2.12}$$

The stretch factor, s_f, can now be computed directly using Eq. A2.12. Then the zero shift, δ_{x0}, is computed using Eq. A2.9, and finally the best statistical estimate for each of the down-range coordinates computed using Eq. A2.5.

This completes the methodology behind the determination of the x,y,z, coordinates of the calibration beads. We can now assume that the location of these beads are precisely known. Obviously much reliance has been placed on the fact that a least squares fit to

134

measured data is a better representation of reality than any one measured data point. This is well known and a proven fact as long as the mathematical model used to describe the measured data points adequately represents the true physics of the system.

A2.3 SPARK GAP AND REFERENCE BEAD LOCATIONS

The logic behind the computation of the spark gap and reference bead locations will be illustrated in this section. The mathematics are similar to the vector intersection routine as discussed in Section 5.2 with two exceptions. The first is that here we are looking for the intersection of three vectors instead of two and secondly we will vary one set of coordinates (shadow coordinates of the known beads in space). The mathematical details are presented in Ref. 3.13 and not repeated here, but a simplified discussion using a planar system will be used to illustrate the process. This simplified planar system is shown in the sketch below.
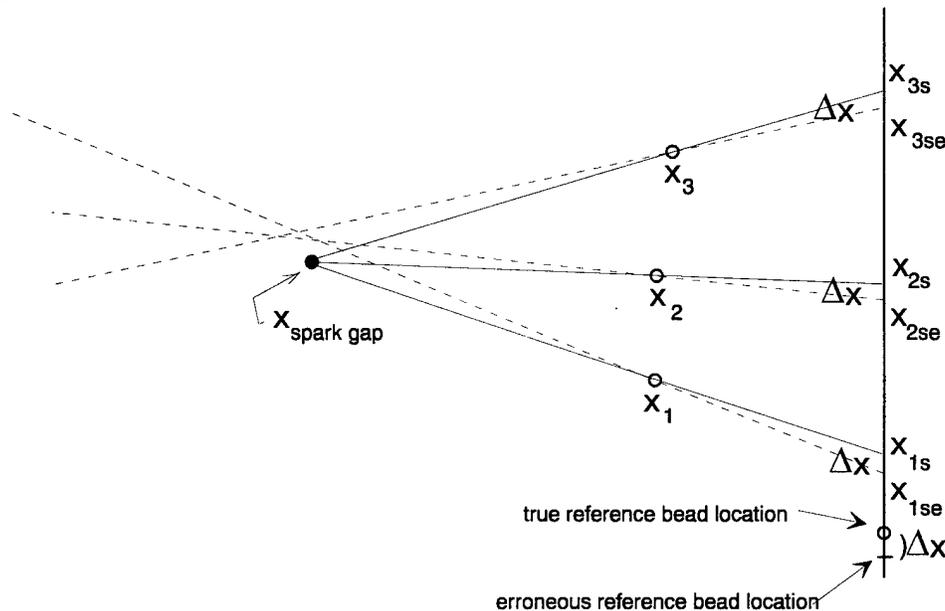
Where, x_1, x_2, x_3 = known points in space

x_{1s}, x_{2s}, x_{3s} = shadow locations of known points

x_{1se}, x_{2se}, x_{3se} = erroneous shadow locations

Δx = error in reference bead location (same error in shadow locations, i.e. $\Delta x = x_{is} - x_{ise}$)

As illustrated in the sketch above, if the location of the reference bead is in error by Δx the measured shadow locations are in error by the same amount(neglecting film reading error). Also illustrated is the fact that the vectors defined by the erroneous shadow locations and the known points in space do not intersect at a point. However, if the erroneous reference bead location is varied (each shadow location is varied by the same amount) until the vectors do intersect at a point then the final location of the reference bead is the true reference bead location and the point of intersection is the

135

updated spark gap location. This essentially is the method as described mathematically in Ref. 3.13.

A2.4 RANGE CALIBRATION EVALUATION

As mentioned previously several sets of shadowgrams were obtained with the calibration wire located at different positions in the range. Three sets of the shadowgrams were used to calibrate the spark source and reference bead locations using the method described in the previous section. The remaining sets of shadowgrams are used to establish the measurement precision and to evaluate possible station biases. The beads on these shadowgrams are read and analyzed as if they represented a free-flight test item in space. The measured range coordinates of calibration beads are then fit using the straight line, quadratic, and sliding-stretching technique as previously discussed. The differences between the measured coordinates and the statistically determined best estimates are then analyzed at each shadowgraph station to determine possible measurement biases. These biases are then recorded and subtracted from all future measurements up until the time the facility is recalibrated and the process is repeated. An estimate of the position measurement precision is determined from the variation in the measurements at each station.

The precision of the attitude measurements is obtained by comparing the theoretical local slopes of the calibration wire at each shadowgraph station with the measured slopes obtained from the shadowgraph film. The theoretical local slopes can easily be determined from the curve fits. The measured slopes are determined by locating two points on the wire at each shadowgraph station and computing the corresponding attitudes.

Using the techniques discussed above the measuring capability of the ARF is approximately 0.08 degrees and 0.08 cm respectively for the orientation and position of well defined points in space. This measurement precision has also been confirmed from the analysis of numerous free-flight trajectories as measured in the facility. However, it must be noted that the measurement precision can be a function of the test item's size and geometry. For example the attitude of a short blunt configuration cannot be measured as precisely as a long slender configuration.

APPENDIX 3

CURVE FITTING PROCEDURE FOR THE
TRICYCLIC EQUATION OF MOTION

A 3.1 STATEMENT OF THE PROBLEM

The problem at hand is to fit the theoretical equation of the angular motion to the experimentally measured data points and determine the unknowns such that they represent a best fit to the data. The theoretical equation of motion (Eq. 6.20) is repeated below,

$$\beta + i\alpha = K_P \exp[(\mu_P + i\phi_P')x] + K_N \exp[(\mu_N + i\phi_N')x] + K_T \exp(ipx) \qquad \text{A3.1}$$

and the unknowns to be determined are: K_P, μ_P, ϕ_P', K_N, μ_N, ϕ_N', and K_T. As was indicated in Section 6.1.3 the spin rate, p, is a function of ϕ_P' and ϕ_N' and therefore is not considered as an unknown in Eq. A3.1.

A 3.2 LEAST SQUARES THEORY

The residual is defined as the difference between the fitted angles, $\beta_F + i\alpha_F$, and the measured angles, $\beta_M + i\alpha_M$, as indicated in the sketch below:
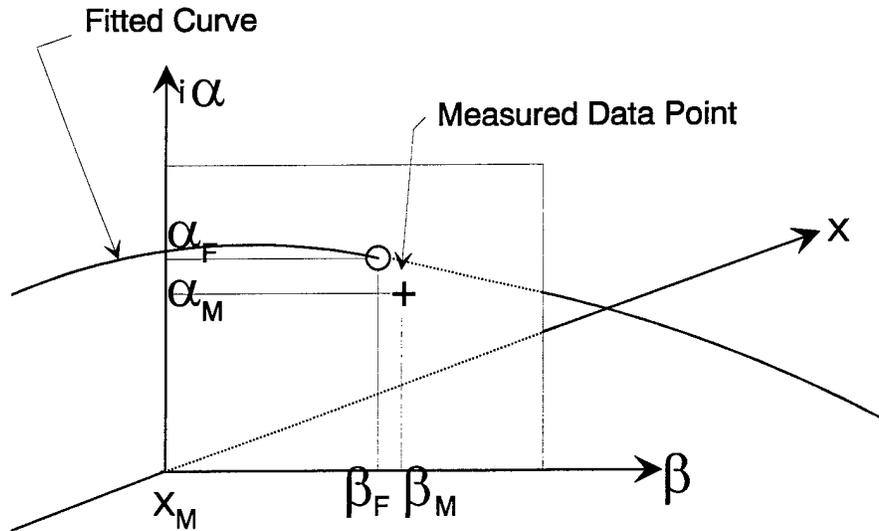
For convenience we will redefine the angles as $\xi_F \equiv \beta_F + i\alpha_F$ and $\xi_M \equiv \beta_M + i\alpha_M$ then the residual, R_M, can be written as shown below:

$$R_M = f(x_M) - \xi_M \qquad \text{A3.2}$$

Where $f(x_M)$ is the tricyclic equation of motion, Eq. A3.1 written for the measured distance x_M, or

$$f(x_M) = K_P \exp \phi_P x_M + K_N \exp \phi_N x_M + K_T \exp \phi_T x_M \qquad \text{A3.3}$$

where

$$K_N = a + ib \quad , \quad K_P = c + id \quad , \quad K_T = f + ig$$
$$\phi_N = \mu_N + i\phi_N' \quad , \quad \phi_P = \mu_P + i\phi_P' \quad , \quad \phi_T = ip$$

and

$$p = (I_y / I_x)(\phi_N' + \phi_P')$$

138

The values of K_N, K_P, K_T, ϕ_N, and ϕ_P which satisfy the least squares requirement that the sum of the residuals squared be a minimum can be found by a simultaneous solution of the set of equations shown below:

$$\partial \sum R_M^2 / \partial K_N = 0 \quad , \quad \partial \sum R_M^2 / \partial K_P = 0 \quad , \quad \partial \sum R_M^2 / \partial K_T = 0$$
$$\partial \sum R_M^2 / \partial \phi_N = 0 \quad , \quad \partial \sum R_M^2 / \partial \phi_P = 0 \qquad\qquad \text{A3.4}$$

This set of equations (A3.4) is nonlinear in respect to the unknowns and hence cannot be solved directly. Therefore, an interative technique must be used for the fitting process.

A 3.3 THE DIFFERENTIAL CORRECTIONS PROCEDURE

The differential corrections procedure is an iterative method which can be used to fit Eqs. A3.4 to the required precision. We are given a set of data points and the function Eq. 3.3 written as,

$$\xi = K_P \exp \phi_P x + K_N \exp \phi_N x + K_T \exp \phi_T x$$

Note that $\xi = \beta + i\alpha$ and the unknowns (K_P, ϕ_P, K_N, ϕ_N, and K_T) are defined as,

$$K_N \equiv a + ib = (a_0 + \Delta a) + i(b_0 + \Delta b) = K_{N0} + \Delta K_N$$

$$K_P \equiv c + id = (c_0 + \Delta c) + i(d_0 + \Delta d) = K_{P0} + \Delta K_P$$

$$K_T \equiv f + ig = (f_0 + \Delta f) + i(g_0 + \Delta g) = K_{T0} + \Delta K_T$$

$$\phi_N \equiv \mu_N + i\phi_N' = \mu_{N0} + \Delta\mu_N + i(\phi_{N0}' + \Delta\phi_N') = \phi_{N0} + \Delta\phi_N$$

$$\phi_P \equiv \mu_P + i\phi_P' = \mu_{P0} + \Delta\mu_P + i(\phi_{P0}' + \Delta\phi_P') = \phi_{P0} + \Delta\phi_P$$

Then it becomes obvious that,

$$
\left.
\begin{array}{ll}
K_{N0} = a_0 + ib_0 & \Delta K_N = \Delta a + i\Delta b \\[2mm]
K_{P0} = c_0 + id_0 & \Delta K_P = \Delta c + i\Delta d \\[2mm]
K_{T0} = f_0 + ig_0 & \Delta K_T = \Delta f + i\Delta g \\[2mm]
\phi_{N0} = \mu_{N0} + i\phi_{N0}' & \Delta\phi_N = \Delta\mu_N + i\Delta\phi_N' \\[2mm]
\phi_{P0} = \mu_{P0} + i\phi_{P0}' & \Delta\phi_P = \Delta\mu_P + i\Delta\phi_P'
\end{array}
\right\} \qquad \text{A3.5}
$$

The subscripted zero values represent the first approximation to the unknowns and the delta terms are the corrections added after each iteration. We now need to determine these corrections such that the sum of the residuals squared is a minimum. Substituting the quantities above into the residual equation, Eq.A3.2, that equation can be written as shown:

$$R_M + \xi_M = (K_{P0} + \Delta K_P) \exp[(\phi_{P0} + \Delta \phi_P)] x_M + (K_{N0} + \Delta K_N) \exp[(\phi_{N0} + \Delta \phi_N)] x_M$$

$$+ (K_{T0} + \Delta K_T) \exp[(\phi_{T0} + \Delta \phi_T)] x_M$$

Expanding the above equation with Taylor's theorem we can obtain,

$$R_M + \xi_M = K_{P0} \exp \phi_{P0} x_M + K_{N0} \exp \phi_{N0} x_M + K_{T0} \exp \phi_{T0} x_M + \Delta K_P \partial F / \partial K_{P0}$$

$$+ \Delta K_N \partial F / \partial K_{N0} + \Delta K_T \partial F / \partial K_{T0} + \Delta \phi_P \partial F / \partial \phi_{P0}$$

$$+ \Delta \phi_N \partial F / \partial \phi_{N0} + (\text{ higher order terms}) \qquad A3.6$$

where,

$$F = K_{P0} \exp \phi_{P0} x_M + K_{N0} \exp \phi_{N0} x_M + K_{T0} \exp \phi_{T0} x_M$$

When the first approximations are reasonably good the Δ's will be small and the higher order terms are neglected.

It is now necessary to define another residual as the difference between the ordinates of the first approximation curve and the data points, or

$$R_i = \xi_M - F$$

Substituting this relationship into Eq. A3.6 we arrive at the equation shown below:

$$R_M = \Delta K_P \partial F / \partial K_{P0} + \Delta K_N \partial F / \partial K_{N0} + \Delta K_T \partial F / \partial K_{T0} + \Delta \phi_P \partial F / \partial \phi_{P0}$$

$$+ \Delta \phi_N \partial F / \partial \phi_{N0} - R_i \qquad A3.7$$

Equation A3.7 can be written for each data point and this series of equations are known as the residual equations. Using this definition for R_M the condition for the sum of the squares to be minimum is,

$$\partial \sum R_M^2 / \partial \Delta K_N = 0 \quad , \quad \partial \sum R_M^2 / \partial \Delta K_P = 0 \quad , \quad \partial \sum R_M^2 / \partial \Delta K_T = 0$$

$$\partial \sum R_M^2 / \partial \Delta \phi_N = 0 \quad , \quad \partial \sum R_M^2 / \partial \Delta \phi_P = 0$$

Substituting Eq. A3.7 into one of the above relations we get,

$$\partial \sum R_M^2 / \partial \Delta K_N = \partial / \partial \Delta K_N \sum [\Delta K_P \partial F / \partial K_{P0} + \Delta K_N \partial F / \partial K_{N0} + \Delta K_T \partial F / \partial K_{T0}$$

$$+ \Delta \phi_P \partial F / \partial \phi_{P0} + \Delta \phi_N \partial F / \partial \phi_{N0} - R_i]^2 = 0$$

Taking the indicated partial derivative this equation can be written as,

$$\partial \sum R_M^2 / \partial \Delta K_P = 2 \sum A_i [\Delta K_P A_i + \Delta K_N B_i + \Delta K_T C_i + \Delta \phi_P D_i + \Delta \phi_N E_i - R_i] = 0 \qquad A3.8$$

140

where,

$$A_i \equiv \partial F / \partial K_{P0} \, , \, B_i \equiv \partial F / \partial K_{N0} \, , \, C_i \equiv \partial F / \partial K_{T0} \, ,$$

$$D_i \equiv \partial F / \partial \phi_{P0} \, , \, E_i \equiv \partial F / \partial \phi_{N0}$$

Similarly the other partial derivatives can be obtained, or

$$\partial \sum R_M^2 / \partial \Delta K_N = 2 \sum B_i \, [\Delta K_P \, A_i + \Delta K_N \, B_i + \Delta K_T \, C_i + \Delta \phi_P \, D_i + \Delta \phi_N \, E_i - R_i] = 0 \quad A3.9$$

$$\partial \sum R_M^2 / \partial \Delta K_T = 2 \sum C_i \, [\Delta K_P \, A_i + \Delta K_N \, B_i + \Delta K_T \, C_i + \Delta \phi_P \, D_i + \Delta \phi_N \, E_i - R_i] = 0 \quad A3.10$$

$$\partial \sum R_M^2 / \partial \Delta \phi_P = 2 \sum D_i \, [\Delta K_P \, A_i + \Delta K_N \, B_i + \Delta K_T \, C_i + \Delta \phi_P \, D_i + \Delta \phi_N \, E_i - R_i] = 0 \quad A3.11$$

$$\partial \sum R_M^2 / \partial \Delta \phi_N = 2 \sum E_i \, [\Delta K_P \, A_i + \Delta K_N \, B_i + \Delta K_T \, C_i + \Delta \phi_P \, D_i + \Delta \phi_N \, E_i - R_i] = 0 \quad A3.12$$

The summations are accomplished over the complete data set or 1 to N. These five equations (A3.8 to A3.12) are usually written in matrix form and solved for the five unknowns: ΔK_P, ΔK_N, ΔK_T, $\Delta \phi_P$, and $\Delta \phi_N$. Once the Δ's are determined they are added to the initial approximations and the process repeated. This iterative process is continued until the Δ's approach zero and then convergence is achieved.

(This page is blank)

142

APPENDIX 4

BIBLIOGRAPHY

There are many good sources of reference material, for example the proceedings of the International Ballistics Conferences, the Aeroballistic Range Association meetings, the Navy Symposiums on Ballistics, AGARD and AIAA sponsored conferences and others.

A 4.1 DATA REDUCTION / THEORY

1. Murphy, C.H., "Advances in Dynamic Analysis of Range Data", BRL Memorandum Report No. 1270, May 1960.
2. Murphy, C.H., "On the Quasi-Linear Substitution Method for Missile Motion Caused by Strongly Nonlinear Static Moment", BRL Memorandum Report No. 1466, April 1963.
3. Murphy, C.H., "Prediction of the Motion of Missiles Acted on by Non-Linear Forces and Moments", BRL Report No. 995, October 1956.
4. Murphy, C.H., "The Effect of Strongly Nonlinear Static Moment on the Combined Pitching and Yawing Motion of a Symmetric Missile", BRL Report No. 1114, August 1960.
5. Murphy, C.H., "Limit Cycles for Non-Spinning Statically Stable Symmetric Missiles", BRL Report No.1071, March 1959.
6. Thomas, L.H., "The Theory of Spinning Shell", BRL Report 839, November 1952.
7. Reed, H.L., "The Dynamics of Shell", BRL Report 1030, October 1957.
8. Tobak, M.,and Lessing, H.C.,"Study of the Aerodynamic Forces and Moments on Bodies of Revolution in Combined Pitching and Yawing Motions", NASA TN D-316 May 1960.
9. MacAllister, L.C."Some Instability Problems with Re-Entry Shapes", BRL Memorandum Report 1224, June 1959.
10. Rasmussen, M.L.,"Determination of Nonlinear Pitching-Moment Characteristics of Axially Symmetric Models From Free-flight Data", NASA TN D-144, February 1960.
11. Zaroodny, S.J.,"Spiral Yawing Motions of 81-mm M56 Shell", BRL Memorandum Report No. 682, May 1953.
12. Lietmann, G.,"Nonlinear Equations of Motion of Spin-Stabilized Missile Solved by a Perturbation Method", NAVORD 3364, August 1954.
13. Murphy, C. H.,"On Stability Criteria of the Kelly-McShane Linearized Theory of Yawing Motion" BRL Report 853, April 1953.
14. Maple, C.G., and Synge, J.L.,"Aerodynamic Symmetry of Projectiles", Q.A.M. Vol. IV, January 1949.
15. Murphy, C.H.,"Effect of Varying Air Density on the Nonlinear Pitching and Yawing Motion of a Symmetric Missile", BRL Report No. 1162, February 1962.
16. Murphy, C.H., and Hodes, B.A."Planar Limit Motion of Nonspinning Symmetric Missiles Acted on by Cubic Aerodynamic Moments", BRL Memorandum Report 1358, June 1961.
17. Murphy, C.H., and Nicolaides, J.D.,"A Generalized Ballistic Force System", BRL Report No. 933, May 1955.
18. Davis, R.A.," The Response of Bisymmetric Aircraft to Small Combined Pitch,Yaw, and Roll Control Actions", Journal of Aeronautical Sciences, Vol. 24, pp 905-910, December 1957.
19. Yonda, A.W.,"Data Reduction of the Yaw and Swerve of a Fin-Stabilized Missile with a Roll Varying Through Resonance for a High Speed Digital Computer", BRL Memorandum Report No. 1042, October 1956.

20. McShane, E.J., Kelley, J.L., and Reno, F."Exterior Ballistics", University of Denver Press,1953.

21. Turetsky, R.A.,"Reduction of Spark Range Data", BRL Report 684, 1948.

22. Karpov, B.G.,"The Accuracy of Drag Measurements as a Function of Number and Distribution of Timing Stations", BRL Report No. 658, 1948.

23. Schmidt, L.E."Aerodynamic Coefficients Determined from the Swerve Reduction", BRL Memorandum Report 599, 1952.

24. Conti, S.,"On the Reduction of Shadowgrams", BRL Report 786,1952.

25. Boltz, R., and Nicolaides, J.D.,"A Method of Determining Some Aerodynamic Coefficients from Supersonic Free-Flight Tests of a Rolling Missile", BRL Report No. 711,1950.

26. MacAllister, L.C.,"Comments on the Preliminary Reduction of Symmetric and Asymmetric Motions of Free-Flight Range Models", BRL Memorandum Report No. 781, 1954.

27. Nicolaides, J.D., and Boltz, R.,"On the Pure Rolling Motion of Winged and/or Finned Missiles in Varying Supersonic Flight", BRL Report No. 799, 1953.

28. Seiff, A.,"A New Method for Computing Drag Coefficients from Ballistic Range Data", J.A.S., Vol. 25, pp 133-134, February 1958.

29. Charters, A,C, and Turetsky, R.A.,"Determination of Base Pressure from Free-Flight Data", BRL Report No. 653, March 1948.

30. Charters, A,C, and Kent, R.A.,"The Relation Between the Skin Friction Drag and the Spin Reducing Torque", BRL Report No. 287, July 1942.

31. Murphy, C.H., and Bradley, J.W.,"Jump Due to Aerodynamic Asymmetry of a Missile with Varying Roll Rate", BRL Report No. 1077, May 1959.

32. Nicolaides, J.D.,"Two Nonlinear Problems in the Flight Dynamics of Modern Ballistic Missiles", I.A.S. Report 59-17, January 1959.

33. Kirk, Donn B.,"A Method for Obtaining the Nonlinear Aerodynamic Stability Characteristics of Bodies of Revolution from Free-Flight Tests", NASA TN D-780, March 1961.

34. VanAllen, J.A., and Hitchcock, H.P.,"Loss of Spin of Projectiles", J.A.S., Vol. 15, pp 35-40, January 1948.

35. Vaughn, H.R.,"A Detailed Development of the Tricyclic Theory", SC-M-67-2933, Sandia National Laboratory, February 1968.

36. Nicolaides, J.D., "Missile Flight and Astrodynamics", Technical Note 1959-61-65, Bureau of Weapons, Dept. of the Navy.

37. Hawkins, J.A.,"Trajectory Equations for Long-Range Bombs and Rockets", APGC-TR-61-18, ASTIA Document, March 1961.

38. Ingram, C.W., "An Approximate Solution of the Nonlinear Differential Equation for the Complex Angle of a Symmetrical Missile", AFATL-TR-68-71, June 1968.

39. Murphy, C.H., "Generalized Subharmonic Response of a Missile with Slight Configurational Asymmetries", BRL Report No. 1591., June 1972.

40. Brunk, J.E., "User's Manual: Extended Capability Magnus Rotor and Ballistic Body 6-DOF Trajectory Program", AFATL-TR-70-40, May 1970.

41. Murphy, C.H., "A Symptom of Payload-Induced Flight Instability", BRL-MR-3867, September 1990.

42. Hall, D.W., "Aerodynamics of Statically Stable Hypersonic Projectiles", AFATL-TR-85-30, June 1985.

43. Nicolaides, J.D., "A Review of Some Recent Progress in Understanding Catastrophic Yaw", University of Notre Dame, UNDAS-TN-669JDN, September 1966.

44. McCoy, R.L., "The Effect of Wind on Flat-Fire Trajectories", BRL Report No. 1900, August 1976.

45. Pepitone, T.R., "The Influence of Roll Orientation-Dependent Aerodynamics of the Stability of Cruciform Missile Configurations", NSWC TR 79-416, January 1981.

46. Murphy, C.H., "Some Special Cases of Spin-Yaw Lock-In", BRL-MR-3609, August 1987.

47. Murphy, C.H., "Effect of Horizontal and Vertical Side Forces and Moments on Stability of a Symmetric Missile in Ascending or Descending Flight", ARBRL-MR-02915, April 1979.

48. Murphy, C.H., "Comments on Projectile Jump", BRL-MR-1071, April 1957.

49. Cooper, G.R., and Bradley, J.W., "Determining Atmospheric Conditions from Trajectory Data", BRL Interim MR No. 952, December 1990.

50. Welsh, C.J., and Watt, R.M., "Effect of Roll on the free-Flight Motion of Statically Stable Bodies", AEDC-TR-67-156., September 1967.

51. Hathaway, W.H., "Analysis of the Free-Flight Aerodynamics on Non-Symmetric Bodies from Ballistic Spark Range Data", M.S. Thesis, University of Vermont, February 1976.

52. Whyte, R.H., and Hathaway, W.H., "Aeroballistic Range Data Reduction Technique Utilizing Numerical Integration", AFATL-TR-74-41, February 1974.

53. Brown, C.B. Jr., "An Extended Kalman Filter for Estimating Aerodynamic Coefficients", AFATL-TR-76-158, December 1976.

54. Hathaway, W.H., and Whyte, R.H., "Aeroballistic Research Facility Free-Flight Data Analysis Using the Maximum Likelihood Method", AFATL-TR-79-98, December 1979.

55. Fischer, M., and Hathaway, W.H., "Aeroballistic Research Facility Data Analysis System(ARFDAS)", AFATL-TR-88-48, September 1988.

56. Cohen, C.J., and Clare, T.A., "Analysis of the Rolling Motion of Finned Missiles at Large Angles of Attack", NWL TR-2671, February 1972.

57. Daniels, P., and Hardy, S.R., "Theoretical and Experimental Methods in the Solution of Missile Nonlinear Roll Problems", NSWC-TR-3773, March 1978.

58. Kain, J.E., and Brown, C.M. "An Evaluation of Aeroballistic Range Projectile Parameter Identification Procedures", AFATL-TR-78-93, August 1978.

59. Whyte, R.H., and Mermagen,W.H., "A Method for Obtaining Aerodynamic Coefficients from Yawsonde and Radar Data", Journal of Space Craft and Rockets, Vol. 10, No. 6, pp 384-388, June 1973.

60. Murphy, C.H., "Gravity-Induced Angular Motion of a Spinning Missile", Journal of Space Craft and Rockets, Vol. 8., No. 8, pp 824-828, August 1971.

61. Byers, M.E., "A new Technique for the Analysis of Non-Linear Free-Flight Motion", AIAA Paper No. 74-614, presented at the 8th Aerodynamic Testing Conference, Bethesda, Maryland, July 8-10, 1974.

62. Chapman, G.T., and Kirk, D.B., "A Method for Extracting Aerodynamic Coefficients from Free-Flight Data", AIAA Journal, Vol. 8, No. 4, pp 753-758, April 1970.

63. Winchenbach, G.L., "The Curve Fitting of an Idealized Equation to the Angular Motions of a Missile When the Aerodynamic Parameters Vary Along the Flight Path", M.S. Thesis, University of Tennessee Space Institute, August 1968.

64. Sabot, S.M., Winchenbach, G.L., and Chapman, G.T., "Comparison of Various Drag Coefficient Expansions Using Polynomials and Splines", Journal of Space Craft and Rockets, Vol. 23, No. 3, pp 259-263, May-June 1986.

65. Winchenbach, G.L., et al, "Subsonic and Transonic Aerodynamics of a Wraparound Fin Configuration", Journal of Guidance, Control, and Dynamics, Vol. 9, No. 6, pp 627-632, November-December 1986.

66. Kim, Y.H., and Winchenbach, G.L., "Roll Motion of a Wraparound Fin Configuration at Subsonic and Transonic Mach Numbers", Journal of Guidance, Control, and Dynamics, Vol. 9, No. 2, pp 253-255, March-April 1986.

67. Oxford, V., and Winchenbach, G.L., "Aeroballistic Free-Flight and Wind Tunnel Data Correlation Techniques", AFATL-TR-86-89, January 1987.

68. Hathaway, W.H., and Whyte, R.H., "Aeroballistic Range Data Analysis for Non-Symmetric Configurations", AFATL-TR-76-109, September 1976.

69. Murphy, C.H., "Free-Flight Motion of Symmetric Missiles", BRL Report No. 1216, July 1963.

70. Murphy, C.H., "Data Reduction for the Free-Flight Spark Ranges", BRL Report 900, February 1954.

71. Nicolaides, J.D., "Free-Flight Dynamics", University of Notre Dame, South Bend, Indiana, 1967.

72. Nicolaides, J.D., "On the Free-Flight Motion of Missiles Having Slight Configurational Asymmetries", BRL Report No. 856, June 1953.

73. Murphy, C.H., "The Measurement of Non-Linear Forces and Moments by Means of Free-flight Tests", BRL Report 974, February 1956.

74. Madagan, A.N. Jr., "An Investigation of the Method Used in Free-Flight Hypersonic Testing for Reducing Total Drag Coefficient to Zero-Lift Drag Coefficient", M.S. Thesis, University of Tennessee Space Institute, June 1968.

75. Murphy, C.H., "Spinning Projectile Instability Induced by an Internal Mass Mounted on an Elastic Beam", ARL-MR- 270, November 1995.

76. Whyte, R.H., et al, "Recent Experience in Extraction of Aeroballistic Performance from Doppler Radar Data", Paper presented at the 46th Meeting of the Aeroballistic Range Association, Minnetonka, Minnesota, September 1995.

77. Yates, L.A., "A Comprehensive Automated Aerodynamic Reduction System for Ballistic Ranges", WL-TR-96-7059, October 1996.

A 4.2 FACILITIES AND INSTRUMENTATION

1. Rogers, W., "The Transonic Free Flight Range", BRL Report 849, 1953.
2. Bouget, C., et al, "The DREV Terminal Ballistics Facility", DREV R-4364/85.

3. Clay, W.H., et al, "Spark Camera Annotation and Control System for the BRL Transonic Range Facility", BRL-TR-3036,1987.

4. Parrish, G.E., "Projectile Measurements and Instrumentation Laboratory", AFATL-TR-74-156, September 1974.

5. Grabarek, C.L., and Herr, L., "X-Ray Multi-Flash System for Measurement of Projectile Performance at the Target", BRL-TN-1634, September 1966.

6. Dugger, P.H., et al, "Development of Microwave Radar and Model Detection Instrumentation Systems for the Aeroballistic Range", AEDC-TR-82-24, December 1982.

7. Clay, W.H., "A Precision Yawsonde Calibration Technique", BRL-MR-2263, January 1973.

8. Burton, L.W., Kaste, R.P., and Stobie, I.C., "A Technique for Measurement of In-Bore Projectile Spin", BRL-TR-3037, September 1989.

9. Brown, R.R., and Parker, J.R., "A High Speed Electronic Imaging Application in Aeroballistic Research", Proceedings of SPIE, Vol. 497, High Speed Photography, Videography, and Photonics II, San Diego, California, August 21-22, 1984.

10. Brown, R., and Parker, J.R., "Conceptual Design and Analysis of High Speed Electronic Imaging- Phase I", AFATL-TR-85-65, October 1985.

11. Brabham, C., "A Multispark Shadowgraph System for a Free-Flight Aeroballistic Range", Paper presented at the 1977 International Congress for Instrumentation in Aerospace Simulation Facilities, England, 1977.

12. Snyder, D.R., and Kosel, F.M., "Application of High Resolution Still Video Cameras to Ballistic Imaging", Proceedings of SPIE, Vol. 1346, Ultrahigh and High-Speed Photography, Videography, Photonics and Velocimetry, 1990.

13. Weber, P.A., and Elrod, W.C., "Time Delay Computer for Precise Control in Recording Transient Events", AIAA Paper 80-1143, Presented at the Joint Propulsion Conference, Hartford Connecticut, June 30-July 2, 1980.

14. Holt, D.M., Kelley, R.J., and Winchenbach, G.L., "A Prototype High Speed Electronic Imaging System for Aeroballistic Research and Analysis", Paper presented at the 12th International Congress on Instrumentation in Aerospace Simulation Facilities, Williamsburg, Virginia, June 1987.

15. Trolinger, J.D., "Laser Applications in Flow Diagnostics", AGARDOGRAPH No. 296, October 1988.

16. Haug, B.T., "Measuring Displacements of Gun System Components by Use of Optron Optical Trackers", ARBRL-MR-03331.

17. Schmidt, E.M., "The Aerodynamics Range: A National Historic Mechanical Engineering Landmark", ARBRL-SP-00028, May 1983.

18. Braun, W.F., "The Free-Flight Aerodynamics Range", BRL Report No. 1048, 1958.

19. Kittyle, R.L.,Packard, J.D., and Winchenbach, G.L., "Description and Capabilities of the Aeroballistic Research Facility", AFATL-TR-87-08, May 1987.

20. Canning, T.S., Seiff, A., and James, C.S., "Ballistic Range Technology", AGARD-AG-138-70, August 1970.

21. Heinrici, U., and Winchenbach, G.L., "Description and Comparison of Photographic Instrumentation Systems Used in Some Free-Flight Facilities", Paper presented at the 32nd Meeting of the Aeroballistic Range Association, Karlsborg, Sweden, August 1981.
22. West, K.O., "Yaw Card Range Tests of a 30-mm Frangible T.P. Projectile", AFATL-TR-76-5, January 1976.
23. Anderson, R.C., "Six View Holographic Interferometer", WL-TR-96-7034, April 1966.
24. Trolinger, J.D., Millerd, J., and Gran, M., "Development of an Interferometry / Tomography Data Reduction System", WL-TR-96-7023, February 1996.

A 4.3 NOTABLE DATA PUBLICATIONS

1. Roeker, E.T., "Large Yaw Firings of 20-mm HEI, T282E1 Shell with Fuze T196 at Mach Number 2.3", BRL Memorandum Report No. 888, April 1955.
2. Charters, A.C., and Thomas, R.N., "The Aerodynamic Performance of Small Spheres from Subsonic to High Supersonic Velocities", J.A.S., Vol. 12, pp 468-476, October 1945.
3. May, A., and Witt, W.R. Jr., "Free-Flight Determination of the Drag Coefficients of Spheres", J.A.S. Vol. 20, pp 635-638, September 1953.
4. Murphy, C.H., and Schmidt, L.E., "The Effect of Length on the Aerodynamic Characteristics of Bodies of Revolution in Supersonic Flight", BRL Report No. 876, August 1953.
5. Davis, J.M., "The Aerodynamics of Golf Balls", Journal of Applied Physics, Vol. 20, pp 821-828, September 1949.
6. Murphy, C.H., and Piddington, M.J., "Aerodynamic Properties of Ring Airfoils in Supersonic Flight", J.A.S, Vol. 27, pp 954-955, December 1960.
7. MacAllister, L.C., "The Aerodynamic Properties of a Simple Non-Rolling Finned Cone-Cylinder Configuration Between Mach Numbers 1.0 and 2.5", BRL Report 935, May 1955.
8. Nicolaides, J.D., "A Transonic Range Study of the Free-Flight Performance of the 127/60 mm Anti-Aircraft Missile T-144E2", BRL MR No. 746, December 1953.
9. Boyer, E.D., "Free-Flight Range Tests of a 10-Caliber Cone Cylinder", BRL MR No. 1258, April 1960.
10. Wood, R.M., and Murphy, C.H., "Aerodynamic Derivatives for Both Steady and Non Steady Motion of Slender Bodies", J.A.S., Vol. 22, pp 870-871, December 1955.
11. Nicolaides, J.D., and Bradley, J.J., "Magnus Moment on Pure Cones in Supersonic Flight", NAVORD Report 6183, January 1959.
12. Intrieri, P.F., "Free Flight Measurements of the Static and Dynamic Stability and Drag of a 10° Blunted Cone at Mach Numbers 3.5 and 8.5", NASA TN D-1299, May 1962.
13. Kirk, D.E., and Miller, J.R., "Free Flight Tests of Fifth Stage Scout Entry Vehicle at Mach Numbers of 5 and 17", NASA TN D-1425, October 1962.

14. Watt, R.M., and Winchenbach, G.L., "Free-Flight Range Tests of Blunted 4-,4.5-, and 5-Caliber Bodies of Revolution of Secant-Ogive, Tangent-Ogive and Conical Nose Shapes", AEDC-TR-71-166, December 1971.

15. Winchenbach, G.L., Watt, R.M., and Skinner, A.J.,"Free-Flight Range Tests of Basic and Boattail Configurations of 3- and 5-Caliber Army-Navy Spinner Projectiles", AEDC-TR-70-12, March 1970.

16. Welsh, C.J., and Winchenbach, G.L., "Free-Flight Investigation of Ablation Effects on the Stability of Conical Reentry Configurations", AEDC-TR-71-242, February 1972.

17. Carman, J.B., Uselton, B.L., and Winchenbach, G.L., "Wind Tunnel and Free-Flight Range Tests of 3- and 5-Caliber Army-Navy Spinner Projectiles with Rotation Bands", AEDC-TR-71-119, June 1971.

18. Welsh, C.J., Winchenbach, G.L., and Madagan, A.N., "Free-Flight Investigation of the Aerodynamics Characteristics of a 10-Deg. Semiangle Cone at Mach Numbers from 6 to 16", AEDC-TR-69-63, April 1969.

19. Winchenbach, G.L., Watt, R.M., and Welsh, C.J., "Free-Flight Range Tests of 20-mm M56A2 Shell with the M505A3 Fuze", AEDC-TR-65-258, January 1966.

20. Whyte, R.H., Winchenbach, G.L., and Hathaway, W.H., "Subsonic Free-Flight Data for a Complex Asymmetric Missile", AIAA Paper 79-1689R, Journal of Guidance and Control, January-February 1981.

21. Winchenbach, G.L., Daniel, D.C., and Edgar, J.D., "Aeroballistic Range Tests of Tubular Projectiles at Mach Numbers from 1.0 to 3.2", AFATL-TR-75-106, August 1975.

22. Winchenbach, G.L., and Cobb, K.K., "Free-Flight Range Tests of Spinning Tubular Projectiles at Mach Numbers from 2.0 to 3.2", AFATL-TR-79-18, February 1979.

23. Winchenbach, G.L., and Chelekis, R.M., "Free- Flight Range Tests of the Standard Dynamics Model (SDM) at Transonic Mach Numbers", AFATL-TR-82-5, December 1981.

24. Buff, R.S., Winchenbach, G.L., and Whyte, R.H., "Aerodynamics of Spin Stabilized Projectiles with Exterior Dimples", AIAA Paper 82-2144, August 15-17,1983.

25. Gates, R.S., et al, "Aerodynamic Test and Analysis of a Slender Generic Missile Configuration", AIAA Paper No. 89-3368, August 1989.

26. Abate, G.L., and Winchenbach, G.L., "Aerodynamics of Missiles with Slotted Fin Configurations ", AIAA Paper No. 91-0676, January 1991.

27. McCoy, R.L., "Aerodynamic Characteristics of Caliber .22 Long Rifle Match Ammunition", BRL-MR-3877, November 1990.

28. Wikoff, D., Cottrell, C., and Packard, J., "An Investigation of Controlled Vortex Drag Using Stepped Afterbodies from M = 0.5 to 3.0", AFATL-TR-88-123, September 1988.

29. Braun, W.F., "Aerodynamic Data for Small Arms Projectiles", BRL Report No. 1630, January 1973.

30. Hitchcock, H.P., "Aerodynamic Data for Spinning Projectiles", BRL Report No. 620, October 1947.

31. Goldstein, D. L., "Summary of Aerodynamic Data on German Projectiles", BRL-MR-410, February 1946.

32. McCoy, R.L., "The Aerodynamic Characteristics of Caliber 0.50 Ball, M333, API, M8, and APIT, M20 Ammunition", BRL-MR-3810, December 1989.

33. Roschke, E.J., "The Effect of Nose Truncation on the Aerodynamic Properties of 9-Caliber Long Army-Navy Spinner Rocket Models Near Sonic Velocity", BRL-TN No. 902.

34. Schmidt, L.E., and Murphy, C.H., "The Aerodynamic Properties the 7-Caliber Army-Navy Spinner Rocket in Transonic Flight", BRL-TR No. 775.

35. Abate, G.L., and Winchenbach, G.L., "Free-Flight Range Tests of High Fineness Ratio (L/D = 27 to 50) Configurations at Mach Numbers of 1.6 to 5.1", AFATL-TR -90-89, November 1990.

36. Dupris, A.D., "Aerodynamic Characteristics of a dart Model with Various Surface Roughnesses from Free-Flight Tests", DREV M-2956/89, January 1989.

37. Clare, T.A., and Daniels P., "Effect of Fin Slots on the Static and Dynamic Stability Characteristics of Finned Bodies", NWL-TR-2582, June 1971.

38. McCoy, R.L., "Free-Flight Range Tests of the Copperhead Projectile", ARBRL-MR-03090, March 1981.

39. Schmidt, L.E., "The Dynamic Properties of Pure Cones and Cone Cylinders", BRL Report No. 759.

40. Danberg, J.E., Sigal, A., and Celmins, I., "Aerodynamic Characteristics of a Family of Cone-Cylinder-Flare Projectiles", Journal of Space Craft and Rockets, Vol. 27, No. 4, July-August 1990.

41. Warren, H.R., Templin, R.J., and Cheers, B., "Aeroballistic Range Measurements of the Performance and Stability of Supersonic Aircraft", Canadian Aeronautical Journal, Vol. 4, No. 10, December 1958.

42. Dupris, A.D., "High Spin Effect on a 27 L/D Finned Projectile from Free-Flight Tests", AIAA Paper 87-2430.

43. Dupris, A.D., "Aeroballistic Range Tests of Flechette Anti-Tank Penetrator", Defense Research Establishment (DREV), Valcartier, Report 4443/88, April 1988.

44. Abate, G.L., et al, "Aeroballistic Range Tests: Scaled Models of the 105mm M1 Projectile and Modified Configurations", WL-TR-95-7059, September 1995.

45. Winchenbach, G.L., and West, K.O., "Free-Flight Range Test of the MK84, GBU-15 Cruciform Wing Weapon (CWW) at Mach Numbers of 0.5 to 1.2", AFATL-TR-78-85, March 1978.

46. Whyte, R.H., et al, "Aerodynamic Data Base of the C130 Gunship 105mm Projectile", WL-TR-7059, October 1995.

47. Dupris, A.D., Edwards, J., and Normand, M., "Aerodynamic Characteristic and Aeroheating Aspects of Two Hypersonic Configurations from Free-Flight Tests", DREV-R-9428, October 1995.

A 4.4 INTERIOR BALLISTICS / LAUNCHERS

1. Heiny, O.K., "Analytic and Experimental Interior Ballistics of Closed Breach Guns", AFATL-TR-69-42, May 1969.

2. Boehman, L.I., and Swift, H.F., "Analysis of Captured Piston Compressed Gas Guns", AFATL-TR-81-98, November 1981.

3. Fisher, E.B., "USER / Analyst Manual for Gun Model II", AFATL-TR-84-17, February 1984.
4. Heiny, O.K., "Engineering Interior Ballistics of Closed Breach Guns", AFATL-TR-73-189, September 1973.
5. Heiny, O.K., and West, R.J., "Interior Ballistics, Muzzle Flash and Gas Gradients of Aircraft Cannon", AFATL-TR-76-34, March 1976.
6. Swift, H.F., and Szczepansky, R.J., "75mm High Performance Solid Propellant Launcher", Physics Applications, Inc. Report, 1982.
7. Patin, R.M., "The mathematical Modeling of a Two-Stage Light gas Gun with a Deformable Piston", M.S. Thesis, Dept. of Mechanical Engineering, Louisiana State University, May 1985.
8. Swift, H.F., McDonald, J.W., and Chelekis, R.M. "Description and Capabilities of a Two-Stage Light Gas Launcher", Paper presented at the 35th Meeting of the Aeroballistic Range Association, Meppen, Germany, September 1984.
9. Mayer, P.C., "Compressed Air Gun Test Equipment and Testing Techniques", Paper presented at the 25th Meeting of the Aeroballistic Range Association, Silver Springs, Maryland, October 1974.
10. Chelekis, R.M., Swift, H.F., and McDonald, J.W., "Description and Capabilities of a High Performance Single Stage Launcher", Paper presented at the 34th Meeting of the Aeroballistic Range Association, Williamsburg, Virginia, October 1983.
11. Strange, D.E., and Swift, H.F., "Approximate Methods for Evaluating Light-Gas Gun Performance", Paper presented at the 43rd Meeting of the Aeroballistic Range Association, Columbus, Ohio, October 1992.
12. Winchenbach, G.L., Adelgren, R., and McClenahan, C., "Launching a Surf Zone Mine Countermeasure Explosive Array from a Double Barreled Single Stage Compressed Gas Gun", Paper presented at the 44th meeting of the Aeroballistic Range Association, Munich, Germany, September 1993.

DISTRIBUTION LIST
(WL-TR-1997-7006)

Defense Technical Info. Center
DTIC-OCP
8725 John J. Kingman Road, Suite 0944
Fort Belvoir,VA 22060-6218   1

WL/FIMCC
2145 5th St Ste 1, Bldg, 24C
Attn : Dr.George L. Siebert
Wright Patterson AFB ,OH 45433-756   1

WL/FIMD
2145 5th St Ste 1,Bldg, 24C
Attn : Charles Tyler
Wright-Patterson AFB,OH 45433-7562   1
NASA Langley Research Center
Technical Library Branch, MS 185
Attn: Document Cataloging
Hampton,VA 23665   1

Commander
U.S. Army Missile Command
Redstone Sci. Info. Center
Attn: AMSMI-RD-CS-R/Documents
Redstone Arsenal ,AL 35898-5241   1

Commander
U.S. Army Missile Command
AMSI RD SI AT (Dave Washington)
Redstone Arsenal ,AL 35898-5241   1

Commander
Naval Weapons Center (Code 3431)
Attn: Technical Library
China Lake ,CA 93555-6001   1

Director
U.S. Army Research Laboratory
Attn: AMSRL-OP-CI-B (Tech . Lib.)
Aberdeen Proving Ground
MD 21005-5006   1

Director
U.S. Army Research Laboratory
Attn: Dr. C.H. Murphy
      Dr. W. D'Amico
      F. Brandon
Aberdeen Proving Ground
MD 21005-5006   3

Commander
U.S. Army Armament Research
Development, and Engineering Center
Attn: SMCAR-TDC
Picatinny Arsenal, NJ 07806-5000   1

Commander
U.S. Army Armament Research
Development, and Engineering Center
Attn: SMCAR-AET
Picatinny Arsenal, NJ 07806-5000   1

Wright-Patterson AFB,OH 45433-6503
ASC/ENSTA   1
ASC/XRH   1
WL/CA-F   1
WL/FIM   1
WL/FIV   1

Eglin AFB offices:
WL/MNSI   2
WL/MNAV   19
WL/MNM   1
WL/MNMF   1
WL/MNA   2
WL/CA-N   1
WL/MNP-1(Tech library)   1

Aerospace Computing,Inc
339 Paone Drive
Boulder Creek,CA 95006
Attn : Dr. Leslie Yates   3

University of Alabama in Huntsville
Attn: Dr Gary Hough
Aerophysics Research Center
P.O.Box 999
Huntsville ,AL 35899   1

Institute for Advanced Technology
4030-2 West Bracker Lane
Attn: Dr. Don Berry
Austin, TX 78759   1

Calspan Corp.
Dept. 89
4455 Gennessee St
Buffalo , NY 14225
Attn : Mr Dick Bergman   1

AEDC
Attn : Tech Library
Arnold Air Force Base , TN 37389-4001 1

AEDC / SUT
Attn : Joel Shaver
        Richard Dix
Arnold Air Force Base , TN 37389-4001 2

AEDC / Operations   .
Attn : Larry Campbell
Arnold Air Force Base , TN 37389-4001 1

AEDC / VKF
Attn : Randall Watt
Arnold Air Force Base , TN 37389-4001 1

Sandia National Laboratories
Division 1401
P. O. Box 5800
Albuquerque , NM 87185-5800
Attn : Dr. Lalit Chhabildas   1

Southwest Research Institute
6620 Culebra Road
San Antonio , TX 78228-0510
Attn : Jack Riegal   1

Physics Applications, Inc.
7635 Wilmington Pike
Dayton ,OH 45458-5413
Attn : Hal Swift
        Dave Strange   2

University of Dayton Research Institute
300 College Park Drive
Dayton ,OH 45469-0182
Attn : Dr. Lloyd Huff   1

University of California,Berkeley
Dept of Engineering
6107 Etchverry Hall
Berkeley , CA 94720
Attn : Dr. Gary Chapman   . 1

University of Florida
Graduate Engineering Research Center
1350 N. Poquito Road
Shalimar , FL 32579
Attn : Dr. Chris Anderson
        Dr. J. E. Milton   2

NASA Ames Research Center
Moffett Field , CA 94305-1000
Attn : Mr Joseph Hartman
        MS 229-4   1

MetroLaser
18006 Skypark Circle , Suite 108
Irvine , CA 92714
Attn : Dr. Jim Trolinger   1

GASL
Attn : Technical Library
77 Raynor Ave.
Ronkonkoma , NY 11779   1

U.S. Naval Surface Weapons Lab.
Attn : Dr William Yanta
Code : K24 , Aerodynamics Branch
10901 New Hampshire Ave.
Silver Springs, M.D. , 20903-5000   1

NASA Lewis Research Center
Attn : Mr Arthur Decker , COTR
21000 Brookpark Road M/S 77-1
Cleveland ,OH 44135-3191   1

Attn : Dr. Richard P. Miles
Dept of Mechanical & Aerospace Eng.
D414 Engineering Quadrangle
P.O. Box CN5263
Princeton ,N.J. 08544-5263   1

Arrow Tech Assoc's
Lakewood Common
1233 Shelbourne Rd.
Pearson House Suite D8
So. Burlington VT 05403
Attn: Mr Bob Whyte
        Mr. Wayne Hathaway
        Mr. John Burnet   3

Institute for Advanced Technology
4030-2 West Braker Lane
Austin , TX 78759
Attn : Mr. Don Berry   1

Louisiana State University
Mechanical Engineering Dept.
CEBA 2805, LSU Campus
Baton Rouge , LA 70803
Attn : Dr. Robert Courter   1

Terma Electronics
46313 Stratton Terrace
Sterling VA, 20165
Attn : Mr. Jorgen Groth   1

Instut Franco-Allemand de
Researches de Saint-Louis
5 Rue du General Cassagnou ,B.P.34
68301 Saint Loius Cedex, France
Attn : Dr. M. Giraud
        Dr. Claude Berner
        Eckhard Summer   3

Naval Surface Warfare Center
17320 Dahlgren Road
Dahlgren, VA 22448
Attn : Dr. Frank Moore   1

Defense Research Est. Valcartier
P.O. Box 8800
Courcelette Q.C. , GOA1R0
Canada
Attn : Mr. Alain Dupris   1

UTSI
Tullahoma TN 37388
Attn : Dr. Roy Schulz   1

Nielsen Engineering & Research Inc.
526 Clyde Avenue
Mountain View , CA 94043-2212
Attn : M.R. Mendenhall
        Tom Canning   2

JPL
4800 Oak Grove Drive
Pasadina , CA 91109
Attn : Eric Slimco , MS 158-224   1